NORTHWESTERN UNIVERSITY

Studying and Engineering the *E. coli* 70S Ribosome *in vivo* and *in vitro* for the Synthesis of Abiological Polymers

A DISSERTATION

SUBMITTED TO THE GRADUATE SCHOOL

IN PARTIAL FULFILLMENT OF THE REQUIREMENTS

for the degree

DOCTOR OF PHILOSOPHY

Field of Biological Sciences

By

Anne Elizabeth d'Aquino

EVANSTON, ILLINOIS

March 2020

ABSTRACT

Studying and Engineering the *E. coli* 70S Ribosome *in vivo* and *in vitro* for the Synthesis of Abiological Polymers

Anne Elizabeth d'Aquino

The ribosome, the cell's machine for synthesizing proteins, can be thought of as the chef of the cell. Just as a chef reads a recipe and combines ingredients to create a dish, the ribosome reads cellular instructions and connects building block molecules (amino acids) to construct proteins. Like the final dish that nourishes us, proteins maintain the health of the cell. In culinary arts, a chef's training dictates their specialty; a chef with basic training prepares traditional staples, while a chef with specialized training masters a specific dish– for example, sushi. This thesis describes how changes (mutations) to the ribosome impact its function and how these mutations can be leveraged to design and build specialized ribosomes. The active site of the ribosome, or the functional heart of the machine, is arguably the most important part of protein synthesis, also known as translation. This site carefully positions amino acid monomers such that they react to form a protein. Studying and mutating the ribosome's active site has been difficult because changes to the ribosome cause cell sickness and death. This lack of mutational knowledge has hindered the biology and engineering fields and precluded the possibility of leveraging the ribosome for the synthesis of novel polymers.

Two key technologies have emerged as a powerful means to design, build, and characterize mutant or engineered ribosomes: cell-free ribosome synthesis, and cellular orthogonal ribosomes. This thesis describes the design, construction, and characterization of ribosomal mutant variants in a cell-free, or *in vitro* integrated ribosome synthesis, assembly, and translation (iSAT) platform.

Using this platform, we have generated sets of fundamental knowledge on the mutational flexibility of the ribosome's active site and mapped our findings onto the crystal structure to generate structure-function relationships. Furthermore, we have leveraged this platform to rapidly construct and study extended backbone incorporating ribosome constructs. Finally, in an effort to begin studying novel changes to the ribosome in the context of a living cell, efforts to improve an *in vivo* orthogonal ribosome platform, and use that platform to design and build engineered ribosomes in a cell are described. An overview of the ribosome's structure, function, and engineering efforts are outlined in Chapter 1. In Chapter 2, a cell-free ribosome synthesis, assembly, and translation (iSAT) platform is leveraged to generate a comprehensive mutational map of the ribosome's active site. As described in Chapter 3, this system can be used in the construction of multi-mutants for the rapid construction and characterization of ribosomes that incorporate extended backbone monomers. In Chapters 4 and 5, we leverage an *in vivo* ribosome engineering platform to design, characterize, and use orthogonal tethered ribosomes for expanding biological function. Finally, in Chapter 6, new basic science and synthetic biology questions surrounding the ribosome and translation are explored.

ACKNOWLEDGEMENTS

Although I am ultimately responsible for the final products, this dissertation was made possible by the support, guidance, and mentorship of many people. I am immensely grateful for the direct and indirect support I received throughout the journey of my PhD.

I cannot adequately express my gratitude for my family. Thank you to my mom and dad, Katherine and João d'Aquino – Two of the smartest and hardest working individuals I know. Your parenting has shaped me into who I am today. I want the world to know you and your story, because you are incredible humans. I frequently reflect on where you've come from, where you are now, and all that you have accomplished. You are both role models to me, and truly amazing individuals. Thank you to my twin sister, Andrea. I am so inspired by you! You are a force of nature. You have motivated me and pushed me to be a better scientist and human being. Your introspection, advocacy, creativity, guidance, and drive light my life up in unpredictable ways. I am so lucky to have you as a partner in this life, and I would not be where I am today without you. Thank you to my sister, Aurea – I strive to be a fraction of the human being that you are. Your strength, love, knowledge, creativity, kindness, and persistence are truly humbling. I treasure our chats, whether it be over the phone or with cats in our laps on your couch. Everything you do amazes me! Thank you to Valentina, for your unwavering support and love. I am so proud to have you as my sister, my friend, my confidant and my world travel partner. There is nothing you cannot do! Our time together is always pure joy – Like being kids again! I can't wait to see where we go together next. And thank you to my brother, Anthony, for being a constant source of love and encouragement. As the oldest child, you truly blazed a trail for all of your sisters. I look up to you in so many ways. Thank you for always making me laugh, smile, and forget about my worries. I

am so lucky to be your little sister. I am looking forward to many trips to visit you, Ashley, Leilani, and George in the near future! Thank you to Dion, Sandy, Aaron, Luis, Ashley and Steven, for being a part of my life and my family; I am incredibly fortunate to have received so much love and support from each of you.

I would like to express my deep gratitude for my advisor, Professor Mike Jewett, for seeing my potential and allowing me to rotate and subsequently join the lab. Thank you for your support, advice, mentorship and supervision throughout the completion of my PhD. Professor Jewett has been an invaluable source of guidance and encouragement and has always been supportive of my academic and career interests. The insightful criticisms and suggestions he offered throughout my research has shaped its direction and outcome considerably. Thank you to my other committee members: Professor Amy Rosenzweig, Professor Bob Lamb, and Professor John Marko for providing me with constructive feedback, mentorship, and support throughout my PhD. Professor Rosenzweig, as my chair, you have been an incredible source of insight and perspective. I can't thank you enough for being an ally as well as a mentor to me throughout my PhD. I would also like to thank my undergraduate advisor, Professor Clint Spiegel. I would not be where I am without Professor Spiegel's mentorship during my time as an undergraduate at Western Washington University.

My intellectual and professional development has been greatly shaped by my fellow graduate students and peers at Northwestern. Thank you to all my colleagues, labmates, and collaborators, who have made this work possible, including Dr. Erik Carlson, Lauren Clark, Dr. Jessica Perez, Dr. Rey Martin, Dr. Rui Gan, Dr. Ashty Karim, Dr. Jessica Stark, Jazzy Hershewe, Dr. Adam Hockenberry, Tasfia Azim, Kim Hoang, Alysse DeFoe, Dr. Kolya Aleksashin, Dorota

Klepacki, Teresa Szal, Dr. Antje Kruger, Dr. Joseph Yesselman, Dr. Rhiju Das, and Dr. Andrew Watkins. Thank you to Professor Shura Mankin and Professor Nora Vazquez-Laslop, for your invaluable support and guidance on all of my projects. Your insights and collaboration significantly enhanced the research we published. Furthermore, I will miss beach volleyball on summer Sundays with the entire Mankin lab—There we formed something more than peptide bonds. We formed bonds of friendship! Special thanks to my mentor and close friend, Dr. Erik Carlson, who taught me how to merge my basic science background with an engineering lab, and how to critically evaluate my work and the work of others. I am so honored to have worked with you and to have published with you! I can't wait to work with you at Stanford! And a huge thank you to Lauren Clark, who is a sister to me. You have grounded me, supported me, and encouraged me in so many ways. You were there for me during some of the most difficult events in my life. You hear me and see me; and you always have a way of saying just the right thing. I would also like to thank all other members of team ribosome (past and present) and the Jewett Laboratory for their help, inspiration and countless scientific discussions.

Thank you to my closest friends who, without them, I would be lost. Thank you to Drew Bauman, Andrea d'Aquino, Steven Swick, Ellie Page, Kari Tanaka, Koko Lawson, Jasmine Lucas, Chamille Lescott, Lam-Kiu Fong, Lisa Cole, Kevin Metcalf, Ryan Ross, and WeiTing Chen for always being there for me, and helping guide me when I've lost my direction. No matter what amount of time passes before we see each other, every meet-up is always a beautiful reminder of our friendship. From Saturday brunches, to late night drinks, morning tea times, going on adventures, traveling, or just laughing and talking; you have all filled me with the positive energy to persist, understand myself, and understand the world we live in. Each of you have not only

challenged me to consider new ways of thinking and approaching problems, but you have also supported me during difficult moments in my graduate career. Furthermore, you have all reminded me to rest – The work that each of us does is not trivial. Our goals, hopes, and dreams take an enormous amount of work to accomplish. You all reminded me in gentle and beautiful ways to slow down, stop, rest, and enjoy life along with the work I do. A very special thanks to Chamille – I am so thankful to have met you in the last year of my PhD. You are an incredible scientist and human being. You have an indescribable energy that you so graciously share with all those around you. I have been so lucky to learn from you.

Thank you to Northwestern University's Summer Research Opportunity Program (SROP). There is a possibility that I would not be at Northwestern if it was not for this program. A very special thank you to my SROP advisor, Professor Heather Pinkett for truly sparking the joy of academic research in me. Heather saw something in me and lifted me up, nominating me to give the SROP class final presentation in science as well as nominating me for early admission to Northwestern University. This was the first time that I truly felt like I belonged in this field and this work. I can never thank you enough for that. And to my SROP graduate student mentor and friend, Dr. Kari Tanaka. You were so patient with me, and despite your seniority to me, you made me feel accepted, comfortable, and accomplished. I learned so much from you over that summer and am still learning so much from you now! I am incredibly fortunate to have you as a science sister and best friend. Thank you to all of the undergraduate students who I have mentored throughout my PhD: Tasfia Azim, Kim Hoang, and Alysse DeFoe. I learned so much from all of you, and am always blown away by your thoughtfulness, insight, creativity, and drive. I have

greatly benefited from conversations and scientific discussions with each of you and am grateful to have had the opportunity to learn and grow from you.

Thank you to Northwestern's Prison Education Program (NPEP). NPEP transformed me in unpredictable and incredible ways. This program is not only the highlight of my graduate school experience, but the apex of my PhD—In this program I truly learned and applied critical thinking, questioning, mentorship, and teaching in some of the most challenging and enriching ways. Every aspect of my life has been transformed by this program. A very special thank you to Professor Jennifer Lackey. I can't say it enough, but you truly are a role model to me. You have impacted my PhD immensely, and I am unbelievably thankful for this. Thank you to the NPEP Graduate Student Advisory Committee members and alum: Dr. Andrea d'Aquino, Dr. Steven Swick, Hansen Breitling, Magda Boutros, Charlotte Rosen, Jonas Rosenbrück, Jake Rothschild, Ari Tolman, Dr. Anya Degenshein, Dr. Lauren Leydon-Hardy and Professor Barron Reed. You are all a family to me. You have supported me during some of the most difficult moments in my PhD and were allies to me and advocates for me in the most important ways. I feel so lucky to have found a family in graduate school who is so willing to devote their time, talents, and energy to such an important mission. Everyone in this program is a constant reminder of the beauty in this world. Magda – I am so thankful to have worked with you on the Cook County Jail partnership. You are absolutely incredible, and I don't know how you do everything! I am so lucky to call you both my colleague and friend. Not many people would sit outside for hours in the peak Chicago summer heat to help us host a garage sale for NPEP! You are truly an incredible human being – I hope that I am there for you as you have always been there for me. Hansen, I will always cherish our car rides to-and-from Stateville, where we learned from and about each other. You opened my eyes to philosophical

terms and concepts that helped me articulate for the first time, my experiences and feelings surrounding my identity. You saw me and you heard me. You have always made a safe space for me to learn and share. As an ally to me, and all minorities and marginalized identities in science (and beyond); you never made the conversation about you. You stood in solidarity with me, listened, and even absorbed my (and others') struggles as your own. You have been a powerful voice alongside mine. I appreciate you immensely and am so looking forward to seeing even more of what you accomplish! Thank you to our absolutely incredible students at Stateville Correctional Center – I could not ask for a better group of students. You are an inspiration to me and saw something in me that I didn't initially see myself. I am so fortunate to be spending my remaining time in Chicago working with you all! Thank you to my students at the Cook County Jail. I wish my mini-course could have lasted longer. You affirmed my love for teaching and inspired me to think about new research avenues with your questions.

Thank you to the members of the NU HerStory leadership team (past and present), especially Andrea d'Aquino, Constanza Vasquez-Doorman, Lam-Kiu Fong, Alicia McGeachy, and Jessica Perez. Thank you for your unwavering passion in fighting to bring change and equity to science. Thank you to Deborah and Cathy, for always advocating for students and for all the work you have done to help me—and many other graduate students—through innumerable challenges we have faced here as graduate students at Northwestern, over the years.

Thank Drew Bauman for being a good friend, and listener. When I was down, you lifted me up; when I was sad, you helped me laugh; and when I was struggling, you supported me. Your light heartedness and jokes made my graduate school experience a much more positive one. We learned and grew so much together. My PhD would not be the same without you. We overcome

many obstacles and expanded our minds in beautiful and challenging ways. Thank you for the stories that we share together.

Finally, an extra special thanks to Dr. Andrea d'Aquino and Dr. Steven Swick – My two best friends. You two helped me with my papers and thesis in ways that I could have never imagined. Between editing my writing, and helping me conjure meaningful text, and tasteful reviewer responses, you both carried me through the most difficult part of the finish line. Andrea – thank you for taking care of me during the last days of thesis writing. Between cooking for me, letting me share your space, bringing me snacks, helping me with formatting, and making sure I was well-rested; you helped me during the most difficult part of my graduate school experience. Steven – thank you for always thoughtfully listening to me and giving invaluable feedback. Your perspectives are always so enlightening. Thank you to you both for sharing your time and space with me.

I have been so fortunate to have taken part in so many incredible opportunities throughout my PhD. These beautiful moments in my graduate career have been possible only through the liberating love and support of my friends and family. During this time, I learned many things, but perhaps the most important piece of knowledge gained was the importance of these relationships. Thank you to my friends and family for always being there for me.

"I've learned that I still have a lot to learn." – Maya Angelou

LIST OF ABBREVIATIONS

aaRS	Aminoacyl tRNA synthetase
Amp	Ampicillin
A-site	Aminoacyl-site
BB	Backbone
BME	β-mercaptoethanol
Cb	Carbenicillin
CFPS	Cell-free protein synthesis
DHFR	Dihydrofolate reductase
DNA	Deoxyribonucleic acid
DTT	Dithiothreitol
EF-Tu	Elongation factor thermo unstable
FPLC	Fast protein liquid chromatography
GA	Gibson Assembly
GFP	Green fluorescent protein
His	Histidine
IPTG	Isopropyl β- d-1-thiogalactopyranoside
iSAT	Integrated synthesis, assembly, and translation
Kan	Kanamycin
LB	Luria broth
MALDI	Matrix-assisted laser desorption/ionization
MBP	Maltose binding protein
mg	milligrams
mRNA	Messenger RNA
MWCO	Molecular weight cutoff
ncAA	Non-canonical amino acid
ng	nanograms
NTP	Nucleoside triphosphates
OD	Optical density
PCR	Polymerase chain reaction
PEG	Polyethylene glycol
PEP	Phosphoenolpyruvate
P_L	Strong leftward promoter
PMSF	Phenylmethylsulfonyl fluoride
P-site	Peptidyl site
PTC	Peptidyltransferase center
RISE	Ribosome synthesis and evolution
RM	RNAMake
RNA	Ribonucleic acid

RNAP	RNA polymerase
rRNA	Ribosomal RNA
RPM	Revolutions per minute
R-protein	Ribosomal protein
SDP	Sequence defined polymer
SDS-PAGE	Sodium dodecyl sulfate polyacrylamide gel electrophoresis
sfGFP	Superfolder GFP
SOB	Super optimal broth
SOC	Super optimal broth with catabolite repression
SPPS	Solid phase peptide synthesis
TP70	Total protein of the 70S *E. coli* ribosome
tRNA	Transfer RNA
TH	Toehold
tRNA	Transfer RNA
WT	Wild type

DEDICATION

To my nephew, Mateo Miguel Roedell.

Thank you for all of the joy you brought and continue to bring, despite your short time in this world.

TABLE OF CONTENTS

ABSTRACT 3
ACKNOWLEDGEMENTS 5
LIST OF ABBREVIATIONS 12
DEDICATION 14
TABLE OF CONTENTS 15
LIST OF TABLES AND FIGURES 22
CHAPTER 1 35
The *Escherichia coli* ribosome: Engineered ribosomes for basic science and synthetic biology 35
1.1 Introduction 36
1.2 The ribosome's parts 39
1.2.1 Nucleic acids of the ribosome: Structure and Function 39
1.2.2 The polypeptides of the ribosome: Ribosomal proteins 42
1.2.3 The site of translation initiation: Shine-Dalgarno and Anti-Shine-Dalgarno sequences 43
1.2.4 The ribosome's catalytic peptidyl transferase center: A-, P-, and E-Sites 44
1.3 Engineered ribosomes for advancing basic biology 46
1.3.1 Reconstructing the ribosome from its parts: Ribosome reconstitution 46
1.3.2 Probing the ribosome's active site 50
1.3.3 Specializing the ribosome 55
1.3.4 Isolating the ribosome by affinity purification 56
1.3.5 Developing and using the Squires strain 58
1.4 Engineered ribosomes for synthetic biology 60
1.4.1 Engineered ribosome-associated translation machinery 61

1.4.2 Limitations of wild-type ribosomes for genetic code expansion 64

1.4.3 Engineering the ribosome's active site 65

1.4.4 Orthogonal ribosomes: message decoding, tRNA interactions, subunit tethering .. 68

1.5 Perspectives, conclusions, and outlook 72

1.6 Introduction to dissertation topics 78

CHAPTER 2 81

Studying and engineering ribosomes *in vitro*: Mutational characterization and mapping of the 70S ribosome active site 81

2.1 Abstract 82

2.2 Introduction 83

2.3 Materials and methods 88

2.3.1 Plasmid construction 88

2.3.2 Sequence alignment and analysis 88

2.3.3 Strain culture and harvest 89

2.3.4 Component preparation 90

2.3.5 iSAT reactions 90

2.3.6 Ribosome sedimentation analysis 91

2.3.7 iSAT ribosome purification 92

2.3.8 Nucleotide distance calculations 92

2.4 Results 93

2.4.1 Examining mutational flexibility of PTC rRNA *in vitro* 93

2.4.2 Characterizing PTC mutant ribosome translation readthrough 97

2.4.3 Incorporation of ribosomes with PTC active site mutations into functional polysomes 100

2.4.4 The ribosome's active site is composed of high- and low-flexibility pockets and shells 102
2.4.5 Studying multi-mutant ribosomes *in vitro* 106
2.5 Discussion 109
2.6 Data availability 114
2.7 Acknowledgements and contributions 115
2.8 Patent information 115
2.9 Supplementary figures and tables 116
CHAPTER 3 144
Studying and engineering β-amino acid incorporating ribosomes 144
3.1 Abstract 145
3.2 Introduction 145
3.3 Materials and methods 148
3.3.1 Plasmid construction 148
3.3.2 Strain and culture harvest 149
3.3.3 Component preparation 150
3.3.4 iSAT reactions 150
3.3.5 Ribosome sedimentation analysis 151
3.3.6 iSAT ribosome purification 152
3.3.7 MS2-tagged ribosome construct preparation and isolation 152
3.3.8 Expression and purification of MBP-MS2-His protein 154
3.3.9 Purification of MS2 tagged ribosomes 156
3.3.10 Testing β-amino acid incorporation 158

3.4 Results 158

3.4.1 Characterizing iSAT and MS2-purified β-incorporating ribosomes' functionality 158

3.4.2 Characterizing the assembly of β-incorporating ribosomes 162

3.4.3 β-amino acid incorporation with purified β-ribosomes 163

3.5 Discussion 165

3.6 Acknowledgements and author contributions 165

3.7 Supplementary tables and figures 165

CHAPTER 4 166

Studying and engineering ribosomes *in vivo*: Improvements to a ribosome with tethered subunits for *in vivo* ribosome engineering 166

4.1 Abstract 167

4.2 Introduction 167

4.3 Materials and Methods 171

4.3.1 Construction of the tether libraries 171

4.3.1 Replacement of the wild-type ribosome by Ribo-T v2 173

4.3.2 Selecting mutants, evaluating growth rate and analyzing tethers 174

4.3.3 Liquid culture competition assay 174

4.3.4 Total RNA analysis of tethered Ribo-T v2 175

4.3.5 Selection of new orthogonal pairs 175

4.3.6 Evaluation of new orthogonal pairs 183

4.3.7 Evaluation of Ribo-T growth in minimal media 184

4.3.8 Expression and purification of recombinant proteins using oRibo-T v2 184

4.3.9 Strain construction for ncAA incorporation with oRibosomes 186
4.3.10 Combined orthogonal ribosome-sf-GFP reporter system 188
4.3.11 Incorporation of p-azido-phenylalanine using oRibo-T 189
4.3.12 Chemical probing of the structure of the Ribo-T tethers 190
4.3.13 RNA structure modeling 191
4.3.14 Protein secondary structure map generation 192
4.4 Results 192
4.4.1 Tether optimization improves growth of Ribo-T cells 192
4.4.2 Improvement of Ribo-T orthogonal function 197
4.4.3 Evaluation of evolved orthogonal pairs 200
4.4.4 Orthogonal pair activity in other *E. coli* strains 203
4.4.5 Synergistic effect of evolved tethers and orthogonal pairs 204
4.4.6 Incorporation of non-canonical amino acids by Ribo-T 205
4.5 Discussion 207
4.6 Acknowledgements and contributions 209
4.7 Patent information 210
4.8 Supplementary figures and tables 210
CHAPTER 5 225
Studying computationally designed ribosome variants *in vivo* and *in vitro* 225
5.1 Abstract 226
5.2 Introduction 226
5.3 Materials and methods 228
5.3.1 Design of ribosome tether constructs 228

5.3.2 Construction and experimental testing of ribosome tether constructs 228

5.3.3 *In vivo* replacement of the wild-type ribosome by tethered ribosome variants 229

5.3.4 *In vitro* construction, testing, and characterization of ribosomes 230

5.3.5 Selecting tether mutants, evaluating growth rate and analyzing tethers 231

5.3.6 Total RNA analysis of tethered ribosomes 231

5.4 Results 232

5.4.1 Characterizing computationally designed tethered ribosomes 232

5.4.2 Characterizing ribosomes with RNA aptamer tethers 237

5.5 Discussion 241

5.6 Acknowledgements and contributions 242

5.7 Supplementary figures and tables 244

CHAPTER 6 265

Dissertation Overview and Future Outlook 265

6.1 Dissertation Overview 266

6.2 Future work 267

6.2.1 Probing single and multi-mutations in other key regions of the ribosome 267

6.2.2 Leveraging SHAPE-Seq for characterizing mutant rRNA interactions 267

6.2.3 Rescuing translation and improving ncAA incorporation with translation factors 268

6.2.4 Novel circular permutations with computationally designed tethers 269

CHAPTER 7 270

Conclusion 270

CHAPTER 8 272

Appendix 272

8.1 Improving ribosome orthogonality with translational riboregulators 273

8.1.1 Background 273

8.1.2 Experimental setup and future work 275

8.2 Expressing ribosomal proteins *in vitro* 277

8.2.1 Background 277

8.2.2 Experimental setup and future work 279

8.3 Educational tools: studying mutations in protein structure and function 280

8.3.1 Background 280

8.3.2 Experimental setup and future work 281

8.4 Nature Protocols: A ribosome tethering strategy for an orthogonal ribosome-messenger RNA system 282

8.4.1 Abstract 282

8.4.2 Overview of the technique 282

8.5 Giving back to the scientific and broader community 290

REFERENCES 292

LIST OF TABLES AND FIGURES

CHAPTER 1

Figure 1.1 Ribosome engineering in context: protein translation in a cell. Free transfer RNAs (tRNAs) are charged (aminoacylated) with amino acids by the aminoacyl-tRNA synthetase (aaRS). Aminoacyl-tRNA molecules can also be generated *in vitro* using Flexizymes of pdCpA. Next, the aminoacyl-tRNA molecule is delivered to the ribosome by elongation factor Tu (EF-Tu). The tRNA, whose anticodon loop corresponds to a messenger RNA (mRNA) codon, delivers the amino acid to the ribosome, where it is polymerized into a protein. Abbreviations: nsAA, nonstandard amino acid; PTC, peptidyl transferase center. 38

Figure 1.2 Map of the ribosome's parts. The ribosome is a complex machine composed of numerous parts. Some of the integral parts are mapped here. These include 3 different ribosomal RNA (rRNA) molecules (5S rRNA and 23S rRNA in the large subunit are depicted in grey, and 16S rRNA in the small subunit is depicted in wheat); ribosomal proteins (r-proteins) (the 33 large subunit r-proteins are depicted in teal, and the 21 small subunit r-proteins are depicted in orange); the catalytic peptidyl transferase center (PTC); the A-, P-, and E-sites; and the anti-Shine-Dalgarno sequence for decoding. Figure rendered using PyMol and PDB ID 4V5H. 40

Figure 1.3 In vitro synthesis, assembly, and translation (iSAT) for ribosome design and engineering. (a) The iSAT method enables efficient one-pot co-activation of ribosomal RNA (rRNA) transcription, (b) assembly of rRNA with native ribosomal proteins into *Escherichia coli* ribosomes, and (c) synthesis and analysis of functional proteins from these ribosomes in a S150 extract lacking native ribosomes. This purely *in vitro* strategy for *E. coli* ribosome construction offers a powerful technique to study and exploit engineered ribosomes. 49

Table 1.1 Proposed roles of select 23S rRNA nucleotides in translation. 52

Figure 1.4 Orthogonal ribosomes. (a) For an orthogonal Shine-Dalgarno:anti-Shine-Dalgarno (o-SD:aSD) system, tuning of the SD sequence of the mRNA in conjunction with the aSD sequence of the 16S rRNA allows for orthogonal message decoding. Of note, the 50S subunit is not orthogonal and freely associates with both wild-type and orthogonal 30S subunits. (b) in the tethered ribosome system, the entire ribosome, including the catalytic 50S subunit, is orthogonal and does not interfere with the wild-type ribosomes. (c) In the orthogonal transfer RNA (tRNA):ribosome system, tuning the interaction between the 3' tRNA sequence and the ribosome's 23S rRNA establishes orthogonality to wild-type tRNAs and wild-type 23S rRNAs. Abbreviation: o-mRNA, orthogonal messenger RNA. 56

Figure 1.5 Cartoon depiction of the MS2 ribosome purification technique. (a) A 17-nucleotide RNA hairpin that binds the MS2 phage coat protein is engineered into the terminal loop of *Escherichia coli* 23S rRNA helix 98. (b) upon lysin cells possessing the tagged ribosomes, binding the ribosomes to an affinity matrix, washing, and eluting, purified MS2-tagged ribosomes can be characterized and studied. 58

Figure 1.6 The Squires strain. The Squires strain is an experimental system that can be used for studying and engineering ribosomes. In traditional Escherichia coli strains (such as MRE600), ribosomal RNA (rRNA) genes are highly repeated on the genome (red triangles). Ribosomes are synthesized based on seven genomic copies of the ribosomal operon. In the Squires strain, all seven chromosomal rRNA operons are deleted. A single E. coli rRNA operon carried by a multicopy plasmid (ptRNA67) supplies 16S rRNA and 23S rRNA to the cell. Using this strain, ribosome variants can be introduced into the Squires strain cells, and ptRNA67 removed. This permits the in vivo study of ribosome variants without the contamination of endogenous wild-type ribosomes. Abbreviation: mRNA, messenger RNA. 59

Figure 1.7 23S ribosomal RNA (rRNA) residues in the peptidyl transferase center engineered for new chemistries. Featured in work by both the Hecht and Schepartz groups, key residues in the 23S rRNA (2057-2063 and 2492-2507) are highlighted in magenta and red, respectively. The rest of the 23S rRNA and 16S rRNA are shown in gray and wheat, respectively. These key residues were selected for mutation based on their role in peptide bond formation and their vicinity to the 3’ end of both the A-site tRNA and P-site tRNA (green) which carries the activated amino acid monomer for polymerization. The messenger RNA (mRNA) is shown in lime for reference, near the bottom of the tRNAs. 67

Table 1.2 Freely available online tools, software, and resources for aiding ribosome design and engineering efforts. 73

Table 1.3 Summary of translation apparatus parts, pieces and tools for incorporating various nonstandard monomers. 75

CHAPTER 2

Figure 2.0 Graphical abstract. Studying ribosome active site mutants using an *in vitro* platform. Peptidyl transferase center (PTC) mutant plasmids were introduced into *in vitro* integrated synthesis, assembly, and translation (iSAT) reactions along with cell-free iSAT reagents. Once iSAT reactions are initiated, T7 RNA polymerase transcribes sfGFP mRNA as well as rRNA. The rRNA coassembles with ribosomal proteins (TP70) to form iSAT ribosomes. These ribosomes can then translate the reporter protein mRNA (sfGFP). Upon completion of an iSAT reaction, kinetics, structure, fidelity, and assembly analyses can be carried out to characterize ribosomes *in vitro*. 83

Figure 2.1 The ribosome’s peptidyl transferase center (PTC) is important for translation and can be studied *in vitro*. (a) Secondary structure and (b) crystal structure model of the PTC-ring nucleotides probed in this study. (c) Secondary structure and crystal structure model of the A- and P-loop nucleotides probed in this study. Ribosome structure accessed from PDB ID: 4YBB, with tRNAs from PDB ID: 1VY4. 85

Figure 2.2 The ribosome’s peptidyl transferase center (PTC) is amenable to mutation, despite high sequence conservation. (a) Shannon entropy plot representing the conservation of PTC nucleotides across 1,614 of bacterial and archael species. All large subunit (LSU) sequences were taken from

alignments found at the Silva database (43). Shannon entropy values of zero represent 100% conservation across all species. Despite the high conservation of the ribosome's PTC, there is high plasticity within its catalytic core. (b) Mutational flexibility of each PTC mutation relative to the activity of WT iSAT ribosomes. Nucleotides are color coded according to the legend. The original WT nucleotide activity is normalized to 1, and resides below the red line on the graph. Each possible nucleotide change at the corresponding position is color coded in the bars above the red line, with bar size representing relative activity. Single asterisks are placed above nucleotides wherein the sum of mutant activity (mutational flexibility) results in activity ≥ 1 (PTC-ring: G2057, A2058, A2062, A2448, C2496, A2497, A2503, U2504, G2505, U2584, U2586, A2587, G2588, G2607, G2608, and U2609; A- and P-loops: U2548, G2550, C2551, U2554, U2555, C2556, G2557, C2558, C2559, A2560, G2253, C2254). A second asterisk is placed above nucleotides wherein at least one nucleotide mutation results in activity ≥ 75% of WT activity (PTC-ring: G2057, A2058, A2062, C2496, A2503, G2505, A2587, G2608, and U2609; A- and P-loops: U2548, G2550, C2551, U2555, C2556, C2558, C2559, A2560, C2554). **(C)** Protein synthesis curves for representative nucleotide mutations have been included in this graph: wild-type, high activity (A2062U and G2057U), medium activity (C2496G and A2451C), medium-low activity (U2585G and A2451U), and low activity (G2455A and C2452G) mutants were chosen. Translation rates for representative PTC mutants in this study are represented in Supplementary Table S2. For simplicity and ease of visualization, only a subset of 180 nucleotide mutation kinetic curves are included on the graph and the X-axis is restricted to 8 hours..... 94

Table 2.1 Bulk translation rates of wild-type and representative mutant 70S iSAT ribosomes. Bulk translation rates for iSAT ribosomes were determined from protein synthesis kinetics curves, for reactions after 2 h incubations. 96

Figure 2.3 Ribosomal PTC mutations increase stop-codon readthrough. (a) Schematic of translation fidelity assay using premature stop codon constructs. Assays were adapted from O'Connor *et al*. (37). Premature stop codon readthrough from wild-type ribosomes was normalized to 1. Mutant ribosome premature stop codon readthrough was quantified through fluorescence and set relative to WT. Mutants with lower fidelity (higher readthrough of premature stop codons) produce higher relative sfGFP titers. (b) UAG stop codon readthrough at amino acid position 50, 100 ,116, and 216. (c) UAG, UGA, and UAA stop codon readthrough at amino acid position 100. Relative activity in translation fidelity assays using premature stop codons was assessed using sfGFP fluorescence. The pJL1-sfGFP plasmid possessing a UAG stop codon at the specified locations were introduced into iSAT reactions as the reporter plasmid along with the mutant or wild-type rRNA plasmids. Values represent averages and error bars represent one standard deviation from the mean, with n ≥ 3 for n number of independent reactions. 98

Figure 2.4 Sucrose gradient fractionation identifies assembly differences across ribosomal PTC mutants. (a) The five nucleotide mutations chosen for sucrose gradient fractionation based on their activity. One high activity (A2062U) mutant was chosen, two medium activity (U2585G and A2451U), and one low activity mutant (G2455A) was assessed for assembly and compared to WT. (b) A wild-type sucrose gradient fractionation trace (black) is compared to 4 representative mutant

traces (color coded based on nucleotide mutation activity graph). From bottom to top, the mutants are positioned in decreasing activity order. (c) Relative areas under sucrose gradient fractionation trace curves were used to calculate ratios of subunits to 70S and polysome particles as well as the ratio of 70S particles to polysomes. 101

Figure 2.5 A mutational map reveals that the ribosome's PTC is composed of functional pockets and shells. (a) Secondary structure and (b) crystal structure model of the PTC-ring nucleotides probed in this study (heat mapped), along with the A-site tRNA, and P-site tRNA. (c) Crystal structure and secondary structure models of the A- and P-loop nucleotides probed in this study (heat mapped), A-site tRNA (green), P-site tRNA (blue), and PTC ring nucleotides (grey). (d-j) Crystal structure model of the PTC-ring nucleotides possessing: (d) the lowest mutational flexibility (red and magenta), (e) medium/low mutational flexibility (red-violet), (f) medium/high mutational flexibility (violet), and (g) the highest mutational flexibility (violet-blue). (h) Crystal structure model of the A-loop nucleotides probed in this study (heat mapped), A-site tRNA (green). (i) Crystal structure model of the P-loop nucleotides probed in this study (heat mapped), P-site tRNA (blue). (j) Structure model highlighting the nucleotides with mutants possessing increased translation readthrough (C2496, U2585, and A2451), as well as assembly defects (G2455). Ribosome structure accessed from PDB ID: 4YBB, with tRNAs from PDB ID: 1VY4. 104

Figure 2.6 Sequence alignment and Shannon entropy plot representing the conservation of PTC nucleotides across 1,614 bacterial and archael species. Shannon entropy values of zero represent 100% conservation across all species. The black boxes and lines highlight the positions of co-variance. 107

Figure 2.7 Activity of each PTC multi-mutant relative to the activity of wild type iSAT ribosomes. The multi-mutants highlighted with green boxes represent those multi-mutants whose activity exceeded that of one or more of the individual single mutants. 108

Supplementary Figure 2.1 The ribosome's peptidyl transferase center (PTC) is highly conserved. (a) Phylogenetic tree of the species used for the rRNA sequence alignment. The left to right distance for any branch of the tree represents the amount of sequence divergence from the "root" (far left) to the actual sequence (the leaves, far right). (b) Sequence alignment matrix illustrating the conservation of PTC nucleotides across 1,614 species of bacterial and archael species. All LSU sequences were taken from alignments found in the SILVA database (43). The ribosome's PTC is highly conserved across both bacterial and archael species. 116

Supplementary Figure 2.2 The ribosome's A- and P-loops are highly conserved. Sequence alignment illustrating the conservation of PTC nucleotides across 1,614 species of bacterial and archael species. All LSU sequences were taken from alignments found at https://www.arb-silva.de/projects/living-tree/. The ribosome's PTC is highly conserved across both bacterial and archael species. Shannon Entropy scores are akin to variance scores (though we caution that they ignore phylogenetic relatedness), with a Shannon Entropy of zero representing zero variance (100% conservation across the 1,614 species). Any values above zero indicate that evolutionary changes have occurred and result in multiple nucleotides within a given site in the alignment. 117

Supplementary Figure 2.3 Protein synthesis kinetic time course curves from iSAT reactions for all individual nucleotide mutations probed in the PTC-ring, A-loop, and P-loop. Smoothed data from samples taken every 15 minutes are shown. Values represent averages and error bars represent one standard deviation from the mean, with n ≥ 3 for n number of independent reactions. 118

Supplementary Figure 2.4 Ribosomes with mutations in the A- and P-loops demonstrate decreased bulk protein synthesis rates. (a) Relative protein synthesis activity of A-loop mutants tested in translation assays. (b) Protein synthesis kinetic time course curves from iSAT reactions for the following A-loop nucleotide mutations have been included in this graph: C2559A, C2551A, U2552G. Protein synthesis rates are proportional to relative protein synthesis titers. For simplicity and ease of visualization, not all nucleotide mutation kinetic curves are included on the graph. Values represent averages and error bars represent one standard deviation from the mean, with n ≥ 3 for n number of independent reactions. (c) Relative protein synthesis activity of P-loop mutants tested in translation assays. (d) Protein synthesis kinetic time course curves from iSAT reactions for the following P-loop nucleotide mutations have been included in this graph: C2254A, G2253A, G2250U. Protein synthesis rates are proportional to relative protein synthesis titers. For simplicity and ease of visualization, not all nucleotide mutation kinetic curves are included on the graph (see Supplementary Figure 2.3). Values represent averages and error bars represent one standard deviation from the mean, with n ≥ 3 for n number of independent reactions. 119

Supplementary Figure 2.5 Regression models of Shannon entropy (nucleotide conservation) against mutational flexibility (the sum of all nucleotide mutations' relative activity). (a) The regression plot for the PTC-ring possesses a low R^2 value (R^2 =0.117, p=0.025) demonstrating difficulty in predicting mutational flexibility from nucleotide conservation. (b) The regression plot for the A- and P-loops also possesses a low R^2 value (R^2 =0.173, p=0.086) demonstrating difficulty in predicting mutational flexibility from nucleotide conservation. 120

Supplementary Figure 2.6 Ribosomal A-loop mutations do not increase stop-codon readthrough. (a) Relative protein synthesis activity of A-loop mutants tested in translation fidelity assays. (b) A-loop secondary structure. (c) UAG stop codon readthrough at amino acid position 50, 100 ,116, and 216 of sfGFP. (d) UAG, UGA, and UAA stop codon readthrough at amino acid position 100 of sfGFP. As described in the main text, the relative readthrough activity in translation fidelity assays using premature stop codons was assessed using sfGFP fluorescence. sfGFP levels obtained with wild-type rRNA plasmids are normalized to 1, and values obtained with each of the mutants were expressed relative to that obtained with the respective wild-type rRNA plasmid. To enable comparison with Figure 3 from the main text, the y-axis values are extended to 10 in c and d. Values represent averages and error bars represent one standard deviation from the mean, with n ≥ 3 for n number of independent reactions. 121

Supplementary Figure 2.7 Ribosomal P-loop mutations do not increase stop-codon readthrough. (a) Relative protein synthesis activity of P-loop mutants tested for fidelity. (b) P-loop secondary structure. (c) UAG stop codon readthrough at amino acid position 50, 100 ,116, and 216 of sfGFP. (d) UAG, UGA, and UAA stop codon readthrough at amino acid position 100 of sfGFP. As

described in the main text, the relative readthrough activity in translation fidelity assays using premature stop codons was assessed using sfGFP fluorescence. sfGFP levels obtained with wild-type rRNA plasmids are normalized to 1, and values obtained with each of the mutants were expressed relative to that obtained with the respective wild-type rRNA plasmid. To enable comparison with Figure 3 from the main text, the y-axis values are extended to 10 in c and d. Values represent averages and error bars represent one standard deviation from the mean, with n ≥ 3 for n number of independent reactions. 122

Supplementary Figure 2.8 The ribosome's peptidyl transferase center (PTC) is composed of functional pockets. (a) Heat map of rRNA PTC-ring and (b) A- and P-loop mutational activity against their distance from the P-site tRNA (top) and A-site tRNA (bottom). White shading illustrates zero activity, while dark orange shading illustrates WT-activity..... 123

Supplementary Figure 2.9 Regression models of nucleotide distance against mutational flexibility. (a) Regression model of distance from A-site (R^2=0.154, p=0.13) and P-site (R^2=0.001, p=0.93) tRNA against mutational flexibility of PTC-ring nucleotides suggests a non-significant (p>0.05) and weak (low R^2 values) relationship. (b) Regression model of distance from A-site and P-site tRNA against mutational flexibility of A- (red) and P-loop (blue) nucleotides. The regression plots for the A-loop nucleotides possess R^2 values of 0.35 (p=0.03) and 0.32 (p=0.04), respectively. The regression plots for the P-loop nucleotides possess R^2 values of 0.61 (p=0.12) and 0.43 (p=0.23), respectively. The regressions and p-values for the A-site nucleotides suggests a significant and predictive relationship between mutational flexibility and distance from tRNA molecules; while the P-site nucleotides suggests a predictive relationship, however this relationship is non-significant due to a small sample size. 124

Supplementary Figure 2.10 Comparison of ribosomal mutant activity vs. nucleotide base change within the PTC-ring. Nucleotide changes from C to A, C to G, and G to C have the lowest activity, with ~70-90% of the nucleotides exhibiting less than 20% of WT activity. In contrast, changes from G to A, A to U and G to U exhibit the highest activity, with ~20-30% of the nucleotides exhibiting 80-100% of WT activity. 125

Supplementary Figure 2.11 Growth curve of E. coli MRE600 strain used in this study. Cells were grown in 10L of 2xYTPG media and harvested from the fermenter at OD = 2.9–3.1. Cells were grown at 37C, as previously reported. 126

Supplementary Figure 2.12 Extract testing and optimization. (a) Protein concentration of S150 extract used in this paper. Values represent average concentrations as determined by Bradford assay with bovine serum albumin (BSA) as a standard. Error bars represent one standard deviation from the mean for triplicate measurements. (b) Magnesium optimization of S150 extract for reporter protein synthesis in iSAT reactions. Standard 15 µL batch reactions were performed at 37°C for 20 h, with varying magnesium glutamate concentrations the S150 extract used. Total protein concentration of each S150 extract added to reactions was standardized at 3.6 mg mL^{-1}. Synthesis of active wild-type (wt) sfGFP was measured after 20 h using fluoresence. Optimal magnesium glutamate concentrations for iSAT reactions was determined to be: 13 mM for

MRE600. This concentration was then used for subsequent experiments. Values represent averages and error bars represent one standard deviation from the mean, with n ≥ 3 for n number of independent reactions..... 127

Supplementary Figure 2.13 Gel electrophoresis analysis of WT and mutant iSAT ribosomes following sucrose density centrifugation. A 120 µL iSAT reaction possessing a reporter plasmid was analyzed by polysome profiling in a 10-40% sucrose gradient. The resulting 500 µL – 1 mL fractions were run by electrophoresis on a 1% agarose gel (one fraction per well). The rRNA contained within each fraction was used to confirm the predominate peaks as containing 30S, 50S, or 70S subunits..... 128

Supplementary Table 2.1 *E. coli* 23S rRNA PTC nucleotides and their published mutational studies. 129

Supplementary Table 2.2 Bulk translation rates of wild-type and PTC-ring mutant 70S iSAT ribosomes. Bulk translation rates for iSAT ribosomes were determined from protein synthesis kinetics curves, for reactions after 2 h incubations, and normalized to wild-type..... 136

Supplementary Table 2.3 Equations and examples scores for relative activity calculations, and overall mutational flexibility scores. Relative activity was calculated to compare performance of each mutant by normalizing wild-type protein synthesis yields to one and mutant yields to the normalized wild-type yields. An overall mutational flexibility score was then determined for each nucleotide position by adding the relative activities of every possible point mutation. The highest mutational flexibility score of three indicates that all three nucleotide changes possess wild-type activity, while the lowest mutational flexibility score of zero indicates that all three nucleotide changes preclude any protein synthesis. 140

Supplementary Table 2.4 Sucrose gradient fractionation profiles of rRNA PTC mutants. Representative nucleotide mutations were chosen for sucrose gradient fractionation based on their activity. iSAT reactions were separated through sucrose gradients, and fractions were collected. The relative average abundance of rRNA in each fraction was quantified by calculating the area under each curve. 141

Supplementary Table 2.5 PTC-ring nucleotide distances calculated in PyMol. PTC nucleotide distances were calculated from either the A-site or P-site tRNAs. Using the *E. coli* ribosome structure (PDB- 4YBB), we measured the distance between A76 of the A-site and P-site tRNAs and within one angstrom of the geometric center of each PTC nucleotide. 142

Supplementary Table 2.6 A- and P-loop nucleotide distances calculated in PyMol. Distances were calculated from either the A-site or P-site tRNAs. Using the *E. coli* ribosome structure (PDB-4YBB), we measured the distance between A76 of the A-site and P-site tRNAs and within one angstrom of the geometric center of each PTC nucleotide. 143

CHAPTER 3

Figure 3.1 Enabling non-canonical amino acid incorporation requires many parts. 146

Figure 3.2 (a) β-amino acids are attractive building blocks for therapeutic peptidomimetics. These extended backbone monomers are biologically active, mimic natural peptides, and form secondary structure. Additionally, they have structural diversity, evade protease degradation, and can have increased affinity for active sites. (b) β-peptides are currently synthesized with solid phase peptide synthesis (SPPS). 147

Figure 3.3 SDS-PAGE gel of MS2-MBP-His protein expression and purification..... 156

Figure 3.4 A 0.7% agarose gel used to visualize the binding, washing, and elution fractions during the purification of MS2-tagged ribosomes. 157

Figure 3.5 A map of the β-incorporating ribosomal mutations from the Hecht and Schepartz lab. The mutational map is color coded based on high mutational flexibility (green) and low mutational flexibility (red). 159

Figure 3.6 Assessing the functionality of iSAT assembled β-incorporating ribosome mutants. (a) A schematic of the iSAT workflow for synthesizing and studying β-incorporating ribosomes in vitro. (b) Relative protein synthesis titers of wt and β-incorporating ribosomes. (c) Protein synthesis kinetics for wt and β-incorporating ribosomes. 160

Figure 3.7 *In vitro* translation activity of purified MS2-tagged ribosomes and wild-type ribosomes possessing no MS2 stem loop. In both cases, the ribosomes were wild-type in that they do not possess any mutations in the 23S rRNA. 161

Figure 3.8 Assessment of ribosome assembly through sucrose gradient fractionation. Top panel illustrates the fractionation trace possessing the peaks for 30S, 50S, 70S, and polysomes. The large peak for the β-amino acid incorporating ribosomes which is positioned near the wild-type polysome peak, may in fact be a hibernating 100S dimer. The bottom panel represents an RNA agarose gel of select sucrose gradient fractions. 163

Figure 3.9 Testing the incorporation of β-phenylalanine into a short peptide (12 amino acids) using a pre-charged tRNA (charged with flexizyme) and β-incorporating ribosomal mutants. (a) Schematic of the workflow for testing mutant ribosomes for incorporation of ncAAs. (b) the MALDI trace demonstrating no β-phenylalanine incorporation with mutant ribosomes..... 164

Supplementary Table 3.1 Relevant plasmid DNA constructs for MS2-tagged ribosome purification. 165

CHAPTER 4

Figure 4.1 Ribo-T system improvement strategies. (a) Schematic of Ribo-T showing tether (red) and orthogonal ribosome binding site (yellow). (b) The tether is optimized in cells growing exclusively from the Ribo-T plasmid. (c) Previously published Ribo-T tether sequence. (d)

Orthogonal function evolved for Ribo-T. € Previously published orthogonal mRNA (o-mRNA) Shine-Dalgarno (SD) sequence and orthogonal 16S rRNA anti-SD (o-ASD) sequence shown. 169

Figure 4.2 Optimizing tether sequence improves performance. (a) Wild-type 23S rRNA helix 101 and 16S rRNA helix 44 are connected to create Ribo-T with 9A for 5' tether, T1 and 8A for 3' tether, T2. (b) Library 1: paired 5' tether T1 poly A from 7-20 nucleotides, with 3' tether T2 poly T from 7-20 nucleotides. Library 2: unpaired polyA on both T1 and T2, ranging in 7-20 nucleotides long. Library 3: randomized T1 (8N) and T2 (9N) keeping residues of opened H101 and h44 apex loops. Library 4: randomized apex-to-apex T1 (15N) and T2 (10N) of tether. (c) Selection scheme for improved tethers. Strains lacking genomic copies of rRNA operons (Δ7rrn) are transformed with plasmid-based Ribo-T tether libraries, and the wild-type pCSacB plasmid (wt) is removed. (d) Tether sequences and growth rates of analyzed colonies. Error bars = 1SD of noted independent colonies, n. The top 15 Ribo-T design winners (L4-1 through L4-13) were co-cultured and passaged for 3 days. Between each passage, the bulk culture populations were sequenced and analyzed. 173

Figure 4.3 Optimizing tether sequence improves performance. a. Ribo-T v1: previously published tether sequence. Ribo-T v2: fastest growing and most frequent selected tether sequence. b. Growth rate and max OD_{600} of SQ171 slow growing (sg) and SQ171 and fast growing (fg) cells growing with pAM552 (wild-type *rrnb* operon), pRibo-T v1 and pRibo-T v2 (n=6; paired t-test [two-sided], $p<0.05$). Error bars = 1 SD. c. Spot plated SQ171 and SQ171fg cells growing with pAM552, pRibo-T v1 and pRibo-T v2 imaged after 48 hours at 37 °C. d. Total RNA extraction from SQ171 and SQ171fg cells growing with pAM552, pRibo-T v1 and pRibo-T v2. 195

Figure 4.4 Improving orthogonal pairs. Selection scheme to optimize orthogonal Shine-Dalgarno (SD) and anti-Shine-Dalgarno (ASD) pairs in untethered and tethered context. 198

Figure 4.5 Selected orthogonal pair sequences and function in Ribo-T v2. (a) Top evolved orthogonal mRNA and 16S with predicted pairing. Selection round is noted by round 1 or round 2 to the right of each pair. n denotes number of isolated members with that sequence from the selection. (b-e) Orthogonal pair notation: Original orthogonal Ribo-T system denoted by v1, and x.y where x is o16S number and y is o-mRNA letter (pORTx.y plasmid name format). (b) Orthogonal expression of super folder green fluorescent protein (*sf-gfp*) in BL21(DE3)Δupp. + pair: both o-rRNA and o-mRNA expressed, - pair: just o-mRNA expressed without cognate o-rRNA. Percent orthogonality is shown below column labels. A higher percentage value is desired, indicating a lower background expression of o-mRNA as compared to the expression with the cognate orthogonal rRNA. Error bars = 1 SD of n=3 independent experiments. The protein's structure and details are listed to the right of the graph. (c) Orthogonal expression of Cm acetyltransferase (*cat*) in BL21(DE3)Δupp. Error bars = 1 standard error in IC_{50} curve fitting. The protein's structure and details are listed to the right of the graph. (d) Orthogonal expression of *N*-glycosyltransferase of *A. pleuropneumoniae* (*ApNGT*) in BL21(DE3). The protein's structure and details are listed to the right of the graph. (e) Orthogonal expression of Beta-galactosidase (LacZ) in BL21(DE3). The protein's structure and details are listed to the right of the graph. 202

Figure 4.6 Incorporation of ncAA p-azido-L-phenylalanine (pAzF) by orthogonal Ribo-T. (a) Combined rRNA and *sf-gfp* plasmid with *sf-gfp* gene is replaced with a 1TAG or 5TAG version to create pORT3B.gfp1TAG and pORT3B.gfp5TAG (orthogonal Ribo-T with aSD sequence 3 and orthogonal sfGFP message B containing 1 TAG or 5 TAG, respectively). Wild-type *rrnb* operon was cloned as a negative control for background orthogonal expression (pAM.B.gfp1TAG and pAM.B.gfp5TAG). (b) Expression of *sf-gfp* with 1TAG or 5TAG in C321.ΔA derived strain MCJ.1217 (C321.ΔA.mutS^{+}.Δλred.Δupp), in the presence of (+) or absence of (-) pAzF. Error bars = 1 SD of n=6 independent experiments. 207

Supplementary Figure 4.1. Library construction and selection strategy for tether optimization. 210

Supplementary Figure 4.2. Total RNA gel of selected library members. WT: wildtype ribosomes extracted from SQ171 cells with pAM552 plasmid. Sample names are organized as LX-Y; where X is the library number (1-4), and Y is a clone number from that library. 211

Supplementary Figure 4.3 Liquid culture enrichment and competition assay shows Ribo-T v2 as the dominant genotype following multiple generations of growth. The top 15 Ribo-T winners identified were co-cultured in triplicate and passaged for 3 days. Between each passage, the bulk populations from the culture were sequenced and analyzed. 212

Supplementary Figure 4.4 Ribo-T v2 improvements enhance growth of SQ171 and SQ171fg cells in which Ribo-T replaces wild-type ribosomes. Growth curves of (a) SQ171 cells (Error bars = 1 SD; n=5). and (b) SQ171fg cells (Error bars = 1 SD; n=3) transformed with pAM552 DNA (wild-type, black), or Ribo-T v1 (blue) or Ribo-T v2 (green). 213

Supplementary Figure 4.5 Ribo-T v2 enhances cell fitness as compared to Ribo-T v1 when grown on minimal media (M9 casamino acids, M9CA) at various temperatures in different cell backgrounds. (a) Orthogonal and non-orthogonal untethered ribosomes, Ribo-T v1, and Ribo-T v2, were grown in and on M9CA media in a-b. POP cells (n=6-8), c-d. SQ171fg cells (n=5-6), and e-f. SQ171 cells (n=6). Final OD_{600} and doubling times were analyzed. Error bars = 1 SD..... 214

Supplementary Figure 4.6 Chemical probing and prediction of the structure of the Ribo-T v2 linkers. (a) The diagrams represent the structures of helices H101 and h44 in wild-type ribosomes (left), Ribo-T v1 (middle), and Ribo-T v2 (right), with the nucleotide accessible to the dimethyl sulfate (DMS modification indicated by green dots). Highly accessible residues are indicated by brightly-colored dots. (b) The predicted secondary structure formed by the Ribo-T v2 tethers with the nucleotides most accessible for DMS modifications indicated. 215

Supplementary Figure 4.7 Reporter plasmid and ribosome plasmid maps. (a) Reporter plasmid with Ptrp or lpp5 promoter, and chloramphenicol acetyltransferase-uracil phosphoribosyltransferase (*cat-upp*), super folder green fluorescent protein (*sf-gfp*) (reporter plasmid: plpp5.gfp), or *cat* gene (reporter plasmid: plpp5.cat). Plasmid contains kanamycin resistance and p15A origin of replication. (b) Plasmid coding for untethered ribosomal RNA (rRNA) from *rrnb* operon, with either p_L promoter or p_{LT} promoter for orthogonal expression.

Plasmid contains ampicillin resistance gene lactamase, and ColE1 origin of replication. rRNA processing stems (PS) and anti-Shine-Dalgarno (aSD) sites indicated. (c) Plasmid coding for tethered ribosome Ribo-T. 5' tether 1 (T1) and 3' tether 2 (T2), and 23S circular permutation connecting piece C3 noted (plasmid name: pRibo-T vX; where X is either 1 or 2)..... 216

Supplementary Figure 4.8 Combined positive and negative selection scheme for evolving new orthogonal Shine-Dalgarno/anti-Shine-Dalgarno pairs. (a) BL21(DE3)Δupp cells with pPtrp-catupp-p15A and *cat-upp* expressed die in the presence of 5-Fluorouracil. (b) BL21(DE3)Δupp cells with pPtrp-catupp-p15A and *cat-upp* expressed gain resistance to the antibiotic chloramphenicol. Plates shown are representative of at least 3 independent experiments..... 217

Supplementary Figure 4.9 Evolved orthogonal pairs. (a) Activity testing of untethered orthogonal ribosomes and mRNA following first round of positive selection. Controls: pAM552/wt: wild-type SD expression. pAM552o/A, original orthogonal system in untethered context. (b) Selected Shine-Dalgarno (SD) and anti-SD sequences. Round of selection and number of colonies (n) noted for each pair sequence. Orthogonal mRNA SD sequence is labeled with letters, and orthogonal 16S aSD sequence is labeled with numbers. Pair 1A is the previously published orthogonal pair noted as "v1 o-pair" [175]. Error bars = 1 SD for pairs possessing n>1 colonies. 218

Supplementary Figure 4.10 Orthogonal Ribo-T v2 is capable of synthesizing diverse proteins of different sizes, compositions, and functions. (a) Orthogonal expression of *sf-gfp* in BL21 Star (DE3) strain (top panel). Orthogonal expression of *sf-gfp* in C321.ΔA derived strain MCJ.1217 (bottom panel). MCJ1217 (C321.ΔA.mutS^{+}.Δλred.Δupp) is a variant of the fully recoded C321.ΔA strain [178,258], and provides benefits for non-canonical amino acid incorporation using amber suppression. (b) SDS PAGE gels of the expression and purification of non-model proteins. (c) SDS-PAGE expression gel comparison between oRibo-T v1 and oRibo-T v2. oRibo-T v2 had a 37% improved expression level of LacZ (n=3, paired t-test, 2 df) and a 22% improved expression level of ApNGT (n=3, paired t-test, 2 df) over oRibo-T v1. Error bars = 1 SD. Gel is representative of three independent replicates (n=3). (d) The secondary structure maps of each protein..... 219

Supplementary Figure 4.11 (a) Orthogonal pair activity in untethered ribosomes in BL21(DE3)Δupp strain. (b) Orthogonal pair activity in untethered ribosomes in BL21 Star (DE3) and (c) recoded TAG-less strain MCJ.1217 (C321.ΔA.mutS^{+}.Δλred.Δupp). Error bars = 1 SD. 220

Supplementary Figure 4.12 Comparison between original published tether (v1) and improved v2 tether with a) *sf-gfp* and b) *cat* reporters. poRibo-T2 is the original orthogonal Ribo-T as published. poRiboT*x.y* contain v1 tethers and pORT*x.y* contain v2 tethers, where *x* indicates rRNA anti-Shine Dalgarno (ASD) species and *y* indicates the cognate mRNA SD species. The bars with corresponding percent values above each set of data represents the percent improvement of the orthogonal pairs with v2 tethers vs. v1 tethers. Error bars = 1 SD. 221

Supplementary Figure 4.13 Incorporation of non-canonical amino acid p-azidophenylalanine (pAzF) by orthogonal ribosomes. (a) Combined rRNA and sfGFP reporter plasmid system. The orthogonal reporter sfGFP is inserted in the forward (light green) and reverse (dark green) direction

relative to the *rrn* operon. (b) Expression of orthogonal *sf-gfp* from a combined plasmid in POP2136. Representative ribosome constructs include pAM = wild-type untethered ribosomes, pO2 = orthogonal untethered ribosomes possessing optimized aSD sequence 2 (3'-UGGUGU), and pORT3 = orthogonal Ribo-T possessing optimized aSD sequence 3 (3'-GGUGUC). Each construct was combined with the orthogonal sfGFP reporter B (5'-CAACCAC) in the forward (f) or reverse (r) orientation. Fluorescence is normalized by OD_{600} and is the average of at least 3 independent colonies. Error bars = 1 SD. (c) Combined rRNA and *sf-gfp* plasmid with reverse orientation. For amber suppression, the *sf-gfp* gene is replaced with a 1TAG or 5TAG version as noted. (d) Expression of *sf-gfp* with 1TAG or 5TAG in C321.ΔA.mutS^{+}.Δλred.Δupp (MCJ.1217), in the presence of pAzF (+) or absence of pAzF (-). Fluorescence is normalized by OD_{600} and is the average of at least 3 independent colonies. Error bars = 1 SD. 222

Supplementary Table 4.1 Primers used for the construction of Ribo-T tether libraries and gBlocks used in cloning steps. 223

CHAPTER 5

Figure 5.1 (a–d) Modelling (top panels) of tethers (green and magenta strands) that connect 16S and 23S rRNA into a single rRNA, and agarose gel electrophoresis (bottom panels) of RNA extracted from *E. coli* (Squires strain) in which wild-type ribosomes were completely replaced with the designed molecules (top): an early U3 tether (Umbilical 3) designed by the Jewett lab, cleaved into two bands in vivo (a), a stapled ribosomes developed by a separate group (three replicates shown), also cleaved in this plasmid context and strain *in vivo* (b), the successful Ribo-T design developed after a year of manual trial and error to withstand cleavage in vivo (c) and RM-Tether 4, a design automatically generated by RNAMake, which also presents as a single band *in vivo* (d). (e) Sucrose gradient fractionation prepared from in vitro iSAT reactions that express wild-type ribosomes, Ribo-T version 1.0 and RM-Tether 4. Peaks correspond to small subunits (30S), large subunits (50S), monosomes/70S and polysomes (standard assignments of the peaks are given in, for example, Underwood et al.). (f) Agarose electrophoresis analysis confirms that the polysome fraction of **e** is composed of tethered ribosomes. Full gels are given in Figure 5.2. 234

Figure 5.2 Secondary structure comparison and full gels for ribosome tethering studies (a) Secondary structure of 16S helix 44 (h44) and wild-type 23S helix 101 (H101). (b) Published Ribo-T secondary structure. (c) (left) Secondary structure of RM-Tether 4 designed with RNAMake. Each motif is colored as in the 3D structure model (right). (d) Culture density of *E. coli* cells containing RNAMake RM-Tether design 4. (e) Gel assay of 8 distinct colonies, verifying the RNAMake-designed Ribo-T. In one case, lane 4, we observed very faint 16S and 23S-like rRNA bands, possibly reflecting linker cleavage either in the cell or during ribosome isolation. (f) Agarose gel electrophoresis of RNA extracted from E. coli (Squires strain SQ171fg) in which wild type ribosomes were completely replaced with the indicated ribosomes. The double band under

the wild type lane indicates the 16S and 23S rRNA in the two separate subunits of the ribosome. The Ribo-T lane represents the original Ribo-T construct published by Orelle *et al*. The Ribo-T variants (a-d) represent tether variants of Ribo-T (unpublished data from the Jewett lab) that remain tethered, and the stapled ribosomes represent tethers generated from published work by Fried, *et al*. In our system and constructs, stapled tethers do not maintain a single-subunit entity, resulting in a 3-band pattern. (g) U3 tether (Umbilical 3) designed by the Jewett lab, presents as three bands in vivo (last lane). 236

Figure 5.3 MS2 tethered ribosome design, with an MS2 RNA aptamer linking H101 and h44 of the large and small subunits, respectively..... 237

Figure 5.4 Initial MS2-Ribo-T constructs either possessing or lacking linker spacers were tested in the Squires strain. (a) The secondary structure of the MS2-Ribo-T construct with linker spacers that was successful in maintaining the life of the cell. Tether sequences are as follows: T1= TTTGATGAGGAATTACCCATCTTT; T2= TTTGATGAGGATTACCCATCTTTAAA. (b) RNA extraction gel demonstrating that MS2-Ribo-T constructs possessing linker spacers are capable of maintaining their tethered identities after introduction into the Squires strain. 238

Figure 5.5 The impact of MS2 tether composition on doubling time. (a) RNA gels of the various MS2-Ribo-T constructs. (b) Growth curves of the MS2-Ribo-T constructs as well as wild-type and Ribo-T controls. (c)..... 240

Figure 5.6 (a) Doubling time characterization of MS2-Ribo-T library members; and (b) RNA gel confirmation of tethered identities in living Squires strain *E. coli* cells. 241

Supplementary Table 5.1 Ribosome tether primers for pRibo-T template. 244

Supplementary Table 5.2 Ribosome tether sequences from RNAMake. 245

Supplementary Table 5.3 Tether designs that were designed, built, and characterized in the Squires strain. 263

Supplementary Figure 5.1 All 9 RNAMake RM-Tether designs, colored according to the motifs that were used to generate it, helices (gray), small subunit (orange), and large subunit (blue).. 264

CHAPTER 6

Figure 6.1 Using SHAPE-Seq in combination with iSAT ribosome synthesis or orthogonal tethered ribosomes (Ribo-T) will enhance our understanding of structure and function relationships within RNA designs and the ribosome. 268

Figure 6.2 Schematics of the various translation factors that could be used in ribosome and translation engineering. Titrating in these factors may help elucidate basic biology of their structural and functional impacts in translation, while also aiding the improved incorporation of ncAAs. 269

CHAPTER 1
The *Escherichia coli* ribosome: Engineered ribosomes for basic science and synthetic biology

The work presented in this chapter is based upon work published in:

d'Aquino, A. E.; Kim, D. S.; Jewett, M. C. Engineered Ribosomes for Basic Science and Synthetic Biology. *Annu. Rev. Chem. Biomol. Eng*. **2018**, *9*, 311–340. DOI: 10.1146/annurev-chembioeng-060817-084129

1.1 Introduction

The ribosome is a ribonucleoprotein machine, comprised of RNA and proteins. In all kingdoms of life, the ribosome is made up of one large and one small subunit. In bacteria, these correspond to the 50S large subunit and the 30S small subunit. The large 50S subunit of the *Escherichia coli* ribosome is comprised of 33 ribosomal proteins (r-proteins), the 23S ribosomal RNA (rRNA), and the 5S rRNA. The corresponding small 30S subunit is comprised of 21 r-proteins and the 16S rRNA [1].

One can think of the ribosome as the catalytic workhorse of the cell, since it carries out the polymerization of α-amino acids into polypeptides called proteins. To achieve this function, the ribosome has several tasks. These tasks include accommodating aminoacyl-transfer RNA (aa-tRNA) monomers, decoding mRNAs, catalyzing polypeptide synthesis, and excreting polypeptides [2]. The shape, physiochemical, and dynamic properties of the ribosome have been evolutionarily optimized to polymerize ~20 different canonical amino acids. With protein elongation rates of up to 20 amino acids per second in bacteria [3] at an error rate of approximately 1 in 10,000 [4], the extraordinary synthetic capability of the protein biosynthesis system has driven extensive efforts to harness it for societal needs in areas as diverse as energy, materials, and medicine. For example, recombinant protein production has transformed the lives of millions of people through the synthesis of biopharmaceuticals like insulin and industrial enzymes like subtilisin. In nature, however, only limited sets of protein monomers are utilized, thereby resulting in limited sets of biopolymers (i.e., proteins). Expanding nature's repertoire of ribosomal monomers could yield new classes of enzymes, therapeutics, materials, and chemicals with diverse genetically encoded chemistry. For instance, sequence-defined polypeptides made of protease-

resistant monomers (D-, β-amino acids) could lead to antimicrobial drugs that combat rising antibacterial resistance. Such sequence-defined molecules have never been synthesized before. Yet, their synthesis would redefine biomanufacturing and become a major driver of global innovation and economic growth.

Unfortunately, expanding the range of genetically encoded chemistry into proteins presents a complex and formidable challenge for many reasons. One of the main challenges is that modifying the ribosome is a systems-level challenge. This is because many factors are involved in protein synthesis that must be tuned (Figure 1.1). These factors include: (i) aminoacyl-tRNA synthetases (aaRSs) which covalently link amino acid monomers with their cognate transfer RNA (tRNA) delivery vehicles, (ii) aminoacyl-transfer RNA (aa-tRNA) monomers that decode codons, and (iii) elongation factor Tu (EF-Tu) which delivers a correctly activated monomer (aminoacyl-tRNA) to the ribosome, and also serves as a gateway to ensure sequence fidelity. Another challenging constraint is that the ribosome is required for life, which restricts the mutations that can be made to ribosomes. In practice, these constraints have made the natural ribosome essentially un-evolvable and, so far, there has not been a generalizable method for designing and modifying the ribosome to work with substrates beyond those found in nature. Despite these challenges, new tools are emerging to derive general paradigms for engineering translation systems for basic science and advanced applications.

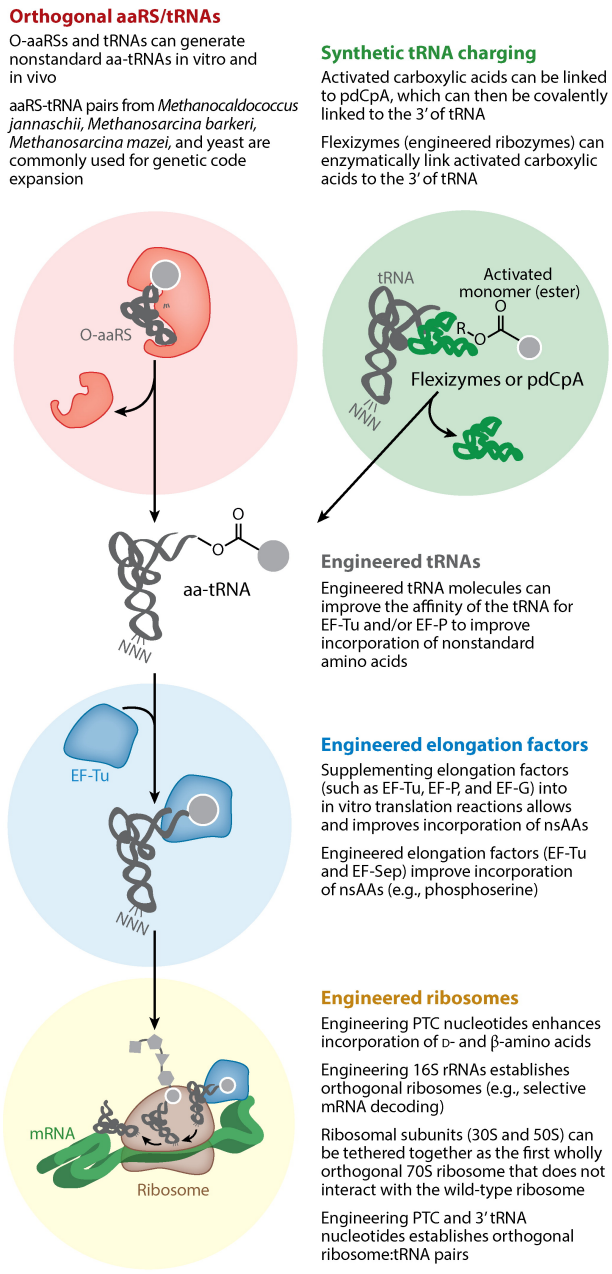

Figure 1.1 Ribosome engineering in context: protein translation in a cell. Free transfer RNAs (tRNAs) are charged (aminoacylated) with amino acids by the aminoacyl-tRNA synthetase (aaRS). Aminoacyl-tRNA molecules can also be generated *in vitro* using Flexizymes of pdCpA. Next, the aminoacyl-tRNA molecule is delivered to the ribosome by elongation factor Tu (EF-Tu). The tRNA, whose anticodon loop corresponds to a messenger RNA (mRNA) codon, delivers the amino acid to the ribosome, where it is polymerized into a protein. Abbreviations: nsAA, nonstandard amino acid; PTC, peptidyl transferase center.

In this chapter, the growing body of work on the design and engineering of bacterial ribosomes is summarized, with a focus on *E. coli*, for applications in both basic and synthetic biology research. Four key categories in ribosome design and engineering are reviewed: (i) understanding the parts and pieces of the ribosome and the translation system, (ii) designer ribosomes for basic biology, (iii) designer ribosomes for synthetic biology, and (iv) the progress, prospects, and challenges of designing and engineering ribosomes. Along the way, the numerous methodologies that have been developed to advance ribosome engineering are summarized. Finally, this chapter highlights how ribosome engineering can impact fields as diverse as materials, energy, and medicine and end with future outlooks on the field.

1.2 The ribosome's parts

To design and engineer a machine as complex as the ribosome for novel purposes, it is critical to first understand the various functional moieties. From the structural and interwoven proteins, to the subsequent RNA helices and loops, to the active site of the machine, identifying and characterizing the pieces at play before manipulating them is a critical requirement. Below is a summary of the key ribosomal parts whose understanding will facilitate engineering and design.

1.2.1 Nucleic acids of the ribosome: Structure and Function

The bacterial ribosome has three rRNAs. The three rRNAs that constitute the *E. coli* ribosome (5S, 16S, and 23S) are necessary for ribosomal structure and function (Figure 1.2). Noller and colleagues solved the sequences of the DNA genes encoding the 16S, 23S, and 5S rRNAs, establishing a foundation in our molecular understanding of rRNA molecules [5-7]. After the discovery of catalytic RNA [8,9], biochemical evidence proposing the role of 23S RNA in peptidyl transferase [10], and finally, a high-resolution crystal structure of the 50S subunit [11], the ribosome

was declared a ribozyme which catalyzes peptide bond formation via an RNA-based mechanism. Additionally, Steitz and colleagues established that no protein moiety resides within several angstroms of the PTC, confirming RNA catalysis [11].

Of the three rRNAs, the 5S rRNA, which is approximately 120 nucleotides in length, is arguably the least understood. The 5S rRNA resides on almost all ribosomes, with the exception of some fungal mitochondrial ribosomes, higher animals, and certain protists [12] (Figure 1.2). Structurally, this rRNA molecule can bind proteins and other molecules, suggesting that it is involved with and connected to several translation elements. Functionally, it has been proposed that the 5S rRNA interacts with key domains of the ribosome, including domain V containing the active site, and GTPase-associated domains [13]. Although many studies have been carried out to characterize this molecule, details surrounding its activity and specific mechanism are still unclear. As described in Section V of this review, there still remains future work to understand this ribosomal component.

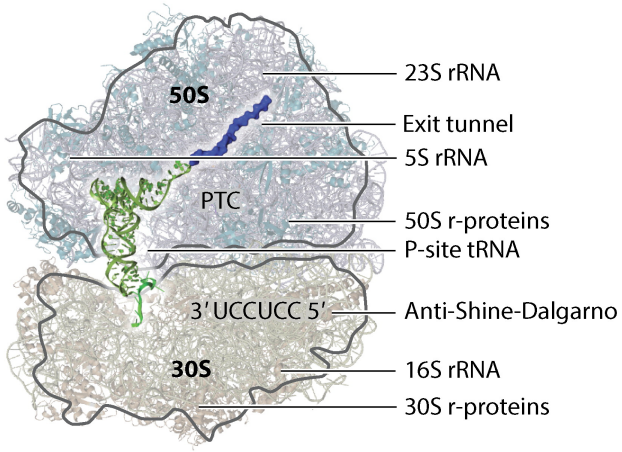

Figure 1.2 Map of the ribosome's parts. The ribosome is a complex machine composed of numerous parts. Some of the integral parts are mapped here. These include 3 different ribosomal RNA (rRNA) molecules (5S rRNA and 23S rRNA in the large subunit are depicted in grey, and 16S rRNA in the small subunit is depicted in wheat); ribosomal proteins (r-proteins) (the 33 large

subunit r-proteins are depicted in teal, and the 21 small subunit r-proteins are depicted in orange); the catalytic peptidyl transferase center (PTC); the A-, P-, and E-sites; and the anti-Shine-Dalgarno sequence for decoding. Figure rendered using PyMol and PDB ID 4V5H.

The 16S rRNA makes up the small (30S) subunit (Figure 1.2) and is involved in early and intermediate steps of translation including translation initiation and decoding. During translation initiation, the 3' end of the 16S rRNA (the anti-Shine-Dalgarno sequence, as discussed in the following subsections) base pairs with a purine-rich element of messenger RNA (the Shine-Dalgarno sequence), which is positioned upstream of the start codon [14]. Importantly, the 16S rRNA also interacts with initiation factors (IF), impacting the kinetics of translation initiation [15]. Regarding translation decoding, the 16S rRNA possesses the site of codon-anticodon interactions, wherein 16S nucleotides G530, A1492, and A1493 effectively stabilize base pairing formed between tRNA anticodons and the mRNA [16]. Methyl-modifications and mutations to 16S rRNA modulate and impact translation fidelity and kinetics [17].

The 23S rRNA makes up the 50S subunit, which is responsible for accommodation, peptidyl transferase, and protein excretion. Biochemical studies and crystal structures of the ribosome have shown that many of these key activities are mediated through specific nucleotides within the 23S rRNA (Figure 1.2). Over the past approximately two decades, crystal structures have played an increasing role in our understanding of how the ribosome works, especially the peptidyl transferase center (PTC). The groundbreaking high-resolution crystal structures were solved using a small molecule which mimics the tetrahedral intermediate in peptide bond formation and inhibits peptidyl transferase activity [11,18]. In these studies, the structures elegantly illustrated that the ribosome specifically positions the 3' terminus CCA ends (which is acylated to amino acids) of the A- and P-site tRNAs via interactions with the 23S rRNA at highly conserved

A- and P-loops, respectively [11]. The structure also suggests that rRNA residues stabilize the intermediate state of the tRNA-peptide complex. Additionally, the authors' structure implies involvement of two key nucleotides in peptide bond formation: A2451 and G2447. Steitz and colleagues found that the N3 of nucleotide A2451 resides in closest proximity (3 Å) to the peptide bond being synthesized, thus playing a key role in monomer positioning for translation elongation[11].

The insights gained regarding rRNAs have had significant impacts on both basic biology and engineering. Understanding the significance of the three rRNAs in the synthesis of proteins has resulted in growing research interest to manipulate and design parts of this rRNA for purification and novel functions. With the plethora of rRNA knowledge in hand, we can now begin to imagine engineering these rRNA components. Because sequence defines structure, and structure defines function, we can begin from our knowledge of rRNA sequences to understand how we might design rRNA with new functions. In the following discussion of the next section, I aim to describe in more detail the remaining parts of the ribosome and their mechanisms of action.

1.2.2 The polypeptides of the ribosome: Ribosomal proteins

The *E. coli* ribosome contains 54 ribosomal proteins (r-proteins) that are synthesized in cells under tight regulation to ensure stoichiometric expression [19]. The small 30S subunit contains 21 r-proteins, while the 50S subunit contains 33 r-proteins [1]. Ribosomal proteins play essential, and sometimes mysterious, roles in ribosome assembly and function. These proteins have attracted the attention of both basic and synthetic biologists who are interested not only in understanding their function in translation, but also leveraging our understanding for novel purposes.

The functions of r-proteins range from structural support, to mRNA decoding, to chaperone and cofactor binding, and to catalytic activity near the PTC [20]. Mutations in r-proteins have been shown to convey resistance to antibiotics through direct and indirect disruption of antibiotic binding sites [21,22], but the precise roles of all proteins in translation have yet to be fully elucidated. Although we know that protein synthesis is catalyzed by rRNA, it has been demonstrated that this catalytic activity still requires certain r-proteins [23]. Conversely, while the *E. coli* ribosome is said to include 54 r-proteins, ribosomal mutants have been found that lack certain ribosomal proteins, and gene knockout studies have illustrated that 22 r-proteins can be individually deleted from the *E. coli* genome without lethality [24,25]. Work from Noller and colleagues has suggested a minimum number of macromolecules required for peptidyl transferase, specifically the 23S rRNA and r-proteins L2 and L3 [26]. L2 and L3 are near the PTC in the assembled ribosome [27-29]. Additionally, Schulze, Nierhaus and Mankin demonstrated via single-omission tests that L2, L3, and L4 are essential for peptidyl transferase activity [30,31].

Knowledge gained from ribosomal protein studies have helped demystify their contributions to protein translation, ribosome assembly, antibiotic resistance, and more. With this knowledge in hand, many scientists have begun utilizing these proteins for purification, tagging, dynamics studies, and reconstitution. Section 1.3 of this thesis, titled Engineered ribosomes for advancing basic biology, further elaborates on this progress. Next we discuss the components of the ribosome involved in translation initiation, monomer accommodation, peptide elongation, and peptide release.

1.2.3 The site of translation initiation: Shine-Dalgarno and Anti-Shine-Dalgarno sequences

In bacteria, one mechanism through which open reading frames in mRNAs are recognized and translated by ribosomes includes the interaction of two complementary sequences: the Shine-Dalgarno (SD) and anti-Shine-Dalgarno (aSD) sequences. Translation initiation and translation efficiency are both controlled by these sequences [32]. The Shine-Dalgarno (SD) sequence is found approximately 8 bases upstream from the start codon in *E. coli* mRNA sequences. Its complementary anti-Shine-Dalgarno (aSD) sequence is part of the highly conserved 3' end of the small subunit 16S rRNA [14] (Figure 1.2). The SD sequence in the mRNA interacts with the aSD region of the 16S rRNA such that the mRNA-rRNA base pairing facilitates the initiation of protein translation and synthesis.

Extensive work has been carried out to support, define, and characterize the SD-aSD interactions. Recently, the anti-Shine-Dalgarno sequence interaction and its functional role in regulating translation efficiency was characterized. By analyzing data from experiments measuring translation activity across different SD-aSD pairs, Hockenberry and co-workers found that translation efficiency is maximized for sequences with intermediate aSD binding strengths [33]. Additionally, numerous publications have demonstrated that mutations altering mRNA sequence complementarity and binding have significant impacts on translation efficiency and ability [34-36]. Finally, complete substitution of the SD sequence with a non-SD sequence was demonstrated to completely abolish mRNA translation [37].

1.2.4 The ribosome's catalytic peptidyl transferase center: A-, P-, and E-Sites

Following translation initiation via the SD-aSD sequences, protein translation enters the elongation phase. During elongation, both the incoming amino acid and the nascent peptide are simultaneously bound to tRNA molecules within the ribosome's active site (Figure 1.2). There

exist three binding sites for tRNA molecules in the ribosome. These sites include: the A-site, which accepts the incoming aminoacyl-tRNA (aa-tRNA), the P-site, which holds the elongating peptidyl chain attached to tRNA (peptidyl-tRNA), and the E-site, through which the deacylated tRNA exits the ribosome. These three binding sites account for the codon-anticodon (mRNA-tRNA) interaction, the precise arrangement of tRNA acceptor and donor arms during peptide bond formation, and the successive movement, or translocation, of mRNA relative to the ribosome [10].

In the first step of translation, aa-tRNA is delivered to the A-site of the ribosome as a complex with elongation factor Tu (EF-Tu) and GTP. The tRNA anticodon associates with the complementary codon in the 30S A-site, while the aminoacyl acceptor end (CCA) remains bound to EF-Tu. The codon-anticodon pairing and binding instigates a conformational change in EF-Tu, subsequently leading to GTP hydrolysis. This hydrolysis triggers EF-Tu to dissociate from the ribosome, releasing the aminoacyl end of the tRNA molecule to fully enter the A-site of the large 50S subunit. This process is known as accommodation [38].

This accommodated aa-tRNA quickly undergoes the peptidyl transferase reaction. In the first step of the reaction, the A- and P-site tRNA molecule acceptor arms are arranged in the 50S subunit through interactions with 23S rRNA nucleotides [39]. Specifically, the CCA end (which carries the amino acid) of the P-site tRNA is base paired to G2251, G2252, and G2583 while the A-site tRNA CCA end is base paired to G2553 and A2450 (*E. coli* numbering). During this reaction, peptide bond formation takes place via the transfer of the growing peptidyl group from the CCA terminus of the P-site tRNA to the aminoacyl group attached to the CCA terminus of the A-site tRNA [38]. This reaction is facilitated through interactions with conserved 23S rRNA bases located at the center of the PTC: A2451, U2506, U2585, C2452, and A2602 [11].

Finally, the now empty tRNA that previously resided in the P-site translocates to the E-site where it will subsequently exit the ribosome; and the A-site tRNA, esterified to the growing peptide chain, translocates to the P-site. The E-site, although still not fully understood, contributes significantly to the fidelity and process of translation. Importantly, the E-site maintains the reading frame of the ribosome, permitting faithful translation of genetic information. Having a tRNA molecule in the E-site prevents loss of the ribosome's reading frame [40]. The results of these structural biology breakthroughs have provided biochemists, engineers, and synthetic biologists with the foundation to probe the role of PTC nucleotides.

Each of the parts of the ribosome can be thought of as components of a machine. These components work harmoniously in a rhythmic dance, performing the task of decoding, synthesizing, and excreting the proteins of the cell. In the following sections, we discuss how the ribosome's parts have been designed and engineered for a better understanding of their roles in the overall process of translation, and furthermore, how these parts can be repurposed for novel functions.

1.3 Engineered ribosomes for advancing basic biology

Learning by building is a powerful approach for probing fundamental biological processes. These insights into basic biology permit the efficient engineering of these machines for novel purposes. From understanding how the ribosome assembles, to how it decodes, accepts, and processes tRNAs charged with amino acids, to the intricacies in how it dynamically rotates and moves -- understanding how the ribosome functions represents basic biology discoveries which also embody subtle but significant engineering feats.

1.3.1 Reconstructing the ribosome from its parts: Ribosome reconstitution

Structure, function, and assembly studies of the ribosome have been greatly facilitated by reconstitution of both the large and small subunits. These advances have defined necessary components, elucidated key ribosomal mechanisms, and facilitated the construction of minimal cell systems.

The *E. coli* 30S ribosomal subunit was the first to be reconstituted. In 1968, Traub and Nomura demonstrated that a mixture of the 30S ribosomal proteins (TP30) could be reconstituted with 16S ribosomal RNA (rRNA) to form fully functional 30S subunits [41]. This conventional 30S subunit reconstitution protocol involves a one-step incubation at 20mM Mg2+ and 40°C [41]. In 1999, Culver and Noller improved the reconstitution of the small subunit substantially, alleviating challenges in cost, time, resources, and cross contamination associated with traditional reconstitution. They developed an ordered assembly protocol that allowed efficient reconstitution of 30S subunits using the purified recombinant proteins. Their reconstitution method represented the first means for exhaustive mutational analysis of each ribosomal protein of the small subunit [42]. More recently, Maki and Culver showed that 30S assembly can be facilitated at lower temperatures by chaperones [43].

The reconstitution and assembly of the large 50S subunit was not elucidated until after the 30S subunit. Due to the increased number of ribosomal proteins (33) and larger size of rRNA (the 23S rRNA is 2904 nts and the 5S rRNA is 120 nts), bottom-up 50S assembly was significantly more complex compared to the small subunit, and was first achieved by Nierhaus in 1974 [44], and extended in years that followed [45]. The conventional 50S subunit reconstitution protocol involves a non-physiological two-step high temperature incubation, first at 4mM Mg2+ and 44°C, then at

20mM Mg2+ and 50°C. Total reconstitution of the 50S subunit with an in vitro transcribed 23S rRNA was later carried out by Green and Noller [46].

While studies using the conventional reconstitution approach with *E. coli* ribosomes have revealed much of today's knowledge regarding the assembly of the ribosomal subunits from the deconstruction and reconstitution procedures described above [47-49], inefficiencies in reconstitution make the construction and analysis of engineered variants difficult [50]. For example, conventionally reconstituted 50S subunits made with in vitro transcribed 23S rRNA (lacking the naturally occurring post-transcriptional modifications) are up to 10,000 times less efficient in reconstitution than those using mature 23S rRNA as measured by the fragment reaction, where single peptide bonds are formed on isolated 50S subunits [50]. Furthermore, the non-physiological two-step conditions for 50S assembly preclude coupling of ribosome synthesis and assembly in a single integrated system.

To overcome limitations in conventional reconstitutions, Jewett and coworkers developed the integrated synthesis, assembly, and translation (iSAT) method that enables efficient one-pot co-activation of rRNA transcription and processing, assembly of rRNA with native ribosomal proteins (TP70) into *E. coli* ribosomes, and synthesis of functional proteins from assembled ribosomes in a S150 crude cell extract lacking native ribosomes (Figure 1.3) [51]. This work is significant because it is the first demonstration that rRNA from any organism has been co-synthesized and assembled into functional ribosomes in a single compartment in vitro. A novel feature of iSAT is that it mimics co-transcription of rRNA and ribosome assembly as it occurs in cells. iSAT activity has been improved >1000-fold by optimizing extract preparation methods, tuning rRNA transcription levels, alleviating substrate limitations, and using macromolecular

crowding and reducing agents [51-53]. Another key feature of this system is the ability to generate rRNA variants by simply changing the rDNA input; making it an attractive platform for probing the ribosome in vitro and engineering modified ribosomes. Indeed, the concept, carried out in a purified translation system, was recently extended to evolving the 16S rRNA.

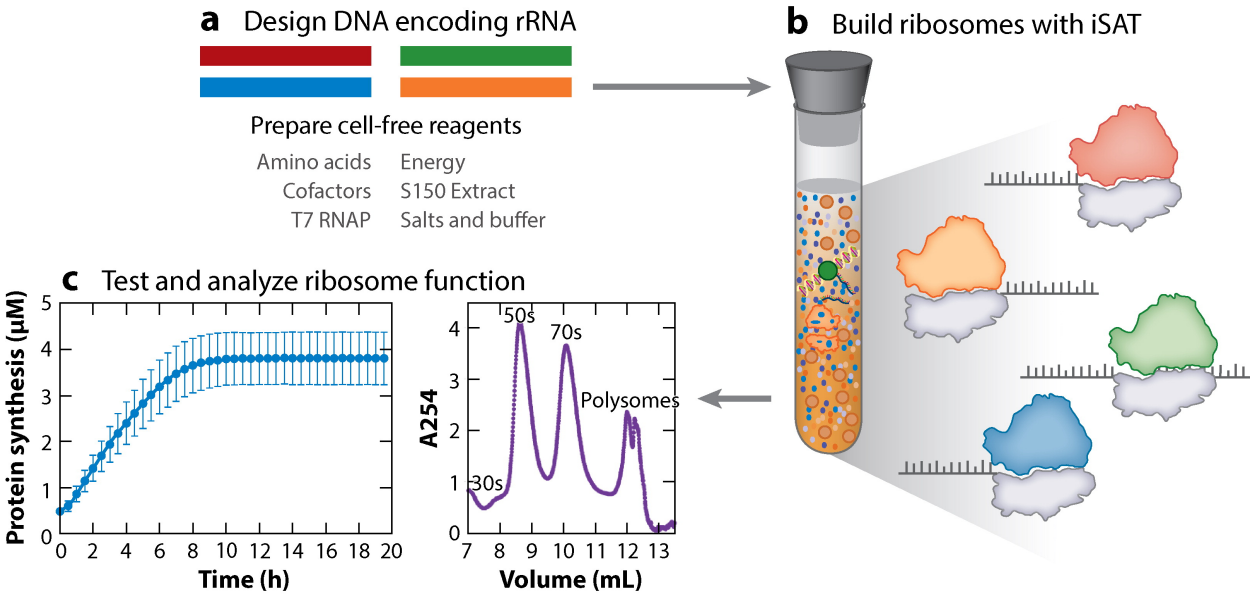

Figure 1.3 In vitro synthesis, assembly, and translation (iSAT) for ribosome design and engineering. (a) The iSAT method enables efficient one-pot co-activation of ribosomal RNA (rRNA) transcription, (b) assembly of rRNA with native ribosomal proteins into *Escherichia coli* ribosomes, and (c) synthesis and analysis of functional proteins from these ribosomes in a S150 extract lacking native ribosomes. This purely *in vitro* strategy for *E. coli* ribosome construction offers a powerful technique to study and exploit engineered ribosomes.

Beyond engineering the ribosome, the in vitro construction of ribosomes is a topic of rapidly growing interest in systems and synthetic biology for designing and building minimal cells to understand the origins of life [54,55]. The idea is that one could enable self-replication by pooling together essential purified biological macromolecules, their genes and their small molecule substrates. Towards this goal, researchers in the Church lab reported on the construction of

functional *E. coli* 30S ribosomal subunits using a defined, purified cell free system lacking ribosomes (PURE Δribosome system) under physiological conditions [56]. Using this system, the authors achieved high engineering flexibility, effectively permitting the screening and testing of ribosome biogenesis factors and assembly cofactors, and their impacts on and functions in ribosome assembly [57]. Importantly, their method was used to demonstrate that 30S ribosomes can be constructed solely from in vitro synthesized 30S r-proteins and in vitro transcribed 16S rRNA. Their small subunits assembled from in vitro synthesized parts resulted in ribosomes with 17% activity as compared to wild type ribosomes. Additionally, the authors further demonstrated the synthesis of 50S r-proteins and the co-synthesis of 30S and 50S r-proteins in the PURE system. Thus, their integrated method can potentially be applied to construct fully synthetic ribosomes, endowing even greater control over finely probing various parts of the ribosome.

Traditional and engineered ribosome reconstitution efforts described above have been highly impactful on the ribosome field. Indeed, the ability to deconstruct and reconstruct the ribosome precisely defines its parts and functional moieties, which is crucial in future efforts to engineer it for novel purposes. Importantly, it changed the perspective with which scientists and engineers viewed the ribosome, from a black-box macromolecular machine to a precise machine with well-defined parts. In the text that follows, further efforts to probe and understand those parts are described.

1.3.2 Probing the ribosome's active site

The PTC is the active site of the ribosome. It resides in Domain V of the 23S rRNA in the large 50S subunit and is comprised solely of rRNA. The PTC is the site of peptide bond formation,

tRNA positioning, peptide stalling, and antibiotic binding. This catalytic core holds many key functions, and has been studied using biochemistry, genetics, structural biology, and engineering.

Many labs have studied the PTC and its role in translation using crystallography and structural studies, chemical crosslinking and foot printing, as well as genetics. These techniques represent the most established methods for probing the PTC and its role in peptide bond formation. Groundbreaking bacterial ribosome structures provided the first suggestions into the role of rRNA in translation [11]. Pioneering work from the lab of Dr. Harry Noller implicated important contacts between the tRNA and nucleotides in both the large and small subunit rRNAs [58,59]. Other classical techniques for probing the PTC include puromycin assays, translation fidelity assays, NMR, ribosome foot printing, and sucrose gradient fractionation. Notably, engineering efforts in basic biology have probed the PTC through mutational studies. In 2006, Sato and coworkers carried out a comprehensive genetic selection revealing essential nucleotides in the peptidyl-transferase center [60]. Specifically, they leveraged systematic selection of functional sequences by enforced replacement (SSER) wherein they generated randomized rRNA libraries of critical regions in and around the PTC and then introduced these into *E. coli* cells. This study resulted in elucidation of essential bases within the PTC. However, like many mutational studies of the active site, dominant lethal phenotypes prevented complete mutational characterization. Toxic mutation sequences that did not produce transformants in vivo were not further investigated. Studies of these lethal mutations are critical though, as they improve our understanding of the ribosome and antibiotic resistance, and open doors to engineering efforts. For example, in their 2007 paper, Yassin and Mankin leveraged deleterious mutations in the large ribosomal subunit to identify potential antibiotic binding sites [61].

All the works described above have helped us gain insight into how the ribosome catalyzes peptide bond formation, translocation, and peptide release. In Table 1.1, a non-comprehensive list has been assembled outlining the 23S rRNA active site nucleotides studied, how they were studied, and their proposed roles in translation. Basic biology studies of the PTC have been invaluable, however, investigations into the ribosome's PTC have so far been limited, primarily due to the dominant lethal phenotype of many mutants as described above. Dominant growth defects caused by mutations in the ribosome can preclude identification of mutants that confer desired functions. In Sections IV and V, we discuss more avenues for filling this gap in knowledge and facilitating engineering of the ribosome's active site. Below, we describe three important techniques for studying ribosome function, which have been crucial for enabling studies of rRNA mutants.

Table 1.1 Proposed roles of select 23S rRNA nucleotides in translation.

rRNA nucleotide	**Proposed role in translation**	**Reference**
A2451	• First proposed to be involved in peptide bond formation. Crystal structures show that it is closest (3 Å) to the peptide bond being catalyzed. • Studies demonstrate that all base changes confer dominant lethal phenotype. • Proposed to be involved in peptide release based on kinetic studies • Proposed to stabilize the ordered structure of the PTC	• Nissen, P., et al. 2000. Science 289: 920-30 • Thompson, J., et al. 2001. PNAS 98(16): 9002-9007 • Youngman, et al. 2004. Cell. 117(5): 589-599
G2447	• Proposed involvement in peptide bond formation. Believed to render catalytic properties to A2451. • G2447A and G2447C maintain cell viability. G2447A synthesizes protein at rates similar to WT.	• Nissen, P., et al. 2000. Science 289: 920-30 • Thompson, J., et al. 2001. PNAS 98(16): 9002-9007

G2251, G2252, and G2583	• Base pairs with P-site tRNA to position tRNA acceptor arms.	• Nissen et al, 2000
G2253 and A2450	• Base pairs with A-site tRNA to position tRNA acceptor arms.	• Nissen et al, 2000
A2451, U2506, U2585, C2452, and A2602	• Proposed to be involved in peptide bond formation, based on crystal structure. • A2451, U2506, U2585, and A2602 proposed to be involved in peptide release based on kinetic studies. • Release factors may promote conformational rearrangements of U2585 to promote peptide release.	• Nissen et al, 2000 • Youngman, et al. 2004. Cell. 117(5): 589-599 • Schmeing et al. 2005. Nature. 438(7067): 520-4
C2394	• Contacts E-site tRNA. C2394G impacts ribosome's ability to bind deacylated tRNA to the E- and P/E-sites, and reduces translation fidelity.	• Schmeing, T.M., et al. 2003. RNA 9:1345-52; • Moazed, D., and Noller, H.F. Cell 57:585-97
G2112 and G2116	• Contacts E-site tRNA.	• Schmeing, T.M., et al. 2003. RNA 9:1345-52; • Moazed, D., and Noller, H.F. Cell 57:585-97
G2655	• Part of the sarcin-ricin loop (SRL) which interacts with and binds EF-G. • G2655C is lethal in vivo. Ribosomes carrying the G2655C mutation are defective in EF-G driven translocation.	• Leonov, et al. 2003. JBC. 278, 25664-25670.
A2450 and C2063	• Proposed to form an A-C wobble base pair essential for tRNA translocation.	• Chirkova, et al. 2010. NAR. 38(14): 4844-4855

C2063, A2451, U2506, and A2602	• Proposed (based on crystal structure) to surround the GGQ motif of RF2 during translation termination and peptide release. • Mutational studies of A2602 suggest that this nucleotide is most essential for hydrolysis.	• Petry et al. 2005. Cell. 123:1255-1266 • Youngman, et al. 2004. Cell. 117(5): 589-599 • Polacek et al. 2003. Cell. 11(1): 103-12
C2573 and A2572	• Mutations do not impact aa-tRNA accommodation, peptide bond formation, or fidelity of aa-tRNA selection. The mutations do impair RF2-catalyzed peptide release.	•
A2058 and A2059	• Mutations A2058G and A2059G confer resistance to macrolides such as clindamycin and erythromycin.	• Sigmund, C., and Morgan, E. 1982. PNAS. 79: 5602-6.
G2057	• G2057A confers low-level resistance to erythromycin in *E. coli*.	• Ettayebi, M., Prasad, S.M., and Morgan, E.A. J Bacteriol. 1985. 162(2): 551-557.
A2062	• A2062G confers clindamycin resistance in E. coli and macrolide resistance in other bacteria.	• Cochella & Green. PNAS. 2004. 101(11): 3786-3791.
A2503	• Located at the start of the exit tunnel. • Involved in nascent-peptide recognition and ribosome stalling. • Only A2503G is viable, all other mutations are dominant lethal.	• Vazquez-Laslop, N., et al. 2010. EMBO J. 29(18): 3108-17.
U2609	• U2609C mutation renders E. coli cells resistant to two ketolides: telithromycin and ABT-773.	• Garza-Ramos, G., et al. 2001. J Bacteriol. 183(23): 6898-6907.

1.3.3 Specializing the ribosome

To overcome the dominant lethality problem, de Boer and colleagues pioneered a specialized ribosome system using orthogonal Shine-Dalgarno (SD) sequences in specific reporter protein mRNAs that target orthogonal anti-SD sequences in 16S rRNA (Figure 1.4) [62]. The authors accomplished this by altering the SD sequence preceding the human growth factor gene from 5' GGAGG (wt) to 5' CCTCC or 5' GTGTG. In doing this, these modified mRNAs could not be recognized and translated by wild type bacterial ribosomes. However, upon changing the aSD region in the 3' end of the 16S rRNA gene from 5' CCTCC (wt) to 5' GGAGG or 5' CACAC, they could restore Watson-Crick base-pairing between the complementary sequences and achieve significant expression of the human growth factor. This groundbreaking work not only opened the door to numerous basic biology studies, but importantly, also initiated in vivo ribosome engineering efforts to be discussed below.

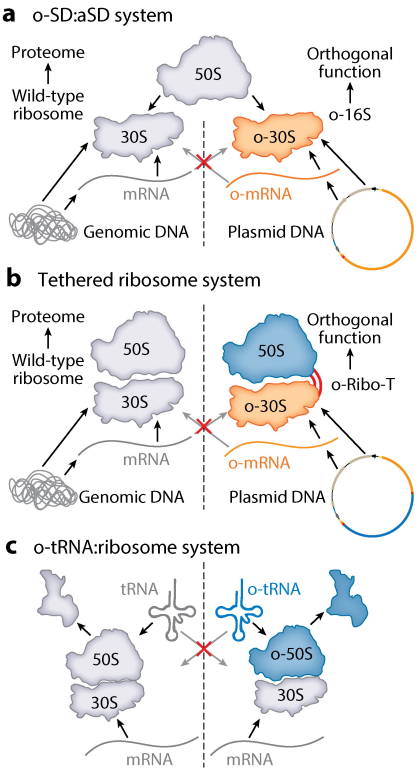

Figure 1.4 Orthogonal ribosomes. (a) For an orthogonal Shine-Dalgarno:anti-Shine-Dalgarno (o-SD:aSD) system, tuning of the SD sequence of the mRNA in conjunction with the aSD sequence of the 16S rRNA allows for orthogonal message decoding. Of note, the 50S subunit is not orthogonal and freely associates with both wild-type and orthogonal 30S subunits. (b) in the tethered ribosome system, the entire ribosome, including the catalytic 50S subunit, is orthogonal and does not interfere with the wild-type ribosomes. (c) In the orthogonal transfer RNA (tRNA):ribosome system, tuning the interaction between the 3' tRNA sequence and the ribosome's 23S rRNA establishes orthogonality to wild-type tRNAs and wild-type 23S rRNAs. Abbreviation: o-mRNA, orthogonal messenger RNA.

1.3.4 Isolating the ribosome by affinity purification

As noted above, a purely in vitro strategy for ribosome construction offers a powerful solution for studying and exploiting engineered ribosomes. With the development of ribosome assembly and reconstitution, as well as high interest in ribosome mutational studies, researchers have become interested in an efficient, easy, and high-throughput method for purifying the bacterial ribosome. Particularly challenging aspects have been mutations in the rRNA of the PTC,

which often confer dominant lethal phenotypes in *E. coli*. This makes it prohibitively difficult to synthesize and express pure populations of mutant ribosomes. Often, researchers have resorted to expressing mixed populations of mutant and wild type ribosomes, and subsequently parsed out the "noise" contributed by wild type ribosomes. Recently, however, three approaches to selectively tag and purify mutant ribosomes from a mixed population have been developed.

In 2003, Leonov and coworkers [63] developed a method based on site-directed incorporation of a streptavidin binding tag into functionally neutral sites of the large subunit 23S rRNA. Using this tag, they successfully leveraged affinity chromatography to isolate ribosomes carrying a lethal G2655C mutation. The authors then utilized this technique to further demonstrate that G2655C plays a key role in interacting with EF-G in tRNA translocation in the ribosome. Youngman et al. described the use of another affinity-tagging system for the purification of mutant ribosomes [64]. In their work, they inserted a 17 nucleotide RNA hairpin that binds the MS2 phage coat protein into the terminal loop of *E. coli* 23S rRNA helix 98 (Figure 1.5). Using their purification system, they isolated and analyzed four universally conserved nucleotides in the PTC: A2451, U2506, U2585, and A2602. Using kinetic analyses, the authors found that each of these mutant ribosomes possesses defects in peptide release, suggesting that these nucleotides are intimately involved in peptide release but not in peptide bond formation. Similarly, Hesselein and coworkers leveraged a U1A protein-binding tag inserted onto the 23S rRNA to probe the conserved A2450+C2063 wobble pair within the PTC. Another example of ribosome purification came in 2009, when Ederth and coworkers developed a novel strain of *E. coli* (JE28) by fusing the nucleotide sequence encoding a hexa-histidine affinity tag at the 3′-end of the single copy *rplL* gene (encoding the large subunit ribosomal protein L12) in the *E. coli* MG1655 strain. The JE28 strain produces a

homogeneous population of ribosomes with a (His)6-tag at the C-termini of all four L12 proteins. Additionally, the authors developed and optimized a high-throughput method for a single-step purification of tetra-(hexa-His)-tagged 70S ribosomes from this strain using affinity chromatography. The authors further describe how this method can be adapted for purification of ribosomal subunits and mutant ribosomes [65].

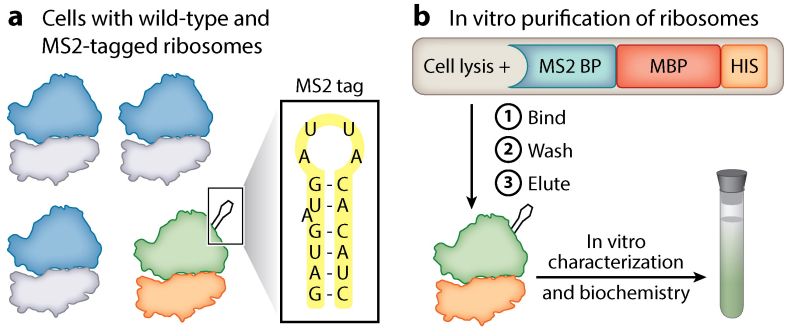

Figure 1.5 Cartoon depiction of the MS2 ribosome purification technique. (a) A 17-nucleotide RNA hairpin that binds the MS2 phage coat protein is engineered into the terminal loop of *Escherichia coli* 23S rRNA helix 98. (b) upon lysin cells possessing the tagged ribosomes, binding the ribosomes to an affinity matrix, washing, and eluting, purified MS2-tagged ribosomes can be characterized and studied.

Developments in ribosome purification and isolation have allowed studies into mutant ribosomes, defining the role of key rRNA nucleotides in translation. Future efforts to understand the impact of ribosomal mutations, and develop multiply-mutated ribosomes for novel purposes will undoubtedly leverage these techniques to isolate and probe new modified machines.

1.3.5 Developing and using the Squires strain

As described above, many studies on ribosomal structure and function have been carried out on the *E. coli* ribosome in vitro, which have enabled precise, well-controlled findings on ribosome structure and function. Verification of these findings in vivo, enable further insight into ribosome function in a cell, but can be hindered by the presence of wild type ribosomes. In 1999,

Asai and coworkers successfully developed an *E. coli* strain (Δ7 prrn) commonly referred to as the Squires Strain, in which all seven chromosomal rRNA operons were deleted, and all rRNA was transcribed from a single plasmid-based rRNA operon [66]. The plasmid containing the rRNA operon can be swapped with another plasmid coding for a variant rRNA operon, thereby allowing isolated studies of a rRNA variant (Figure 1.6). This strain has enabled studying of the basic biology of engineered ribosomes *in vivo*.

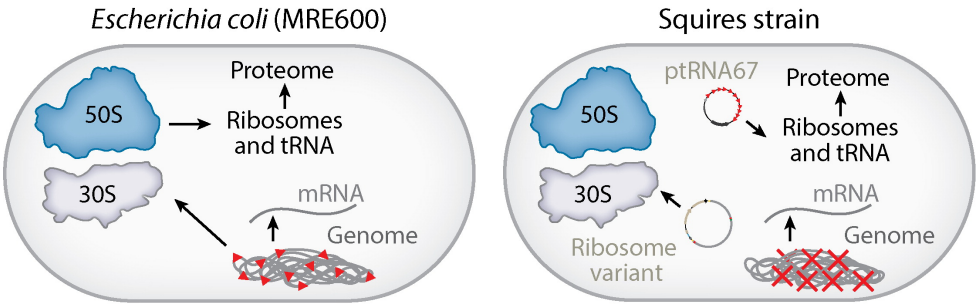

Figure 1.6 The Squires strain. The Squires strain is an experimental system that can be used for studying and engineering ribosomes. In traditional Escherichia coli strains (such as MRE600), ribosomal RNA (rRNA) genes are highly repeated on the genome (red triangles). Ribosomes are synthesized based on seven genomic copies of the ribosomal operon. In the Squires strain, all seven chromosomal rRNA operons are deleted. A single E. coli rRNA operon carried by a multicopy plasmid (ptRNA67) supplies 16S rRNA and 23S rRNA to the cell. Using this strain, ribosome variants can be introduced into the Squires strain cells, and ptRNA67 removed. This permits the in vivo study of ribosome variants without the contamination of endogenous wild-type ribosomes. Abbreviation: mRNA, messenger RNA.

In one example, Vazquez-Laslop et al. leveraged this strain to study mutations of A2503 in the 23S rRNA. Specifically, the authors demonstrated that of the three possible mutations, only A2503G was capable of supporting cell growth in the absence of wild type ribosomes [67]. Additionally, Sahu and coworkers utilized this strain to study the functional replacement of two highly conserved tetraloops in the bacterial ribosome. Using this strain, the authors estimated the frequency of missense error and nonsense error read-through, in addition to assessing whether mutated ribosomes could sustain the life of the cell [68]. Furthermore, Burakovsky and coworkers

studied ribosome accommodation gate mutations using the Δ7 prrn strain. The authors designed a variety of mutations at C2573 and A2572 and found that mutations at these positions did not impact aa-tRNA accommodation, peptide bond formation, or the fidelity of aa-tRNA selection. However, the mutations did impair RF2-catalyzed peptide release [69].

The results of these studies, and many more, in the Squires strain demonstrate that it is indeed possible and important to assess the impacts of ribosome design and engineering in the context of the cell. The Squires strain has been invaluable in synthetic biology research, as described in the sections below.

In summary, advances in basic biology have unlocked fundamental knowledge and developed tools for manipulating the ribosome. Synthetic biology, a burgeoning field of research, has been able to leverage these advances to develop new translation systems that address societal and scientific needs. In the following sections, advances and efforts in synthetic biology to design and engineering the ribosome are described and summarized.

1.4 Engineered ribosomes for synthetic biology

The precise and robust nature of the translation apparatus has attracted significant efforts to engineer it for compelling applications in energy, medicine, and materials [70-75]. For example, establishing novel message-reading capabilities of the ribosome could result in the ability to run orthogonal genetic programs inside a living cell [76,77] as well as expansion of the genetic code beyond the canonical triplet codon-anticodon model [78] or even the canonical 4-base code [79]. Given this promise, recent efforts to expand and enhance the function of the ribosome for synthetic biology applications have produced important milestones in ribosome engineering at an

accelerated pace. Below, we examine the ribosome and protein translation machinery that have been engineered for applications in synthetic biology (Figure 1.1).

1.4.1 Engineered ribosome-associated translation machinery

Pioneering works have opened the possibility to overcome the sparse chemical space afforded by natural translation. These pioneering efforts have shown site-specific incorporation of more than 150 non-standard α-amino acids (nsAAs) into proteins using an engineered translation apparatus to generate biological insights and new applications [80-82]. The natural ribosome is also capable of producing polymers with non-peptide backbones (*e.g.,* polyesters) [83-85], and has even incorporated select exotic monomers [85-94]. Photocaged [95], fluorescent [96], and bioorthogonally reactive [97,98] monomers have provided new ways to study protein structure, dynamics, and post-translational modifications [80,99-109]. Further, the generation of proteins with non-natural chemistry has enabled the synthesis of novel therapeutics [102-104,110,111] and genetically-encoded materials [101,112-114]. As a result of these impressive efforts, expanding the genetic code has emerged as a major opportunity in synthetic and chemical biology [99,115-117].

Given the ribosome's flexibility in accommodating the ~20 different standard amino acid functional groups found in nature, the bulk of initial efforts in engineering the translation apparatus have focused on the three peripheral machines involved in translation: tRNAs, aminoacyl-tRNA synthetases, and elongation factors [118,119]. The key need is to prepare aminoacyl-tRNA substrates that can be polymerized by the ribosome bearing the nsAAs. This has been done using protein and RNA based enzymes. Often, the ability to generate nsAA-tRNA monomers is achieved by evolving orthogonal aminoacyl-tRNA synthetase (aaRS)::orthogonal tRNA pairs. These "orthogonal" translation components do not recognize natural amino acids or cross-react with

native translational machinery, yet can deliver nsAA-tRNA monomers to the ribosome. To achieve this task, synthetic biologists frequently use the *Methanocaldococcus jannaschii* tyrosyl synthetase, *Methanosarcina barkeri /Methanosarcina mazei* pyrrolysyl synthetases, and the yeast tryptophanyl synthetase. In such efforts, the substrate preference of the amino acid binding pocket of an aminoacyl-tRNA synthetase is modified, and thereby generates a novel, orthogonal aminoacyl-tRNA molecule for incorporation into a protein. In one illustrative example, Amiram et al. used a multiplex automated genome engineering (MAGE) strategy [120,121] to generate highly selective and orthogonal aaRS/tRNA pairs that enhance the insertion of nsAAs into proteins in vivo [122]. Guided by the three dimensional crystal structures, the authors simultaneously varied 12 residues surrounding the amino acid side chain binding pocket and five residues at the aaRS-$tRNA_{CUA}$ anticodon interface to generate $>10^9$ variants [122]. From this library, they isolated aaRS variants with up to 17- (*p*-acetyl phenylalanine: pAcF-m4) and 25-fold (*p*-azido phenylalanine: pAzF-m4) higher activity than either progenitor enzyme. Importantly, library diversity can be modified by increasing the number of MAGE cycles, changing the mutagenic ssDNA pool, targeting different aaRS regions, or changing the conditions applied during negative selection, without the need for plasmid reconstruction and retransformation and loss of library diversity. Such efforts hold promise for future work in improving translation machinery outside of the ribosome for genetic code expansion.

As an alternative approach, Flexizymes can also be used to generate novel aminoacyl-tRNA molecules. Flexizymes are synthetic RNA molecules with catalytic capabilities (thereby classifying them as ribozymes), capable of acylating tRNA molecules with an activated amino acid monomer [123-126]. This system requires activation of the monomer with a leaving group, such as

cyano-methyl ester, dibenzyl ester, or chlorobenzyl thioester, and tolerates a large diversity of side chains and backbones of amino acid monomers being acylated onto the tRNA. Flexizymes recognize the 3' end of a tRNA molecule (R-CCA-3', where R is a G or an A depending on the tRNA), and acylate the terminal 3' A with the activated monomer, forming the aminoacyl-tRNA molecule. Interestingly, it can also act on activated monomers with alternate backbones, such as β-, D-, and N-alkyl amino acids, as well as hydroxy-acids. This technology is less synthetically laborious than traditional chemical ligation with an activated nucleotide (pdCpA), and has been shown to enable incorporation of many different nonstandard monomers into sequence-defined polymers. The Suga group has been instrumental in developing, implementing, and advancing Flexizyme technology, and has so far developed three kinds of Flexizymes (aFx, dFx, eFx). Furthermore, the Suga lab has demonstrated the synthesis of peptides containing α-L-nonstandard-, β-, D-, N-methyl-, N-acyl-, and N-alkyl-amino acids as well as synthesis of sequence-defined polyesters [127-135], allowing researchers to stretch the bounds of possible substrates that can be used by the ribosome.

Beyond engineering the process of loading amino acids onto tRNAs, recent work has been carried out to study, understand, and engineer the tRNA molecule itself to facilitate non-standard amino acid incorporation at single and multiple positions. In their 2017 paper, Katoh et al. engineered the D-arm and T-stem of tRNA to enhance D-amino acid incorporation [136]. Specifically, they leveraged their previous basic science breakthroughs to rationally design an optimal tRNA. In their first set of prior work, Katoh and coworkers demonstrated that the T-stem sequence on aminoacyl-tRNAs modulates strength of interactions with EF-Tu, which can in turn be exploited to improve incorporation of non-standard amino acids [134]. In their second

breakthrough, a collaborative effort between the Suga and Rodnina labs demonstrated that translation factor EF-P alleviates ribosomal stalling through recognition of a D-arm motif found in $tRNA^{Pro}$ [137]. EF-P effectively accelerates peptidyl transfer when a proline is being processed. Based on these two discoveries, Katoh and coworkers logically engineered tRNAs' D-arm and T-stem sequences to improve consecutive incorporation of D-amino acids as well as an α-disubstituted amino acid. The chimeric tRNA possessed the T-stem of $tRNA^{GluE2}$, which was previously shown to have a higher binding affinity to EF-Tu, and the D-arm of $tRNA^{Pro1}$. As a result of this engineering, the authors successfully synthesized two macrocyclic peptides possessing four and five consecutive D-amino acids.

1.4.2 Limitations of wild-type ribosomes for genetic code expansion

Despite the fact that many types of monomers can be incorporated into a growing polymer chain by the ribosome, incorporation of backbone-modified monomers has been shown to be very limited in the total peptide length and efficiency. Backbone-modified β- or D-amino acids face a challenge in the ribosome, specifically in the ribosome's catalytic active site and nascent peptide exit tunnel [134,138]. In certain cases, such as the naturally modified amino acid phosphoserine, engineered elongation factors (EF-Sep) have been shown to aid the ribosome during the polymerization reaction for inefficiently accommodated substrates. For example, engineering of EF-Sep and the tRNA body have improved the binding and delivery of phosphoseryl-tRNA to the ribosome [139], hence enhancing incorporation of phosphoserine into proteins.

Modifying non-ribosomal factors involved in translation has been shown to aid in incorporation of challenging unique monomers as well. Proline, one of the naturally occurring amino acids, has been known to stall the ribosome [140]. The presence of EF-P, a specialized

elongation factor, effectively alleviates the stalling caused by stretches of amino acid sequences containing this monomer [141,142]. The pyrrolidine side chain present in proline presents a steric deviation from the other 19 amino acids, as the α-amino group is relatively displaced. Because the ribosome is hypothesized to catalyze peptide bond formation through careful positioning of the reactive moieties in the PTC [143] and the consequential lowering of the entropy of peptide bond formation [144], the spatial deviation as observed in proline processing has been observed to stall the ribosome. Proline-driven stalling of the ribosome may hint at the fact that the ribosome is sensitive to the backbone geometry of the monomer substrate, which has been useful for alleviating ribosome stalling with backbone modified nsAA.

In 2016, Suga and colleagues demonstrated that supplementing elongation factors (EF-G and EF-Tu) into in vitro translation reactions helps alleviate ribosome stalling, thus allowing multiple consecutive incorporations of D-amino acids by the ribosome [134,137]. However, such approaches may face a fundamental limit in accommodation of the ribosome active site. For this reason, engineering the ribosome may represent a key target for expanding such monomers in the future. In the following section, we discuss examples of ribosome engineering efforts for expanding the genetic code and the chemistry of life.

1.4.3 Engineering the ribosome's active site

The fundamental limits of the chemistry that the ribosome can carry out are currently unknown, but based on recent work from Englander and colleagues highlighting the discrimination of the PTC towards D-amino acids [138], utilization of exotic monomers (*e.g.,* β-, D-, or γ–amino acids) by the wild type ribosome may be limited. Ribosome engineering may address this key limitation. Recent work by the Hecht and Schepartz groups mutagenized key residues in the

ribosome's active site known to be involved, at least spatially, in peptide bond formation between the P-site and A-site monomer-tRNA molecules [118,145-147]. Using puromycin screening, mutant sequences of the 23S rRNA that include residues 2057-2063 and 2492-2507 were isolated (Figure 1.7). Such mutant ribosomes have been isolated and demonstrated to increase incorporation of D- and β-amino acids, both in vitro and in vivo [118,145-147]. However, the isolated mutant ribosomes alone have not been shown to incorporate multiple, or consecutive residues of backbone-modified monomers. Multiple, consecutive incorporation may trigger stalling of the ribosome that is not alleviated by the currently isolated mutant ribosomes, providing a challenge for the future. In addition, mutant ribosomes have only been identified for D- and β-amino acid incorporation, each with distinct 23S rRNA sequences. It may be possible that there is no "holy grail" sequence of a mutant 23S rRNA that permits incorporation of all backbone modified monomers, but rather, each exotic monomer is best incorporated by a specific mutant ribosome. In this case, efforts in ribosome engineering should be applicable towards a variety of exotic monomers, given the evidence that each exotic monomer may require a distinct mutant ribosome for polymerization.

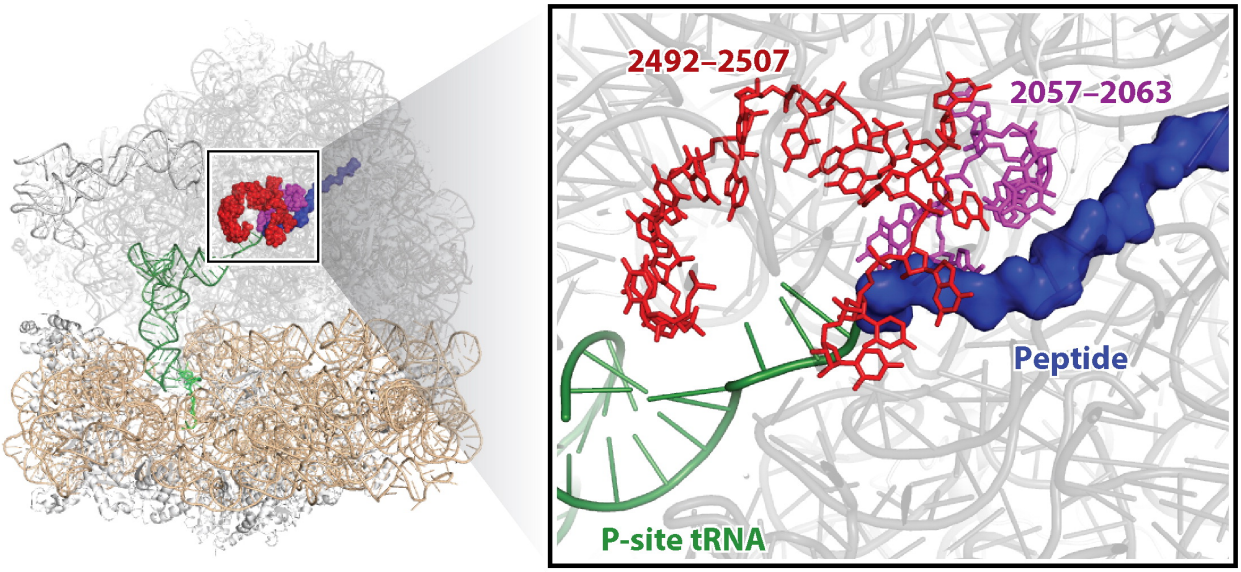

Figure 1.7 23S ribosomal RNA (rRNA) residues in the peptidyl transferase center engineered for new chemistries. Featured in work by both the Hecht and Schepartz groups, key residues in the 23S rRNA (2057-2063 and 2492-2507) are highlighted in magenta and red, respectively. The rest of the 23S rRNA and 16S rRNA are shown in gray and wheat, respectively. These key residues were selected for mutation based on their role in peptide bond formation and their vicinity to the 3' end of both the A-site tRNA and P-site tRNA (green) which carries the activated amino acid monomer for polymerization. The messenger RNA (mRNA) is shown in lime for reference, near the bottom of the tRNAs.

Efforts to engineer the ribosome's active site for novel functions remain one of the most complex challenges faced by synthetic biologists, and the lessons learned from such efforts including fundamental knowledge, novel function, and experimental techniques, can be leveraged to design and engineer parts of the ribosome beyond the PTC. Below, we describe a different approach to repurpose the ribosome, primarily in establishing orthogonal translation systems with orthogonal ribosomes. Orthogonal ribosomes may hold the key to accelerating ribosome design and engineering efforts as well as unlocking new functions in ribosomes.

1.4.4 Orthogonal ribosomes: message decoding, tRNA interactions, subunit tethering

Expanding the decoding and catalytic capabilities of the ribosome is often at the expense of diminishing its endogenous function in protein synthesis. To bypass this limitation, recent developments in cells have focused on the creation of specialized ribosome systems. The concept is to create an independent, or orthogonal, translation system within the cell while wild-type ribosomes continue to synthesize genome-encoded proteins to ensure cell viability and productivity. The orthogonal ribosome is thus excluded from the production of the endogenous polypeptides and ideally exclusively translates only specific, targeted mRNA(s). Therefore, the orthogonal translation apparatus can be engineered to carry out new functions, even if such modifications may negatively affect the operation of the orthogonal ribosome in normal translation.

Initial efforts focused on the small 30S subunit of the bacterial ribosome. The small subunit is primarily responsible for decoding the mRNA message [14]. As mentioned above, by modifying the SD sequence of an mRNA and the corresponding aSD sequence in 16S rRNA, it is possible to create specialized ribosomes capable of translating only a specific kind of engineered mRNAs, while simultaneously excluding them from translating endogenous cellular mRNAs. In recent years, efforts from the Chin lab have extended and improved the approach pioneered by Hui and deBoer in several important ways. For example, by testing various combinations of bases that comprise the SD (on the mRNA) and the aSD (on the 16S rRNA) sequences, Rackham and colleagues identified new pairs of SD-aSD sequences that enable robust orthogonal translation (Figure 1.4) [77]. Specifically, the authors identified orthogonal SD (oSD) sequences by randomizing the -13 to -7 positions in the mRNA, and subjected this randomized library to negative selection,

such that any oSD sequences translated by wild type ribosomes were eliminated. With the remaining sequences, a plasmid coding for the 16S rRNA was introduced, with randomization of eight nucleotides, including the aSD sequence, that are hypothesized to play a role in ribosome-mRNA interactions. Specifically, nucleotides 722, 723, and 1536-1541 of the 16S rRNA (*E. coli* ribosome numbering) were selected. In a positive selection, the gene for chloramphenicol acetyl transferase (CAT) coupled with each oSD sequence, and variants of the 16S rRNA library best able to translate CAT and therefore survive, were selected and identified. These identified pairs of orthogonal SD:aSD sequences were instrumental in subsequent work evolving the ribosome for message decoding capabilities, such as more efficient incorporation of nonstandard amino acids at UAG stop codons [148] and decoding quadruplet codons [78]. Building upon orthogonal pairs of SD:aSD sequences, Chubiz and colleagues computationally identified additional oSD:oaSD pairs [149]. The work is based on the hypothesis that SD:aSD interactions are primarily driven by thermodynamics (Watson-Crick pairing), and best-functioning orthogonal SD-aSD sequence pairs would be less energetically favored to interact with the wild type SD-aSD sequences while being favored to interact with each other.

Until two years ago, such techniques have been limited to the 30S small subunit because the 50S large subunits freely exchange between pools of native and orthogonal 30S subunits. This has previously constrained the engineering potential of the large subunit. However, a significant advance in orthogonal ribosomes came with the advent of tethered ribosomes, in which the bipartite design of ribosomes conserved in all of nature was re-conceptualized through the linking of the 16S and 23S rRNAs into a hybrid chimera [150]. These ribosomes with tethered 50S and 30S subunits (termed Ribo-T) are capable of successfully carrying out protein synthesis. The

construction of Ribo-T is based on identifying all viable circular permutants of the 23S rRNA in the Squires strain. Through this effort, new 5' and 3' ends of functional 23S rRNA constructs were identified. This identification was key because the native 5' and 3' ends of the 23S rRNA are not spatially close to the 16S rRNA 5' and 3' ends according to known crystal structures of the ribosome. After identification of functional circular permutants, helix H101 of the 23S rRNA and helix h44 of the 16S rRNA were identified as possible targets for tethering the rRNAs together. After optimization of the RNA linker, referred to as the tether, Ribo-T was shown to successfully conduct protein synthesis, and even support cell growth in the Squires strain. This represented, for the first time, a completely *in vivo* orthogonal ribosome where both subunits are isolated from the wild type ribosome population [150]. Importantly, Ribo-T can operate both as an o-mRNA decoding ribosome that works alongside a wild type population or as a wild type mRNA decoding ribosome that can meet cellular demands for sustaining life (Figure 4). When operating as an orthogonal ribosome, the catalytically active 50S subunit is sequestered and isolated from the wild type ribosome population, and therefore can harbor dominant lethal mutations in the 23S rRNA that were not possible in the previous state-of-the-art orthogonal ribosome system. Ribo-T offers an exciting opportunity for ribosome engineering, as it enables in vivo engineering of different parts of the ribosome, namely the peptidyl transferase center, free from cell viability constraints. Subsequent to the development Ribo-T, Fried and colleagues described the development of a "stapled" ribosome [151], which also featured conjoined ribosomal subunits at H101 and h44. The stapled ribosome was demonstrated to be capable of orthogonal message decoding, but was not shown to be capable of supporting life.

While the orthogonal Ribo-T–mRNA system opens new opportunities for engineering ribosomes in vivo, in vitro systems still offer potential advantages to precisely control the reaction environment in a manner that may allow for the isolation of certain mutant ribosomes not possible in cells. For example, Teresaka and colleagues engineered the interaction between tRNA molecules and the 23S rRNA in the ribosomal 50S subunit to establish orthogonal tRNA-ribosome pairs [152]. In this work, the authors identified key residues in the tRNA 3' end (C74 and C75) that interact with the peptidyl transferase center of the ribosome's 23S rRNA to deliver the aminoacyl-tRNA monomer. The corresponding residues in the 23S rRNA (G2251, G2252, and G2553) were mutated and pairs of tRNA-ribosome variants were tested for peptide synthesis activity. Through screening, the double 23S rRNA mutant (G2251C/G2553C) and double mutant tRNA (CGA 3' end, deviated from wild type CCA 3' end) were identified as orthogonal to wild type ribosomes and tRNAs, but active in translating when both the mutant ribosome and mutant tRNA are present (Figure 1.4). Of note, many aminoacyl-tRNA synthetases, responsible for generating the aminoacyl-tRNA monomer required for protein synthesis, recognize and require the CCA 3' end of cognate tRNAs, and therefore this work is currently limited to Flexizyme-charged tRNAs for use in in vitro translation systems.

Taken together, recent works in orthogonal ribosomes have pushed the boundaries of ribosome engineering to new heights. It establishes targeted populations of ribosomes for engineering that can operate in parallel with the cell's native ribosomes, and thereby carry out functions that supplement or are completely separate from the synthesis of natural proteins. We can imagine such populations of ribosomes can be engineered further and further away from natural functions, towards human-defined functions.

In summary, ribosome design and ribosome engineering efforts for the advancing synthetic biology have opened new doors for exploring poorly understood functions of the ribosome (*e.g.,* antibiotic resistance mechanisms), enabling orthogonal genetic systems, and engineering ribosomes with altered chemical properties. These advancements are built upon knowledge and techniques from basic biology, and in turn can develop tools and insights for elucidating fundamental mechanisms of the ribosome. We expect basic and synthetic biology to become increasingly complimentary and believe ribosome design and engineering is a research area keenly positioned for these advancements.

1.5 Perspectives, conclusions, and outlook

This thesis chapter provides a broad examination of the innovations in our understanding, design, and engineering of the ribosome. The findings, systems, tools, and techniques described provide an overview of the current state of ribosome engineering but are not completely comprehensive. Below, we highlight future challenges and opportunities on the horizon.

One key challenge is the ability to effectively and efficiently evolve ribosomes for new functions. This challenge is further exacerbated by cell viability constraints, especially in efforts to redesign and reshape parts of the ribosome critical to protein synthesis activity, such as the peptidyl transferase center. Improvements and innovations in in vivo and in vitro ribosome evolution platforms will provide scientists and engineers with unprecedented tools to understand how this machine has evolved, while providing a platform for rapidly evolving novel ribosomes.

Second, current tools in RNA modeling and computational design are not yet capable of "designing" a ribosome de novo, given the complexity of the ribosome's structure and assembly.

Advancements in such tools, as well as freely available online resources (Table 1.2), would allow engineers to rationally design and repurpose the ribosome. The combined efforts of basic, synthetic, and computational biologists would permit the rapid and efficient identification of rRNA targets, and the subsequent engineering of those targets.

Table 1.2 Freely available online tools, software, and resources for aiding ribosome design and engineering efforts.

Resource	Description and potential use
The Center for Molecular Biology of RNA: RNA Center Software	• A freely available center for RNA software • Possesses databases, tools for editing and manipulating rRNA secondary structure, plugins for working with ribosome crystal structure files, and links to software for producing sequence logos of RNA sequences
RiboKit (Das Lab, Stanford University)	• PyMol commands for various RNA manipulation tools • RiboVis: a set of useful and short Python functions for rendering RNA and proteins in PyMol • RNAMake: a toolkit for designing and optimizing RNA 3D structure. Allows the alignment between RNA motifs. • BIERS: Best Inference Engine for RNA Structure
RNAstructure: webservers for RNA secondary structure prediction	• DuplexFold: predicts the lowest free energy structure for two interacting sequences, not allowing intramolecular base pairs • AllSub: Generates all possible low free energy structures for a nucleic acid sequence

	• Bifold: predicts the lowest free energy structure for two interacting sequencing, allowing intramolecular base pairs
PDB	• A free archive containing structures of ribosomes (as well as other proteins, nucleic acids, and complex assemblies).
Ribosome Binding Site Calculator (Salis Lab, Pennsylvania State University)	• Predicts the translation initiation rates of natural bacterial mRNA sequences (validated in many bacterial hosts) and designs synthetic ribosome binding sites for targeted translation initiation rates.
RiboVision (Georgia Institute of Technology)	• Ribosome information viewer, including domain/helix definitions, protein contacts, base pairing, and sequence conservation. • Archive of rRNA secondary structures annotated with precomputed data such as domain/helix labels, possible contacts, and conservation. • Pending update to RiboZones, comprehensive suite of ribosome tools and datasets.
Comparative RNA Website (CRW, University of Texas at Austin)	• Collection of RNA data sets, focusing in comparative analysis (structure models, sequence alignment, etc). • Contains significant metadata on rRNAs yet to be analyzed in detail.
Silva: high quality ribosomal RNA database (Denmark)	• Large database of rRNA sequences (both prokaryotic and eukaryotic) • Both curated/annotated and raw data. • Tools for phylogenetic analysis of ribosomal RNA sequences, including graphically oriented software (ARB).

Another opportunity for investigation lies in the understanding and engineering of the 5S rRNA. As mentioned above, there are still many uncertainties surrounding this molecule. What

exactly is the role of this molecule, and why might it be required for translation? Why has the ribosome evolved to have this small and separate rRNA? Engineering efforts carried out with this molecule may reveal the role of this rRNA in translation, and polypeptide synthesis.

Broadly, we need to continue to build our toolkit. We lack complete characterization of translation machines. For instance, if one's goal is to incorporate a nsAA with specific characteristics (*i.e.*, long flexible backbone, mirror image monomer, specific pKa, etc); what parts should be used to incorporate the monomer into a growing peptide? Which synthetase should be used? Should chemical ligation or Flexizymes be leveraged? We have useful parts and pieces, but they still require characterization (Table 1.3). Thus, these questions remain unanswered, and a thorough characterization of the parts and how or when they are to be used will provide a translation machinery toolkit for basic and synthetic biologists.

Table 1.3 Summary of translation apparatus parts, pieces and tools for incorporating various nonstandard monomers.

Part / Piece / Tool	Description and use
Engineered tRNAs	• Designated orthogonal tRNA for acylation with nonstandard monomer. Should not interact with cellular tRNAs and aaRSs. • Often paired with orthogonal aaRSs from M. jannaschii, M. barkeri, M. mazei, or the mutated yeast tryptophanyl-tRNA synthetase. • $tRNA^{GluE2}$ has been demonstrated to possess a high affinity for EF-Tu, and thus improve incorporation of D-amino acids. • A chimeric tRNA bearing the D-arm of $tRNA^{Pro1}$, and the T-stem of $tRNA^{GluE2}$ has been used to further improve incorporation of multiple D-amino acids.
Engineered aaRS	• Specifically acylate orthogonal tRNAs with a nonstandard amino acid.

	• The tyrosyl-tRNA (*Methanocaldococcus jannaschii*), pyrrolysyl-tRNA (*Methanosarcina barkeri/ Methanosarcina mazei*) and yeast phenylalanyl-tRNA synthetases have been popular starting points for engineering. • Works both in vivo and in vitro.
Flexizymes	• Ribozymes capable of charging tRNAs with monomers containing a carboxylic acid moiety. • Does not require primary amine moiety, capable of charging non-amino acids onto tRNA. • tRNAs are charged with Flexizymes in vitro, then supplemented into translation reactions (genetic code reprogramming) • Enabled incorporation of hydroxy acids, β-amino acids, D-amino acids, N-acyl/N-methyl/N-alkyl amino acids, and nonstandard α-amino acids
pdCpA	• Activated nucleotide that can be used in chemoenzymatic synthesis of nonstandard monomer-tRNAs. • Attached to nonstandard monomer in synthetic in vitro reaction, then ligated to 3' end of tRNA using ligase enzyme.
EF-Tu/EF-Sep/EF-G/EF-P	• EF-Tu with an altered amino acid binding pocket allows for site-specific incorporation of selenocysteine (Sec) into proteins at the UAG codon. • EF-Sep is an engineered EF-Tu with an amino acid binding pocket specific to phosphoserine, and allows direct incorporation of phosphoserine into proteins. • EF-G is proposed to play a crucial role in tRNA translocation in the ribosome and polypeptide elongation, and supplementing EF-G to in vitro translation reactions have been shown to enable consecutive and improved incorporation of D-amino acids into proteins. • EF-P has been used to incorporate multiple D-amino acids into proteins. When used with a tRNA molecule bearing the D-arm of $tRNA^{Pro1}$, D-amino acid incorporation is improved.
Orthogonal SD:aSD pairs	• Engineering the 16S rRNA's aSD and the corresponding mRNA SD sequence makes possible orthogonal translation, where the orthogonal ribosome selectively translates orthogonal mRNAs. • Orthogonal 30S subunits enable selective engineering of ribosome demonstrating improved amber suppression and quadruplet codon decoding for nonstandard amino acid incorporation.

Tethered ribosomes	• Tethered ribosomes (Ribo-T) link the 23S rRNA and 16S rRNA through RNA tethers, forming a chimeric 16S/23S rRNA-based ribosome. • This for the first time establishes orthogonal ribosomes, where message decoding and peptide bond formation is sequestered from the wild-type ribosome population. • Makes possible in vivo engineering of both small and large subunits of ribosomes without being hindered by cell viability constraints.
Schepartz and Hecht Ribosomes	• Engineered ribosomes featuring mutations in 23S rRNA residues that enable improved incorporation of β-amino acids (Schepartz-in vivo and Hecht-in vitro) and D-amino acids (Hecht). • Ribosomes screened/selected using puromycin as a tRNA mimic.

Finally, a grand challenge remains in developing and understanding rules and patterns in designing the ribosome. What does it mean to be a ribosome designer? Currently, studies are limited to a small number of nucleotides (Table 1.1), and frequently only explore single or double mutants. Although these studies have yielded invaluable insights on the role of key nucleotides in ribosome function, fully comprehensive maps of ribosomal variants do not currently exist. Furthermore, the ribosome as a machine works through a dynamic consortium of rRNAs. A platform to enable engineering the ribosome beyond single, double, or even triple rRNA changes across an expansive section of the ribosome would enable truly transformative engineering for both basic and synthetic biology applications. Expansive characterization of ribosomal variants will enable a thorough understanding of the form and function of the ribosome's domains, helices, and nucleotides. This complete characterization will additionally provide the groundwork and footing for ribosome evolution targets by providing rules for permissible alterations to this machine.

1.6 Introduction to dissertation topics

The following chapters represent research performed towards understanding the basic biology of the ribosome *in vitro* and *in vivo* to facilitate ribosome engineering efforts. Each chapter represents a complete story that has either been published in a peer-reviewed scientific journal (in full or in part) or is intended for submission to journals in the near future.

Chapter 2 of this thesis details the development of a mutational flexibility map of the ribosome's active site, the peptidyltransferase center (PTC). In this work, we quantified the conservation of every PTC-loop, A-loop, and P-loop nucleotide, and subsequently constructed and characterized every possible single point mutation at these locations. This work resulted in the design, building, synthesis, and characterization of 180 unique single point mutations within the ribosome's PTC. Additionally, this chapter also discusses the impacts of combining multi-mutations within the ribosome's active site; work that is ongoing. This chapter represents a significant breakthrough in the study of mutations within the highly conserved active site of the *E. coli* ribosome. This work serves as a foundation for subsequent chapters of this dissertation, as well as future work within the lab.

Chapter 3 of this thesis outlines *in vitro* work leveraging both the iSAT platform as well as ribosome purification methods for the isolation and characterization of β-amino acid incorporating ribosomes. These ribosomes, which were previously published on, could potentially be leveraged for the incorporation of expanded backbone monomers, as well as other non-canonical amino acids. To this end, this chapter represents the first efforts to use the iSAT platform for the incorporation of expanded backbone monomers. Despite a lack of translational activity, our

characterizations point to possible areas for system optimization, and lay the groundwork for a high-throughput in vitro workflow for studying and testing ribosomes capable of incorporating expanded backbone monomers.

Chapter 4 of this dissertation highlights a transition from working *in vitro* to studying and engineering ribosomes *in vivo*. In an effort to begin imagining mutating the ribosome for new functions within the cell, we worked to employ an *in vivo* orthogonal system. This work improves a tethered ribosome system, called Ribo-T, to generate a new state-of-the-art orthogonal ribosome platform, termed Ribo-T v2. Using library selection and evolution methods, we were able to identify an optimized set of Ribo-T v2 tethers, which possessed a mix of paired and unpaired RNA bases. Ribo-T v2 not only features improved growth rates and healthier overall fitness, the tethers remain uncleaved and the cells are capable of growing on a variety of medias at different temperatures. Furthermore, orthogonality of Ribo-T v2 was optimized through rigorous *in vivo* selections. Together these tether and orthogonality improvements enabled expanded biological function, permitting the incorporation of up to 5 non-canonical amino acids.

In chapter 5 of this thesis, we expand our studies and engineering of the tethered Ribo-T construct to probe computationally and user-designed tethers. This work includes both published and unpublished sections. Importantly, we demonstrate for the first time, the effective tethering of ribosomal subunits with a computationally designed tether. We further investigate the use of other well-characterized RNA motif tethers, such as the MS2 RNA aptamer. Here we demonstrate for the first time, the ability to generate functional RNA aptamer tethers on a Ribo-T construct; including tethers capable of binding protein (MS2 binding protein). The unpublished results from this work will undoubtedly lead to further investigations of functional RNA aptamer tethers which

possess the ability to carry out functions such as sequestering small molecules, binding proteins, restricting translation, localizing substrates, and more.

Chapter 6 and 7 summarize the dissertation, propose future work, and draw conclusions from this thesis. The most important findings from each section are summarized, and subsequently we describe future efforts in both studying the basic biology of the ribosome, as well as applying these findings to more engineering efforts. These sections highlight where the work of this thesis fits into the greater ribosome and synthetic biology fields, and includes predictions of where the fields are headed, and how future work might fit into this vision.

Finally, chapter 8, the appendix, includes our initial efforts on other projects spanning both ribosome work (both *in vivo* and *in vitro*) as well as educational tools. These projects have not yet been published or completed but represent important steppingstones for the next generation of ribosome biochemists, synthetic biologists, and scholars. Ideally, the appendix will represent a resource for younger graduate students and new postdocs to find inspiration and the beginnings of a project or paper. Lastly, the concluding section of the appendix highlights perhaps one of the most important aspects of this dissertation: Giving back to the scientific and broader community through scientific communication, outreach, education, and mentorship. The dissertation marks the transition from a student to a scholar; and as part of a scholar's responsibility, one must train, teach, and give back to the community that supported their own education and scholarly growth.

CHAPTER 2

Studying and engineering ribosomes *in vitro*: Mutational characterization and mapping of the 70S ribosome active site

The work presented in this chapter is based upon work accepted in Nucleic Acids Research. d'Aquino, A. E.; Azim, T.; Aleksashin, N.A.; Hockenberry, A. J.; Jewett, M. C. Mutational characterization and mapping of the 70S ribosome active site. Accepted December 2019: *NAR*. **2020**.

2.1 Abstract

The synthetic capability of the *Escherichia coli* ribosome has attracted efforts to repurpose it for novel functions, such as the synthesis of polymers containing non-natural building blocks. However, efforts to repurpose ribosomes are limited by the lack of complete peptidyl transferase center (PTC) active site mutational analyses to inform design. To address this limitation, we leverage an *in vitro* ribosome synthesis platform to build and test every possible single nucleotide mutation within the PTC-ring, A-loop and P-loop, 180 total point mutations. These mutant ribosomes were characterized by assessing bulk protein synthesis kinetics, readthrough, assembly, and structure mapping. Despite the highly-conserved nature of the PTC, we found that >85% of the PTC nucleotides possess mutational flexibility. Our work represents a comprehensive single-point mutant characterization and mapping of the 70S ribosome's active site. We anticipate that it will facilitate structure-function relationships within the ribosome and make possible new synthetic biology applications.

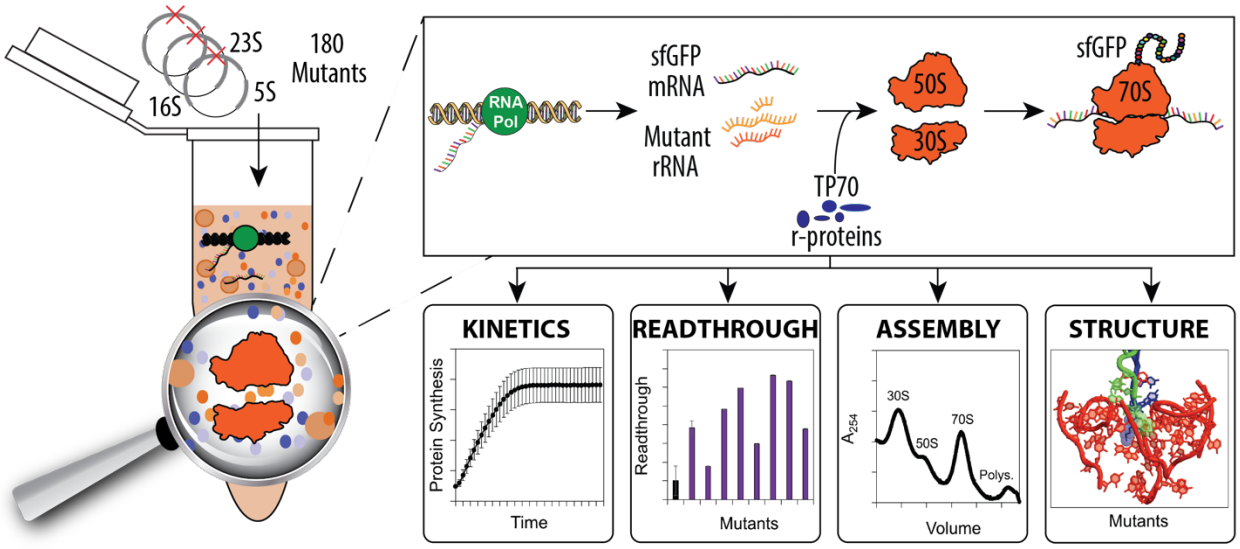

Figure 2.0 Graphical abstract. Studying ribosome active site mutants using an *in vitro* platform. Peptidyl transferase center (PTC) mutant plasmids were introduced into *in vitro* integrated synthesis, assembly, and translation (iSAT) reactions along with cell-free iSAT reagents. Once iSAT reactions are initiated, T7 RNA polymerase transcribes sfGFP mRNA as well as rRNA. The rRNA coassembles with ribosomal proteins (TP70) to form iSAT ribosomes. These ribosomes can then translate the reporter protein mRNA (sfGFP). Upon completion of an iSAT reaction, kinetics, structure, fidelity, and assembly analyses can be carried out to characterize ribosomes *in vitro*.

2.2 Introduction

The *Escherichia coli* ribosome is the molecular machine that polymerizes α-amino acids into polypeptides using information encoded in messenger RNAs (mRNAs). This machine is composed of two distinct subunits: the large (50S) subunit, responsible for accommodating tRNA-amino acid monomers, catalyzing peptide bond formation, and excreting polypeptides, and the small (30S) subunit, primarily responsible for decoding the mRNA. The active site of the ribosome, or the peptidyl transferase center (PTC), residing in the 23S rRNA of the 50S subunit, is composed primarily of conserved catalytic rRNA nucleotides, but has been demonstrated to possess ribosomal protein as well [153-156].

Previous works have revealed that the key catalytic functions of the ribosome are executed by its RNA components; making the ribosome an ancient ribozyme [11]. These rRNA nucleotides of the PTC play a key role in positioning the CCA ends of the aminoacyl (A)-site and peptidyl (P)-site tRNA monomers to catalyze peptide bond formation and facilitates peptide release [157]. Additional studies suggest that ribosomal proteins may contribute to function as well [153-156]. Most notably, a number of L27 residues are positioned to interact with the peptidyl-tRNA, potentially stabilizing the 3' ends of the tRNA substrates in the PTC for catalysis [153]. Within the PTC, sets of key rRNA nucleotides are arranged as rings and loops, with the central PTC-ring, A-loop, and P-loop playing pivotal roles in translation [11,158,159] (Figure 2.1). The central PTC-ring (defined in our study as G2057-C2063, G2447-C2456, C2496-C2507, G2582-G2588, A2602, and C2606-C2611) surrounds the A- and P-site tRNA monomers and has been implicated in antibiotic binding [160], tRNA positioning [161], and peptide stalling [162,163]. As their names suggest, the A-loop (defined in our study as U2548-A2560) is essential in interacting with A-site tRNA during translation, while the P-loop (defined in our study as G2250-C2254) makes contacts with P-site tRNA [158,164-166]. The A- and P-loops are co-located on either side of the central PTC-ring, above the peptide exit tunnel (Figure 2.1). All of these nucleotides have previously been identified as essential catalytic bases, as their identities are highly conserved [60].

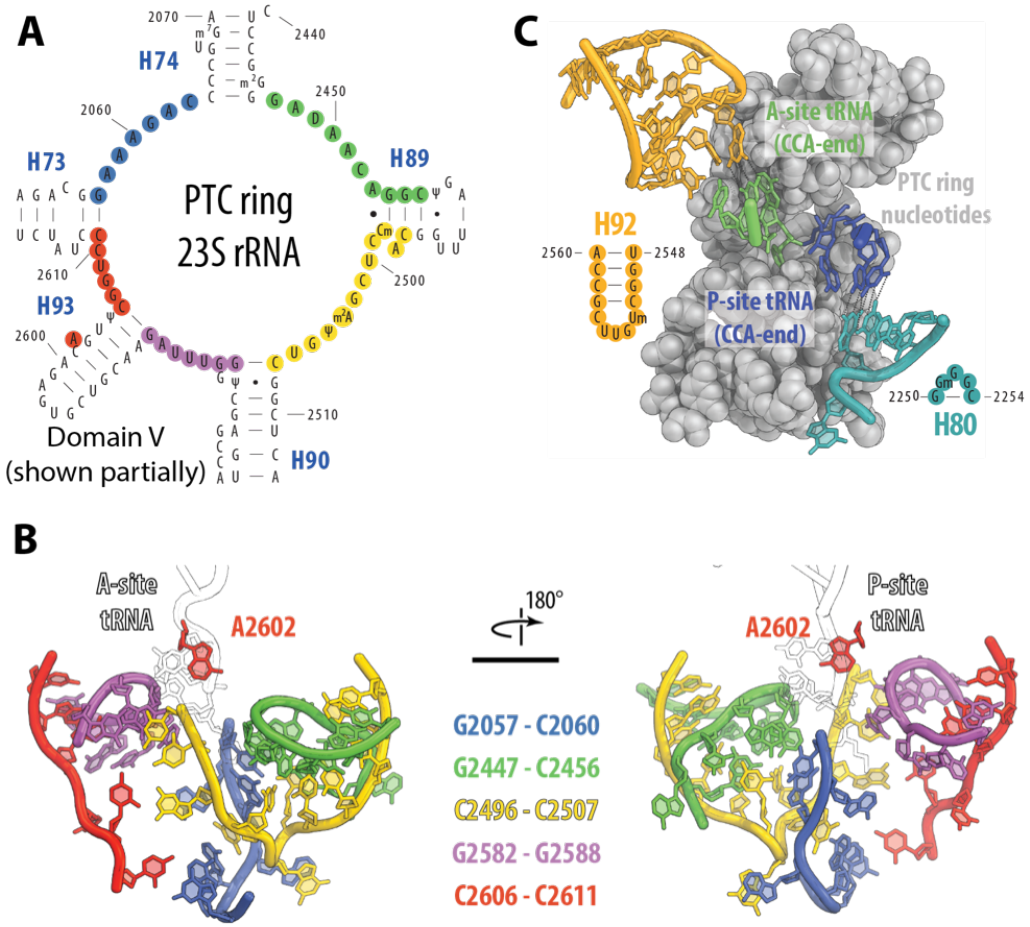

Figure 2.1 The ribosome's peptidyl transferase center (PTC) is important for translation and can be studied *in vitro*. (a) Secondary structure and (b) crystal structure model of the PTC-ring nucleotides probed in this study. (c) Secondary structure and crystal structure model of the A- and P-loop nucleotides probed in this study. Ribosome structure accessed from PDB ID: 4YBB, with tRNAs from PDB ID: 1VY4.

Both *in vivo* and *in vitro* studies of the *E. coli* ribosome's active site have provided a foundational understanding of ribosome structure, function, and mechanism [1,42,167-170]. However, we lack a comprehensive understanding of the PTC, in part, because a complete functional mutational analysis does not exist. This gap in knowledge is rooted in several challenges. One challenge, for example, includes insufficient high-throughput methods to synthesize and

characterize a large number of ribosomal mutations. As a result, existing ribosomal mutation studies typically focus only on a few mutations at a time (*i.e.*, one to six in depth characterizations per paper) [64,171], use characterization techniques that can be difficult to compare (spanning *in vitro* biochemistry, *in vivo* genetics, computational modelling, antibiotic resistance probing, and more), and sometimes examine different bacterial species. This has led to a segmented and heterogeneous image of the ribosome's mutational space (Supplementary Table 2.1). Another challenge is the highly-conserved nature and functional importance of many active site nucleotides. Characterization of mutations at these locations has proven difficult as nucleotide changes confer deleterious phenotypes [61,172,173]. Thus, despite insights gained from crystal structures and 30+ years of biochemical analyses, we still currently lack direct mutational and functional knowledge for many key nucleotides in the ribosome's active site. A comprehensive mutational map of the rRNA within the ribosome's active site would facilitate antibiotic resistance studies [61], active site and rRNA engineering efforts [174-176], and substantially build on our current understanding of structure-function relationships within the ribosome [174].

To circumvent cell-viability constraints [177], a cell-free [178-182], or *in vitro*, ribosome synthesis approach could be used for identifying structurally and functionally critical sites in the ribosome useful for both basic biology and future ribosome engineering advances [49]. For example, the elegant "atomic mutagenesis" approach developed by Polacek and colleagues has helped unravel the detailed contributions of rRNA nucleotides in protein synthesis [183-185]. In previous work, we developed and optimized a different approach for use with *Escherichia coli* ribosomes; the integrated synthesis, assembly, and translation (iSAT) platform for the *in vitro* construction and characterization of ribosomes [51-53,186]. The iSAT platform leverages a ribosome-free S150 crude

extract to enable the efficient transcription of template-derived rRNA. Importantly, iSAT co-activates the processes of rRNA synthesis and processing, ribosome assembly, and translation in a one-pot reaction, mimicking natural *in vivo* processes. The iSAT system therefore provides a unique and powerful approach for the interrogation and manipulation of *E. coli* ribosomes in a cell-like environment. This system contrasts with previous approaches for *in vitro* ribosome reconstitution, which have played important roles in elucidating our understanding of the ribosome [64], but are unable to incorporate synthetic *in vitro* transcribed 23S rRNA of the large subunit into highly active *E. coli* ribosomes [43,44,49,50,184,187]. Key advantages of this platform include no wild-type ribosome contamination, facile and rapid mutant construction and testing, and a reaction environment that closely resembles the cell.

In this work, we use the *in vitro* iSAT platform to rapidly characterize ribosomal active site mutations. Importantly, these catalytic regions of the ribosome are highly conserved, implying that these interactions are essential for peptide-bond formation. Thus, studies of these regions will help further define the structural and functional importance of these particular sequences in the ribosome. Specifically, we probed all nucleotides in the catalytically critical PTC-ring, A-loop, and P-loop by: i) constructing single point mutations at every possible rRNA position within these loops (180 total mutations); ii) testing their translational activity *in vitro*; iii) assaying translation readthrough of a premature stop codon as a proxy for translation accuracy and release factor fidelity [171,188-190] and; iv) characterizing ribosomal assembly. Finally, we analyzed our mutational activity data in the context of the three-dimensional ribosome structure by mapping our findings directly onto the crystal structure (Figure 2.1). We report the first, to our knowledge, comprehensive molecular dissection of the ribosome's active site in the context of mutational

flexibility, and the development of a high-throughput and standardized workflow for rapidly constructing and characterizing rRNA mutants. We envision these findings to be a steppingstone for both basic biologists and engineers to target, study, and engineer single or multiple ribosomal nucleotides.

2.3 Materials and methods

2.3.1 Plasmid construction

The 7,300-bp plasmid pT7rrnB carries an *Escherichia coli* rRNA operon, *rrnB*, under the control of the T7 promoter and the ampicillin resistance gene as a selective marker. All ribosomal mutant plasmids are derivatives of pT7rrnB carrying single point mutations in the 23S rRNA gene. Briefly, site-directed mutagenesis was used to construct each individual point mutant. Nucleotide point mutations were introduced into primers and amplified using pT7rrnB as a template for PCR amplification. PCR products were blunt end ligated, transformed into DH5α using electroporation, and plated onto LB-agar/ampicillin plates at 37°C. Plasmid was recovered from resulting clones and sequence confirmed.

Similarly, premature stop codon readthrough constructs were generated by introducing a premature stop sequence (UAG, UGA, of UAA) into primers, and amplified using pJL1-sfGFP as a template for PCR amplification. PCR products were blunt end ligated, transformed into DH5α using electroporation, and plated onto LB-agar/Kanamycin plates at 37°C. Readthrough controls were generated from reporter constructs by introducing all possible stop codon permutations (UGA, UAA, and UAG) at various positions within the reporter (Figure 2.3A). All constructs were verified by DNA sequencing.

2.3.2 Sequence alignment and analysis

A dataset consisting of 1,614 pre-aligned and phylogenetically arranged 23S sequences were downloaded from the All Species Living Tree Project (version 123, compiled using the SILVA reference database LSUref123) [191]. This dataset included the *E. coli* sequence (AJ278710) that was used as a reference to find regions of interest in the full species alignment using custom scripts (available at https://github.com/adamhockenberry/23s-alignment-LTP). All species were used in visualizations, but entropy calculations included only analysis of ungapped sequences. Specifically, for each position in the alignment of a region of interest we first removed any sequence where that position was denoted by a '-' character. With the remaining sequences we calculated the entropy values (H) as:

$$H = - \sum_{i \in (A,U,G,C)} p_i \log (p_i)$$

where the probability of nucleotide *i* (p_i) comes from the counts of nucleotide *i* divided by the number of all non-gapped sequences at that position. In this formulation, *H* has a minimum of 0 when all sequences in an alignment column are one nucleotide and a maximum of ~1.386 when all nucleotides are equally likely (i.e. occurring with a probability of 0.25).

2.3.3 Strain culture and harvest

E. coli cells for S150 extract and TP70 preparation were grown in 10L of 2xYPTG in a fermenter (Sartorius) (Supplementary Figure 2.11). MRE600 strain was grown at 37°C. Cells were harvested at OD_{600} = 2.8-3.0, washed twice in S150 lysis buffer (20 mM Tris-chloride pH 7.2 at 4°C, 100 mM ammonium chloride, 10 mM magnesium chloride, 0.5 mM EDTA, 2 mM DTT), pelleted, and flash frozen at -80°C using liquid nitrogen for storage. Buffer was added at a ratio of 5 mL of buffer per 1 g of cells. 200 µL of Halt Protease Inhibitor Cocktail (Thermo Fisher Scientific Inc.) and 75 µL RNase Inhibitor (Qiagen) were added for every 4 g of cells in the

suspension. The cells were lysed at approximately 20,000 psi with an EmulsiFlex-C3 homogenizer (Avestin). An equivalent dose of RNase Inhibitor and 3 μL of 1M DTT per millilitre were added to the lysate prior to two clarification spins at 30,000 g and 4°C for 30 min. Supernatant equivalent to S30 crude extract was recovered and gently layered into Ti45 ultracentrifuge tubes on top of an equivalent volume of sucrose cushion, buffer B (20 mM Tris-HCl (pH 7.2 at 4°C), 100 mM NH4Cl, 10 mM MgCl2, 0.5 mM EDTA, 2 mM DTT, 37.7% sucrose). Samples were then centrifuged (at 35000 rpm in Ti70 rotor) and 4°C for 20 h. Supernatant was recovered for S150 extract, and the remaining clear ribosome pellet was gently washed and resuspended in buffer C (10 mM Tris-OAc (pH 7.5 at 4°C), 60 mM NH_4Cl, 7.5 mM $Mg(OAc)_2$, 0.5 mM EDTA, 2 mM DTT). Concentration of resuspended ribosomes was determined from A_{260} NanoDrop readings (1 A_{260} unit of 70S = 24 pmol 70S [192]). Ribosomes were then aliquoted and flash-frozen for use as purified 70S ribosomes and for purification of native rRNA and r-proteins.

2.3.4 Component preparation

S150 crude cell-free extracts, *E. coli* 70S ribosomes, total protein of 70S ribosomes (TP70) and T7 RNA polymerase (RNAP) were prepared as previously reported [52,193]. S150 and TP70 were prepared from MRE600 cells. Protein concentrations of each S150 extract were measured using Bradford assay with bovine serum albumin (BSA) as a standard.

2.3.5 iSAT reactions

iSAT reactions of 15 μL were set-up as previously described [52]. Briefly, reactions were prepared in polymerase chain reaction tubes with optically clear flat caps and incubated at 37°C in a CFX96 real-time thermal cycler (Bio-Rad). iSAT reactions contained reporter protein plasmids encoding superfolder GFP (sfGFP). Green fluorescence of sfGFP was monitored using the

CFX96real-time thermal cycler as (excitation: 450-490 nm, emission: 510-530 nm). Additives were included at the described final concentrations. Specifically, crowding agent (2% PEG-6000) and reducing agent (2 mM DTT) were added to each reaction. iSAT reactions for S150 extracts were optimized for concentrations of magnesium glutamate to maximize reaction productivity and minimize consumption of parts (Supplementary Figure 2.12). sfGFP quantification was performed as previously reported [53], using measurements of relative fluorescence units (RFU) from CFX96 real-time thermal cycler (BioRad, Hercules, CA) and BioTek Synergy 2 plate reader (Winooski, VT). RFU values were converted to molar concentration using a linear standard curve made in-house by expressing ^{14}C-leucine labelled sfGFP in *E. coli* PANOx CFPS reactions and relating RFUs to trichloracetic acid precipitable soluble protein yield.

2.3.6 Ribosome sedimentation analysis

Sucrose gradients were prepared from gradient buffer (20 mM Tris-HCl (pH = 7.5 at 4°C), 100 mM NH_4Cl, 10 mM $MgCl_2$) with 10 and 40% sucrose in SW41 polycarbonate tubes using a Biocomp Gradient Master. Gradients were placed in SW41 buckets and chilled to 4°C overnight. Meanwhile, approximately 3 x 15 µL iSAT reactions were prepared and incubated at 37°C, for 2 hours. Reactions were flash frozen in liquid nitrogen. The next day, reactions were pooled and 45 µL of iSAT reactions were diluted to 100 µL with gradient buffer, and carefully loaded onto chilled gradients. The gradients were ultra-centrifuged to 39,000 rpm for 2.5 hours at 4°C, using an Optima L-80 XP ultracentrifuge (Beckman-Coulter) at maximum acceleration and braking. Gradients were analyzed with a Piston Gradient Fractionator (Biocomp). Traces of A254 readings versus elution volumes were obtained for each gradient, with readings adjusted to match baselines based on blank sucrose readings. iSAT reactions without the operon plasmid were performed to

establish a background reading that was subtracted from experimental traces. Gradient fractions were collected and analyzed for rRNA content by gel electrophoresis in 1% agarose and imaged in a GelDoc Imager (Bio-Rad) (Supplementary Figure 2.13). Ribosome profile peaks were identified based on the rRNA content as representing 30S or 50S subunits, 70S ribosomes, or polysomes, as well as a control peak with purified 70S. To calculate the area under each curve, Riemann sums were taken with the 30S x-axis boundaries ranging from ~13 mm gradient distance to ~21 mm, the 50S x-axis boundary ranging from ~22 to ~28 mm, the 70S x-axis boundary ranging from ~30 to 40 mm, and the polysomes x-axis boundary ranging from ~42 to 59 mm. Sums between each X-axis coordinate were taken, and totals were calculated for the given boundaries.

2.3.7 iSAT ribosome purification

Several (approximately 8) 15 µL iSAT reactions were prepared and incubated for 2 hours at 37°C, then pooled together. Purified 70S *E. coli* ribosomes were recovered as previously described [52], with pelleted iSAT ribosomes resuspended in iSAT buffer, aliquoted and flash-frozen.

2.3.8 Nucleotide distance calculations

Nucleotide distances were measured between the average center of each nucleotide to the average center of A76 of each respective tRNA and the attached amino acid residue of each the A-site and P-site tRNA molecules. Distances were calculated from the structure file of PDB ID: 4YBB, with tRNAs from PDB ID: 1VY4 [143] (Supplementary Table 2.5 and 2.6).

2.4 Results

2.4.1 Examining mutational flexibility of PTC rRNA *in vitro*

The goal of this study was to use the iSAT platform to construct and characterize ribosomal active site mutants and generate a functional map of mutational flexibility. However, the ribosome's active site has evolved to accurately and efficiently process α-amino acid monomers using catalytic rRNA, that we would expect to exhibit high levels of conservation and would be less permissible, or flexible, to mutation. In fact, previous work has demonstrated *in vivo* that many nucleotide changes to highly-conserved nucleotides are detrimental [61], but the ribosome can still withstand some small changes at select positions [194] (Supplementary Table 2.1). As a first step in characterizing the ribosome's active site, we quantitatively evaluated conservation at every nucleotide position within the PTC. Large subunit (LSU) sequences were taken from the Silva ribosomal-RNA database and aligned at PTC-nucleotide positions [191]. Sequences were aligned for 1,614 species of bacteria and archaea (Supplementary Figure 2.1 and Supplementary Figure 2.2) and Shannon Entropy values were calculated (Figure 2.2A). Shannon Entropy scores are akin to variance scores (though we caution that they ignore phylogenetic relatedness), with a Shannon Entropy of zero representing zero variance (100% conservation across the 1,614 species). Any values above zero indicate that evolutionary changes have occurred and result in multiple nucleotides within a given site in the alignment. As expected, the entire PTC active site (PTC-ring, A-loop, and P-loop) exhibited a high-level of conservation, with approximately 75% of the nucleotide positions possessing a Shannon Entropy value at or near zero.

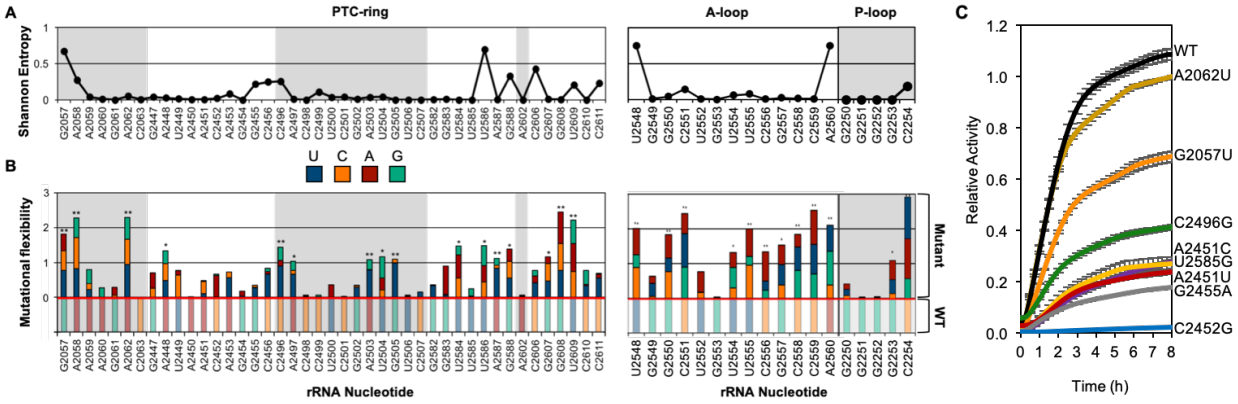

Figure 2.2 The ribosome's peptidyl transferase center (PTC) is amenable to mutation, despite high sequence conservation. (a) Shannon entropy plot representing the conservation of PTC nucleotides across 1,614 of bacterial and archael species. All large subunit (LSU) sequences were taken from alignments found at the Silva database (43). Shannon entropy values of zero represent 100% conservation across all species. Despite the high conservation of the ribosome's PTC, there is high plasticity within its catalytic core. (b) Mutational flexibility of each PTC mutation relative to the activity of WT iSAT ribosomes. Nucleotides are color coded according to the legend. The original WT nucleotide activity is normalized to 1, and resides below the red line on the graph. Each possible nucleotide change at the corresponding position is color coded in the bars above the red line, with bar size representing relative activity. Single asterisks are placed above nucleotides wherein the sum of mutant activity (mutational flexibility) results in activity ≥ 1. A second asterisk is placed above nucleotides wherein at least one nucleotide mutation results in activity ≥ 75% of WT activity. **(C)** Protein synthesis curves for representative nucleotide mutations have been included in this graph: wild-type, high activity (A2062U and G2057U), medium activity (C2496G and A2451C), medium-low activity (U2585G and A2451U), and low activity (G2455A and C2452G) mutants were chosen. Translation rates for representative PTC mutants in this study are represented in Supplementary Table S2. For simplicity and ease of visualization, only a subset of 180 nucleotide mutation kinetic curves are included on the graph and the X-axis is restricted to 8 hours.

While the PTC active site exhibits high levels of nucleotide conservation, we can assess mutational flexibility at each rRNA nucleotide position by building rRNA mutants in the iSAT system. We constructed iSAT reactions, as previously described [51-53,186], possessing wild-type and all 180 mutant ribosomes, separately, and measured reporter protein biosynthesis yields via fluorescent activity over the course of 16-20 hours (Figure 2.2B, 2.2C, and Supplementary Figure 2.3). When looking at all 180 mutants, we observe a wide range of translation rates *in vitro*.

Importantly, these rates are representative of overall activity, and have been summarized in numerical order in tabular form in Supplementary Table 2.2 (also Figure 2.2C, Table 2.1, Supplementary Figure 2.3 and 2.4). Relative activity was subsequently calculated to compare performance of each mutant by normalizing wild-type protein synthesis yields to one and mutant yields to the normalized wild-type yields. An overall mutational flexibility score was then determined for each nucleotide position by adding the relative activities of every possible point mutation. The highest mutational flexibility score of three indicates that all three nucleotide changes possess wild-type activity, while the lowest mutational flexibility score of zero indicates that all three nucleotide changes preclude any protein synthesis (Supplementary Table 2.3).

Table 2.1 Bulk translation rates of wild-type and representative mutant 70S iSAT ribosomes. Bulk translation rates for iSAT ribosomes were determined from protein synthesis kinetics curves, for reactions after 2 h incubations.

rRNA Mutation	Bulk translation rate (μM protein/hr)
WT	1.03 ± 0.03
A2062U	1.02 ± 0.02
G2608C	0.57 ± 0.03
G2057U	0.63 ± 0.02
U2449C	0.52 ± 0.02
C2452A	0.52 ± 0.02
C2496G	0.31± 0.02
A2451C	0.15 ± 0.01
U2585G	0.20 ± 0.01
A2451U	0.14 ± 0.01
G2455A	0.13 ± 0.01
C2452G	0.004 ± 0.01

Despite the highly-conserved nature of the ribosome's active site, the majority (>85%) of the PTC-ring nucleotides possessed some degree of flexibility to mutational changes (one or more mutations at that position permitted full-length protein synthesis, determined by protein activity), as did 80% of A- and P-loop nucleotides (Figure 2.2). Of the 43 PTC-ring nucleotides, 16 positions

(G2057, A2058, A2062, A2448, C2496, A2497, A2503, U2504, G2505, U2584, U2586, A2587, G2588, G2607, G2608, and U2609) possessed a mutational flexibility score ≥ 1. And across the A- and P-loop nucleotides, 12 positions (U2548, G2550, C2551, U2554, U2555, C2556, G2557, C2558, C2559, A2560, G2253, C2254) resulted in a mutational flexibility score ≥ 1. Additionally, 9 PTC-ring nucleotides (G2057, A2058, A2062, C2496, A2503, G2505, A2587, G2608, and U2609) and 9 A- and P-loop nucleotides (U2548, G2550, C2551, U2555, C2556, C2558, C2559, A2560, C2554) possessed at least one nucleotide mutation that resulted in ≥ 75% of WT activity.

We then tested the degree to which our findings relate to natural sequence diversity of 23S rRNA sequences by correlating mutational flexibility for individual sites with their Shannon Entropy values measured across the 1,614 species. For the PTC-ring, we found a significant (p=0.025) but weak (R^2=0.117) relationship, indicating that sequence diversity explains only a minor fraction of the observed variation in mutational flexibility (Supplementary Figure 2.5). For the A- and P-loops, we found a non-significant (p=0.086) and weak (R^2=0.173) relationship, indicating that the sequence diversity does not explain the observed variation in mutational flexibility. In total, these results illustrate a large degree of mutational flexibility that exists within the PTC and the difficulty in predicting mutational flexibility solely from nucleotide conservation.

2.4.2 Characterizing PTC mutant ribosome translation readthrough

With the PTC exhibiting a high degree of mutational flexibility, we wondered if mutants of highly-conserved nucleotides that possessed observable translational activity were exhibiting readthrough impairments during protein synthesis. Readthrough impairments could be a product of either decreased translation accuracy, or release factor fidelity (decreased binding affinity or hydrolysis) [195-197]. Previously, mutations in the active site of the *E. coli* ribosome were reported to

have a negative impact on translation readthrough and fidelity [64,171,190,198], suggesting that our mutant ribosomes might have the same issues. To assess whether our rRNA mutants' functionality was being impacted by impaired translation readthrough, we carried out a series of experiments involving premature stop codon readthrough adapted from previously-reported assays [171] (Figure 2.3A). Specifically, the readthrough assay measures fluorescence output of iSAT reactions using sfGFP reporter constructs separately possessing UAG premature stop codons at amino acid positions 50, 100, 116, or 216 of sfGFP, and comparing three different stop codons (UAG, UGA, and UAA) all positioned at amino acid 100 of sfGFP. Readthrough efficiencies were determined by comparing relative active sfGFP produced from iSAT reactions using each rRNA mutant construct to wild-type ribosome constructs for each reporter. These relative readthrough efficiencies were then normalized by each mutants' translation activity. We tested whether ribosomes with mutations possessing high, medium, and low activity (PTC-ring: A2062U, G2608C, G2057U, U2559C, C2452A, C2496G, A2451C, U2585G, A2451U, G2455A, C2452G; A-loop: C2559A, C2551A, U2552G; and P-loop: C2254G, G2253C, G2251A) could readthrough engineered stop codons in sfGFP mRNA (Figure 2.3; Supplementary Figures 2.6 and 2.7).

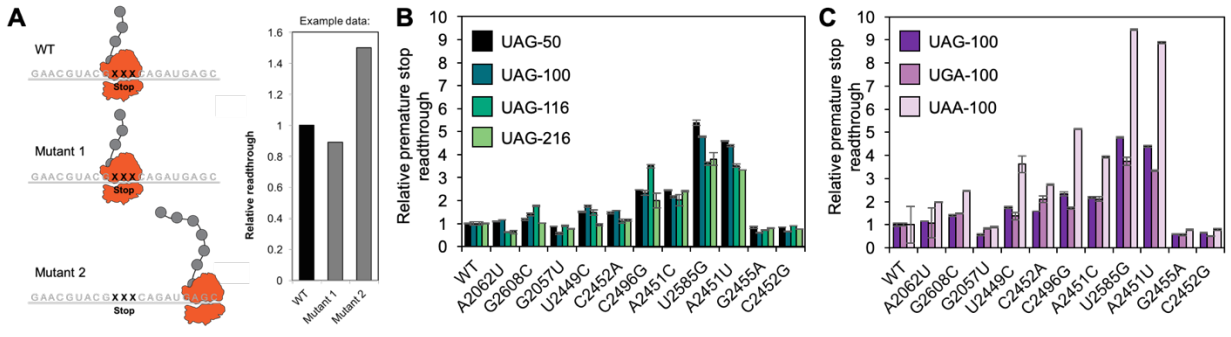

Figure 2.3 Ribosomal PTC mutations increase stop-codon readthrough. (a) Schematic of translation fidelity assay using premature stop codon constructs. Assays were adapted from

O'Connor *et al*. (37). Premature stop codon readthrough from wild-type ribosomes was normalized to 1. Mutant ribosome premature stop codon readthrough was quantified through fluorescence and set relative to WT. Mutants with lower fidelity (higher readthrough of premature stop codons) produce higher relative sfGFP titers. (b) UAG stop codon readthrough at amino acid position 50, 100 ,116, and 216. (c) UAG, UGA, and UAA stop codon readthrough at amino acid position 100. Relative activity in translation fidelity assays using premature stop codons was assessed using sfGFP fluorescence. The pJL1-sfGFP plasmid possessing a UAG stop codon at the specified locations were introduced into iSAT reactions as the reporter plasmid along with the mutant or wild-type rRNA plasmids. Values represent averages and error bars represent one standard deviation from the mean, with $n \geq 3$ for n number of independent reactions.

Our results demonstrate that PTC-ring mutations C2496G, A2451C, U2585G, and A2451U exhibit a high-degree of stop codon readthrough (Figure 2.3B-C), while the A- and P-loop mutations we probed maintain minimal readthrough, similar to wild-type ribosomes (Supplementary Figures 2.6 and 2.7). Importantly, the overall readthrough trends across the mutants are mirrored across each unique premature stop codon construct (the same 4 ribosome mutants exhibiting a higher-degree of readthrough compared to wild-type ribosomes); however, normalized relative readthrough signals for UAA were greater than those for stop codons UAG and UGA. We hypothesize that these results are attributed to both release factors, RF1 and RF2, recognizing the UAA stop codon during wild-type translation (while UAG is only recognized by RF1 and UGA is only recognized by RF2) [199,200]. This increased recognition may result in higher UAA termination efficiencies in our system and thus reduced fluorescence signals for wild-type ribosomes reading this construct. Thus, when relative readthrough is normalized across the mutants compared to wild-type, any small amount of readthrough from a mutant ribosome is further amplified with this stop codon. In summary, the results of our readthrough assay emphasize the important role that PTC-ring nucleotides play in translation readthrough, whether it be accuracy or termination fidelity, as compared to A- and P-loop bases.

2.4.3 Incorporation of ribosomes with PTC active site mutations into functional polysomes

For all the PTC mutants, but especially those with low activity, we wondered if activity was related to the mutants' ability to assemble into functional 70S ribosomes and translate in polysomes. This is because iSAT combines ribosome assembly and translation in a single-pot reaction. It is possible that an rRNA mutation may impact assembly (as opposed to molecular function), resulting in reduced translation activity. To this point, we analyzed assembly of a subset of mutant ribosomes by observing the 30S subunit, 50S subunit, 70S particles, and polysomes (disomes and trisomes) using sucrose gradient fractionation as previously described [53] (Figure 2.4). Using a sucrose gradient, iSAT reactions were centrifuged, fractionated, and trace peaks analyzed (Supplementary Table 2.4). A set of high-, medium-, and low-activity mutants were chosen for analysis, with a few mutants also possessing compromised translation fidelity (U2585G, and A2451U). In the PTC-ring, all mutants except for G2455A broadly possessed similar assembly profile traces to wild-type iSAT ribosomes (Figure 2.4B), but exhibited reduced populations of 70S species and polysomes (disomes and trisomes), matching their decreasing activity (Supplementary Table 2.4). Of note, G2455A, exhibited a very different profile, accumulating almost entirely as free 30S and 50S subunits and only 4% 70S species, 2% disomes, and no trisomes (Supplementary Table 2.4).

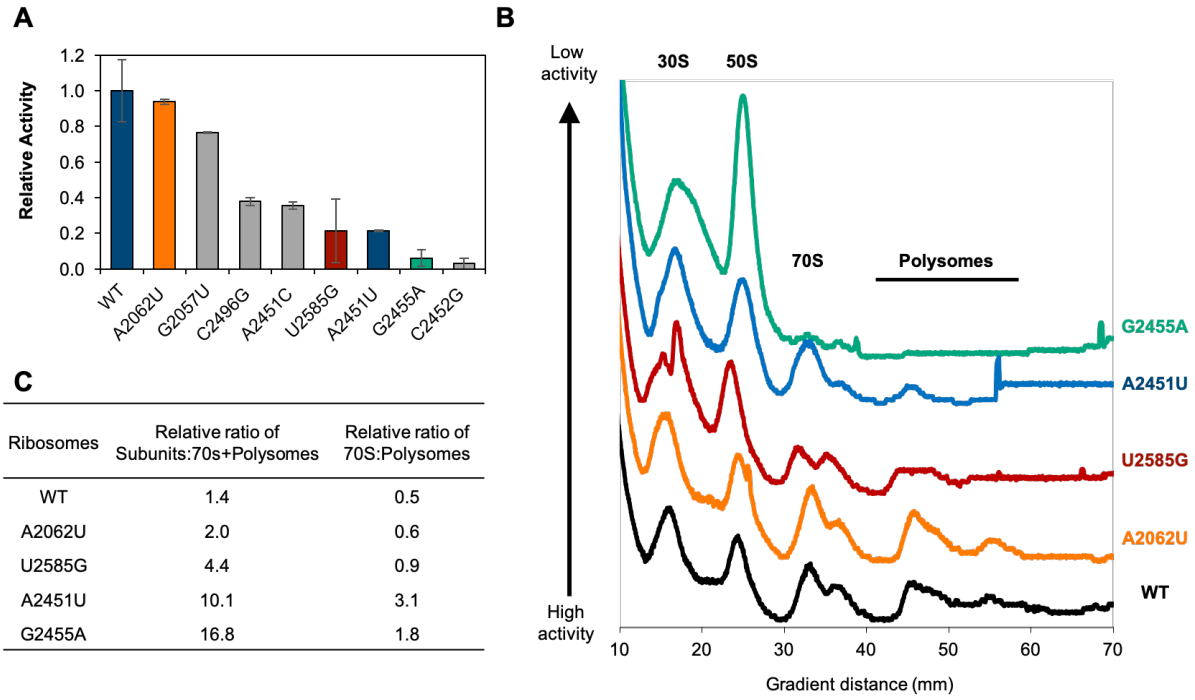

C

Ribosomes	Relative ratio of Subunits:70s+Polysomes	Relative ratio of 70S:Polysomes
WT	1.4	0.5
A2062U	2.0	0.6
U2585G	4.4	0.9
A2451U	10.1	3.1
G2455A	16.8	1.8

Figure 2.4 Sucrose gradient fractionation identifies assembly differences across ribosomal PTC mutants. (a) The five nucleotide mutations chosen for sucrose gradient fractionation based on their activity. One high activity (A2062U) mutant was chosen, two medium activity (U2585G and A2451U), and one low activity mutant (G2455A) was assessed for assembly and compared to WT. (b) A wild-type sucrose gradient fractionation trace (black) is compared to 4 representative mutant traces (color coded based on nucleotide mutation activity graph). From bottom to top, the mutants are positioned in decreasing activity order. (c) Relative areas under sucrose gradient fractionation trace curves were used to calculate ratios of subunits to 70S and polysome particles as well as the ratio of 70S particles to polysomes.

Notably, upon analyzing the relative abundance of species, we observed that compared to wild-type—which has a relative ratio of subunits to 70S+polysomes value of ~1.4—G2455A has an approximately 11-fold greater population of individual subunits (relative ratio of G2455A subunits to 70S+polysomes is ~16.8) (Figure 2.4C). These results closely mirror the stark difference in translation activity between wild-type. When comparing the relative ratio of 70S to polysomes, wild-type and the mutant with highest activity (A2062U) have similar ratios

(70S:polysomes values of 0.5 to 0.6). As activity decreases, this ratio tends to increase roughly proportionately, suggesting that fewer 70S ribosomes are accumulating as polysomes.

2.4.4 The ribosome's active site is composed of high- and low-flexibility pockets and shells

We next set out to map our analysis of mutational flexibility, translational readthrough, and ribosome assembly onto the ribosome's three-dimensional structure, which would facilitate understanding of the PTC active site. Toward this goal we first wanted to gain insight into how proximity to tRNA molecules impacts mutational flexibility. We measured distances from A76 of the A- or P-site tRNAs to the average geometric center of each nucleotide (Supplementary Table 2.5 and 2.6). We then organized the nucleotides in order of closest to furthest from the P-site tRNA (and compared to distances from the A-site tRNA). Upon generating a one-dimensional heat map (Supplementary Figure 2.8), we find different patterns in the PTC-ring compared to the A- and P-loop. Specifically, we found that the PTC-ring possesses pockets of high mutational flexibility (dark orange) and low mutational flexibility (white) regardless of distance from tRNA molecules. Whereas in the A- and P-loops there exists a more evident gradient of flexibility and activity, with the nucleotides residing closest to the P-site tRNA (4Å) having the least amount of activity upon mutation, and the nucleotides residing furthest from the P-site tRNA (36Å) having the greatest mutant activity.

By mapping our ribosome mutants' activity onto the 3D ribosomal crystal structure, we then generated a mutational flexibility map of the active site (Figure 2.5 and Supplementary video). Upon deconvolution of the map into high-, medium-, and low- mutational flexibility groups, we found mutationally flexible and inflexible shells, pockets, and a gradient of flexibility in the PTC-ring, A-, and P-loops (Figure 2.5, Supplementary Figure 2.9 and Supplementary video).

Furthermore, there were no major trends in maintaining high activity with nitrogenous base identity (purine vs pyrimidine) (Supplementary Figure 2.10). Within the PTC-ring, the first shell of nucleotides with the lowest mutational flexibility are shaded in red-magenta. Of these nucleotides, A2450, C2063, and C2501 possess the lowest mutational flexibility, and form a functionally critical pocket surrounding the P-site tRNA molecule with P-loop nucleotides G2252 and G2251 (Figure 2.5D) [201]. In the next shell, nucleotides possessing medium/low mutational flexibility are shaded in red-violet, and on average reside in closer proximity to the P-site tRNA than the A-site tRNA. This nucleotide group includes G2455, which possesses assembly defects when mutated to G2455A, as well as U2585 and A2451, which possess increased translation readthrough when mutated to U2585G and A2451U, respectively (Figure 2.5E). The next shell of increasing mutational flexibility is shaded in violet. This shell of nucleotides spans both sides of the tRNA molecules and begins surrounding the exit tunnel **(**Figure 2.5F**)**. Finally, within the shell of highest mutational flexibility (violet-blue), there resides a prominent pocket surrounding the exit tunnel. Of note, this shell houses the nucleotide C2496, which possesses high translation readthrough when mutated to C2496G (Figure 2.5G).

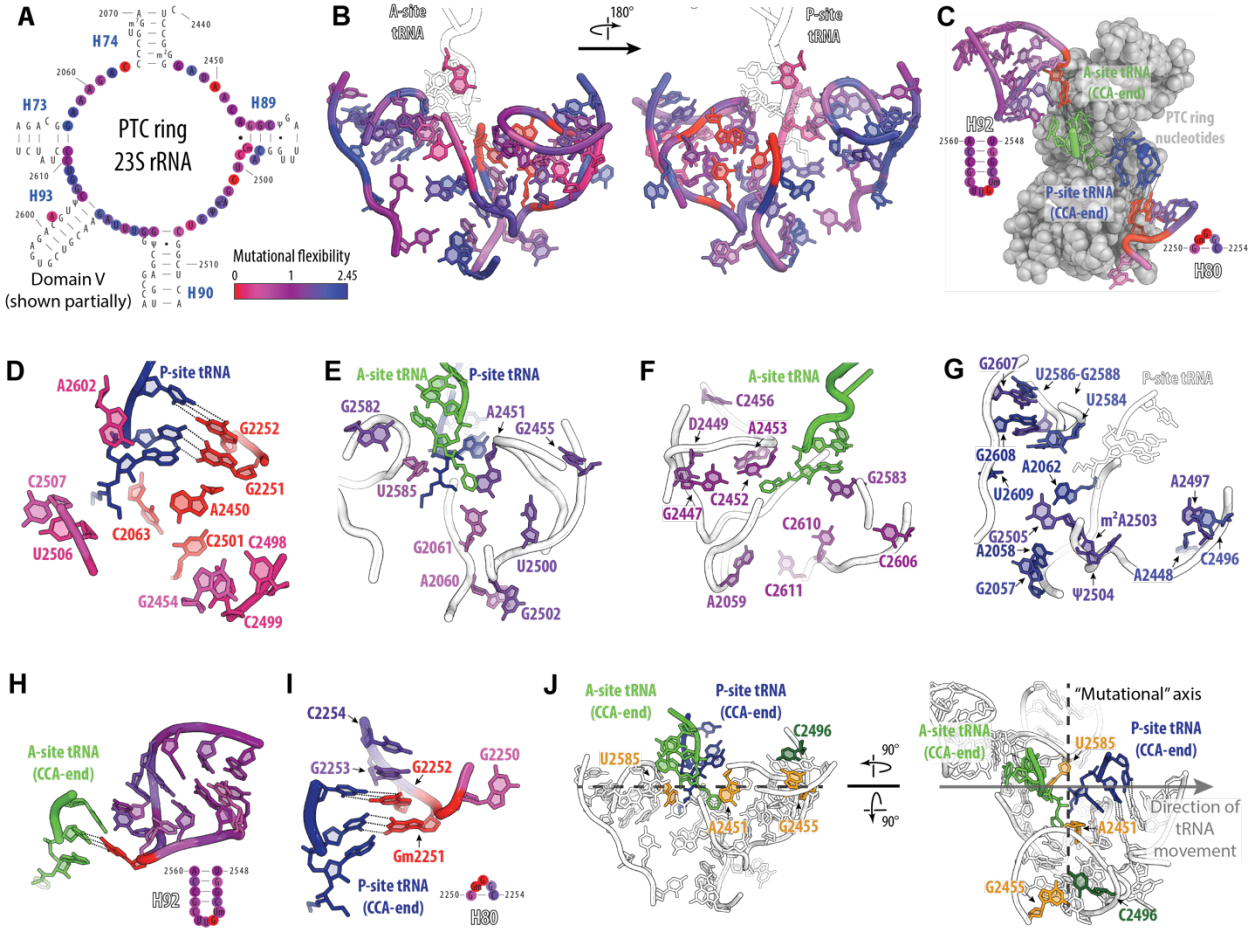

Figure 2.5 A mutational map reveals that the ribosome's PTC is composed of functional pockets and shells. (a) Secondary structure and (b) crystal structure model of the PTC-ring nucleotides probed in this study (heat mapped), along with the A-site tRNA, and P-site tRNA. (c) Crystal structure and secondary structure models of the A- and P-loop nucleotides probed in this study (heat mapped), A-site tRNA (green), P-site tRNA (blue), and PTC ring nucleotides (grey). (d-j) Crystal structure model of the PTC-ring nucleotides possessing: (d) the lowest mutational flexibility (red and magenta), (e) medium/low mutational flexibility (red-violet), (f) medium/high mutational flexibility (violet), and (g) the highest mutational flexibility (violet-blue). (h) Crystal structure model of the A-loop nucleotides probed in this study (heat mapped), A-site tRNA (green). (i) Crystal structure model of the P-loop nucleotides probed in this study (heat mapped), P-site tRNA (blue). (j) Structure model highlighting the nucleotides with mutants possessing increased translation readthrough (C2496, U2585, and A2451), as well as assembly defects (G2455). Ribosome structure accessed from PDB ID: 4YBB, with tRNAs from PDB ID: 1VY4.

Within the A-loop nucleotides, there is a clear gradient of mutational flexibility, with the least flexible nucleotide being G2553 (red) and residing nearest to the A-site tRNA (4 angstroms). Importantly, this nucleotide makes key Watson-Crick interactions with the CCA-end (specifically C75) of the A-site tRNA [164] (Figure 2.5H), while nucleotides possessing high mutational flexibility (violet-blue) make minimal contacts with the A-site tRNA molecule (Figure 2.5C and 2.5H). Much like the A-loop nucleotides, the P-loop nucleotides also possess a gradient of mutational flexibility corresponding with distance from the CCA-end of the P-site tRNA molecule. Importantly, the least mutationally flexible nucleotides, G2252 and G2251, make key Watson-Crick base pairing interactions with C75 and C76, respectively (Figure 2.5C and 2.5I). Interestingly, when modelled onto the heat map of the PTC-ring nucleotides with the lowest mutational flexibility, there is a clear pocket of translationally critical nucleotides that begin with Watson-Crick base pairing interactions at C75 and stretch down to the attached amino acid (**Figure 5D**). Finally, for the A- and P-loops, we also analyzed regression models of distance from A-site and P-site tRNAs against mutational flexibility of A- (red) and P-loop (blue) nucleotides (Supplementary Figure 2.9). The regression plots for the A-loop nucleotides possess R^2 values of 0.35 (p=0.03) and 0.32 (p=0.04), respectively. The regression plots for the P-loop nucleotides possess R^2 values of 0.61 (p=0.12) and 0.43 (p=0.23), respectively. The regressions and p-values for the A-site nucleotides suggests a significant and predictive relationship between mutational flexibility and distance from tRNA molecules; while the P-site nucleotides suggests a predictive relationship, however this relationship is non-significant due to a small sample size.

We next combined our mutational flexibility maps with knowledge from the translation readthrough and assembly experiments. Upon analyzing the PTC-ring nucleotides with translation

readthrough defects (C2496, U2585, and A2451), our mutational map highlights their unique positioning along the tRNA path through the ribosome (Figure 2.5J). Additionally, G2455, which possesses an assembly defect, resides just behind the A-site tRNA molecule. Finally, the nucleotides with the highest (violet-blue) mutational flexibility and lowest (red-magenta) mutational flexibility, reside in pockets that span opposite sides of the tRNA molecules (Figure 2.5D and 2.5G). Upon analyzing regressions for the PTC-ring nucleotides' mutational flexibility against distance from each tRNA, we found no significant relationships (Distance from A-site tRNA: R^2=0.154, p=0.13; Distance from P-site tRNA: R^2=0.001, p=0.93), indicating that nucleotide distance alone does not explain the observed variation in mutational flexibility within this loop (Supplementary Figure 2.9).

2.4.5 Studying multi-mutant ribosomes *in vitro*

A core hypothesis of the work in this chapter is that mutations in the PTC of the ribosome can promote routes to novel sequence defined polymers (SDPs). Testing this requires the ability to rapidly build both single and multi-mutant ribosomes, which we demonstrate here. Using iSAT, we have conclusively demonstrated that even though the ribosome's active site is highly conserved, it is amenable to both single and multi-mutations. Furthermore, we have demonstrated that multi-mutations can impact synergies between single mutations and in some cases, rescue translational activity. Specifically, we used iSAT to expand our mutational mapping studies and synthesized a subset of rRNA multi-mutant base changes in the ribosome's active site (PTC-, A-, and P-loops), revealing a set of compensatory mutations that improve translational activity above that of single mutations.

As a first step in characterizing multi-mutants in the ribosome's active site, we used our sequence alignment and nucleotide conservation analysis to identify nucleotide positions where two or more base changes were shared across a subset of species (Figure 2.6). These changes and positions we termed co-variation mutants; or mutants that have more than one nucleotide change at different positions, across the same subset of species. We then used traditional cloning techniques to build these constructs, and subsequently tested these in iSAT.

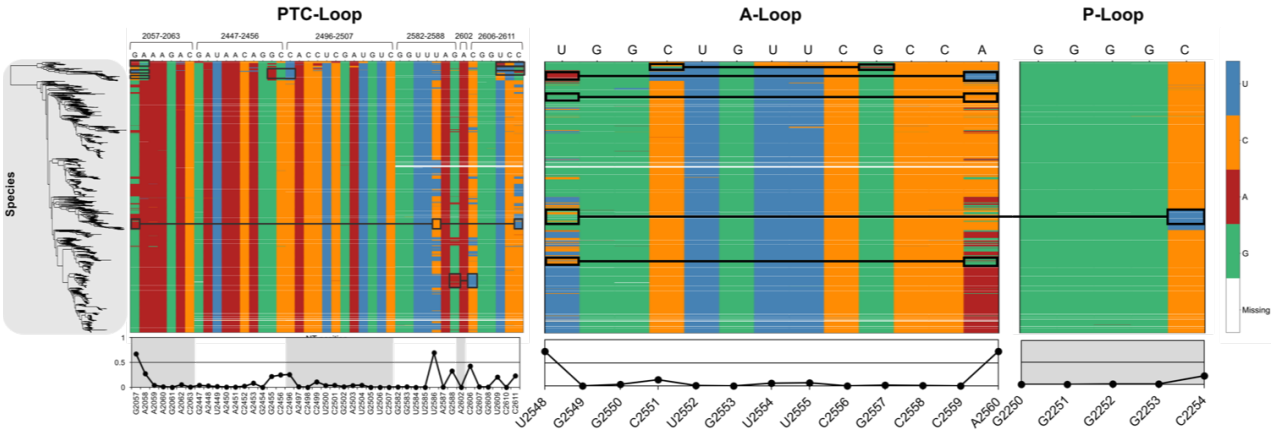

Figure 2.6 Sequence alignment and Shannon entropy plot representing the conservation of PTC nucleotides across 1,614 bacterial and archael species. Shannon entropy values of zero represent 100% conservation across all species. The black boxes and lines highlight the positions of co-variance.

To assess translational activity of each multi-mutant, we measured the protein synthesis yields of iSAT reactions possessing wild-type and multi-mutant ribosomes after 20-hour reactions (Figure 2.7). Relative activity was subsequently calculated. First, wild-type protein synthesis yields were normalized to one, and mutant yields were normalized and set relative to wild-type.

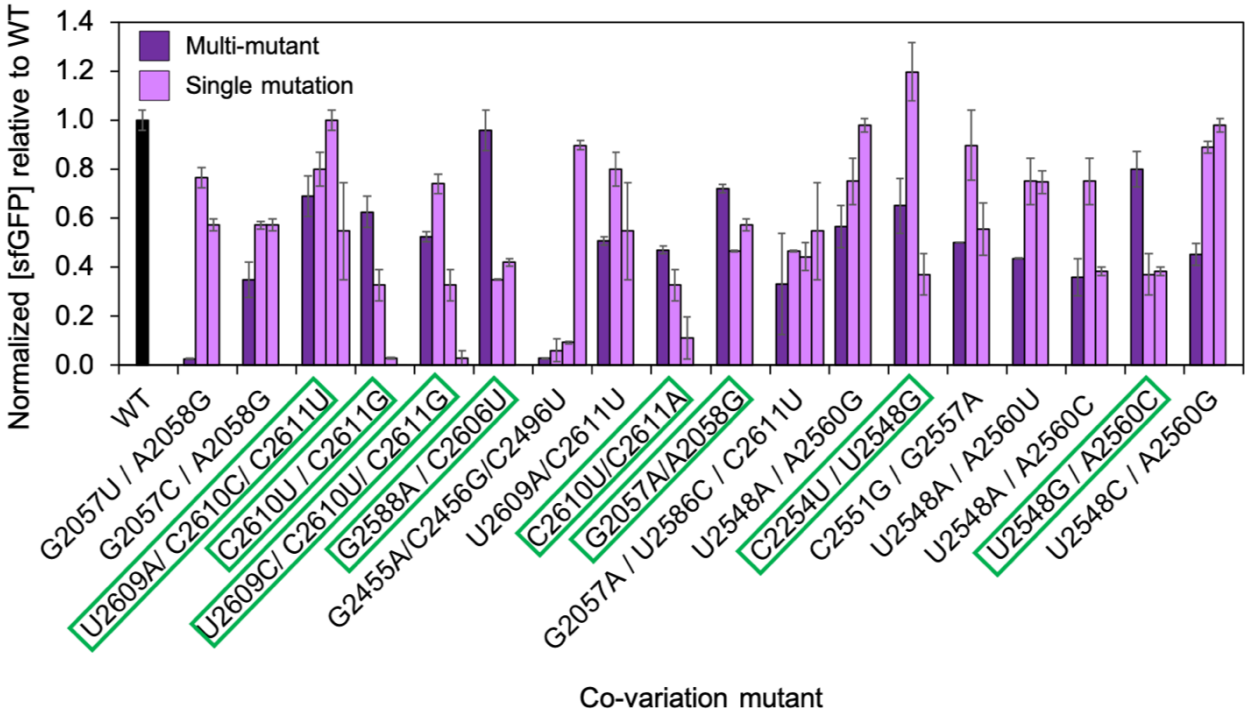

Figure 2.7 Activity of each PTC multi-mutant relative to the activity of wild type iSAT ribosomes. The multi-mutants highlighted with green boxes represent those multi-mutants whose activity exceeded that of one or more of the individual single mutants.

Surprisingly, despite the highly-conserved nature of the ribosome's active site, almost half (~45%) of the multi-mutants exhibited rescuing activity, wherein the combination of mutations resulted in improved activity as compared to the corresponding single mutations (Figure 2.7). These results will aid future endeavors to combine ribosomal active site mutations for the synthesis of SDPs. Specifically, we have now identified a subset of secondary mutations, that when combined with another active site mutation, can improve its activity. Thus, if engineering the ribosome's active site requires mutations that negatively impact translation, we can imagine coupling those mutations to co-evolved or co-variation base changes to improve their activity while maintaining their engineered identity.

2.5 Discussion

Here, using the iSAT platform, we systematically designed, built, and characterized 180 single point mutations within the ribosome's active site; specifically, targeting rRNA nucleotide positions that have been considered essential to peptide bond formation. Importantly, we have demonstrated that our results: (i) corroborate and build upon previous biochemical and structural studies; (ii) provide a comprehensive mutational map for future synthetic biology and engineering applications; and (iii) provide mechanistic insight into peptide bond formation.

When comparing our results to previously published works, we find that our data fit well into early biochemical and structural studies; validating the power and accuracy of the iSAT system. For example, when looking at translation activity, our results align closely with others. In their 1996 study, Porse and colleagues assayed rRNA mutants for peptidyl transferase activity *in vitro* using a fragment assay [202]. They found that upon mutating U2585 to U2585G, this mutation retained 36% of its peptidyl transferase activity (21% activity in our work) whereas U2585A and U2585C were <6% active (~2% activity in our work). Furthermore, the authors found that G2253A, G2253U, and G2253C carried 19%, 42%, and <5% *in vitro* activity, respectively (in the same order: 55%, 40%, and 14% activity in our work). Additional mutants in their study possess activities comparable to ours. In separate work conducted by Thompson and colleagues, the authors analyzed mutations at nucleotides A2451 and G2447. Upon characterizing peptidyl transferase activity, the authors found A2451C decreases the rate of reaction ~3-fold. In our work the protein synthesis activity of A2451C is reduced 2-fold [171].

Additionally, our results corroborate previous readthrough studies as well. Specifically, we demonstrate impaired readthrough of A2451C, A2451U, C2496G and U2585G mutants. These results are consistent with published findings demonstrating that mutations of U2585 lead to a decrease in rate of factor-catalyzed peptide release [64,197]. Thompson and colleagues also demonstrated that when probing translation readthrough A2451C and A2451U exhibited increased readthrough of a UGA premature stop codon ~2-fold [171]. Similarly, our work shows UGA stop codon readthrough of ~1-fold and ~2-fold for A2451C, and A2451U, respectively.

Upon comparing our assembly profiles to those in the literature, we also find several parallels. First, our assembly assay results confirm that rRNA possessing base changes are still capable of forming functional particles for protein synthesis [171]; but also highlight mutant G2455A as possessing defects in maintaining a fully assembled 70S structure (including polysomes). More specifically, upon assaying incorporation of the mutated 23S rRNA into ribosomal particles, Porse and colleagues found that U2585G possessed a greater fraction of 50S subunits compared to 70S species, which we found in this work as well (Supplementary Table 2.4) [202]. When Thompson and colleagues analyzed mutations at nucleotides A2451 and G2447, the authors found that A2451U assembled into 70S particles and accumulated in polysomes, however, at decreased levels compared to wild-type—mirroring our results [171,203,204].

Lastly, across the literature, there are commonly used antibiotic resistance mutations within the ribosome. A prime example is at positions A2062 and A2058. A2062U and A2058U confer macrolide resistance in *E. coli* and other bacteria [205]. We would expect that if our results match the mutants' activity in the cell, that these well-studied PTC mutations would have high or almost wild-type activity. Indeed, in our results, we found that A2062U and A2058U possess 94% and

84% of wild-type activity, placing these nucleotides in the shell of "highly mutationally flexible nucleotides" on our map. Importantly, the published results presented here align well with our iSAT activity results; confirming that our platform is robust and generates assembled *E. coli* ribosomes with function that closely mimics that of the cell.

In addition to corroborating previous studies, our work has also resulted in a comprehensive mutational flexibility and characterization map of the ribosome's active site. This map represents a significant advancement, especially as an experimental tool, for future ribosome engineering efforts. Specifically, our map highlights (in red) the essential role of G2553, G2252, and G2251 in positioning tRNA molecules for peptidyl transfer [158,173,206], and the dependence of faithful hydrogen bonding and wobble pairing within the triple-base pocket C2501·A2450·C2063 [201] (Figure 2.5D). Our findings corroborate and elaborate on other findings that aimed to pinpoint a more specific mechanism for the role of these bases. For instance, in their 2010 paper, Chirkova and colleagues found that modifications at positions A2450-C2063, impair translation activity, while having little impact on peptide bond formation, tRNA drop-off, or ribosome-dependent EF-G GTPase activity. Together, these data support the hypothesis that the wobble pair between A2450 and C2063 plays a critical role in tRNA translocation through the PTC [207]. Similarly, Bayfield and colleagues found that the A2450-C2063 wobble pair do not play a direct role in peptidyl transferase activity, rather, they may function to maintain the correct structure of the active site in the context of the identity of other residues in the vicinity [208]. Our map also illustrates the flexibility and the dispensable nature of nucleotides surrounding the exit tunnel, offering new questions regarding the evolution and necessity of these positions (Figure 2.5G). Finally, our map also demonstrates the complexity of rRNA loop arrangements within the ribosome. Our results

indicate that a nucleotide's mutational flexibility, or dispensability, can be dependent on its position with respect to tRNA molecules (A- and P-loop flexibility gradients), or simply to neighboring nucleotides (PTC-ring mutational pockets and shells) **(**Figure 2.5A-C and 2.5J). Taken together, our results show that many active site mutated ribosomes can faithfully carry out protein synthesis, implying that these conserved nucleotides are not strictly indispensable for ribosome-catalyzed peptide bond formation.

Finally, when extrapolating our findings to better understand the chemistry and mechanism of peptide bond formation, our work not only corroborates previous findings, but also illuminates new results for mutations that were not previously well-studied. First, our work confirms previous hypotheses that PTC-ring nucleotides may play a key role in release factor binding and peptide release [209], and thus mutating these positions may alter these functions. However, the work presented here also adds a new PTC-ring nucleotide mutation to this growing list: C2496G; which currently lacks functional and mutational studies (Supplementary Table 2.1). On the other hand, the juxtaposed A- and P-loops, which displayed no impact on translation readthrough, do not appear to be implicated in release factor binding or hydrolysis. Instead, these nucleotides may play a role in tRNA selection by the ribosome. Specifically, upon aminoacyl-tRNA release from elongation factor-Tu, the A-loop may aid in accommodation of aminoacyl-tRNA into the A-site, permitting subsequent peptide-bond formation [210]. Thus, binding of tRNA by the A-loop may act as a 50S checkpoint coupled to accommodation in the small subunit's decoding center. Although our assays alone are not capable of discriminating between translation fidelity and termination but rather characterize them together; when taken together with other published findings, our work provides evidence supporting key roles for these nucleotides in substrate positioning and release.

Efforts to identify the molecular mechanism by which mutations in the large subunit incur miscoding are not well-understood. Although the small subunit is largely recognized as the site of decoding, previous studies have identified decoding changes upon mutating the large subunit [188,190,198,211]. It is hypothesized that the arrangement and geometry of the tRNAs in elongating ribosomes is perturbed by these active site mutations, thus decreasing the rate of peptidyl transfer and promoting errors in mRNA decoding [158,159,190,198,212].

In summary, the *in vitro* iSAT platform allowed us to rapidly produce (in hours) and study populations of mutant *E. coli* ribosomes without contamination of wild-type species or cell-viability constraints [51]. In our first step towards characterizing these mutations, we discovered that despite the high degree of conservation within the ribosome's active site (~75% of the nucleotide positions are 100% conserved), more than 85% of the rRNA PTC nucleotides are still mutationally flexible to a variety of base changes. Of note, we found that sequence conservation alone was a poor proxy for predicting mutational flexibility (Supplementary Figure 2.5). Next, we employed a premature stop codon assay to study readthrough impairments, which could be caused by decreased translation accuracy or release factor fidelity (decreased binding affinity or hydrolysis). We observed increased levels of translation readthrough with four unique PTC-ring mutants (C2496G, A2451C, U2585G, and A2451U), but no translation readthrough across a subset of A- and P-loop mutants (C2559A, C2551A, U2552G, C2559A, C2551A, and U2552G). In our final functional assay, we assessed ribosome assembly across a suite of high-, medium- and low-activity mutants with sucrose gradient fractionation. The results of our assay are consistent with the presence of lower activity mutant ribosomes possessing reduced populations of 70S and

polysomes. In particular, G2455A possessed primarily 30S and 50S subunits, and almost no functional 70S or polysomes.

Looking forward, we anticipate that our work may open new opportunities to engineer mutant ribosomes for novel purposes [91-93,175,213-217]. Whether the engineering involves expanding the ribosome's exit tunnel (most mutationally flexible and dispensable) or co-evolving nucleotide pockets that appear to rely on key hydrogen bonding and base-pairing (the most mutationally inflexible nucleotides), our new systems-level understanding could help guide ribosome re-design [218]. This in turn will increase our understanding the process of translation to advance new synthetic biology applications.

2.6 Data availability

The Protein Data Bank (PDB) is an open source archive containing information about experimentally-determined structures of proteins, nucleic acids, and complex assemblies. (https://www.rcsb.org/pdb/home/home.do)

Atomic coordinates and structure factors for the ribosome crystal structure used in the described analyses can be found within the Protein Data bank under accession number 4YBB [219] and 1VY4 (tRNA molecules) [143].

PyMol is a computer software, a molecular visualization system (https://pymol.org/2/).

Code used for sequence aligning, sequence matrix visualization and entropy plotting is open source and available in the GitHub repository (https://github.com/adamhockenberry/23s-alignment-LTP).

2.7 Acknowledgements and contributions

The authors would like to acknowledge Dr. Andrea d'Aquino, Dr. Steven Swick, Dr. Ashty Karim, Dr. Alexander Mankin, and Dr. Nora Vazquez-Laslop for their thoughtful review of the manuscript. The authors would also like to thank Dorota Klepacki for their help and insight with running the sucrose gradient fractionations.

Anne d'Aquino and Dr. Michael Jewett conceived the study and wrote the manuscript, Anne d'Aquino and Tasfia Azim prepared DNA constructs. Anne d'Aquino and Tasfia Azim designed experiments and Anne d'Aquino performed experiments. Nikolay A. Aleksashin computationally calculated nucleotide distances for structural studies, analyzed activity and distance relationships via crystal structure maps, and produced the supplementary video. Adam J. Hockenberry performed and analyzed sequence alignments. Antje Kruger prepared sucrose gradients and performed fractionations.

This work was supported by the Army Research Office Grant W911NF-18-1-0181 and W911NF-16-1-0372 (to M.C.J.); National Science Foundation Grant MCB-1716766 (to M.C.J.); Northwestern University Biophysics Training Program (A.E.D., in part); Northwestern University Ryan Fellowship (A.E.D); Northwestern University Presidential Fellowship (A.E.D.); and National Science Foundation Graduate Research Fellowship Program (A.E.D). M.C.J also acknowledges the David and Lucile Packard Foundation and the Camille Dreyfus Teacher-Scholar Program. Source of open access funding: Army Research Office W911NF-16-1-0372.

2.8 Patent information

Jewett, M.C.; d'Aquino, A.E.; Ribosome Variants for Sequence Defined Polymer Synthesis. **2018**. *US Patent Application Serial No. 62/694,553*.

2.9 Supplementary figures and tables

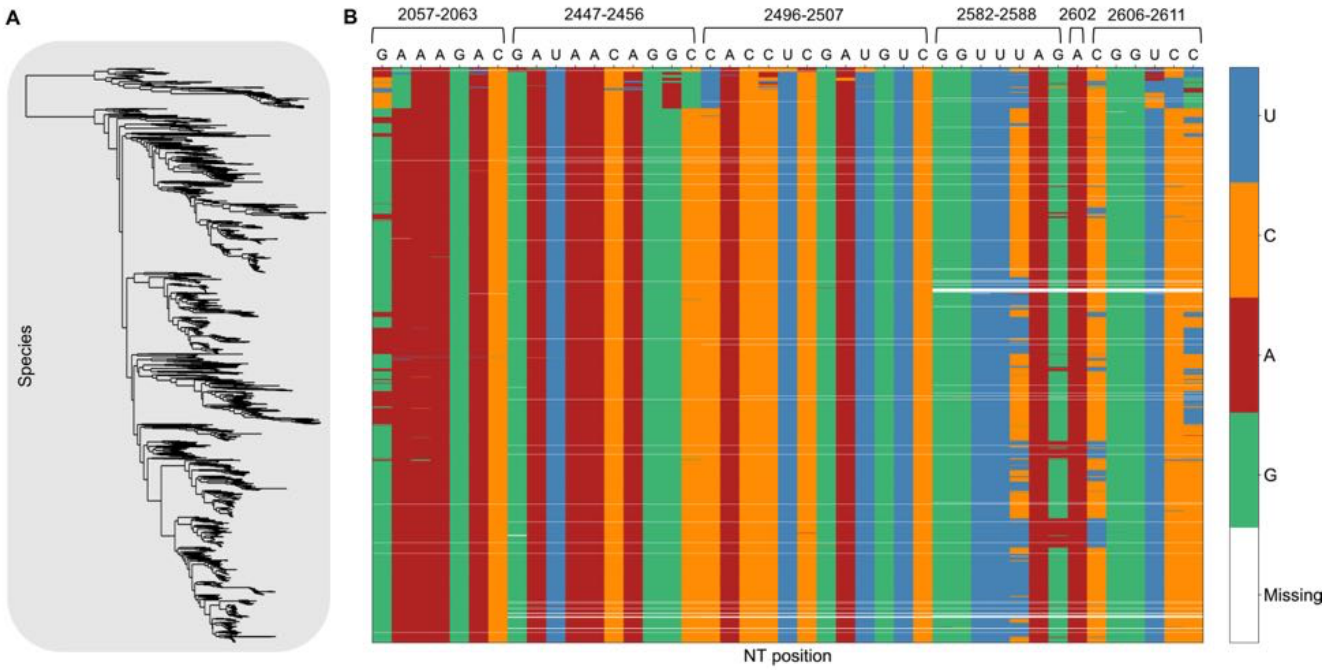

Supplementary Figure 2.1 The ribosome's peptidyl transferase center (PTC) is highly conserved. (a) Phylogenetic tree of the species used for the rRNA sequence alignment. The left to right distance for any branch of the tree represents the amount of sequence divergence from the "root" (far left) to the actual sequence (the leaves, far right). (b) Sequence alignment matrix illustrating the conservation of PTC nucleotides across 1,614 species of bacterial and archael species. All LSU sequences were taken from alignments found in the SILVA database (43). The ribosome's PTC is highly conserved across both bacterial and archael species.

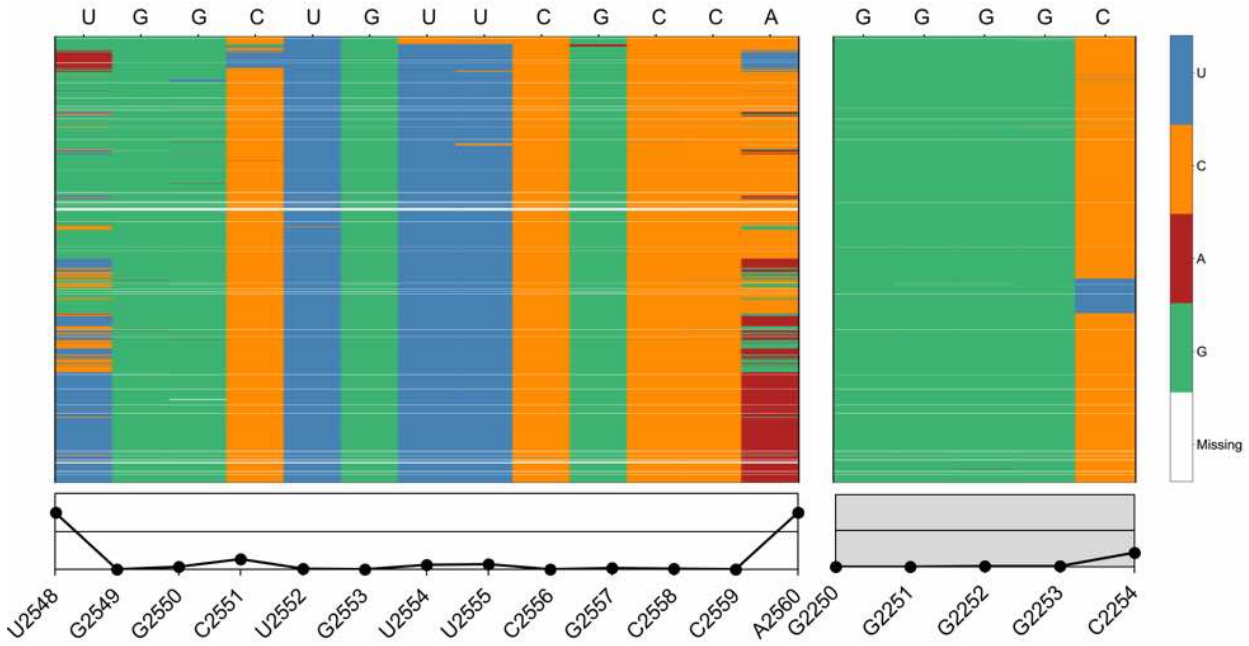

Supplementary Figure 2.2 The ribosome's A- and P-loops are highly conserved. Sequence alignment illustrating the conservation of PTC nucleotides across 1,614 species of bacterial and archael species. All LSU sequences were taken from alignments found at https://www.arb-silva.de/projects/living-tree/. The ribosome's PTC is highly conserved across both bacterial and archael species. Shannon Entropy scores are akin to variance scores (though we caution that they ignore phylogenetic relatedness), with a Shannon Entropy of zero representing zero variance (100% conservation across the 1,614 species). Any values above zero indicate that evolutionary changes have occurred and result in multiple nucleotides within a given site in the alignment.

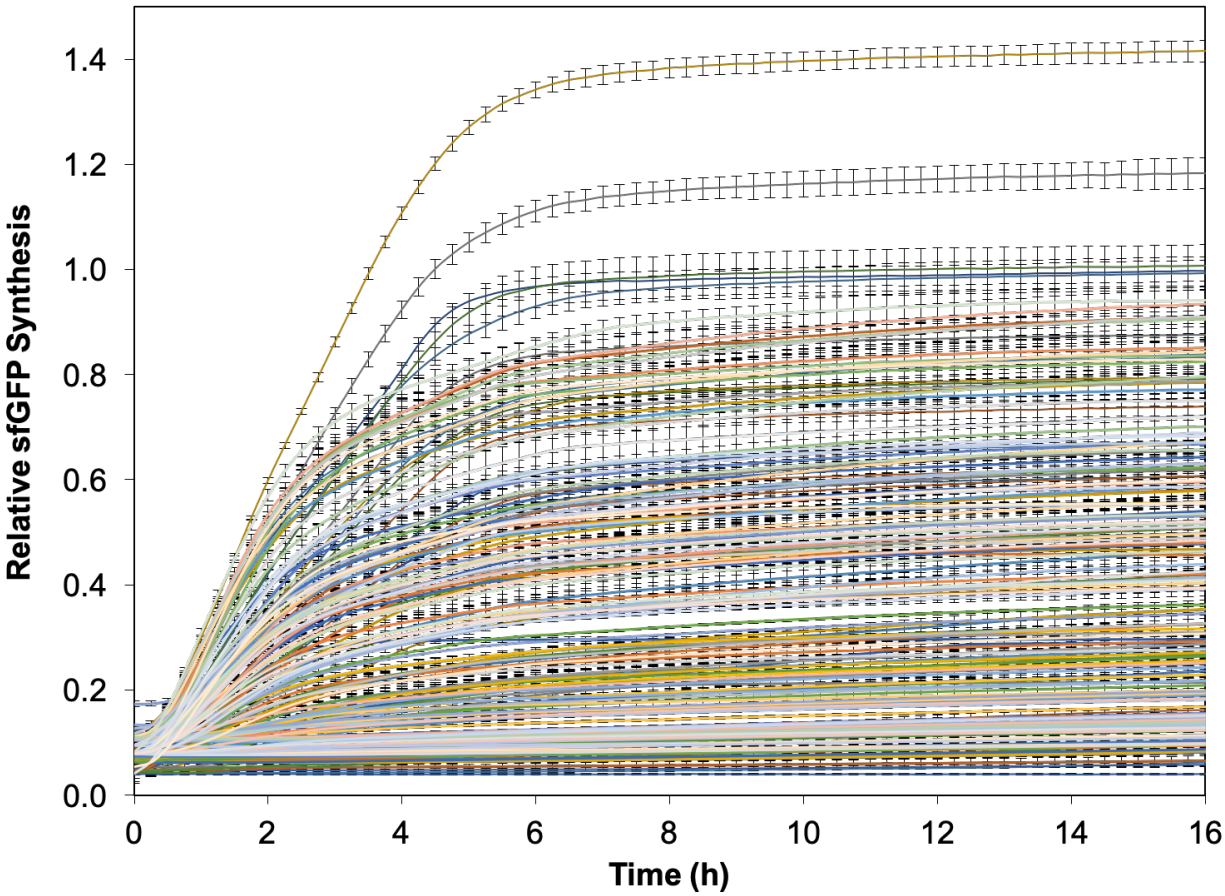

Supplementary Figure 2.3 Protein synthesis kinetic time course curves from iSAT reactions for all individual nucleotide mutations probed in the PTC-ring, A-loop, and P-loop. Smoothed data from samples taken every 15 minutes are shown. Values represent averages and error bars represent one standard deviation from the mean, with $n \geq 3$ for n number of independent reactions.

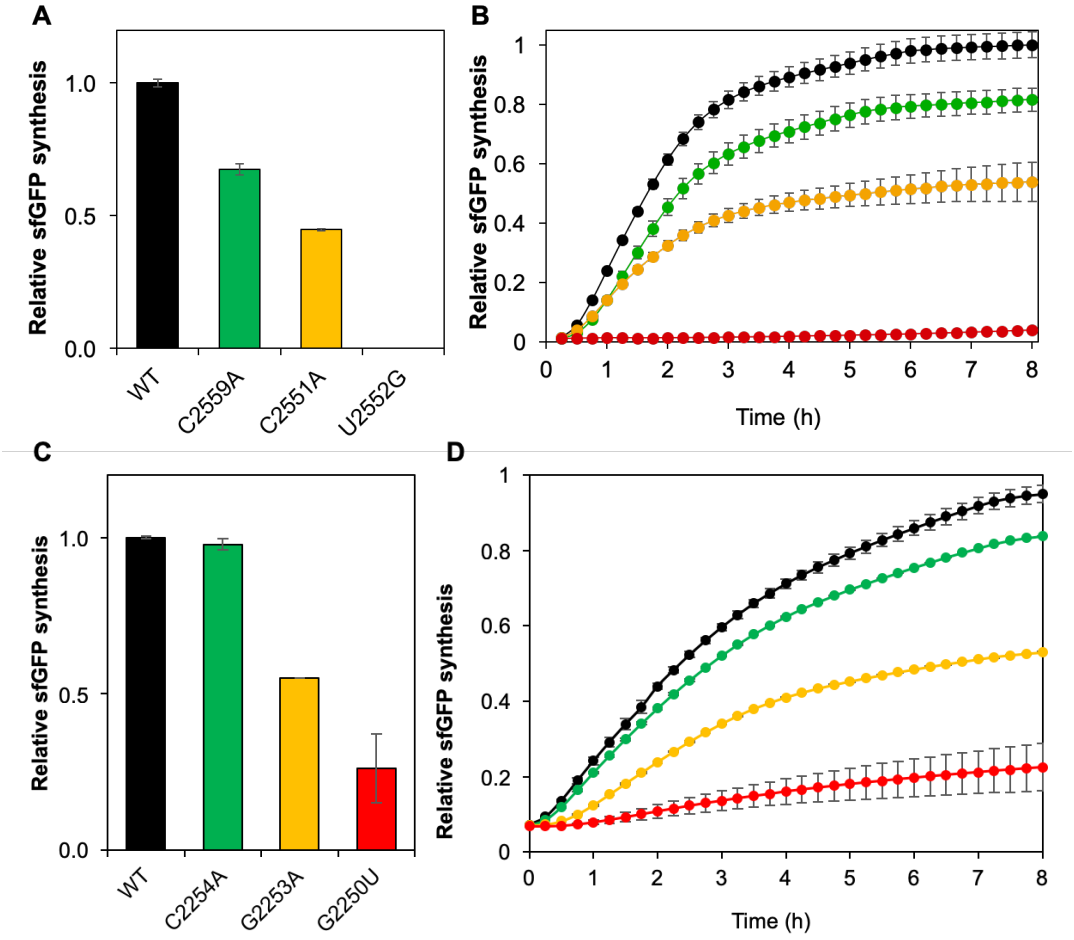

Supplementary Figure 2.4 Ribosomes with mutations in the A- and P-loops demonstrate decreased bulk protein synthesis rates. (a) Relative protein synthesis activity of A-loop mutants tested in translation assays. (b) Protein synthesis kinetic time course curves from iSAT reactions for the following A-loop nucleotide mutations have been included in this graph: C2559A, C2551A, U2552G. Protein synthesis rates are proportional to relative protein synthesis titers. For simplicity and ease of visualization, not all nucleotide mutation kinetic curves are included on the graph. Values represent averages and error bars represent one standard deviation from the mean, with n $\geq$ 3 for n number of independent reactions. (c) Relative protein synthesis activity of P-loop mutants tested in translation assays. (d) Protein synthesis kinetic time course curves from iSAT reactions for the following P-loop nucleotide mutations have been included in this graph: C2254A, G2253A, G2250U. Protein synthesis rates are proportional to relative protein synthesis titers. For simplicity and ease of visualization, not all nucleotide mutation kinetic curves are included on the graph (see Supplementary Figure 2.3). Values represent averages and error bars represent one standard deviation from the mean, with n $\geq$ 3 for n number of independent reactions.

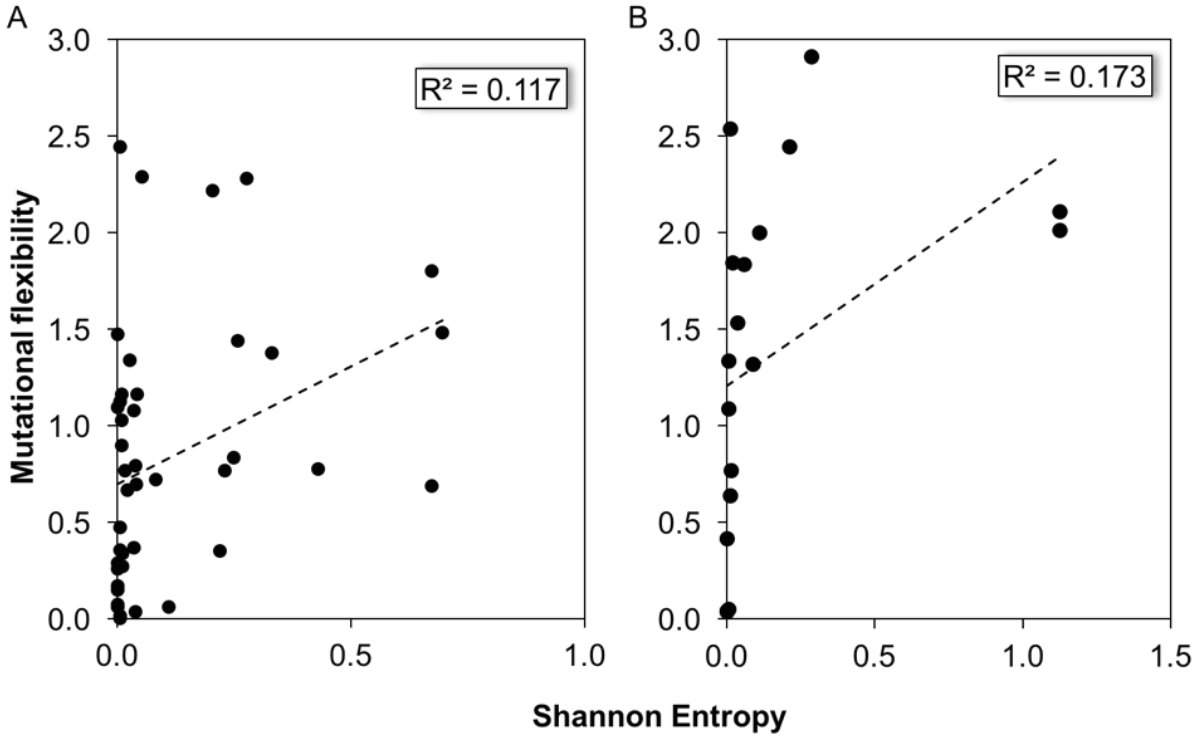

Supplementary Figure 2.5 Regression models of Shannon entropy (nucleotide conservation) against mutational flexibility (the sum of all nucleotide mutations' relative activity). (a) The regression plot for the PTC-ring possesses a low R^2 value (R^2 =0.117, p=0.025) demonstrating difficulty in predicting mutational flexibility from nucleotide conservation. (b) The regression plot for the A- and P-loops also possesses a low R^2 value (R^2 =0.173, p=0.086) demonstrating difficulty in predicting mutational flexibility from nucleotide conservation.

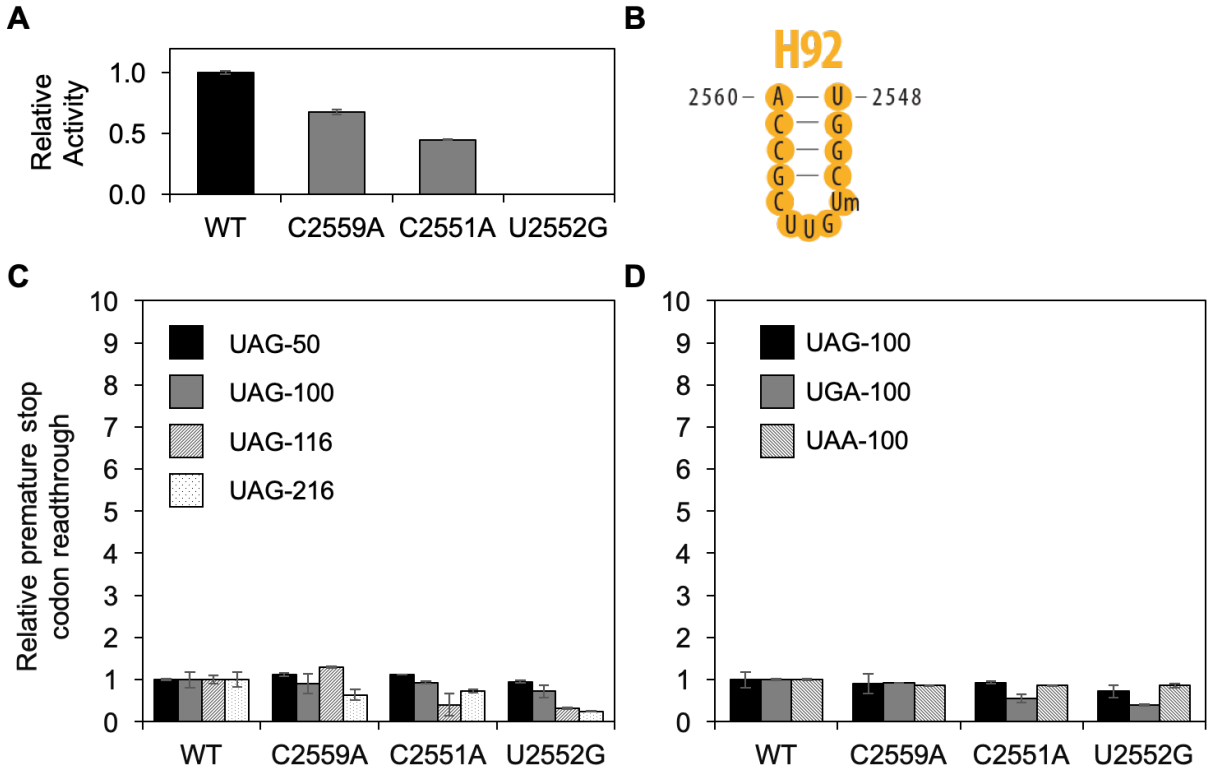

Supplementary Figure 2.6 Ribosomal A-loop mutations do not increase stop-codon readthrough. (a) Relative protein synthesis activity of A-loop mutants tested in translation fidelity assays. (b) A-loop secondary structure. (c) UAG stop codon readthrough at amino acid position 50, 100 ,116, and 216 of sfGFP. (d) UAG, UGA, and UAA stop codon readthrough at amino acid position 100 of sfGFP. As described in the main text, the relative readthrough activity in translation fidelity assays using premature stop codons was assessed using sfGFP fluorescence. sfGFP levels obtained with wild-type rRNA plasmids are normalized to 1, and values obtained with each of the mutants were expressed relative to that obtained with the respective wild-type rRNA plasmid. To enable comparison with Figure 3 from the main text, the y-axis values are extended to 10 in c and d. Values represent averages and error bars represent one standard deviation from the mean, with n $\geq$ 3 for n number of independent reactions.

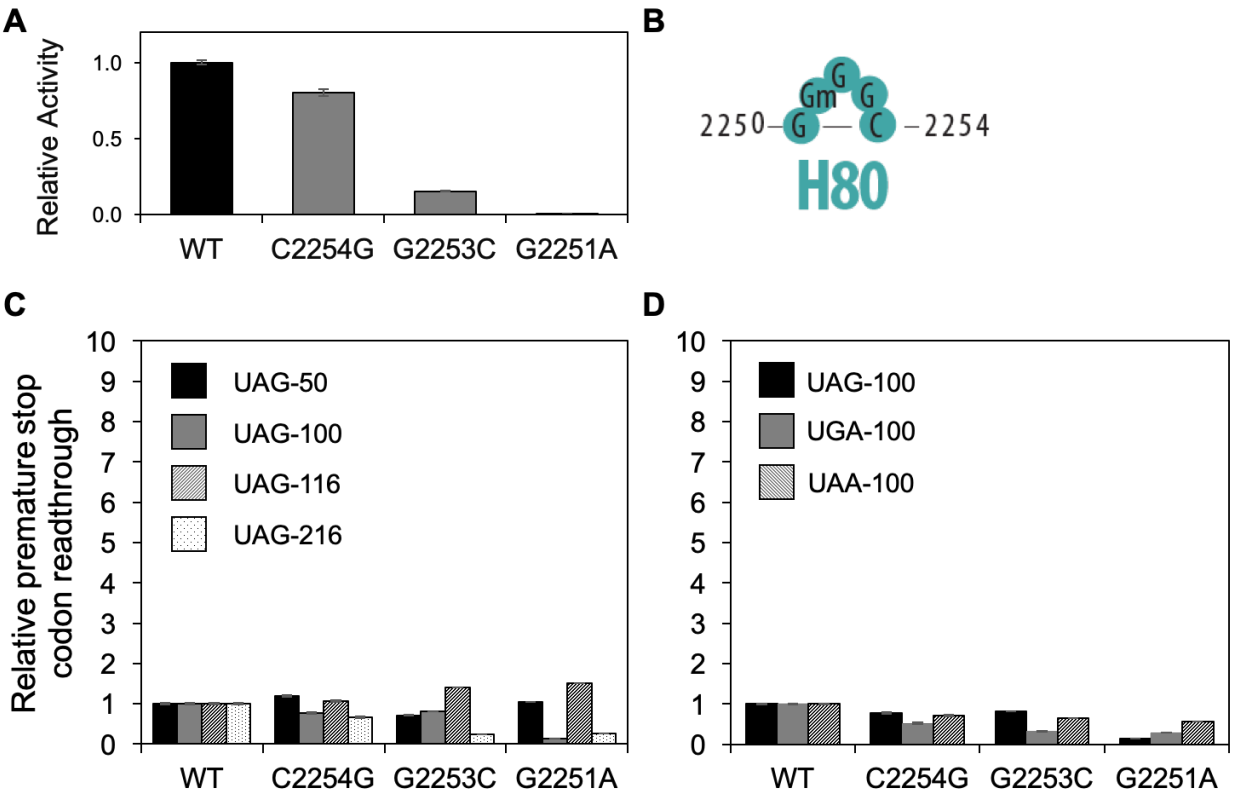

Supplementary Figure 2.7 Ribosomal P-loop mutations do not increase stop-codon readthrough. (a) Relative protein synthesis activity of P-loop mutants tested for fidelity. (b) P-loop secondary structure. (c) UAG stop codon readthrough at amino acid position 50, 100 ,116, and 216 of sfGFP. (d) UAG, UGA, and UAA stop codon readthrough at amino acid position 100 of sfGFP. As described in the main text, the relative readthrough activity in translation fidelity assays using premature stop codons was assessed using sfGFP fluorescence. sfGFP levels obtained with wild-type rRNA plasmids are normalized to 1, and values obtained with each of the mutants were expressed relative to that obtained with the respective wild-type rRNA plasmid. To enable comparison with Figure 3 from the main text, the y-axis values are extended to 10 in c and d. Values represent averages and error bars represent one standard deviation from the mean, with n $\geq$ 3 for n number of independent reactions.

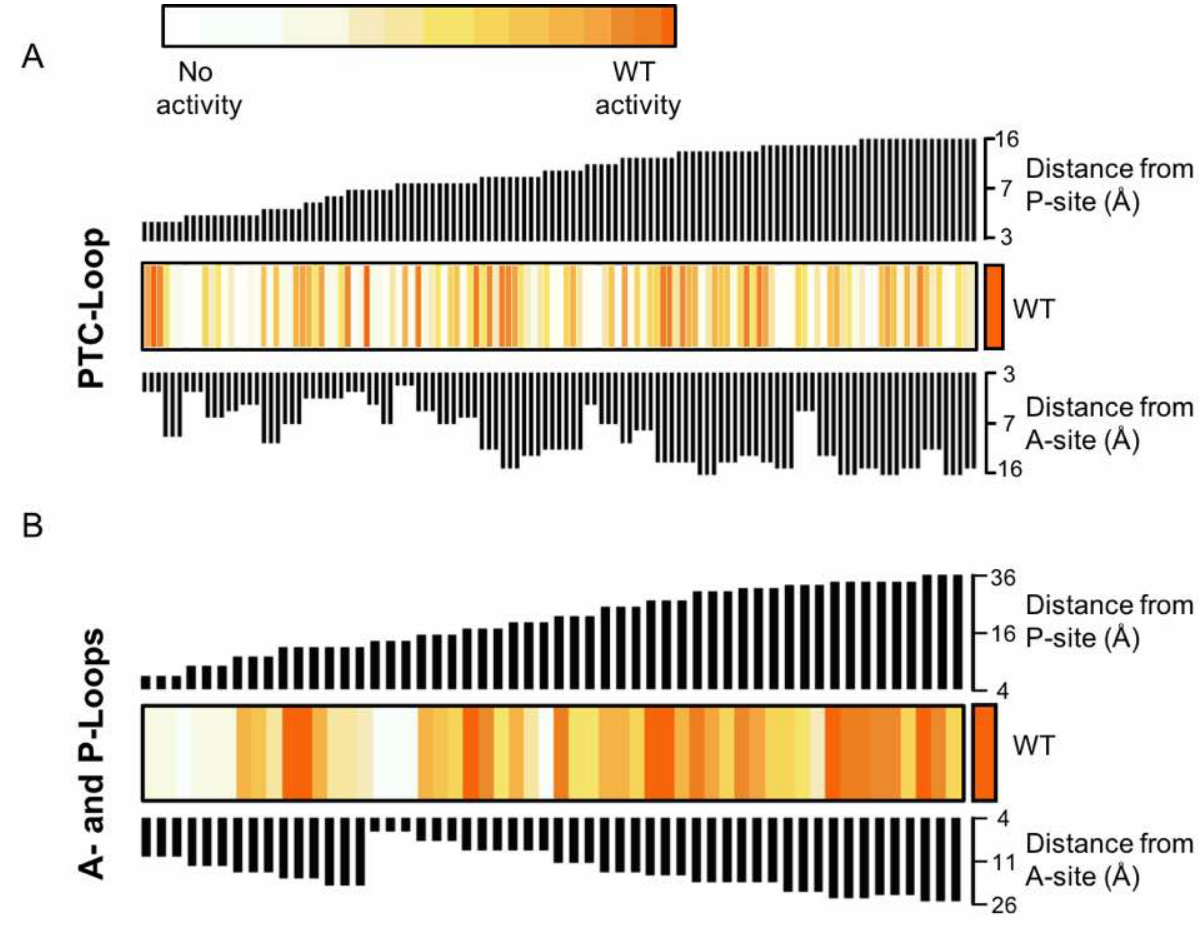

Supplementary Figure 2.8 The ribosome's peptidyl transferase center (PTC) is composed of functional pockets. (a) Heat map of rRNA PTC-ring and (b) A- and P-loop mutational activity against their distance from the P-site tRNA (top) and A-site tRNA (bottom). White shading illustrates zero activity, while dark orange shading illustrates WT-activity.

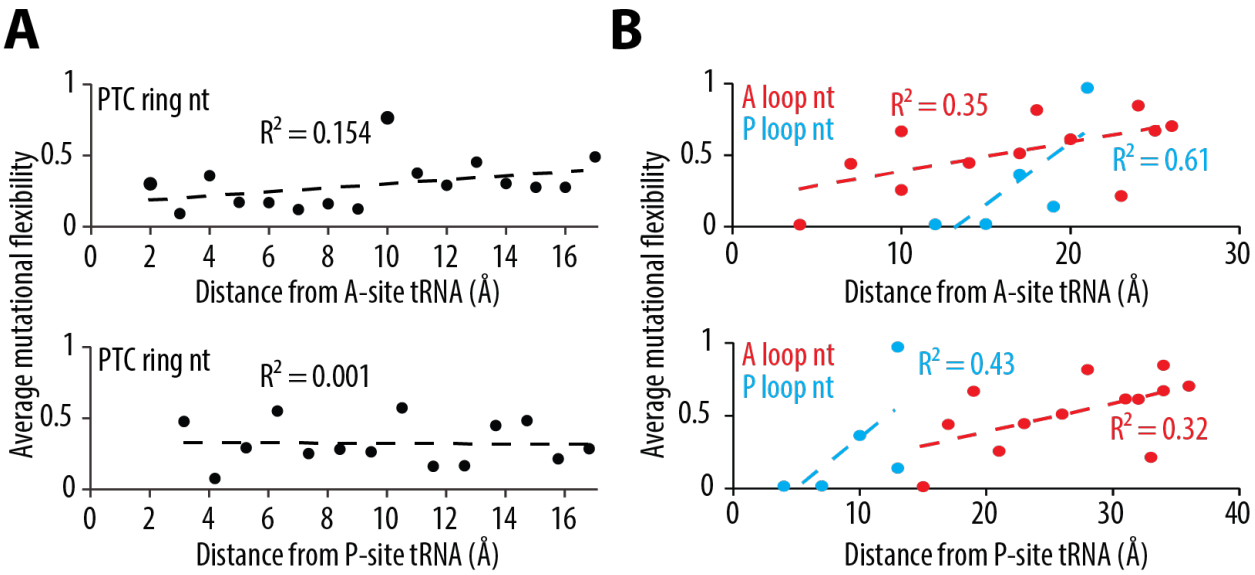

Supplementary Figure 2.9 Regression models of nucleotide distance against mutational flexibility. (a) Regression model of distance from A-site (R^2=0.154, p=0.13) and P-site (R^2=0.001, p=0.93) tRNA against mutational flexibility of PTC-ring nucleotides suggests a non-significant (p>0.05) and weak (low R^2 values) relationship. (b) Regression model of distance from A-site and P-site tRNA against mutational flexibility of A- (red) and P-loop (blue) nucleotides. The regression plots for the A-loop nucleotides possess R^2 values of 0.35 (p=0.03) and 0.32 (p=0.04), respectively. The regression plots for the P-loop nucleotides possess R^2 values of 0.61 (p=0.12) and 0.43 (p=0.23), respectively. The regressions and p-values for the A-site nucleotides suggests a significant and predictive relationship between mutational flexibility and distance from tRNA molecules; while the P-site nucleotides suggests a predictive relationship, however this relationship is non-significant due to a small sample size.

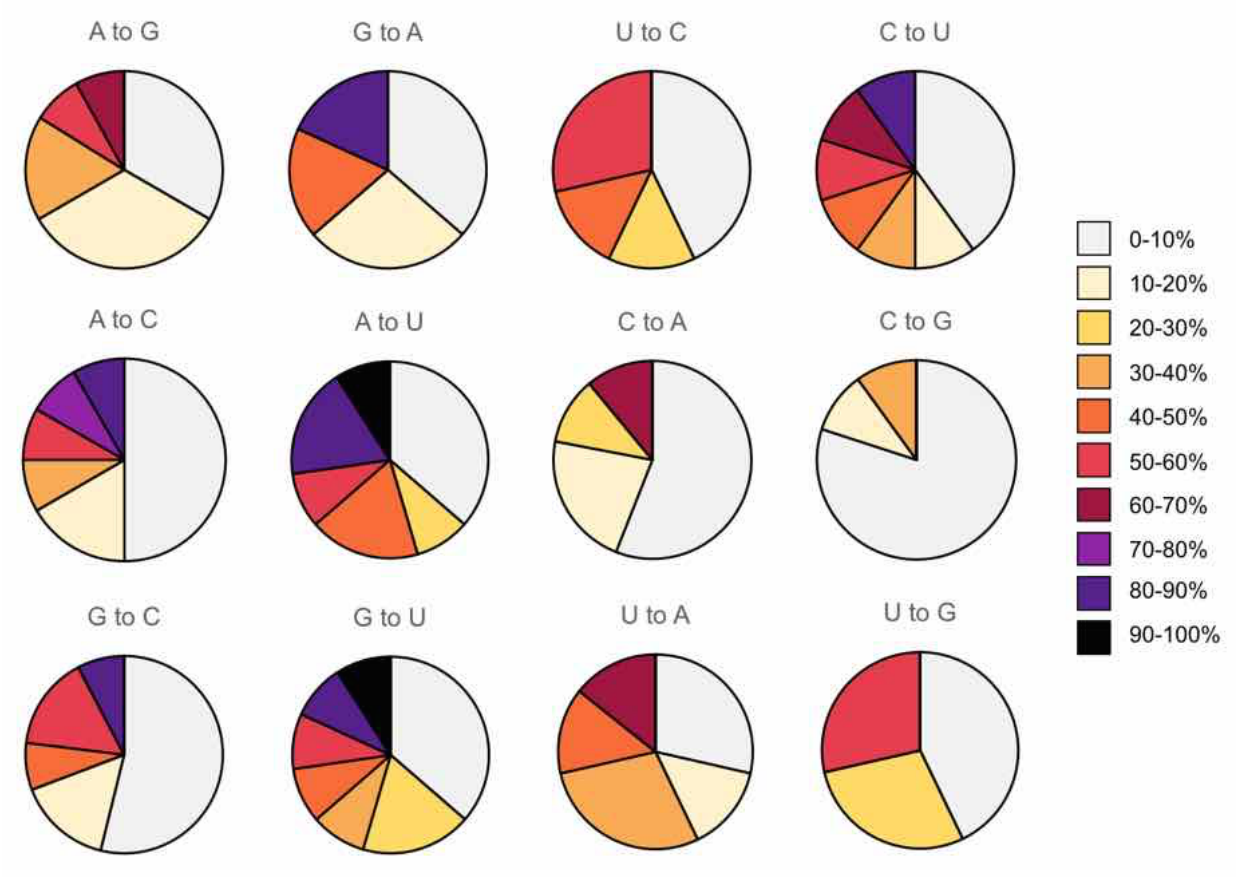

Supplementary Figure 2.10 Comparison of ribosomal mutant activity vs. nucleotide base change within the PTC-ring. Nucleotide changes from C to A, C to G, and G to C have the lowest activity, with ~70-90% of the nucleotides exhibiting less than 20% of WT activity. In contrast, changes from G to A, A to U and G to U exhibit the highest activity, with ~20-30% of the nucleotides exhibiting 80-100% of WT activity.

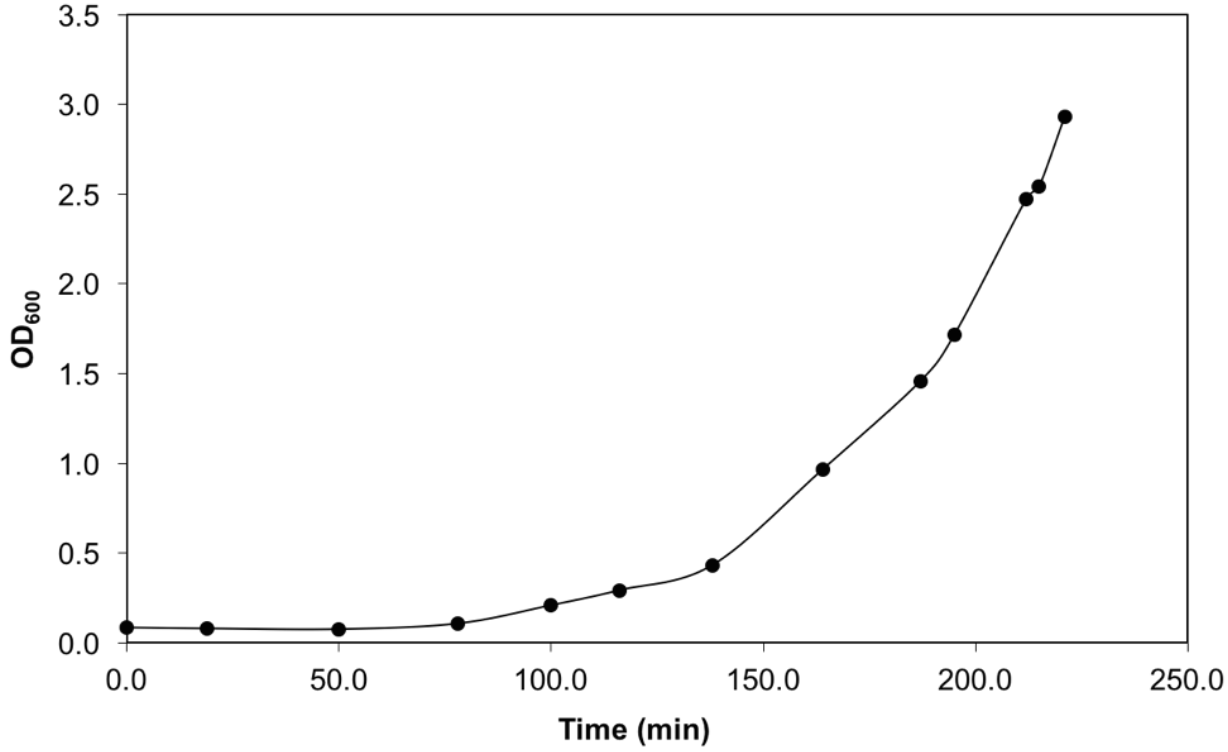

Supplementary Figure 2.11 Growth curve of E. coli MRE600 strain used in this study. Cells were grown in 10L of 2xYTPG media and harvested from the fermenter at OD = 2.9–3.1. Cells were grown at 37C, as previously reported.

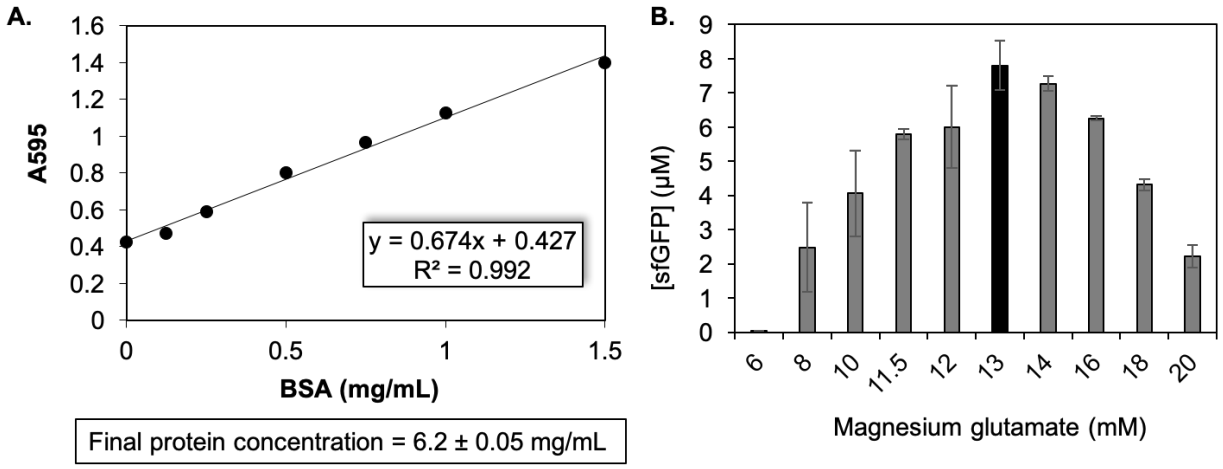

Supplementary Figure 2.12 Extract testing and optimization. (a) Protein concentration of S150 extract used in this paper. Values represent average concentrations as determined by Bradford assay with bovine serum albumin (BSA) as a standard. Error bars represent one standard deviation from the mean for triplicate measurements. (b) Magnesium optimization of S150 extract for reporter protein synthesis in iSAT reactions. Standard 15 μL batch reactions were performed at 37°C for 20 h, with varying magnesium glutamate concentrations the S150 extract used. Total protein concentration of each S150 extract added to reactions was standardized at 3.6 mg mL^{-1}. Synthesis of active wild-type (wt) sfGFP was measured after 20 h using fluoresence. Optimal magnesium glutamate concentrations for iSAT reactions was determined to be: 13 mM for MRE600. This concentration was then used for subsequent experiments. Values represent averages and error bars represent one standard deviation from the mean, with $n \geq 3$ for n number of independent reactions.

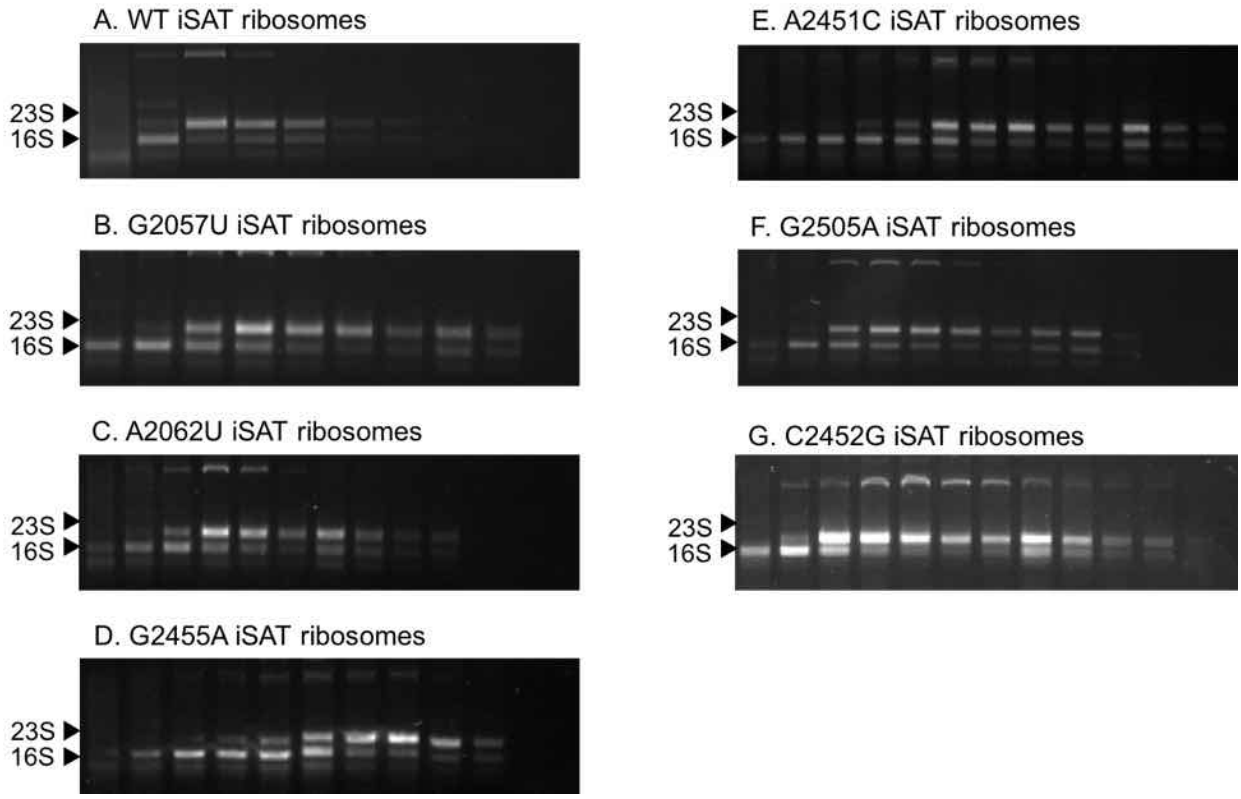

Supplementary Figure 2.13 Gel electrophoresis analysis of WT and mutant iSAT ribosomes following sucrose density centrifugation. A 120 µL iSAT reaction possessing a reporter plasmid was analyzed by polysome profiling in a 10-40% sucrose gradient. The resulting 500 µL – 1 mL fractions were run by electrophoresis on a 1% agarose gel (one fraction per well). The rRNA contained within each fraction was used to confirm the predominate peaks as containing 30S, 50S, or 70S subunits.

Supplementary Table 2.1 *E. coli* 23S rRNA PTC nucleotides and their published mutational studies.

rRNA Nucleotide	Mutational studies	Reference
G2057	• G2057A confers low-level resistance to erythromycin in *E. coli* • G2057C remains unstudied • G2057U remains unstudied	• Ettayebi, M., Prasad, S.M., and Morgan, E.A. J Bacteriol. 1985. 162(2): 551-557.
A2058	• A2058G confers macrolide resistance • A2058U confers clindamycin resistance • A2058C remains unstudied	• Xiong et al. Antimicrob. Agents Chemother. 2005. 49(1): 281-288. • Cochella & Green. PNAS. 2004. 101(11): 3786-3791. • Prunier, A., et al. Antimicrob Agents Chemother. 2002. 46(9): 3054-3056. • Pfister, P., et al. PNAS. 2005. 102(14) 5180-5.
A2059	• A2059G confers macrolide resistance in other bacteria (*E. coli* mutation unstudied) • A2059U remains unstudied • A2059C remains unstudied	• Poehlsgaard, J., et al. Antimicrob Agents Chemother. 2005. 49(4): 1553-1555.
A2060	• A2060G remains unstudied in *E. coli* (*M. bovis* exhibits tiamulin- and valnemulin resistance) • A2060U remains unstudied • A2060C remains unstudied due to lethality in vivo	• Sulyok, K. et al. 2017. Antimicrob Agents Chemother. 61(2): e-01983-16. • Vester, B., and Garrett, R. 1988. EMBO Jour. 7(11):3577-3587.
G2061	• G2061A remains unstudied in *E. coli* (antibiotic resistance in other bacteria – Pristinamycin resistant in *T. therophilus*) • G2061C remains unstudied in *E. coli* • G2061U remains unstudied in *E. coli* (tiamulin and valnemulin resistance in *M. gallisepticum* when in combination with other mutations; and clindamycin resistance in *T. gondii*)	• Gregory, S. et al. 2005. J. Bacteriol. 187(14): 4804-4812 • Li, B., et al. 2010. FEMS Microbiology letters. 308(2):144-149. • Camps, M., et al. Mol. Microbiol. 2002. 43(5): 1309-18.
A2062	• A2062G confers clindamycin resistance in *E. coli*. Confers macrolide resistance in other bacteria • A2062U confers macrolide resistance in other bacteria	• Cochella & Green. PNAS. 2004. 101(11): 3786-3791. • Furneri, P., et al. 2001. Antimicrob Agents

	• A2062C remains unstudied in *E. coli*. Confers 16-memberd macrolide resistance in *S. pneumoniae*.	Chemother. 2001. 45(10): 2958-2960. • Depardieu, F., and Courvalin, P. 2001. Antimicrob Agents Chemother. 2001. 45(1):319-323.
C2063	• C2063A remains unstudied • C2063U only studied in the context of A2450G mutation. The combination of mutations decreases rate of peptide bond formation. • C2063G remains unstudied	• Hesslein, A.E., et al. NAR. 2004. 32(12): 3760-3770.
G2447	• G2447A resistant to oxazolidinones • G2447U dominant lethal in vivo • G2447C resistant to streptomycin, but slow growth.	• Babkova, E.V., et al. JBC. 2003. 278(11): 9802-9807. • Thompson, J., et al. PNAS. 2001. 98(16) 9002-9007.
A2448	• A2448C remains unstudied • A2448G remains unstudied • A2448U remains unstudied	
U2449	• U2449A strongly dominant lethal in vivo • U2449G strongly dominant lethal in vivo • U2449C viable with no impact on growth rate	• Yassin, A.S. & Mankin, A.S. Journal of Biological Chemistry. 2007. 282(33): 24329-24342. • O'Connor, M., et al. NAR. 2001. 239(3): 710-5.
A2450	• A2450G strongly dominant lethal in vivo • A2450U remains unstudied • A2450C remains unstudied	• Yassin, A.S. & Mankin, A.S. Journal of Biological Chemistry. 2007. 282(33): 24329-24342.
A2451	• A2451U strongly dominant lethal in vivo • A2451G strongly dominant lethal in vivo. Deficient in early assembly steps of large subunit. • A2451C peptidyltransferase reaction rate reduced by ~4-fold	• Yassin, A.S. & Mankin, A.S. Journal of Biological Chemistry. 2007. 282(33): 24329-24342. • Thompson, J., et al. PNAS. 2001. 98(16): 9002-9007.
C2452	• C2452A remains unstudied • C2452U confers anisomycin resistance in *H. marismortui* and *S. cerevisiae* • C2452G remains unstudied	• Blaha, G., et al. J. Mol. Biol. 2008. 379(3): 505-519
A2453	• A2453C confers resistance to anisomycin and to linezolid in *H. halobium*. Decreased growth rate. • A2453G strongly dominant lethal in vivo • A2453U confers resistance to anisomycin in *H. marismortui*.	• Kloss, P., et al. JMB. 1999. 294: 93-101. • Yassin, A.S. & Mankin, A.S. Journal of Biological Chemistry. 2007. 282(33): 24329-24342.

		• Blaha, G., et al. J. Mol. Biol. 2008. 379(3): 505-519
G2454	• G2454A moderately dominant lethal in vivo • G2454U remains unstudied • G2454C remains unstudied	• Yassin, A.S. & Mankin, A.S. Journal of Biological Chemistry. 2007. 282(33): 24329-24342.
G2455	• G2455A remains unstudied • G2455U remains unstudied • G2455C remains unstudied	
C2456	• C2456A remains unstudied • C2456U remains unstudied • C2456G remains unstudied	
C2496	• C2496A remains unstudied • C2496U remains unstudied • C2496G remains unstudied	
A2497	• A2497C remains unstudied • A2497G strongly defective in peptidyl transferase activity • A2497U remains unstudied	• Porse, B.T., and Garrett, R.A. JMB. 1995. 249, 1-10.
C2498	• C2498A remains unstudied • C2498U remains unstudied • C2498G remains unstudied	
C2499	• C2499A alone or when paired with G2032A confers linezolid resistance • C2499U strongly dominant lethal in vivo • C2499G remains unstudied	• Fulle, S., et al. NAR. 2015 43(16): 7731-7743. • Yassin, A.S. & Mankin, A.S. Journal of Biological Chemistry. 2007. 282(33): 24329-24342.
U2500	• U2500A confers anisomycin resistance in *H. marismortui* • U2500G remains unstudied • U2500C confers anisomycin resistance in *H. marismortui*. Confers linezolid resistance in *E. coli* and *H. halobium*.	• Blaha, G., et al. J. Mol. Biol. 2008. 379(3): 505-519. • Xion, L.Q., et al. J. Bacteriol. 2000. 182: 5325-5331.
C2501	• C2501A remains unstudied • C2501U remains unstudied • C2501G remains unstudied	
G2502	• G2502A causes a decreasesd growth rate in *E. coli.* • G2502U remains unstudied • G2502C remains unstudied	• Vester, B., and Garrett, R.A. EMBO J. 1988. 7(11): 3577-3587.
A2503	• A2503C leads to increased resistance to proline-rich antimicrobial peptide Onc112 (especially when combined with A2059C).	• Ganon, M.G., et al. NAR. 2016 44: 2439-2450. • Long, K.S., et al. Antimicrob Agents

	• A2503G confers a small susceptibility to linezolid antibiotic in *M. smegmatis* (*E. coli* mutation unstudied) • A2503U confers resistance to valnemulin, chloramphenicol, florfenicol, tylosin, spiramycin, josamycin, and linezolid in *M. smegmatis* (*E. coli* mutation unstudied)	Chemother. 2010. 54(11): 4705-4713. • Li, B.B., et al. J. Antimicrob. Chemother. 2011. 66(9):1983-6.
U2504	• U2504A confer chloramphenicol resistance in mitochondrial rRNA (*E. coli* mutation unstudied). • U2504G growth rate increases to 5.4 h. Cross resistance to both chloramphenicol and linezolid in *M. smegmatis* (*E. coli* mutation unstudied). • U2504C confers linezolid resistance in *H. halobium* (*E. coli* mutation unstudied).	• Long. K.S., et al. Molecular Microbiology. 2009. 71(5): 1218-1217.
G2505	• G2505A confers resistance to oxazolidinone linezolid in Enterococcus faecalis. *E. coli* mutation studied in vitro shows 14% peptidyl transferase activity. Severe to lethal growth defects in vivo. • G2505U shows less than 5% peptidyl transferase activity in vitro. Severe to lethal growth defects in vivo. • G2505C shows 17% peptidyl transferase activity in vitro. Severe to lethal growth defects in vivo. When combined with A1067U, mutation is dominant lethal.	• Bourgeois-Nicolaos, N. et al. J. Infect. Dis. 2007. 195(10): 1480-8. • Saarma, U., and Remme, J. NAR. 1992. 20: 3147-3152. • Porse, B.T., et al. JMB. 1996. 264: 472-483.
U2506	• U2506A impacts ability to catalyze peptidyltransferase with Puromycin. Retains 5% peptidyl transferase activity in vitro. Lethal in vivo. • U2506G displays a cold-sensitive phenotype in which peptide bond formation is efficient at higher temperatures. Retains less than 5% peptidyl transferase activity in vitro. Lethal in vivo. • U2506C impacts ability to catalyze peptidyltransferase with Puromycin. Retains 20% peptidyl transferase activity in vitro. Lethal in vivo.	• Youngman, E.M., et al. Cell. 2004. 117(5): 589-599. • Porse, B.T., et al. JMB. 1996. 264: 472-483.
C2507	• C2507A remains unstudied • C2507U dominant lethal *in vivo*. • C2507G remains unstudied	• Spahn, C., et al. JBC. 1996. 271; 32849-32856.
G2582	• G2582A decreased total protein synthesis by approximately one-third, but not the RNA synthesis. Additionally, this mutation results in an increase in	• Maivali, U., et al. Mol. Biol. (Mosk). 2001. 35(4): 666-71.

	peptidyl-tRNA drop-off, thereby reducing translational processivity. Shows less than 5% peptidyl transferase activity in vitro. Lethal in vivo. • G2582U causes a significant increase in peptidyl-tRNA drop-off from ribosomes, thereby reducing translational processivity. Retains less than 5% peptidyl transferase activity in vitro. Lethal in vivo • G2582C retains <5% peptidyl transferase activity in vitro. Lethal in vivo.	• Porse, B.T., et al. JMB. 1996. 264: 472-483.
G2583	• G2583A readily incorporates into 70S ribosomes and polysomes. When combined with A1067U, mutation is dominant lethal. Alone, mutation is results in very little activity in vitro (less than 5%), growth defects in vivo. • G2583U retains less than 5% peptidyl transferase activity in vitro. Lethal in vivo. • G2583C decreased total protein synthesis by approximately one-third, but not the RNA synthesis. Additionally, this mutation results in an increase in peptidyl-tRNA drop-off, thereby reducing translational processivity. Other studies show this mutation has <5% or no peptidyl transferase activity in vitro. Lethal in vivo.	• Saarma, U., et al. RNA. 1998. 4:189-194. • Saarma, U., and Remme, J. NAR. 1992. 20: 3147-3152. • Maivali, U., et al. Mol. Biol. (Mosk). 2001. 35(4): 666-71. • Porse, B.T., et al. JMB. 1996. 264: 472-483.
U2584	• U2584A retains 22% peptidyl transferase activity in vitro. Lethal in vivo. • U2584G dominant lethal in vivo. Retains 32% peptidyl transferase activity in vitro. • U2584C retains 21% peptidyl transferase activity in vitro. Some growth defect in vivo.	• Porse, B.T., and Garrett, R.A. JMB. 1995. 249:1-10. • Maivali, U., et al. Mol. Biol. (Mosk). 2001. 35(4): 666-71.
U2585	• U2585A lethal in vivo. Causes degradation of both large and small ribosomal subunits in E. coli. Retains 6% peptidyl transferase activity in vitro. • U2585G lethal *in vivo*. Peptidyltransferase rate constant is diminished in vitro by ~7-fold. Retains 36% peptidyl transferase activity in vitro. • U2585C lethal *in vivo*. Peptide release is compromised *in vitro*. Retains less than 5% peptidyl transferase activity in vitro.	• Paier, A., et al. Sci. Rep. 2015. 5:7712. • Youngman, E.M., et al. Cell. 2004. 117: 589-599. • Porse, B.T., et al. JMB. 1996. 264: 472-483.

U2586	• U2586A does not affect wild-type ErmCL peptide stalling. • U2586G does not affect wild-type ErmCL peptide stalling. • U2586C does not affect wild-type ErmCL peptide stalling.	• Arenz, S., et al. Molecular Cell. 2014. 56: 446-452.
A2587	• A2587C remains unstudied. • A2587G remains unstudied. • A2587U remains unstudied.	
G2588	• G2588A alters the interaction of protein substrates and the antiprion compond 6-Aminophenanthridine (6AP) with domain V rRNA, and also decreases protein folding activity of the ribosome (PFAR) • G2588U remains unstudied. • G2588C remains unstudied.	• Pang, Y., et al. JBC. 2013. 288(26): 19081-19089.
A2602	• A2602C completely eliminates RF1-dependent peptidyl-tRNA hydrolysis. • A2602G has diminished peptide release activity. • A2602U has diminished peptide release activity.	• Polacek, N., et al. Molecular Cell. 2003. 11(1):103-112.
C2606	• C2606A remains unstudied. • C2606U remains unstudied. • C2606G remains unstudied.	
G2607	• G2607A remains unstudied. • G2607U remains unstudied. • G2607C remains unstudied.	
G2608	• G2608A does not confer resistance to oxazolidinone antibiotic. • G2608U confers resistance to oxazolidinone antibiotic. • G2608C confers strong resistance to oxazolidinone antibiotic.	• Xu, J., et al. Biochemical and Biophysical Research Communications. 2005. 328(2): 471-476.
U2609	• U2609A results in resistance to klebsazolicin (KLB). • U2609G results in resistance to klebsazolicin (KLB). • U2609C renders *E. coli* resistant to ketolides telithromycin and cethromycin	• Metelev, M., et al. Nature Chemical Biology. 2017. 13: 1129-1136. • Xiong, L., et al. Antimicrob Agents Chemother. 2005. 49(1): 281-288.
C2610	• C2610A remains unstudied. • C2610U in *S. pneumoniae* confers small impacts on the activities of macrolides and clindamycin, but is not categorized as resistance to these antimicrobials. Reduces Erythromycin-dependent ribosome stalling of ErmCL peptide in *E. coli.*	• Canu, A., et al. Antimicrob. Agents. Chemother. 2002. 46(1): 125-131. • Vazquez-Laslop, N. et al. PNAS. 2011. 108: 10496-10501. • Boumghar-Bourtchai, L., et al. Antimicrob. Agents.

	• C2610G is associated with linezolid resistance in *E. faecalis*. Remains unstudied in *E. coli*.	Chemother. 2009. 53(9): 4007-4009.
C2611	• C2611A confers resistance to erythromycin and 14- and 15- membered macrolides in pneumococcal strains. • C2611U in *S. pneumoniae* confers small impacts on the activities of macrolides and clindamycin, but is not categorized as resistance to these antimicrobials. Remains unstudied in *E. coli*. • C2611G confers resistance to erythromycin and 14- and 15- membered macrolides in pneumococcal strains.	• Canu, A., et al. Antimicrob. Agents. Chemother. 2002. 46(1): 125-131. • Tait-Kamradt, A., et al. Antimicrob. Agents. Chemother. 2000. 44(8): 2118-2125.

Supplementary Table 2.2 Bulk translation rates of wild-type and PTC-ring mutant 70S iSAT ribosomes. Bulk translation rates for iSAT ribosomes were determined from protein synthesis kinetics curves, for reactions after 2 h incubations, and normalized to wild-type.

Mutant	Average μM sfGFP	Bulk translation rate (μM protein/hr)	Std. Dev
wt pT7rrnb	1.00	1.03	0.03
G2057U	0.77	0.63	0.02
G2057C	0.57	0.52	0.01
G2057A	0.47	0.33	0.02
A2058C	0.89	0.69	0.03
A2058U	0.82	0.81	0.03
A2058G	0.57	0.51	0.02
A2059G	0.4	0.26	0.01
A2059U	0.22	0.33	0.02
A2059C	0.18	0.09	0.01
A2060G	0.27	0.17	0.01
A2060U	0	0	0.01
A2060C	0	0.02	0
G2061A	0.23	0.35	0.02
G2061C	0.06	0.02	0.01
G2061U	0	0.02	0
A2062U	0.94	1.02	0.02
A2062C	0.72	0.46	0.02
A2062G	0.63	0.43	0.02
C2063U	0	0	0
C2063G	0	0	0
C2063A	0	0	0
G2447A	0.44	0.2	0.01
G2447C	0.25	0.17	0.01
G2447U	0.01	0	0
A2448C	0.49	0.3	0.04
A2448U	0.48	0.21	0.02
A2448G	0.37	0.28	0.04
U2449C	0.64	0.52	0.02
U2449A	0.12	0.02	0
U2449G	0.02	0.01	0.01
A2450G	0.02	0	0
A2450U	0	0	0

A2450C	0	0	0
A2451C	0.36	0.15	0.01
A2451U	0.1	0.14	0.01
A2451G	0.02	0	0
C2452A	0.61	0.52	0.02
C2452G	0.03	0	0.01
C2452U	0.02	0.02	0.02
A2453U	0.57	0.34	0.03
A2453C	0.15	0.05	0.02
A2453G	0	0.01	0
G2454A	0.13	0.09	0.02
G2454U	0.04	0.01	0
G2454C	0	0	0
G2455U	0.27	0.16	0.01
G2455A	0.06	0.13	0.01
G2455C	0.02	0.02	0
C2456U	0.66	0.43	0.1
C2456G	0.09	0.06	0
C2456A	0.08	0.06	0
C2496U	0.9	0.74	0.02
C2496G	0.38	0.31	0.02
C2496A	0.16	0.11	0.01
A2497U	0.67	0.48	0.01
A2497G	0.26	0.12	0.01
A2497C	0.1	0.13	0.01
C2498U	0.06	0	0
C2498A	0	0	0.01
C2498G	0	0	0.02
C2499G	0.04	0.03	0.01
C2499U	0.01	0	0
C2499A	0.01	0.03	0
U2500A	0.36	0.3	0.03
U2500G	0	0.01	0
U2500C	0	0.06	0.02
C2501U	0.03	0.02	0.01
C2501G	0	0	0
C2501A	0	0	0
G2502U	0.29	0.19	0.01

G2502C	0.04	0.02	0.01
G2502A	0.02	0.01	0
A2503U	0.79	0.64	0.02
A2503G	0.28	0.34	0.02
A2503C	0.01	0.31	0.02
U2504G	0.6	0.4	0.01
U2504A	0.35	0.19	0
U2504C	0.21	0.16	0.01
G2505U	0.98	0.85	0.02
G2505A	0.1	0	0
G2505C	0.01	0.49	0.1
U2506G	0.03	0.02	0.02
U2506C	0.02	0.01	0.01
U2506A	0.02	0.02	0.01
C2507U	0.15	0.05	0.01
C2507A	0	0	0
C2507G	0	0.01	0
G2582U	0.34	0.37	0.03
G2582A	0.02	0	0
G2582C	0	0	0
G2583A	0.82	0.53	0.02
G2583U	0.07	0.03	0
G2583C	0.01	0	0
U2584A	0.66	0.44	0.02
U2584C	0.56	0.38	0.02
U2584G	0.25	0.11	0.02
U2585G	0.21	0.2	0.01
U2585A	0.02	0.02	0.03
U2585C	0.02	0.01	0.01
U2586G	0.57	0.52	0.01
U2586A	0.47	0.36	0
U2586C	0.44	0.31	0.04
A2587U	0.83	0.8	0.04
A2587G	0.2	0.02	0.01
A2587C	0.09	0.04	0.01
G2588U	0.56	0.38	0.01
G2588C	0.47	0.49	0.02
G2588A	0.35	0.28	0.01

A2602U	0.03	0.02	0
A2602G	0.02	0.01	0.01
A2602C	0.02	0.01	0
C2606U	0.42	0.3	0.01
C2606A	0.2	0.15	0.01
C2606G	0.15	0.05	0.02
G2607C	0.5	0.45	0.02
G2607U	0.47	0.09	0.01
G2607A	0.2	0.15	0.01
G2608A	0.9	0.58	0.02
G2608U	0.78	0.67	0.02
G2608C	0.77	0.57	0.03
U2609A	0.8	0.55	0.01
U2609C	0.74	0.47	0.02
U2609G	0.68	0.39	0.03
C2610G	0.41	0.49	0.02
C2610U	0.33	0.25	0.02
C2610A	0.04	0	0
C2611U	0.55	0.42	0.02
C2611A	0.11	0.03	0.01
C2611G	0.03	0	0

Supplementary Table 2.3 Equations and examples scores for relative activity calculations, and overall mutational flexibility scores. Relative activity was calculated to compare performance of each mutant by normalizing wild-type protein synthesis yields to one and mutant yields to the normalized wild-type yields. An overall mutational flexibility score was then determined for each nucleotide position by adding the relative activities of every possible point mutation. The highest mutational flexibility score of three indicates that all three nucleotide changes possess wild-type activity, while the lowest mutational flexibility score of zero indicates that all three nucleotide changes preclude any protein synthesis.

Value/Score	Equation used	Example calculations	
Relative activity	$R = \frac{1}{WT} * (Mutant\ activity)$	**Protein synthesis yields** **WT:** 9.6 μM **A2062U:** 9.0 μM **A2062C:** 6.9 μM **A2062G:** 6.0 μM	**Relative activity** **WT:** 1 **A2062U:** 0.94 **A2062C:** 0.72 **A2062G:** 0.63
Mutational flexibility	$R1 + R2 + R3$	**Relative activity** **A2062U:** 0.94 **A2062C:** 0.72 **A2062G:** 0.63	**Mutational flexibility** **A2062:** 2.3

Supplementary Table 2.4 Sucrose gradient fractionation profiles of rRNA PTC mutants. Representative nucleotide mutations were chosen for sucrose gradient fractionation based on their activity. iSAT reactions were separated through sucrose gradients, and fractions were collected. The relative average abundance of rRNA in each fraction was quantified by calculating the area under each curve.

Ribosomes	30S	50S	70S	Disomes	Trisomes
WT	34%	25%	14%	15%	12%
A2062U	36%	30%	12%	12%	8%
U2585G	56%	26%	9%	9%	0%
A2451U	50%	41%	7%	2%	0%
G2455A	46%	48%	4%	2%	0%

Supplementary Table 2.5 PTC-ring nucleotide distances calculated in PyMol. PTC nucleotide distances were calculated from either the A-site or P-site tRNAs. Using the *E. coli* ribosome structure (PDB- 4YBB), we measured the distance between A76 of the A-site and P-site tRNAs and within one angstrom of the geometric center of each PTC nucleotide.

A site (A76 of A-site tRNA + AA)		**P site (A76 of P-site tRNA + AA)**	
Distance	Nucleotides	Distance	Nucleotides
2 Å or less	2583	3 Å or less	2062, 2585
3 Å or less	2506, 2451, 2585	4 Å or less	2061, 2063, 2450, 2451
4 Å or less	2584, 2452	5 Å or less	2586, 2602
5 Å or less	2061, 2505, 2507	6 Å or less	2584
6 Å or less	2063, 2504, 2582	7 Å or less	2452
7 Å or less	2447, 2450	8 Å or less	2503, 2505, 2506
8 Å or less	2501, 2503, 2453, 2602	9 Å or less	2447, 2501, 2504, 2583,
9 Å or less	2500	10 Å or less	2497, 2587, 2608
10 Å or less	2062	11 Å or less	2059, 2449
11 Å or less	2586, 2610	12 Å or less	2453, 2507
12 Å or less	2059, 2454, 2499, 2608	13 Å or less	2496, 2500, 2609, 2610
13 Å or less	2058, 2449, 2497	14 Å or less	2058, 2502, 2588, 2607
14 Å or less	2502, 2496, 2607, 2611	15 Å or less	2060, 2499, 2582, 2606, 2611
15 Å or less	2057, 2455, 2498, 2587, 2606	16 Å or less	2057, 2448, 2454, 2455, 2498
16 Å or less	2060, 2588		
17 Å or less	2448, 2456, 2609		

Supplementary Table 2.6 A- and P-loop nucleotide distances calculated in PyMol. Distances were calculated from either the A-site or P-site tRNAs. Using the *E. coli* ribosome structure (PDB-4YBB), we measured the distance between A76 of the A-site and P-site tRNAs and within one angstrom of the geometric center of each PTC nucleotide.

A site (A76 of A-site tRNA + AA)		**P site (A76 of P-site tRNA + AA)**	
Distance	Nucleotides	Distance	Nucleotides
4 Å or less	2553	4 Å or less	2251
7 Å or less	2554	7 Å or less	2252
10 Å or less	2552, 2555	10 Å or less	2253
12 Å or less	2251	13 Å or less	2250, 2254
14 Å or less	2556	15 Å or less	2553
15 Å or less	2252	17 Å or less	2554
17 Å or less	2253, 2557	19 Å or less	2555
18 Å or less	2551	21 Å or less	2552
19 Å or less	2250	23 Å or less	2556
20 Å or less	2550, 2558	26 Å or less	2557
21 Å or less	2254	28 Å or less	2551
23 Å or less	2549	31 Å or less	2558
24 Å or less	2559	32 Å or less	2550
25 Å or less	2548	33 Å or less	2549
26 Å or less	2560	34 Å or less	2559, 2548
		36 Å or less	2560

CHAPTER 3

Studying and engineering β-amino acid incorporating ribosomes

The work presented in this chapter is unpublished.

3.1 Abstract

Based on the current understanding that substrate positioning results in peptide bond catalysis by the ribosome [11], we hypothesize that the ribosome active site can be engineered to enhance incorporation of non-canonical amino acids, specifically extended backbone β-amino acids. By leveraging *in vitro* ribosome synthesis, assembly, and translation (iSAT), we can now access mutations that are otherwise lethal *in vivo*, providing a means to circumvent evolutionary obstacles that limit experiments in cells. In this work, we sought to (1) build mutant β-amino acid incorporating ribosomes *in vitro*; (2) characterize these mutant ribosomes; and (3) observe their incorporation of at least one expanded backbone monomer. This work focuses on β-amino acids because of their unique ability to enhance resistance to proteolysis, making them ideal candidates for use in peptidomimetic therapeutics [220,221].

3.2 Introduction

All organisms possess a nearly universal genetic code, which encode ~20 canonical amino acids (22 when including selenocysteine and pyrrolysine). Along with post-translational modifications, these naturally occurring amino acids function as the polypeptide backbone to all of life's processes and determine the structure and functional reactivity of the proteins. The incorporation of non-canonical amino acids into proteins has emerged as a significant application in synthetic biology, biochemistry and structural biology [100,222,223].

Producing proteins and peptides with non-canonical amino acids requires an expanded genetic code with multiple biological parts. These parts include (i) an open coding channel reassigned to a non-canonical monomer, (ii) monomer-transfer RNA (tRNA) substrates that can decode the open codon (that are typically produced by an orthogonal aminoacyl-tRNA synthetase

(o-aaRS) specifically charging a non-canonical monomer to its orthogonal tRNA), (iii) delivery of monomer-tRNA substrates to the ribosome by elongation factor Tu (EF-Tu), and (iv) compatible ribosomes (Figure 3.1). To ensure efficient operation of a re-engineered translation apparatus, many parts must be reconfigured. To date, engineering of such parts has resulted in incorporation of more than 150 non-canonical monomers into proteins [81,224].

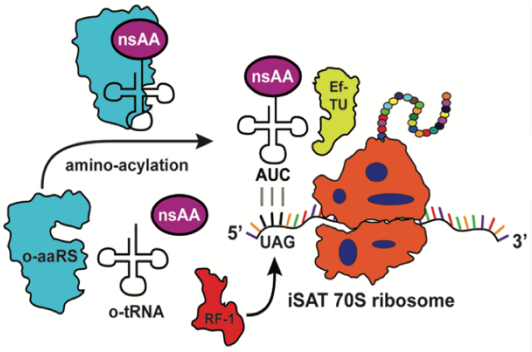

Figure 3.1 Enabling non-canonical amino acid incorporation requires many parts.

It has been demonstrated that the ribosome has an extraordinary tolerance for a number of non-canonical amino acids, although the natural translation machinery only employs ~20 canonical α-amino acids as substrates. Schultz, Hecht, Suga and others have revealed the tolerance of the ribosome towards backbone-modified amino acids [84,85,87,91-94,133,225]. Although these represent breakthroughs in non-canonical amino acid incorporation, each case has its limitations. These limitations include the incorporation of only α-amino acids, the number of non-canonical amino acids incorporated, and the inability to incorporate consecutive non-canonical amino acids.

One family of non-canonical amino acids is the extended-backbone amino acids; which includes β- and γ-amino acids. β-amino acids are not naturally found in proteins, and feature extended backbones compared to α-amino acids (Figure 3.2). These amino acids have gained increasing attention due to their protease resistance and altered immunogenicity, making them

useful sources for therapeutic peptidomimetics [220,221,226,227]. The chemical synthesis of β-peptides is hindered by the difficulty of their solid phase synthesis, insufficient purity, and the requirement of extensive purification [228-232]. Additionally, the synthesis of libraries of β-peptides is prohibitive with chemical synthesis [232]. Thus, leveraging the ribosome as a polymerizing machine is an attractive method for β-peptide synthesis. Incorporation of the β-homoglycine amino acid into a peptide was first demonstrated using amber suppression and β-homoglycine-$tRNA_{CUA}$ prepared by chemoenzymatic acylation [233].

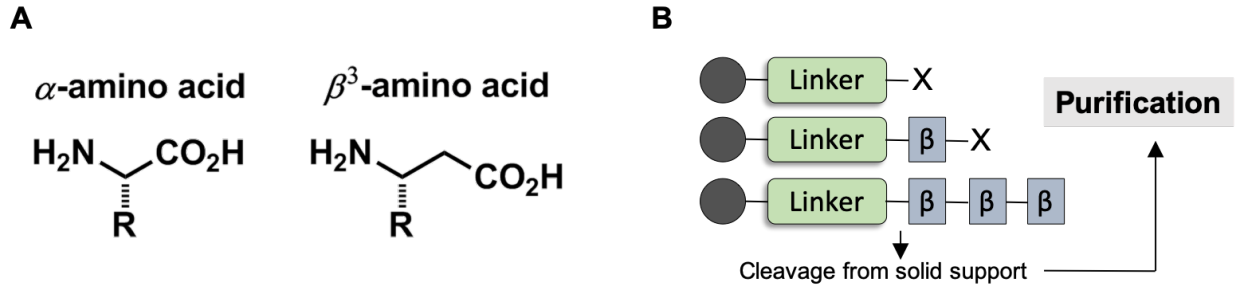

Figure 3.2 (a) β-amino acids are attractive building blocks for therapeutic peptidomimetics. These extended backbone monomers are biologically active, mimic natural peptides, and form secondary structure. Additionally, they have structural diversity, evade protease degradation, and can have increased affinity for active sites. (b) β-peptides are currently synthesized with solid phase peptide synthesis (SPPS).

Incorporating non-canonical amino acids into proteins is heavily dependent on the fidelity of tRNA aminoacylation –or the process of charging a tRNA with its cognate amino acid. In the cell, this process is naturally carried out on α-amino acids by aaRS. Founding research in this field leveraged a chemoenzymatic synthesis technique to produce non-canonical aminoacyl tRNAs. The non-canonical aminoacyl-tRNA was subsequently used to suppress a nonsense codon in an *in vitro* translation reaction [86,234]. This work was groundbreaking in the field, however, the process required laborious organic synthesis and the incorporation efficiency with this technology was

restrictively low. To overcome these challenges, Forster and colleagues prepared a system which was free of aaRSs and introduced chemoenzymatically synthesized aa-tRNA substrates [81]. This improved the efficiency of incorporation, but still relied heavily on the organic synthesis of aa-tRNA substrates. Additionally, in 2011 Suga and colleagues developed a protocol that facilitates genetic code reprogramming using Flexizymes [235]. Flexizymes are flexible tRNA acylating ribozymes that enable the preparation of a diverse array of non-canonical aminoacyl-tRNAs *in vitro*. Although this was a major advance, Flexizymes possess less than optimal activity, limiting non-canonical amino acid incorporation.

A major breakthrough in this field would include the ability to co-evolve the system of translation (e.g., elongation factors, synthetases, etc.) for the incorporation of expanded backbone amino acid monomers into a growing chain. This would permit the incorporation of one, or consecutive (>3), non-canonical expanded backbone amino acid monomers and define design rules for mutating 23S rRNA nucleotides for this incorporation. The cell-free iSAT system is poised to fill these gaps and reveal β-amino acid compatibility with the ribosome. As a first step to co-evolving the system of translation for the incorporation of β-amino acids, this work aims to lay a workflow foundation for constructing and studying ribosomes capable of incorporating expanded backbone monomers *in vitro*.

3.3 Materials and methods

3.3.1 Plasmid construction

The 7,300-bp plasmid pT7rrnB carries an *Escherichia coli* rRNA operon, *rrnB*, under the control of the T7 promoter and the ampicillin resistance gene as a selective marker. All ribosomal

mutant plasmids are derivatives of pT7rrnB carrying multiple mutations in the 23S rRNA gene. Briefly, site-directed mutagenesis was used to construct each individual mutant. Nucleotide point mutations were introduced into primers and amplified using pT7rrnB as a template for PCR amplification. PCR products were blunt end ligated, transformed into DH5α using electroporation, and plated onto LB-agar/ampicillin plates at 37°C. Plasmid was recovered from resulting clones and sequence confirmed.

3.3.2 Strain and culture harvest

E. coli cells for S150 extract and TP70 preparation were grown in 10L of 2xYPTG in a fermenter (Sartorius). MRE600 strain was grown at 37°C. Cells were harvested at OD_{600} = 2.8-3.0, washed twice in S150 lysis buffer (20 mM Tris-chloride pH 7.2 at 4°C, 100 mM ammonium chloride, 10 mM magnesium chloride, 0.5 mM EDTA, 2 mM DTT), pelleted, and flash frozen at -80°C using liquid nitrogen for storage. Buffer was added at a ratio of 5 mL of buffer per 1 g of cells. 200 μL of Halt Protease Inhibitor Cocktail (Thermo Fisher Scientific Inc.) and 75 μL RNase Inhibitor (Qiagen) were added for every 4 g of cells in the suspension. The cells were lysed at approximately 20,000 psi with an EmulsiFlex-C3 homogenizer (Avestin). An equivalent dose of RNase Inhibitor and 3 μL of 1M DTT per milliliter were added to the lysate prior to two clarification spins at 30,000 g and 4°C for 30 min. Supernatant equivalent to S30 crude extract was recovered and gently layered into Ti45 ultracentrifuge tubes on top of an equivalent volume of sucrose cushion, buffer B (20 mM Tris-HCl (pH 7.2 at 4°C), 100 mM NH4Cl, 10 mM MgCl2, 0.5 mM EDTA, 2 mM DTT, 37.7% sucrose). Samples were then centrifuged (at 35000 rpm in Ti70 rotor) and 4°C for 20 h. Supernatant was recovered for S150 extract, and the remaining clear ribosome pellet was gently washed and resuspended in buffer C (10 mM Tris-OAc (pH 7.5 at 4°C),

60 mM NH_4Cl, 7.5 mM $Mg(OAc)_2$, 0.5 mM EDTA, 2 mM DTT). Concentration of resuspended ribosomes was determined from A_{260} NanoDrop readings (1 A_{260} unit of 70S = 24 pmol 70S [192]). Ribosomes were then aliquoted and flash-frozen for use as purified 70S ribosomes and for purification of native rRNA and r-proteins.

3.3.3 Component preparation

S150 crude cell-free extracts, *E. coli* 70S ribosomes, total protein of 70S ribosomes (TP70) and T7 RNA polymerase (RNAP) were prepared as previously reported [52,193]. S150 and TP70 were prepared from MRE600 cells. Protein concentrations of each S150 extract were measured using Bradford assay with bovine serum albumin (BSA) as a standard.

3.3.4 iSAT reactions

iSAT reactions of 15 μL were set-up as previously described [52]. Briefly, reactions were prepared in polymerase chain reaction tubes with optically clear flat caps and incubated at 37°C in a CFX96 real-time thermal cycler (Bio-Rad). iSAT reactions contained reporter protein plasmids encoding superfolder GFP (sfGFP). Green fluorescence of sfGFP was monitored using the CFX96 real-time thermal cycler as (excitation: 450-490 nm, emission: 510-530 nm). Additives were included at the described final concentrations. Specifically, crowding agent (2% PEG-6000) and reducing agent (2 mM DTT) were added to each reaction. iSAT reactions for S150 extracts were optimized for concentrations of magnesium glutamate to maximize reaction productivity and minimize consumption of parts. sfGFP quantification was performed as previously reported [53], using measurements of relative fluorescence units (RFU) from CFX96 real-time thermal cycler (BioRad, Hercules, CA) and BioTek Synergy 2 plate reader (Winooski, VT). RFU values were converted to molar concentration using a linear standard curve made in-house by expressing ^{14}C-

leucine labelled sfGFP in *E. coli* PANOx CFPS reactions and relating RFUs to trichloracetic acid precipitable soluble protein yield.

3.3.5 Ribosome sedimentation analysis

Sucrose gradients were prepared from Buffer C (10 mM Tris-OAc (pH = 7.5 at 4°C), 60 mM NH_4Cl, 7.5 mM $Mg(OAc)_2$, 0.5 mM EDTA, 2 mM DTT) with 10 and 40% sucrose in SW41 polycarbonate tubes using a Biocomp Gradient Master. Gradients were placed in SW41 buckets and chilled to 4°C. Meanwhile, approximately 7-8 x 15 µL iSAT reactions were prepared and incubated at 37°C, for 2 hours. Reactions were pooled and 90-120 µL of iSAT reactions were carefully loaded onto chilled gradients. The gradients were ultra-centrifuged to 22,500 rpm for 17 hours at 4°C, using an Optima L-80 XP ultracentrifuge (Beckman-Coulter) at medium acceleration and braking (setting of 5 for each). Gradients were analyzed with a BR-188 Density Gradient Fractionation System (Brandel) by pushing 60% sucrose into the gradient at 0.75 ml/min (at normal speed). Traces of A254 readings versus elution volumes were obtained for each gradient, with readings adjusted to match baselines based on blank sucrose readings. iSAT reactions without the operon plasmid were performed to establish a background reading that was subtracted from experimental traces. Gradient fractions were collected and analyzed for rRNA content by gel electrophoresis in 1% agarose and imaged in a GelDoc Imager (Bio-Rad). Ribosome profile peaks were identified based on the rRNA content as representing 30S or 50S subunits, 70S ribosomes, or polysomes. To calculate the area under each curve, Riemann sums were taken with the 30S x-axis boundary ranging from 7 mL to 8.35 mL, the 50S x-axis boundary ranging from 8.5 to 9.5 mL, the 70S x-axis boundary ranging from 9.9 to 11.5 mL, and the polysomes x-axis boundary

ranging from 11.725 to 13 mL. X-axis points were taken in 0.00625 mL intervals. Sums between each X-axis coordinate were taken, and totals were calculated for the given boundaries.

3.3.6 iSAT ribosome purification

Several (approximately 8) 15 µL iSAT reactions were prepared and incubated for 2 hours at 37°C, then pooled together. Purified 70S *E. coli* ribosomes were recovered as previously described [52], with pelleted iSAT ribosomes resuspended in iSAT buffer, aliquoted and flash-frozen.

3.3.7 MS2-tagged ribosome construct preparation and isolation

We used a well-characterized and previously published stem-loop from the MS2 phage that binds the MS2 coat protein [236,237]. The relevant constructs are presented in Supplementary Table 3.1. We sought to insert the tag in a position that would not impede ribosome function and dynamics but would be accessible for binding the MS2 coat protein. We used the published construct which inserted the MS2 stem-loop into helix 2791 (previously referred to as helix 98 in earlier work) in *E. coli* 23S rRNA. Constructs possessing the inserted MS2 stem-loop tag were constructed in the pLK35 plasmid, which harbors the *E. coli* rrnC operon under the control of the lambda operator/promoter. Importantly, this promoter system permits inducible expression of tagged ribosomes, allowing for the expression of even dominant-negative rRNA variants.

Electrocompetent DH5a (or BL21) cells were prepared with plasmid pcI857 (Kan50), which encodes the temperature sensitive mutant of lambda repressor protein cI. This strain was used to transform in mutant tagged ribosomes. The tagged constructs (p278MS2 and pEYspurMS2) were derived from pLK35 (Ampicillin resistant). The loop of 23S helix 98

(nucleotides 2707-2799) or 16S helix 6 (nucleotides 83-86, the spur) was replaced with a Spe1 site, into which the MS2 RNA sequence was inserted. The resulting sequence is:

ACTAGTTTT**GATGAGGATTACCCATC**TTT**ACTAGT**

SpeI MS2 aptamer SpeI

The strain DH5a with with pcI857 (Kanamycin resistant) was used for both cloning and ribosome preparation. Cells were grown overnight at 30ºC (Amp^{100}/Kan^{50}), then diluted 1:50 in Luria broth (Amp^{100}/Kan^{50}) prewarmed to 42ºC and grown for 3-4 hours to A_{600} between 0.7 and 0.9. Upon reaching the appropriate absorbance, cells were cooled on ice for about 30 minutes. Cells were then harvested at 6,000 rpm, for 10 minutes in 1-liter bottles. Pellets were pooled for a final spin in 50 mL conical tubes for freezing at -20ºC. Ribosome buffer A (20 mM Tris HCl, pH 7.5, 100 mM NH_4Cl, 10 mM $MgCl_2$, 0.5 mM EDTA, 6 mM BME) was used to wash and pool the cells.

Cells were lysed in ribosome buffer A (20 mM Tris HCl, pH 7.5, 100 mM NH_4Cl, 10 mM $MgCl_2$, 0.5 mM EDTA, 6 mM BME) (30-50 mL) and spun at 30,000 xg for 20 minutes two times (SS-34 tubes). The lysate was carefully layered onto a 35 mL cushion of ribosome buffer D (20 mM Tris-HCl, pH 7.5, 500 mM NH_4Cl, 10 mM $MgCl_2$, 0.5 mM EDTA, 1.1 M Sucrose) in Ti45 tubes (70 mL) or Ti70 tubes (13.5 mL). Samples were centrifuged at 37,000 rpm for 18 hours to pellet ribosomes. Pellets were then resuspsended in 2 mL of ribosome buffer A A (20 mM Tris HCl, pH 7.5, 100 mM NH_4Cl, 10 mM $MgCl_2$, 0.5 mM EDTA, 6 mM BME) with a micro stir bar at 4ºC. Tubes were then washed with another 400 uL of buffer and crude ribosomes were stored at -80ºC.

3.3.8 Expression and purification of MBP-MS2-His protein

We used a fusion between MBP and a 6x-His-tagged MS2 protein, permitting simple and efficient purification on a nickel resin. The MBP-MS2-His plasmid (a gift from Rachel Green's lab) was transformed into BL21(DE3) cells and plated on $Carb^{100}$ LB-agar plates. A freshly transformed colony (less than 1-week old) was used to inoculate a 50 mL overnight culture in LB supplemented with 100 ug/mL ampicillin (or carbenicillin). The next day, one liter of LB with $Carb^{100}$ was inoculated with 10 mLs of overnight culture and grown to an A_{600} of 0.6-0.7 at 37ºC. The cultures were then induced with 1 mM IPTG, and growth was continued for 3-4 hours at 37ºC. The induced culture was pelleted for 10 minutes at 6,000 rpm in a 1-liter rotor. Pellets were resuspended and washed in 50 mL of bindings buffer (50 mM NaH_2PO_4, 300 mM NaCl, 10 mM Imidazol, 6 mM BME, adjusted to pH 8.0). Dry pellets were flash frozen.

The cell pellets were resuspended then lysed in chilled lysis buffer (50 mM Tris-HCl pH 8.0, 200 mM NaCl, 10% glycerol, 1 M DTT, and 1 mM PMSF) via vortexing and rocking. The cell suspension was cooled on ice for 10-30 minutes after resuspension. 100 mM PMSF was added per mL of cell suspension. Cells were lysed via sonication in 10 short bursts of 10 seconds followed by intervals of 10 seconds for cooling. The lysate was subsequently clarified twice by centrifugation for 15 minutes at 11,000 xg at 4ºC, and subsequently mixed with nickel NTA resin that was pre-equilibrated in binding buffer (50 mM NaH_2PO_4, 300 mM NaCl, 10 mM Imidazol, 6 mM BME, adjusted to pH 8.0). Binding was accomplished by mixing the resin and lysate in a cold room for 30 minutes before being prepared for gravity flow or batch purification.

MS2-MBP-His fusion protein was purified in batch mode by loading cell lysate onto NiNTA resin in a 50 mL falcon tube with 10 mL of resin. The resin was washed a total of 5 times

with binding buffer. For each wash, buffer was added, the tube was rotated gently for 1 minute in a cold room, and subsequently centrifuged at 500 xg for 5 minutes. Wash supernatant was carefully removed and collected. In the final step, fusion protein was eluted by adding binding buffer that possessed 200 mM imidazole. 7 mL of elution buffer was added and incubated for 3 minutes with gentle inversions. The resin was then centrifuged at 500 xg for 5 minutes and then the supernatant was carefully pipetted off into a fresh tube. This elution step was repeated 10 times.

The crude lysate, washes, and elutions were run on an SDS-PAGE gel to identify the purified MS2-MBP-His fractions (Figure 3.3). Purified protein fractions were subsequently concentrated using an Amicon Ultra15 3,000 MWCO concentrator. The Amicon Ultra was pretreated at room temperature for 2 hours with 1% skim milk, thoroughly rinsed with water, and subsequently used for concentration. Concentrated protein was subsequently dialyzed in storage buffer (20 mM Tris-HCl, pH 7.5, 150 mM NaCl, 0.02% Sodium azide, and 20% glycerol) at 4ºC.

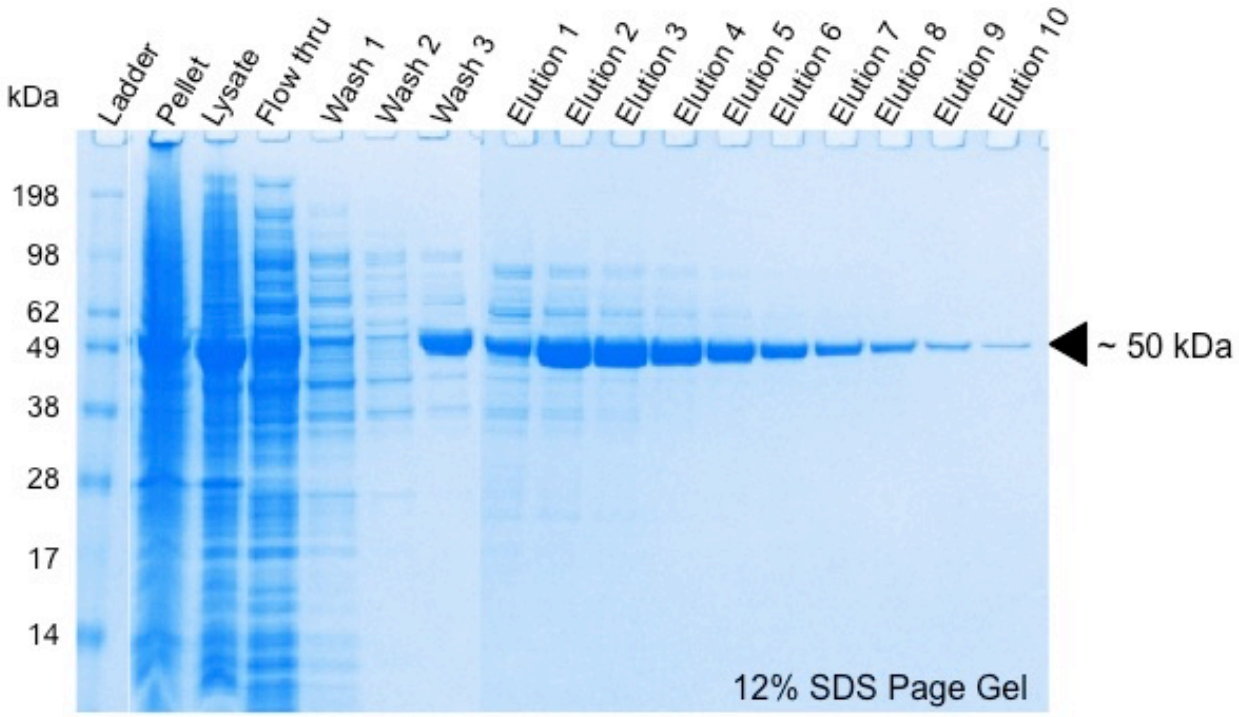

Figure 3.3 SDS-PAGE gel of MS2-MBP-His protein expression and purification.

3.3.9 Purification of MS2 tagged ribosomes

When purifying tagged ribosomes from a crude ribosome preparation, batch purification methods were used. 15 mL of amylose resin was equilibrated in a column in binding buffer (20 mM Tris-HCl, pH 7.5, 100 mM NH_4Cl, 10 mM $MgCl_2$) three times. 15 mL of amylose resin was loaded with 5-8X molar excess of MPB-MS2-His fusion protein (which was previously purified over a NiNTA column) over the amount of tagged ribosomes expected. Specifically, we used 2-3 mg of fusion protein per 70 mg of crude 70S ribosome. Importantly, the fusion protein was not premixed with ribosomes, as this will cause precipitation.

The column was washed with 1-2 column volumes of binding buffer. Crude 70S (diluted 2X in binding buffer) was loaded on the pre-washed, MS2-MBP-His-bound column. The column was then washed with 5 column volumes of binding buffer. Elution was carried out with 3-4

column volumes of elution buffer and collected as 4 mL fractions. Peaks were observed to elute after about 8 mLs, in fractions 3-6. To elute, 5 mL of elution buffer was mixed with the suspension gently and inverted for 3 minutes. The batch tube was centrifuged for 2 minutes at 500 xg, and the supernatant carefully pipetted off into a new fresh tube on ice.

All fractions in eluate peaks were pooled and concentrated. Importantly, we were careful not to pellet eluted ribosomes, as they are sometimes impossible to resuspend once the fusion protein is bound. A 15 mL Amicon Ultra 100K MWCO concentrator was used. Concentrations of eluted ribosomes was measured by taking a 1:1000 dilution of the mixture and reading the absorbance at 260 nm. A 0.7% Agarose gel was used to visualize the elution fractions and identify purified subunits and 70S species (Figure 3.4).

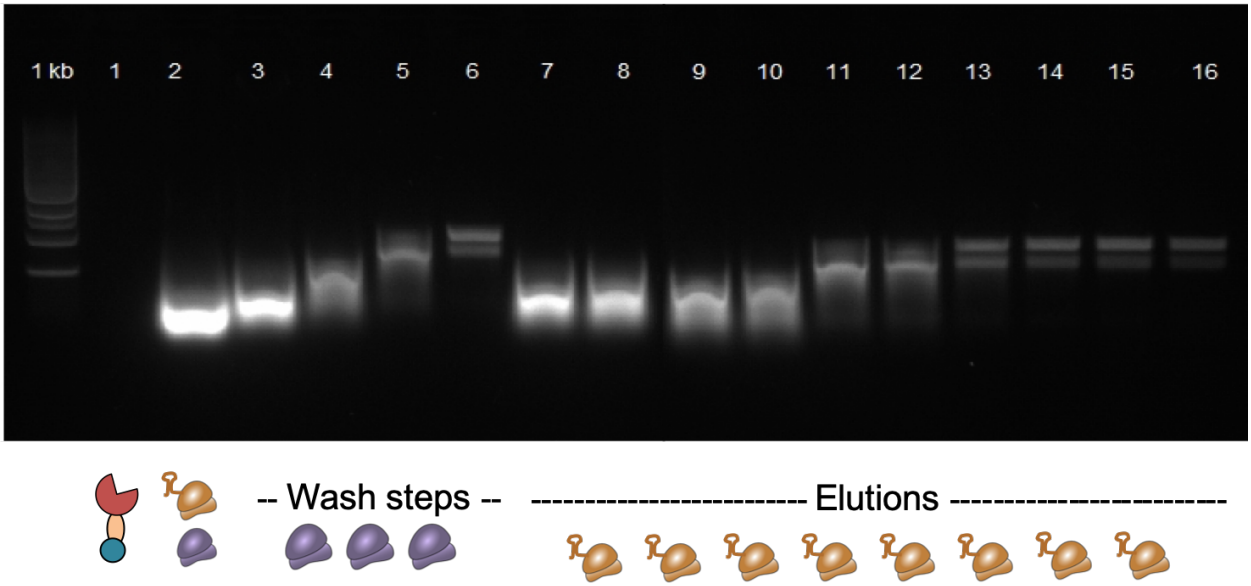

Figure 3.4 A 0.7% agarose gel used to visualize the binding, washing, and elution fractions during the purification of MS2-tagged ribosomes.

3.3.10 Testing β-amino acid incorporation

Both iSAT and MS2-purified β-incorporating ribosomes were assessed for the incorporation of β-amino acids into peptides *in vitro* using MALDI. Specifically, 1.5 μL of the peptides purified by a strep affinity tag was mixed on a MALDI plate with 1 μL of saturated α-cyano-4-hydroxycinnamic acid (CHCA) in THF containing 0.1 % TFA. The samples were dried at room temperature for 30 min. MALDI-TOF mass spectra of the peptides were obtained on a Bruker Autoflex III using the positive reflectron mode.

3.4 Results

3.4.1 Characterizing iSAT and MS2-purified β-incorporating ribosomes' functionality

Our β-incorporating ribosomes were designed based off of previously published mutations by the Hecht and Schepartz lab [91-93,213,217]. Specifically, the Hecht lab β-incorporating ribosomes (040329) possessed the following mutations: 2057-2063: AGCGUGA and 2502-2507: UGGCAG. In their work, they incorporated β-(3)-Phenylalanine analogs into full length DHFR *in vitro*. They also incorporated each of the four isomeric methyl–β-alanines but observed that their system exhibited a preference for incorporation of 3(S)-methyl-β-alanine. To charge their β-amino acid, they used chemical ligation with pdCpA charging, and $tRNA_{CUA}$ was activated with each of the four methyl-β-alanine isomers. The Schepartz lab β-incorporating ribosomes (p7a7) possessed the following mutations: 2057-2063: AGCGUGA and 2502-2507: UGACUU. Importantly, they also incorporated β-(3)-Phenylalanine analogs into full length DHFR but did so *in vivo*. Wild type phenylalanyl-tRNA synthetase was used to charge $tRNA^{Phe}$; and they used a 19/20 minimal media supplemented with a β-amino acid for their assay [213]. A structural analysis of the mutations used

in these two β-amino acid incorporating constructs is mapped onto our mutationally flexibility map from chapter 2 in Figure 3.5.

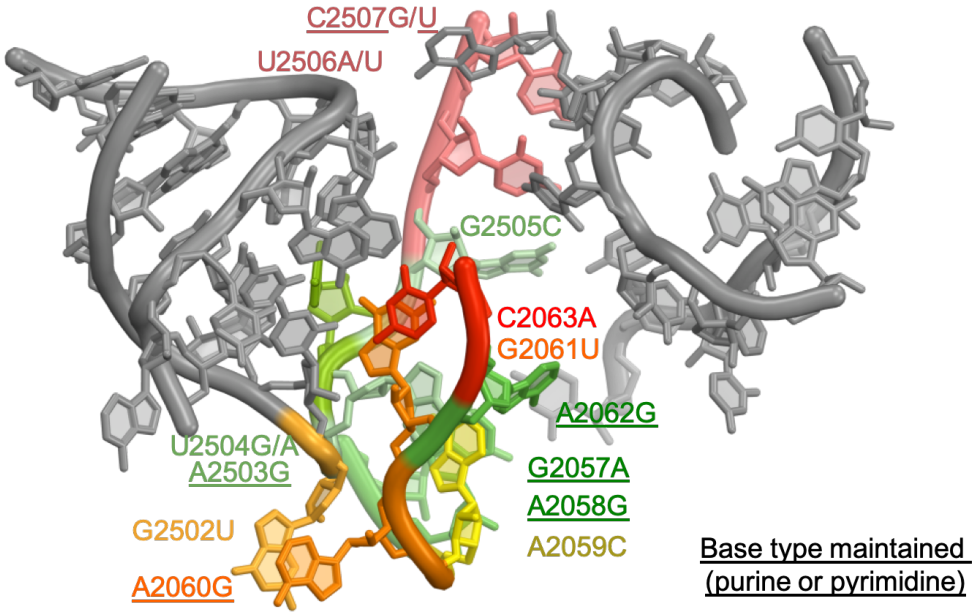

Figure 3.5 A map of the β-incorporating ribosomal mutations from the Hecht and Schepartz lab. The mutational map is color coded based on high mutational flexibility (green) and low mutational flexibility (red).

As a first step in characterizing these β-amino acid incorporating ribosomes, we leveraged the iSAT system [51-53,186] to build and test their translation activity (Figure 3.6 a). Importantly, upon building and assessing their protein synthesis in vitro, we found that compared to wild type ribosomes, both the β-amino acid incorporating ribosomes from the Hecht and Schepartz labs exhibited very low protein synthesis titers and slow protein synthesis kinetics (Figure 3.6 b,c). These results could be attributed to the difference in experimental systems within the two previous publications and the work presented here.

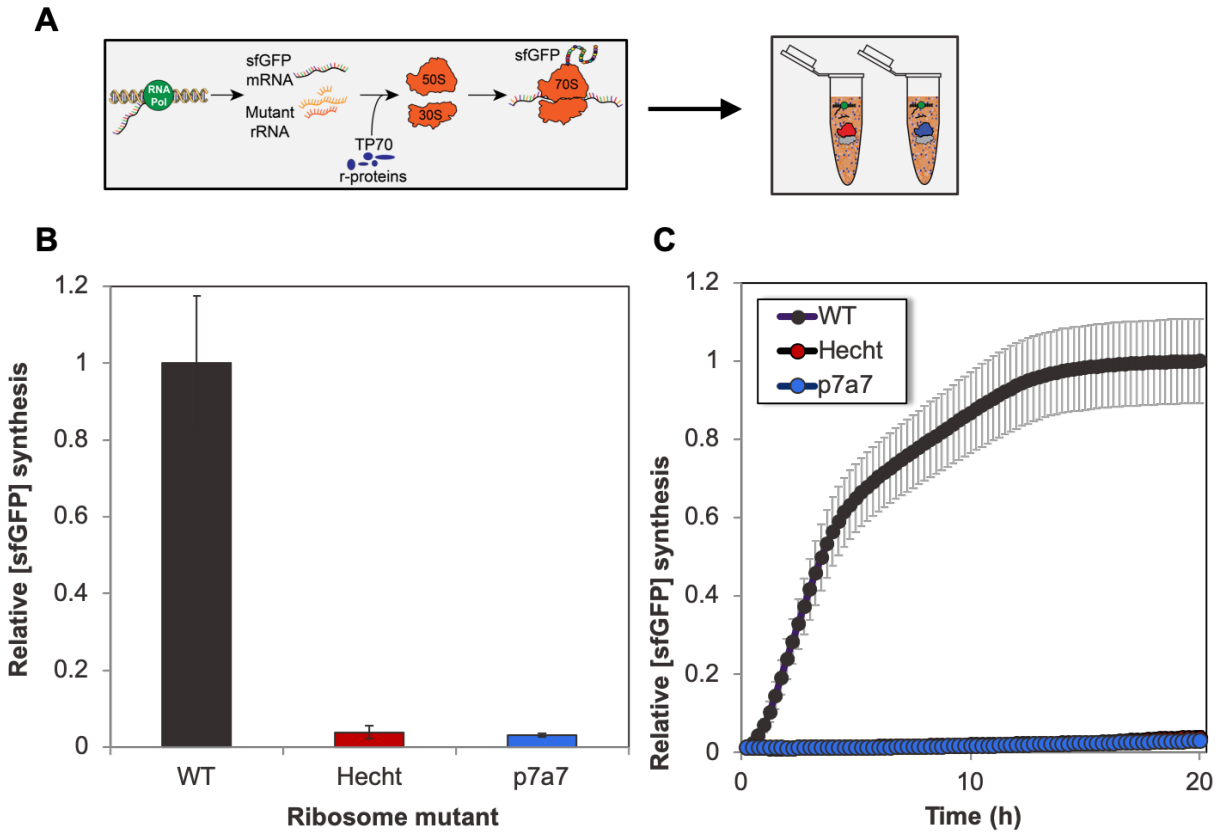

Figure 3.6 Assessing the functionality of iSAT assembled β-incorporating ribosome mutants. (a) A schematic of the iSAT workflow for synthesizing and studying β-incorporating ribosomes in vitro. (b) Relative protein synthesis titers of wt and β-incorporating ribosomes. (c) Protein synthesis kinetics for wt and β-incorporating ribosomes.

Next, we sought to characterize the functionality of the β-amino acid incorporating ribosomes that were synthesized in vivo and purified using MS2 tags. As a first step, we purified wild-type MS2-tagged ribosomes that did not possess any mutations within the large 50S subunit (Figure 3.7). This was an important control to ensure that we were not in fact reducing ribosomal activity by incorporating a purification tag in the large subunit. Additionally, if there was a reduction in activity, this experiment served to normalize the activity by ribosome concentrations. We found that we were successful in purifying MS2-tagged ribosomes that lacked any mutations in the 23S rRNA, and these ribosomes had similar activity to wild-type ribosomes that did not

possess an MS2 stem loop (Figure 3.7). However, when we sought to purify MS2-tagged ribosomes that did possess the β-amino acid incorporating mutations (Hecht or p7a7 mutations), the strains used for the synthesis of MS2-tagged ribosomes grew very poorly, and multiple mutations (that were not the desired β-amino acid incorporating mutations) were consistently incorporated into the ribosomal rRNA. Because of this, we chose to move forward with using iSAT synthesized β-amino acid incorporating ribosomes over the *in vivo* synthesized MS2-tagged constructs. We hypothesized that despite the iSAT mutants' low activity in vitro, it is possible that the synthesis of a protein possessing solely α-amino acids may not be optimized for a mutant designed for the incorporation of β-amino acids. Thus, we set out to characterize the assembly and β-amino acid incorporation abilities of the Hecht and p7a7 ribosomes that were constructed in the *in vitro* iSAT system.

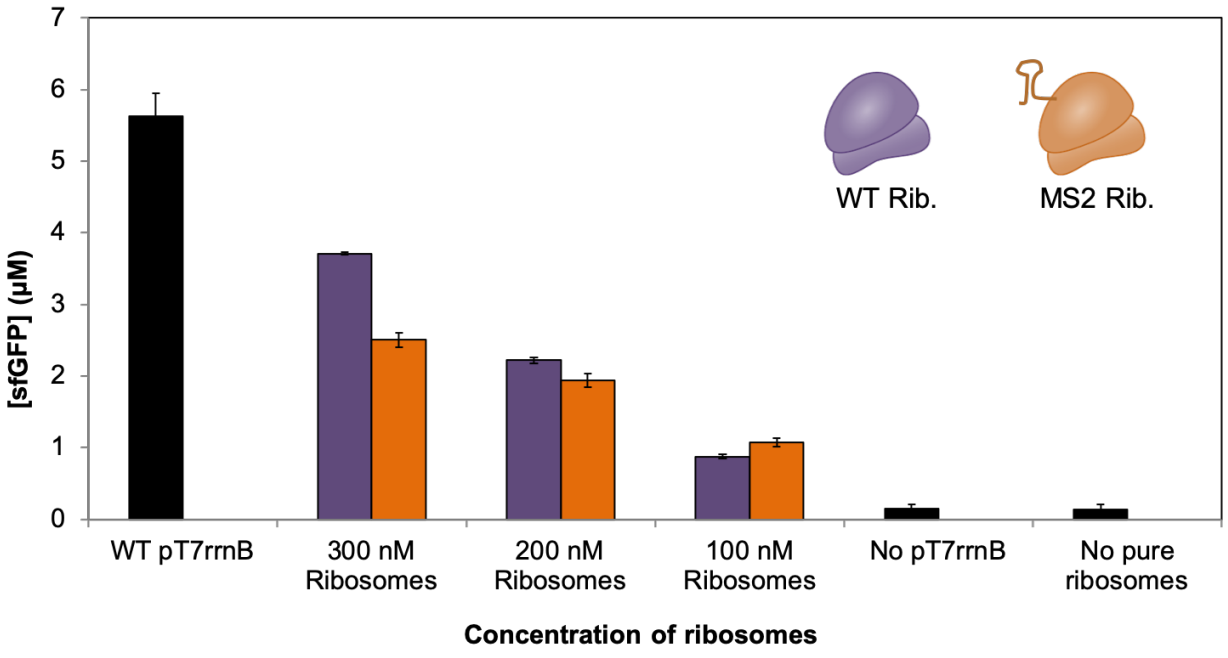

Figure 3.7 *In vitro* translation activity of purified MS2-tagged ribosomes and wild-type ribosomes possessing no MS2 stem loop. In both cases, the ribosomes were wild-type in that they do not possess any mutations in the 23S rRNA.

3.4.2 Characterizing the assembly of β-incorporating ribosomes

Because the Hecht and p7a7 mutants exhibited such low translation activity in our iSAT reactions, we wondered if perhaps the assembly of these ribosomes was somehow being impacted by the suite of rRNA mutations. To assess this, we carried out a sucrose gradient fractionation assay (Figure 3.8). Interestingly, we found that compared to wild type ribosome profiles, the β-amino acid incorporating mutant ribosomes had a different trace profile. Specifically, the trace showed a large peak for individual subunits, almost no 70S peak, and what appeared to be a large polysome peak. Upon searching the literature, this large polysome peak may actually be a hibernating 100S [238] (Figure 3.8). This hypothesis would corroborate our previous finding showing very little translation activity, which would preclude the possibility that these mutant ribosomes are efficiently forming polysomes.

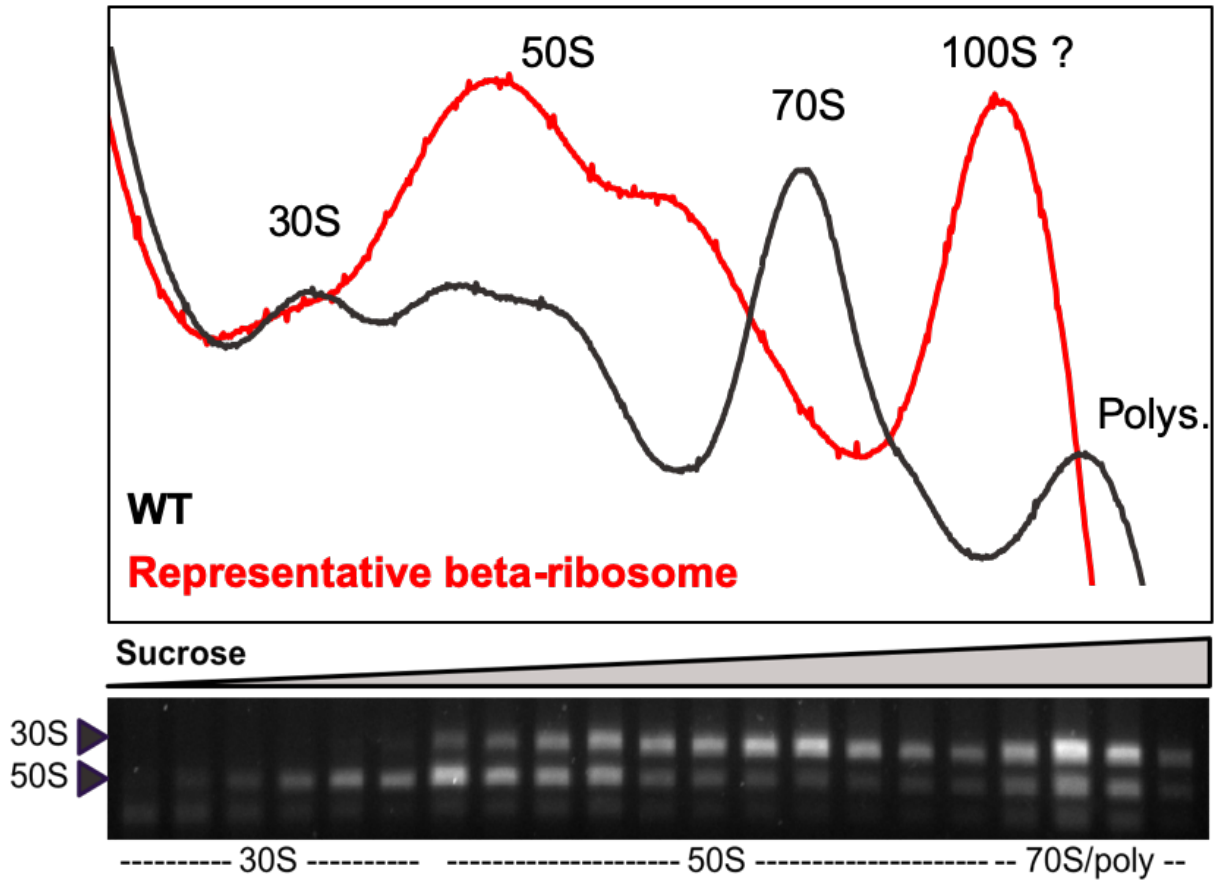

Figure 3.8 Assessment of ribosome assembly through sucrose gradient fractionation. Top panel illustrates the fractionation trace possessing the peaks for 30S, 50S, 70S, and polysomes. The large peak for the β-amino acid incorporating ribosomes which is positioned near the wild-type polysome peak, may in fact be a hibernating 100S dimer. The bottom panel represents an RNA agarose gel of select sucrose gradient fractions.

3.4.3 β-amino acid incorporation with purified β-ribosomes

Finally, despite the evidence suggesting that these mutant ribosomes are not properly assembling or translating, we still sought to characterize their ability to incorporate at least one β-amino acid. To do this, we collaborated with Dr. Joon Lee, who acylated the a tRNA molecule ($tRNA_{GGU}$) with β-phenylalanine using the flexizyme system [123-126]. Using the PURE system, we mixed pre-charged tRNA molecules (possessing β-phenylalanine) with a DNA template encoding

a short mRNA message for the incorporation of β-phenylalanine. We then spiked in each of our β-incorporating ribosomes and compared their incorporation to wild type (Figure 3.9). Interstingly, we found no incorporation of β-amino acids despite previous literature noting that these mutations permit the incorporation. We hypothesize that the differences in our assay and experimental set up and workflow may play a part in this difference in results.

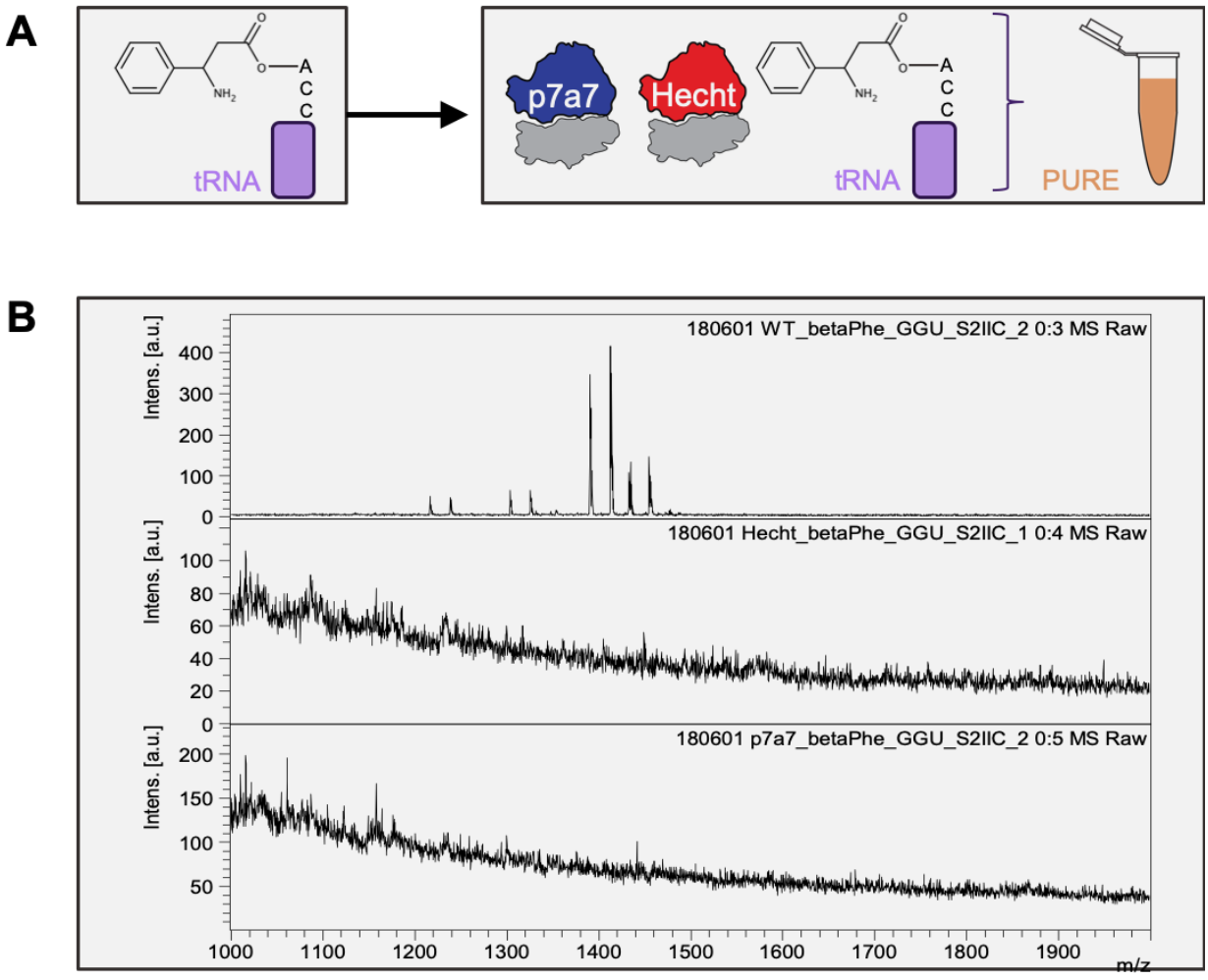

Figure 3.9 Testing the incorporation of β-phenylalanine into a short peptide (12 amino acids) using a pre-charged tRNA (charged with flexizyme) and β-incorporating ribosomal mutants. (a) Schematic of the workflow for testing mutant ribosomes for incorporation of ncAAs. (b) the MALDI trace demonstrating no β-phenylalanine incorporation with mutant ribosomes.

3.5 Discussion

Although we were unsuccessful in observing β-amino acid incorporation using these previously studied and published ribosomal mutants; this chapter represents an important breakthrough in the workflow for designing, building, and testing ribosomal mutants for the incorporation of unusual monomers. Importantly, we compared both *in vivo* and *in vitro* platforms for the construction and characterization of β-amino acid incorporating ribosomes. In the future we hope to use this workflow platform to study other mutant ribosomes and screen them for the incorporation of a variety of ncAAs.

3.6 Acknowledgements and author contributions

Thank you to Tasfia Azim and Kim Hoang for helping clone the mutant ribosome constructs. Thank you to Dr. Joon Lee for his work in precharging tRNA monomers with expanded backbone substrates and testing the incorporation using MALDI, and to Dr. Antje Kruger for her scientific guidance, insight, and conversations. A special thanks to Dr. Antje Kruger for continuing work on this project and similar projecgts.

3.7 Supplementary tables and figures

Supplementary Table 3.1 Relevant plasmid DNA constructs for MS2-tagged ribosome purification.

Plasmid DNA	Resistance and strain notes
MS2-MBP-His protein	[amp^r] grow in BL21 (DE3)
P278 MS2 (for 50S mutations)	[amp^r] grow in DH5a + pCI857
pEY spur MS2 (for 30S mutations)	[amp^r] grow in DH5a + pCI857
pCI857	[Kan^r] grow in DH5a (30C)
MBP-MS2-His + V75E/A81G	Updated version of the MBP-MS2-His construct containing 2 mutations that help with preventing aggregation

CHAPTER 4

Studying and engineering ribosomes *in vivo*: Improvements to a ribosome with tethered subunits for *in vivo* ribosome engineering

The work presented in this chapter is based upon work published in:

*Carlson, E.D.; d'Aquino, *A. E.; Kim, D. S.; Fulk, E.M.; Hoang, K.; Szal, T.; Mankin, A. S.; Jewett, M. C. Engineered ribosomes with tethered subunits for expanding biological function. *Nat. Comm*. **2019**, *10*, 3920. DOI: 10.1038/s41467-019-11427-y

**These authors contributed equally to this work*

4.1 Abstract

Ribo-T is a ribosome with covalently tethered subunits where core 16S and 23S ribosomal RNAs form a single chimeric molecule. Ribo-T makes possible a functionally orthogonal ribosome–mRNA system in cells. Unfortunately, use of Ribo-T has been limited because of low activity of its original version. To overcome this limitation, we used an evolutionary approach to select new tether designs that are capable of supporting faster cell growth and increased protein expression. Further, we evolved new orthogonal Ribo-T/mRNA pairs that function in parallel with, but independent of, natural ribosomes and mRNAs, increasing the efficiency of orthogonal protein expression by 2-fold. The Ribo-T with optimized designs is able to synthesize a diverse set of proteins and can also incorporate multiple non-canonical amino acids into synthesized polypeptides. The enhanced Ribo-T designs should be useful for exploring poorly understood functions of the ribosome and engineering ribosomes with altered catalytic properties.

4.2 Introduction

The ribosome is a molecular machine responsible for the polymerization of α-amino acids into proteins [1,239]. In all kingdoms of life, the ribosome is made up of two subunits [240-242]. In bacteria, these correspond to the small (30S) subunit and the large (50S) subunit. The 30S subunit contains the 16S ribosomal RNA (rRNA) and 21 ribosomal proteins (r-proteins), and is involved in translation initiation and decoding the mRNA message [243]. The *Escherichia coli* 50S subunit contains the 5S and 23S rRNAs and 33 r-proteins, and is responsible for accommodation of amino acid substrates, catalysis of peptide bond formation, and protein excretion [10,244].

The extraordinarily versatile catalytic capacity of the ribosome has driven extensive efforts to harness it for novel functions, such as reprogramming the genetic code [174,176,218,245,246]. For

example, the ability to modify the ribosome's active site to work with substrates beyond those found in nature such as mirror-image (D-α-) and backbone-extended (β- and γ-) amino acids[138,247], could enable the synthesis of new classes of sequence-defined polymers to meet many goals of biotechnology and medicine[174,217]. Unfortunately, cell viability constraints limit the alterations that can be made to the ribosome.

To bypass this limitation, recent developments have focused on the engineering of specialized ribosome systems. The concept is to create an independent, or orthogonal, translation system within the cell dedicated to production of one or a few target proteins while wild-type ribosomes continue to synthesize genome-encoded proteins to ensure cell viability. Pioneering efforts by Hui and DeBoer [248], and subsequent improvements by Chin and colleagues [76,249-251], first created a specialized small ribosomal subunit. By modifying the Shine-Dalgarno (SD) sequence of an mRNA and the corresponding anti-Shine Dalgarno (ASD) sequence in 16S rRNA, they generated orthogonal 30S subunits capable of primarily translating a specific kind of engineered mRNA, while largely excluding them from translating endogenous cellular mRNAs. These advances enabled the selection of mutant 30S ribosomal subunits capable of re-programming cellular logic [76] and enabling new decoding properties[250].

Unfortunately, such techniques have been restricted to the small subunit because the large subunits freely exchange between pools of native and orthogonal 30S. This limits the engineering potential of the large subunit, which contains the peptidyl transferase center (PTC) active site and the nascent peptide exit tunnel. We addressed this limitation with the first fully orthogonal ribosome (termed Ribo-T), whereby the small and large subunits tethered together via helix h44 of the 16S rRNA and helix H101 of the 23S rRNA (Figure 4.1 a,c). Not only could this hybrid

rRNA be assembled into a functional ribosome in a cell, but Ribo-T could support bacterial growth in the absence of wild-type ribosomes (Figure 4.1b). We also used Ribo-T to create the first functionally orthogonal ribosome–mRNA system (Figure 4.1 d,e), and demonstrated that Ribo-T could be evolved to synthesize protein sequences that the natural ribosome cannot easily translate by selecting otherwise dominantly lethal rRNA mutations. This provided the first example of engineering new function in the large subunit of an orthogonal ribosome that was previously inaccessible [175]. Similar results were obtained more recently with an analogously-designed ribosome with conjoined subunits [215, 216]. It should be noted that while remaining functionally independent, orthogonal tethered ribosomes still share many components with native translation machinery (*e.g.,* r-proteins, elongation factors and initiation factors)[218].

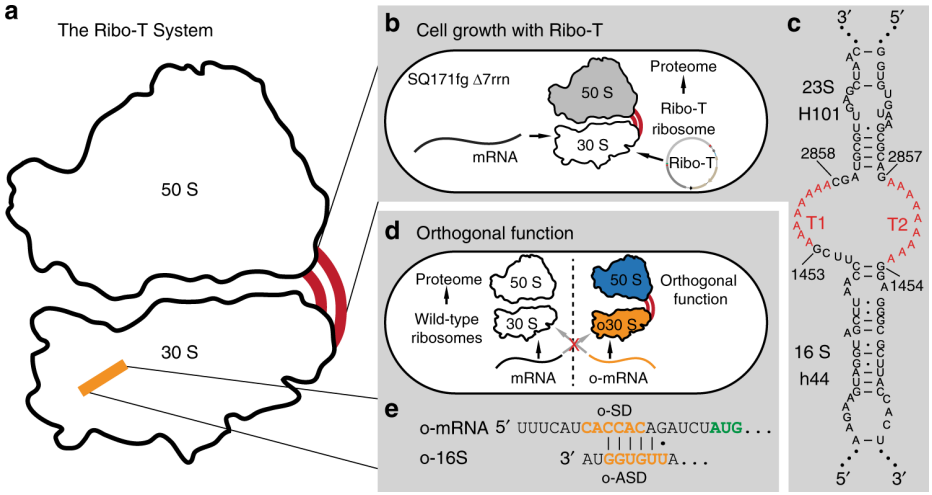

Figure 4.1 Ribo-T system improvement strategies. (a) Schematic of Ribo-T showing tether (red) and orthogonal ribosome binding site (yellow). (b) The tether is optimized in cells growing exclusively from the Ribo-T plasmid. (c) Previously published Ribo-T tether sequence. (d) Orthogonal function evolved for Ribo-T. € Previously published orthogonal mRNA (o-mRNA) Shine-Dalgarno (SD) sequence and orthogonal 16S rRNA anti-SD (o-ASD) sequence shown.

Although the functional independence of Ribo-T conceptually enables new opportunities for exploring poorly understood functions of the ribosome, facilitating orthogonal genetic systems,

and engineering ribosomes with altered chemical properties, Ribo-T possesses limitations that could hinder its broad applications [214]. For example, cells with only Ribo-T exhibit a slower growth rate than cells with natural wild type ribosomes (doubling time $\tau = 70 \pm 2$ min as opposed to $\tau = 35 \pm 1$ min for wild-type), noting that part of this growth rate defect may arise from the circular permutation of the large subunit alone and not the tethering [252]. In addition, the rate of protein synthesis in the Ribo-T cells is approximately 45% of that of the wild-type [175] possibly due to slow assembly and the resulting reduced number of functionally-active translating Ribo-T ribosomes [214]. Furthermore, the implemented orthogonal system was simply a modified version of previous works [249,253], evolved in the context of untethered ribosomes using different plasmid backbones and promoters. Finally, it is not clear if the Ribo-T system is compatible with orthogonal non-canonical amino acid (ncAA) incorporation machinery for applications that could expand the range of genetically encoded chemistry. Taken together, these features of the the initial Ribo-T system limited applications of the original design.

Here, we address these limitations through the development of an improved Ribo-T design. Specifically, we used evolutionary approaches to select new RNA tethers that connect the 16S and 23S rRNA by sampling an extended pool of tether variants differring in their composition and length. By testing libraries amounting to more than 10^{15} members, we isolated Ribo-T variants with improved properties. Specifically, cells carrying the improved variant, which we term Ribo-T version 2 (Ribo-T v2) has a 24% increase in growth rate (0.75 hr^{-1}, in SQ171fg strain) as compared to the original Ribo-T (Ribo-T v1; T1: 9A, T2: 8A) and a 12% increase in final OD_{600} at 37°C as compared to Ribo-T v1 (final Ribo-T v2 $OD_{600} = 0.9$, in SQ171fg strain). In minimal media, these advantages are even more striking, with Ribo-T v2 possessing a 79% improvement

in final OD_{600} at 37°C relative to Ribo-T v1. We then used directed evolution to improve the orthogonal function of Ribo-T. The optimized orthogonal (o)Ribo-T v2 (mRNA Shine-Dalgarno (SD): 5'-CAACCAC-3', 16S anti-SD (ASD): 5'-CUGUGG-3') has a 208% increase in overall expression of the target protein, and possessed a 16% increase in orthogonality (with an orthogonal *cat* reporter) as compared to oRibo-T v1. To demonstrate the utility of the oRibo-T v2, we expressed a variety of diverse proteins ranging from small (25 kDA) to large (116 kDa). Lastly, oRibo-T v2 was leveraged to synthesize superfolder green fluorescent protein (sfGFP) possessing multiple, identical non-cannonical amino acids (ncAAs). Our improvements expand Ribo-T's applications and make the Ribo-T system better suited for studying and leveraging orthogonal translation *in vivo*.

4.3 Materials and Methods

4.3.1 Construction of the tether libraries

Plasmid construction and DNA manipulations were performed following standard molecular biology techniques. The libraries of tether sequences were introduced into the wild-type pRibo-T plasmid by inverse PCR amplification with Phusion polymerase (NEB) with primers listed in Supplementary Table 1. All primers were synthesized by Integrated DNA Technologies. Amplification was followed by re-circularization with the Gibson assembly reaction [55] (Supplementary Figure 4.1). Specifically, Ribo-T backbone plasmid was prepared by PCR amplification with primers 5'-GGAGGGCGCTTACCACTTTG and 5'-GGTTAAGCTACCTACTTCTTTTG using pRibo-T [175] as template. Using Phusion polymerase, PCR was performed at 98 °C initial denaturing for 3 min, (98 °C 30 seconds, 55 °C 30 seconds,

72 °C 70 seconds)x25, and 72 °C final extension for 10 minutes. This amplifies the pRibo-T vector, excluding the tethers and 23S region of the plasmid.

To generate the tether libraries (Figure 4.2b), primer pools were first prepared from primers listed in Supplementary Table 1. For library 1, equimolar amounts of primers T1-A7-f through T1-A20-f were mixed to create the forward primer pool, and equimolar amounts of primers T1-T7-r through T1-T20-r were mixed to create the reverse primer pool. For library 2, equimolar amounts of primers T1-A7-f through T1-A20-f were mixed to create the forward primer pool, and equimolar amounts of primers T1-A7-r through T1-A20-r were mixed to create the reverse primer pool. Library 3 is generated using primers T1-8N-f and T2-9N-r. Library 4 is generated using primers T1-15N-f and T2-10N-r. In 4 separate PCRs under the same reaction conditions just described, respective library primers were used with template pRibo-T to generate PCR products of tether libraries flanking CP23S rRNA (Supplementary Figure 4.1). Following gel extraction of the Ribo-T backbone and 4 tether libraries from 0.7% agarose gels with E.Z.N.A. gel extraction kit (Omega), 50 ng of Ribo-T backbone was re-circularlized in 4 separate Gibson assembly reactions with 3-fold molar excess of respective libraries. 2 μL of each library was transformed into POP2136 cells (F^- *glnV44 hsdR17 endA1 thi-1 aroB mal*$^-$ *cI857* λ *PR* Tet^R) via electroporation and incubated at 30 °C to repress expression of the p_L promoter with POP2136 constitutively expressed cI repressor. 40–80 colonies were selected from each library plate and library diversity was verified by DNA sequencing (Northwestern Sequencing Core). For each library, transformations and plating was scaled until total number of colonies exceeded 3x the theoretical library sizes. Plates were then washed and miniprepped with the E.Z.N.A miniprep kit (Omega) to prepare the 4 plasmid libraries.

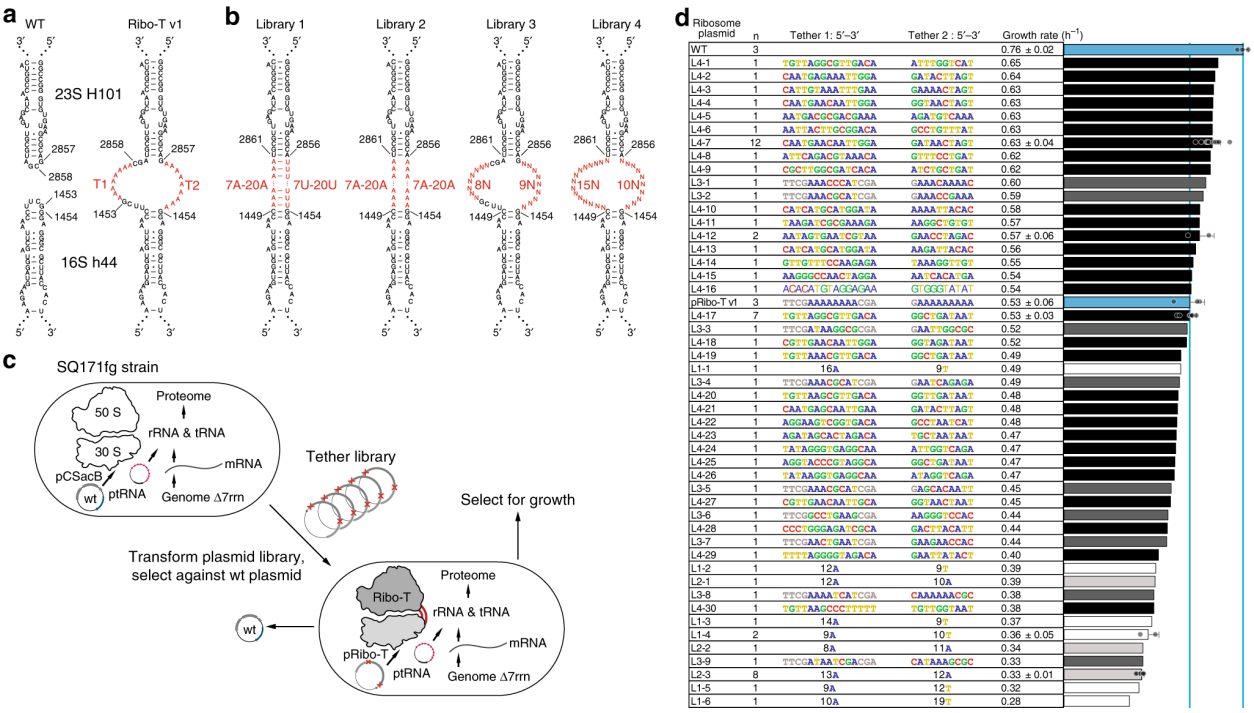

Figure 4.2 Optimizing tether sequence improves performance. (a) Wild-type 23S rRNA helix 101 and 16S rRNA helix 44 are connected to create Ribo-T with 9A for 5' tether, T1 and 8A for 3' tether, T2. (b) Library 1: paired 5' tether T1 poly A from 7-20 nucleotides, with 3' tether T2 poly T from 7-20 nucleotides. Library 2: unpaired polyA on both T1 and T2, ranging in 7-20 nucleotides long. Library 3: randomized T1 (8N) and T2 (9N) keeping residues of opened H101 and h44 apex loops. Library 4: randomized apex-to-apex T1 (15N) and T2 (10N) of tether. (c) Selection scheme for improved tethers. Strains lacking genomic copies of rRNA operons (Δ7rrn) are transformed with plasmid-based Ribo-T tether libraries, and the wild-type pCSacB plasmid (wt) is removed. (d) Tether sequences and growth rates of analyzed colonies. Error bars = 1SD of noted independent colonies, n. The top 15 Ribo-T design winners (L4-1 through L4-13) were co-cultured and passaged for 3 days. Between each passage, the bulk culture populations were sequenced and analyzed.

4.3.1 Replacement of the wild-type ribosome by Ribo-T v2

SQ171 and SQ171fg cells harboring the pCSacB plasmid were transformed with the Ribo-T v2.0 library preparations (Supplementary Figure 4.1). In brief, 20 ng of plasmid was added to 50 µL of electrocompetent cells. Cells were resuspended in 800 µL of SOC and incubated for 1 hour at 37°C with shaking. A 250 µL aliquot of recovering cells was transferred to 1.85 mL of

SOC supplemented with 50 μg mL^{-1} of carbenicillin and 0.25% sucrose (final concentrations) and grown overnight at 37°C with shaking. Cells were spun down and plated on LB agar plates containing 50 μg mL^{-1} carbenicillin, 5% sucrose and 1 mg mL^{-1} erythromycin.

4.3.2 Selecting mutants, evaluating growth rate and analyzing tethers

Colonies that appeared after 24–48 hour incubation of the plates at 37°C were inoculated in a Costar flat bottom 96-well plate containing 100 μL of LB supplemented with 50 μg mL^{-1} carbenicillin and 1 mg mL^{-1} erythromycin. Growth rates were monitored at 37°C in a BioTek microplate reader. Absorbance at 600 nm was read every 10 minutes (continuous linear shaking with a 2-mm amplitude). Doubling times were calculated from the growth curve readings during logarithmic growth as determined by regression.

The fastest growing tether mutants were inoculated in 2 mL LB supplemented with 50 μg mL^{-1} carbenicillin, 5% sucrose and 1 mg ml^{-1} erythromycin and grown for 24–48 hr. Plasmids were isolated from clones and tethers were sequenced (Northwestern Sequencing Core). Tether composition and library diversity were analyzed by sequencing with primers 5'-GCTGTCGTCAGCTCGTGTTG-3' for T1 site and 5'-CTGGAGAACTGAGGGG-3' for T2 site.

4.3.3 Liquid culture competition assay

The top 15 Ribo-T v2 tether winners identified in the initial library screen were transformed individually into SQ171fg cells. Each were grown individually in separate liquid cultures. The cultures were grown overnight at 37°C, with shaking, in LB supplemented with 50 μg mL^{-1} carbenicillin and 1 mg mL^{-1} erythromycin. After ~18 hours, the OD_{600} of each culture was measured. Equal OD_{600} units of each culture were combined into a co-culture, in triplicate, and

passaged for 3 days. Between each passage, both the bulk populations and individual resultant colonies from plated culture were sequenced via sanger sequencing and analyzed.

4.3.4 Total RNA analysis of tethered Ribo-T v2

Successful replacement of the wild type of pCSacB plasmid with the pRibo-T plasmids carrying Ribo-T v2 was confirmed via total RNA extraction. Total RNA was extracted from these clones using RNeasy Mini Kit (Qiagen) and analyzed by agarose gel electrophoresis (Supplementary Figure 4.2).

4.3.5 Selection of new orthogonal pairs

Before selection could be carried out for a highly orthogonal and active 16S/mRNA pair, the BL21(DE3)Δupp strain was prepared by deleting the genomic copy of *upp* from the BL21(DE3) strain using Datsenko-Wanner recombination [254] and replacement with a kanamycin resistance (KanR) cassette. The deletion cassette was PCR amplified from pKD4 plasmid [254] with primers 5'-AATCCGTCGATTTTTTTTGTGGCTGCCCCTCAAAGGAGAAAGAGTTGTGTAGGCTGGAGCTGCTTC and 5'-AAAAAAAAGCCGACTCTTAAAGTCGGCTTTAATTATTTTTATTCTGTCCATATGAATATCCTCCTTAG, with Phusion polymerase (NEB) and 98 °C initial denaturing for 3 min, (98 °C 30 seconds, 55 °C 30 seconds, 72 °C 2 minutes) x 25, and 72 °C final extension for 10 minutes. Plasmid pCP20 was transformed into a kanamycin-resistant colony to remove the KanR cassette by the incorporated flippase sites [254]. Transformed cells were plated on LB agar supplemented with 50 μg ml^{-1} carbenicillin and grown overnight at 30 °C. Colonies were picked, plated on LB agar plates, and grown overnight at 42 °C to select for loss of pCP20 plasmid. Colonies were checked

for kanamycin sensitivity, and deletion was confirmed by sequencing of PCR product from colony PCR using primers 5'-TGCCAGGGTAAAGGTTAG and 5'-GACGGTTGCACCAAAC, and Multiplex PCR mix (Qiagen), flanking the deletion site.

For plasmid compatibility with the rRNA pAM552 plasmid backbone, the origin of replication on pLpp5oGFP [175] was first switched from pMB1 to p15A. Plasmid origin of replication p15A was synthesized by IDT as a gBlock (Supplementary Table 1), and amplified using primers 5'-GATGGCCTTTTTGCGTTTC and 5'-CTGAGAGTGCACCATACAG with Phusion polymerase (NEB) and 98 °C initial denaturing for 3 min, (98 °C 30 seconds, 55 °C 30 seconds, 72 °C 30 seconds) x 25 cycles, and 72 °C final extension for 10 minutes. Plasmid pT7wtK [175] was amplified with primers 5'- GGATCTGTATGGTGCACTC and 5'- TGTAGAAACGCAAAAAGGCCATC with 98 °C initial denaturing for 3 min, (98 °C 30 seconds, 55 °C 30 seconds, 72 °C 2 minutes) x 25 cycles, and 72 °C final extension for 10 minutes. Following digestion with DpnI (NEB), correct sized DNA was gel extracted from a 0.7% agarose gel with E.Z.N.A. gel purification kit (Omega). Using Gibson assembly [255], 50 ng of backbone was recircularized with 3-fold molar excess of p15A insert and transformed into DH5α electrocompetent cells, plated on LB agar plates supplemented with 30 μg ml^{-1} kanamycin and isolated for sequence confirmation.

Next, *cat-upp* gene was prepared from pRepCM3 plasmid [256], containing an internal TAG codon for amber suppression. The TAG codon was mutated back to CAA with inverse PCR using primers 5'- CACCCTTGTTACACCGTTTTCCATGAGCAAACTGAAACGTTTTCATCGCTC and 5'- CTCATGGAAAACGGTGTAAC, pRepCM3 template, and Phusion polymerase (NEB) with 98 °C initial denaturing for 3 min, (98 °C 30 seconds, 55 °C 30 seconds, 72 °C 105 seconds)

x 25, and 72°C final extension for 10 minutes. PCR product was gel extracted from a 0.7% agarose gel with E.Z.N.A. gel extraction kit (Omega), and recircularized with Gibson assembly[255]. Recircularized plasmid was transformed into DH5α electrocompetent cells and plated on LB agar plates supplemented with tetracycline at 20 μg ml^{-1}.

Ptrp promoter through the *cat-upp* was amplified from pRepCM-CAA with primers 5'-GGTGGTAGATCTGTGCACTTCAAAAATCGATG and 5'-GGTGGTGCGGCCGCCAAGCTTCGAATTCTTTATTTCG, adding BglII and NotI sites respectively (underlined), with Phusion polymerase (NEB) with 98 °C initial denaturing for 3 min, (98 °C 30 seconds, 55 °C 30 seconds, 72 °C 1 min) x 25, and 72°C final extension for 10 minutes. Plasmid pT7wtK-p15A and column purified PCR product (E.Z.N.A. cycle pure kit from Omega) were digested with BglII and NotI (NEB) for 1 hour at 37 °C, and gel extracted with E.Z.N.A. gel extraction kit (Omega). 50 ng of pT7wtK-p15A backbone was ligated with 3-fold molar excess Ptrp-cat-upp insert with T4 ligase (NEB) for 14 hours at 16 °C. Product was transformed into DH5α electrocompetent cells and plated on LB agar plates supplemented with kanamycin at 30 μL ml^{-1}. Plasmids were isolated with E.Z.N.A. miniprep kit (Omega) and sequence confirmed. T7 promoter was then deleted using inverse PCR with phosphorylated primers 5'-GTGCACTTCAAAAATCGATG and 5'-GGATCCGTCGACCTGCAG with Phusion polymerase (NEB) with 98 °C initial denaturing for 3 min, (98 °C 30 seconds, 55 °C 30 seconds, 72 °C 3 min)x25, and 72 °C final extension for 10 minutes. Following gel extraction with E.Z.N.A. gel extraction kit (NEB) product was ligated with T4 ligase (NEB) for 14 hours at 16 °C, and transformed into DH5α electrocompetent cells and plated on LB agar plates supplemented with

kanamycin at 30 μL ml^{-1}. Plasmids were isolated with E.Z.N.A. miniprep kit (Omega) and sequence confirmed. This plasmid is named pPtrp-catupp-p15A.

Plasmid pPtrp-p15A (Δcatupp) was prepared from pPtrp-catupp-p15A by PCR with primers 5'-AAGAATTCGAAGCTTGG (forward primer binding at the 3' end of *cat-upp* gene, including a NotI restriction site in PCR product) and 5'-GCATCAGCGGCCGCAACGCTGCGTAGCAACAGATCTCCTCCTTATGAAAGCGAC (reverse primer binding at 5' end of gene), adding a BglII/NotI cloning site. Following column purification (E.Z.N.A. cycle pure kit, Omega), product was digested with NotI (NEB), gel extracted (E.Z.N.A gel extraction kit, Omega), and ligated with T4 ligase (NEB) for 14 hours at 16 °C. Product was transformed into DH5α electrocompetent cells and plated on LB agar plates supplemented with kanamycin at 30 μL ml^{-1}. Plasmids were isolated with E.Z.N.A. miniprep kit (Omega) and sequence confirmed.

Plasmid plpp5-catupp-p15A was prepared from plasmid pPtrp-catupp-p15A and synthesized gBlock (IDT) lpp5-oRBS-BglII (Supplementary Table 1). First, pPtrp-catupp-p15A was amplified with primers 5'-CACTGGATATACCACCGTTG and 5'-GGAAAGCCACGTTGTGTCTC. The linear product is pPtrp-catupp-p15A excluding the Ptrp promoter. Promoter lpp5 [257] with orthogonal ribosome binding site and BglII restriction site [175] was amplified from gBlock lpp5-oRBS-BglII with primers 5'-GAGACACAACGTGGCTTTCC and 5'-CAACGGTGGTATATCCAGTG. Both PCRs were run with Phusion polymerase (NEB) with 98 °C initial denaturing for 3 min, (98 °C 30 seconds, 55 °C 30 seconds, 72 °C 90 seconds) x 25, and 72°C final extension for 10 minutes. Following gel extraction from 0.7% agarose gel with E.Z.N.A. gel extraction kit (Omega), 50 ng of backbone was recircularized with 3-fold molar

excess of lpp5-oRBS-BglII insert using Gibson assembly [255]. Product was transformed into DH5α electrocompetent cells, plated in LB plates supplemented with 30 μg ml^{-1} kanamycin, incubated at 37 °C and plasmids isolated and sequenced.

Selection conditions for BL21(DE3)Δupp strain and plasmid system were determined using the pPtrp-catupp-p15A plasmid with the wild-type Shine-Dalgarno sequence (Supplementary Figure 7a).

Two colonies each of BL21(DE3)Δupp transformed with pPtrp-catupp-p15A (*cat-upp*) or pPtrp-p15A (Δ*cat-upp*) were grown in LB supplemented with kanamycin at 30 μg ml^{-1} at 37 °C overnight with shaking. Fresh LB-kanamycin (30 μg ml^{-1}) was inoculated 1/50 with overnight culture and grown for 3 hours at 37 °C with shaking. Cultures were normalized to 0.1 OD and 1 μL was plated on i) M9 minimal media agar plates supplemented with 0.2% casamino acids, 0.4% glucose, 30 μg ml^{-1} kanamycin and 5-fluorouracil at concentrations 0, 0.25, 0.5, 0.75, 1, 2.5, 5, 10 and 50 μg ml^{-1}, and ii) LB-agar plates supplemented with 30 μg ml^{-1} kanamycin and Cm at concentrations 0, 5, 10, 25, 50, 75, 100, 150 and 200 μg ml^{-1}. Plates were incubated at 37 °C for 18 hours and imaged (Supplementary Figure 8). We observed robust selection conditions and chose 10 μg ml^{-1} 5-FU for the negative selection (background cell growth ceases by 0.5 μg ml^{-1} when *cat-upp* is expressed under the Ptrp promoter and wild-type SD sequence), and 100 μg ml^{-1} Cm was used for the positive selection (minimum inhibitory concentration 5 μg ml^{-1} for the cells not expressing *cat-upp*). Of note, the Ptrp promoter (medium strength) was used in this initial assay optimization experiments along with a wild-type SD sequence (lower mRNA expression with bigger population of wild-type ribosomes) to more accurately reflect standard orthogonal system conditions (high mRNA expression with lower population of o-ribosomes). Using a stronger

promoter at this step, such as lpp5, would result in high cell burden and sickness, and thus give a poor representation of expression levels within the orthogonal system.

For selection of orthogonal pairs, the Shine-Dalgarno site on plasmid plpp5-catupp was fully randomized by PCR mutagenesis using Phusion (NEB), primers 5'-GCATCAAGATCTATGGAGAAAAAAATCACTGG and 5'-CGAGTCCAGATCTNNNNNNNGAAAAAATAACAGATATAGAATTG (IDT), and plpp5-catupp template, with 98 °C initial denaturing for 3 min, (98 °C 30 seconds, 55 °C 30 seconds, 72 °C 90 seconds) x 25, and 72°C final extension for 10 minutes. Following DpnI (NEB) digestion for 1 hour at 37 °C, PCR product was column purified with E.Z.N.A. cycle pure kit (Omega). Product was digested with BglII (NEB) for 1 hour at 37 °C, and purified by gel extraction using E.Z.N.A. gel extraction kit (Omega). Linear product was re-circularized with T4 ligase (NEB) for 14 hours at 16 °C.

Ligated product was transformed into DH5α cells (NEB), and plated on LB-agar plates supplemented with 30 μg ml^{-1} kanamycin and incubated overnight at 37 °C. Transformation and plating was repeated until colony counts exceeded 3x library size. Plates were then washed and miniprepped to generate a plasmid library. Two μL of purified plasmid library was transformed into electrocompetent BL21(DE3)Δupp and plated on M9 minimal media agar plates supplemented with 0.2% casamino acids, 0.4% glucose, 10 μg ml^{-1} 5-FU, 30 μg ml^{-1} kanamycin and 0.1 mM isopropyl-β-D-thiogalactopyranoside (IPTG). Plates were incubated for 24 hours at 37 °C. Plates were washed and the pellet was washed three times with LB-Lennox supplemented with 30 μg ml^{-1} kanamycin, and used to inoculate 500 ml LB-Lennox supplemented with 30 μg ml^{-1} kanamycin to prepare electrocompetent cells.

In a first round of selection, the anti-Shine-Dalgarno of pAM552-LT, encoding for wild-type untethered ribosomes, was fully randomized for a library of 4,096 theoretical members. Specifically, pAM552-LT ASD was fully randomized by PCR mutagenesis using Phusion (NEB), primers 5'-GCATCAGGTAACCGTAGGGGAACCTGCGGTTGGATCANNNNNNTACCTTAAAGAAG CGTAC and 5'- CCCTACGGTTACCTTGTTACG (IDT), with 98 °C initial denaturing for 3 min, (98 °C 30 seconds, 55 °C 30 seconds, 72 °C 2 minutes) x 25, and 72°C final extension for 10 minutes. PCR product was column purified with E.Z.N.A. cycle pure kit (Omega), and digested with BstEII and DpnI (NEB) for 1 hour at 37 °C, and purified by gel extraction using E.Z.N.A. gel extraction kit (Omega). Linear product was re-circularized with T4 ligase (NEB) for 14 hours at 16 °C. Ligated product was transformed into POP2136 electrocompetent cells, and plated on LB-agar plates supplemented with 50 μg ml^{-1} carbenicillin and incubated overnight at 30 °C. Transformation and plating was repeated until colony counts exceeded 3x library size. Plates were then washed and mini-prepped to generate a plasmid library.

The library was transformed into BL21(DE3)Δupp cells containing the negatively selected mRNA library. Cells were recovered in 1 ml SOC, and used to inoculate 50 ml LB supplemented with 30 μg ml^{-1} kanamycin, 50 μg ml^{-1} carbenicillin and 1 mM IPTG. Cultures were grown for 3 hours at 37 °C with shaking at 250 rpm. One ml aliquots were plated on LB agar plates supplemented with 30 μg ml^{-1} kanamycin, 50 μg ml^{-1} carbenicillin, 1 mM IPTG and 100 μg ml^{-1} Cm. Surviving colonies were picked and grown in 96 deep-well format in 750 μL LB media supplemented with 50 μg ml^{-1} carbenicillin and 30 μg ml^{-1} kanamycin at 37 °C for 18 hours. Total plasmids were extracted with Zyppy™-96 plasmid miniprep kit (Zymo Research).

To isolate the pAM552-LT rRNA plasmid and plpp5-catupp reporter plasmids from the total plasmid pool, we identified unique restriction sites on each plasmid that is absent from the other (KpnI present on pAM552-LT, BamHI present on plpp5-catupp). To isolate pAM552-LT, we digested the total plasmid pool with BamHI-HF restriction enzyme (NEB), transformed the digestion pool into POP2136 $CaCl_2$ chemically competent cells, and plated on LB agar plates supplemented with 50 μg ml^{-1} carbenicillin and grown overnight at 30 °C. To isolate plpp5-catupp, total plasmids were digested with KpnI restriction enzyme (NEB), and transformed into DH5alpha $CaCl_2$ chemically competent cells, and plated on LB agar plates supplemented with 30 μg ml^{-1} kanamycin and grown overnight at 37 °C.

Individual plasmids were isolated with E.Z.N.A. miniprep kit (Omega) for sequencing of the Shine-Dalgarno region of plpp5-catupp, and the anti-Shine-Dalgarno region of pAM552-LT (NU genomics core). $CaCl_2$ chemically competent BL21(DE3)Δupp cells containing pAM552 plasmid were transformed with the plpp5-catupp isolated members, and plated on LB agar plates supplemented with 50 μg ml^{-1} carbenicillin and 30 μg ml^{-1} kanamycin and grown overnight at 37 °C. Pair performance was initially evaluated by plating cells on a range of Cm. Colonies were picked into 100 μL of LB supplemented with 50 μg ml^{-1} carbenicillin and 30 μg ml^{-1} kanamycin and grown to saturation overnight at 37 °C with shaking. Cultures were diluted 1/50 into fresh LB supplemented with 50 μg ml^{-1} carbenicillin, 30 μg ml^{-1} kanamycin and 1 mM IPTG and grown at 37 °C with shaking for 3 hours. LB-agar plates supplemented with 50 μg ml^{-1} carbenicillin, 30 μg ml^{-1} kanamycin, 0.1 mM IPTG and Cm at 0, 0.5, 1, 2.5, 10, 20, 40, 60, 80, 100, 200, 300, 400 or 500 μg ml^{-1} were spot plated with 1 μL of induced culture and incubated at 37 °C for 18 hours. Max Cm concentration with growth was noted (Supplementary Figure 9a).

Reporter plasmids from top performing pairs were pooled and transformed into fresh BL21(DE3)Δupp strain. Cells were plated on LB agar plates supplemented with 30 μg ml^{-1} kanamycin and grown overnight at 37 °C. Plates were washed and the pellet was washed three times with LB-Lennox supplemented with 30 μg ml^{-1} kanamycin, and used to inoculate 500 ml LB-Lennox supplemented with 30 μg ml^{-1} kanamycin to prepare electrocompetent cells.

With version 2 tethers evolved and characterized, the improved tether sequences were cloned into poRibo-T2 plasmid [175], named pORT1A. The anti-Shine-Dalgarno sequence of pORT1A was randomized with the protocol described above, and passaged through POP2136 cells at 30 °C (expression from p_{LT} promoter repressed by cI repressor). Positive selection was repeated as described above in the first round. Total plasmid was extracted from colonies using the Zyppy™-96 plasmid miniprep kit (Zymo Research). Reporter and rRNA plasmids were isolated with KpnI and BamHI-HF digestion, respectively, as before.

4.3.6 Evaluation of new orthogonal pairs

Plasmid plpp5.A.cat was prepared by digesting plasmid plpp5.A.gfp with BglII (NEB) and NotI (NEB), restriction sites flanking the *sf-gfp* coding sequence. Backbone was purified by gel extraction using E.Z.N.A. gel extraction kit (Omega). PCR was performed on template pAM552C (Mankin Lab) using primers 5'-GGTGGTAGATCTATGGAAAAAAAAATCACCGG and 5'-GGTGGTGCGGCCGCGCTTATTAGGCGGGCTAGG (BglII and NotI restriction sites underlined) with Phusion polymerase (NEB) with 98 °C initial denaturing for 3 min, (98 °C 30 seconds, 55 °C 30 seconds, 72 °C 2 minutes) x 25, and 72°C final extension for 10 minutes.

For the superfolder green fluorescent protein (*sf-gfp*) assay, 3 colonies for each pair were picked and grown to saturation at 37 °C. Fresh LB supplemented with 30 μg ml^{-1} kanamycin, 50

μg ml^{-1} carbenicillin and 1 mM IPTG was inoculated with 1/50 saturated culture and grown at 37 °C for 18 hours on Biotek Synergy H1 plate reader with linear shaking at 2 mm. OD_{600} and 485/528 excitation/emission were monitored.

For Cm acetyltransferase (CAT) assay, 6 colonies for each pair were picked and grown to saturation at 37 °C. Fresh LB supplemented with 30 μg ml^{-1} kanamycin, 50 μg ml^{-1} carbenicillin and 1 mM IPTG was inoculated with 1/50 saturated culture and grown at 37 °C for 3 hours. 96 well plates containing 100 μL LB supplemented with 30 μg ml^{-1} kanamycin, 50 μg ml^{-1} carbenicillin and 1 mM IPTG, and 0, 0.5, 1, 2.5, 5, 10, 20, 30, 40, 50, 60, 70, 100, 150, 200 or 300 μg ml^{-1} Cm were inoculated with 1/100 induced culture. Plates were incubated for 18 hrs at 37 °C with shaking. OD_{600} was read on BioTek Synergy H1 plate reader, and IC_{50} values (Figure 4.5c) determined using the IC_{50} toolkit (ic50.tk).

4.3.7 Evaluation of Ribo-T growth in minimal media

Wild type ribosomes, Ribo-T v1, and Ribo-T v2 growth (both orthogonal and non-orthogonal) were grown on M9-casamino acids (M9CA) minimal media plates at 30 °C, 37 °C, and 42 °C in a spot-plating format. Colonies appeared after 24–48 hour incubation on each plate, and were subsequently picked and used to inoculate a Costar flat bottom 96-well plate containing 100 μL of M9CA supplemented with 50 μg ml^{-1} carbenicillin (orthogonal constructs) or 50 μg ml^{-1} carbenicillin and 1 mg ml^{-1} erythromycin. Growth rates were monitored at 30 °C, 37 °C, and 42 °C in a BioTek microplate reader. Absorbance at 600 nm was read every 10 minutes (continuous linear shaking with a 2-mm amplitude). Doubling times were calculated from the growth curve readings during logarithmic growth as determined by regression.

4.3.8 Expression and purification of recombinant proteins using oRibo-T v2

Plasmids plpp5.B.LacZ and plpp5.B.ApNGT were prepared by Gibson assembly. Briefly, PCR products were digested with DpnI (NEB), gel extracted as before, and Gibson assembled [255] with 50 ng backbone and 3-fold molar excess insert. Two µL of the assembled products were co-transformed with Ribo-T v2 (pORT3) into BL21(DE3) cells via electroporation, recovered in 1 ml SOC, and plated on LB-agar supplemented with 50 µg ml^{-1} carbenicillin and 30 µg ml^{-1} kanamycin. Plates were grown overnight at 37°C. Plasmids were purified from colonies with E.Z.N.A. miniprep kit (Omega), and sequence-confirmed (Northwestern Sequencing Core).

Sequence confirmed clones were grown overnight in 5 ml LB supplemented with 50 µg ml^{-1} carbenicillin and 30 µg ml^{-1} kanamycin. After ~18 hours, saturated cultures were used to inoculate fresh cultures of 5 ml LB supplemented with 30 µg ml^{-1} kanamycin, 50 µg ml^{-1} carbenicillin. At an OD_{600} of 0.8, the cultures were induced with 1 mM IPTG. Cultures were grown for 3 hours at 37 °C with shaking at 250 rpm. 10 uL of each expression culture was analyzed by SDS-PAGE, on a 4-15% gradient polyacrylamide gel (BioRad). Band intensities were subsequently quantified using Image Studio software.

A sequence confirmed clone containing oRibo-T v2 and the orthogonal protein construct of interest was used to inoculate a 5 mL overnight culture in LB supplemented with 50 µg ml^{-1} carbenicillin and 30 µg ml^{-1} kanamycin. After ~18 hours, saturated cultures were used to inoculate fresh cultures of 5 ml LB supplemented with 30 µg ml^{-1} kanamycin, 50 µg ml^{-1} carbenicillin. At an OD_{600} of 0.8, the cultures were induced with 1 mM IPTG. Cultures were grown for 3 hours at 37 °C with shaking at 250 rpm. The induced cultures were pelleted at 6,170 x g for 10 minutes at 4 °C. The pellets were washed with in 10 mL of binding buffer (50 mM NaH_2PO_4, 300 mM NaCl, 10 mM Imidazole, 6 mM BME, adjusted to pH 8) and stored at -20°C. Cells were resuspended in

cold lysis buffer (1M Tris HCl, pH 8, 3 M NaCl, 50% Glycerol, 1M BME) with vortexing and rocking. The cell suspension was cooled on ice for 10 minutes and then sonicated in 10 bursts of 10 seconds followed by intervals of 10 seconds of cooling. Cellular debris was removed by two centrifugations at 4 °C for 15 minutes at 14,500 x g in SS-34 centrifuge tubes. The lysate was collected after the second centrifugation, and transferred to Ni-NTA resin that was pre-equilibrated with 3 column volumes of binding buffer. Proteins were purified in batch, in 15 mL falcon tubes. The lysate was incubated with the Ni-NTA resin for one hour at 4°C with rocking. After incubation, the resin was centrifuged at 500 x g for 5 minutes, and the supernatant was removed. The Ni-NTA resin was washed 3 times with 3 column volumes of binding buffer, and then incubated with elution buffer (50 mM NaH_2PO_4, 300 mM NaCl, 200 mM Imidazole, 6 mM BME, adjusted to pH 8). Elution fractions were collected, run on an SDS-PAGE gel, and stained with Coomassie.

4.3.9 Strain construction for ncAA incorporation with oRibosomes

Strain C321.ΔA [258] contains the cI repressor, which represses p_L promoter driving expression of the rRNA constructs. Therefore, the strain was prepared for use in the following experiments. Firstly, $mutS^-$ genotype was mutated back to mutS wild-type ($mutS^+$) by multiplex advanced genome engineering (MAGE) [259] and the MAGE oligo accccatgagtgcaatagaaaatttcgacgcccatacgcccatgatgcagcagtatctcaggctgaaagcccagcatcccgagatcctgc. Mutations to $mutS^+$ were screened with colony PCR and primers 5'-CATGATGCAGCAGTATCTCAG and 5'-CTTCTGCATACAGCAGTTC and confirmed by sequencing.

To remove cI repressor, the λ-red machinery and the *bla* resistance marker, a kanamycin knockout cassette was generated from pKD4 plasmid [254] with primers 5'-GTATGTCGTTTCAGCTAAACGGTATCAGCAATGTTTATGTAAAGATGTGTAGGCTGGAGCTGCTTC and 5'-TTTGCCGACTACCTTGGTGATCTCGCCTTTCACGTAGTGGACAAAGTCCATATGAATATCCTCCTTAG with Phusion polymerase and 98 °C initial denaturing for 3 min, (98 °C 30 seconds, 55 °C 30 seconds, 72 °C 30 seconds)x25, and 72 °C final extension for 10 minutes. Product was column purified with E.Z.N.A. cycle pure kit (Omega). Expression of λ-red machinery was induced with a 15-minute incubation at 42 °C, and electrocompetent cells were prepared. KanR knockout cassette was electroporated into the cells, plated on LB agar supplemented with 30 μg ml^{-1} kanamycin and incubated overnight at 42 °C to select against heat-induced toxic expression of λ-red cassette. Kanamycin resistant colonies were screened for sensitivity to carbenicillin, indicating loss of *bla*. A sensitive colony was picked and transformed with pCP20 plasmid for removal of kanamycin marker by the incorporated flippase sites [254]. Transformed cells were plated on LB agar supplemented with 50 μg ml^{-1} carbenicillin and grown overnight at 30 °C. Colonies were picked, plated on LB agar plates, and grown overnight at 42 °C to select for loss of pCP20 plasmid. Colonies were checked for kanamycin sensitivity, and deletion was confirmed by sequencing of PCR product from colony PCR using primers 5'-GCCGACTCTATATCTATACCTTCATC and 5'-GCAACCGAGCGTTCTGAAC, and Multiplex PCR mix (Qiagen), flanking the deletion site. Furthermore, this strain has *upp* gene knocked out using the same methodology described in preparing the BL21(DE3)Δupp strain above. This strain is named MCJ.1217.

4.3.10 Combined orthogonal ribosome-sf-GFP reporter system

The orthogonal *sf-gfp* cassette was amplified from plpp5.B.gfp template with primers 5'-AGAGTTGGATCCCCTTGTATTACTGTTTATGTAAGC and 5'-AAGAGTT**GGCGCGCC***AAAAAAAAGCCCGCCTTTCGGCGGGCTTTG*TTATTTTTCGAACTGCGGATG for forward orientation, and primers 5'-AGAGTT**GGCGCGCC**CCTTGTATTACTGTTTATGTAAGC and 5'-AAGAGTTGGATCC*AAAAAAAAGCCCGCCTTTCGGCGGGCTTTG*TTATTTTTCGAACTGCGGATG for reverse orientation using Phusion polymerase (NEB) with 98 °C initial denaturing for 3 min, (98 °C 30 seconds, 55 °C 30 seconds, 72 °C 2 min)x25, and 72 °C final extension for 10 minutes. Added BamHI restriction site is underlined, added AscI restriction site is bolded, and t500 terminator is italicized. Plasmid backbones were amplified from plasmids pAM552, pO2 or pORT3 with primer 5'-CCTGTCGTCATATCTACAAG flanking the AscI restriction site and primer 5'-AAGAGTTGGATCCTGTAGAAACGCAAAAAGGCCATC, adding in a BamHI restriction site, using Phusion polymerase (NEB) with 98 °C initial denaturing for 3 min, (98 °C 30 seconds, 55 °C 30 seconds, 72 °C 2 min)x25, and 72 °C final extension for 10 minutes. PCR products were individually purified by E.Z.N.A. cycle pure kit (Omega), and digested with BamHI-HF and AscI (NEB) for 1 hour at 37 °C. Digestion products were purified by gel extraction with 1% agarose gel and E.Z.N.A. gel extraction kit (Omega), and ligated in all combinations (Supplementary Figure 13a) with T4 DNA ligase (NEB). Two µL of each ligation product was transformed into POP2136 cells via electroporation, plated on LB-agar supplemented with 50 µg ml^{-1} carbenicillin, and grown overnight at 30 °C to repress plasmid *rrn* expression. Plasmids were purified from colonies with E.Z.N.A. miniprep kit (Omega), and sequence-confirmed

(Northwestern Sequencing Core). Plasmids constructed are named pAM.B.gfp-f, pAM.B.gfp-r, pO2B.gfp-f, pO2B.gfp-r, pORT3B.gfp-f and pORT3B.gfp-r.

Six replicates of each construct were picked and grown to saturation at 30 °C in LB supplemented with 50 μg ml^{-1} carbenicillin. Fresh LB supplemented with 50 μg ml^{-1} carbenicillin, was inoculated with 1/50 volume saturated culture and grown at 30 °C for 4 hours, then 42 °C for 12 hours in the Biotek Synergy H1 plate reader with linear shaking at 2 mm. OD_{600} and fluorescence (485 nm/528 nm excitation/emission) was monitored.

4.3.11 Incorporation of p-azido-phenylalanine using oRibo-T

The integrated ribosome-*sf-gfp* plasmids with the *sf-gfp* gene in the reverse direction relative to rRNA operons were used as the backbone, and amplified with primers 5'-GACCACATGGTTCTGCAC and 5'-CGCTGAATTTGTGACCGTTC with the same PCR conditions as above. Plasmids pDT7sfGFP1TAGTT2 (1TAG) and pDT7sfFP5TAGTT2 (5TAG) [260] were used as templates with primers 5'-CGGTCACAAATTCAGCGTG and 5'-TTCGTGCAGAACCATGTG with the same PCR conditions as above. PCR products were digested with DpnI (NEB), gel extracted as before, and Gibson assembled [255] with 50 ng backbone and 3-fold molar excess insert. Two μL of the assembled products were transformed into POP2136 cells via electroporation, plated on LB-agar supplemented with 50 μg ml^{-1} carbenicillin, and grown overnight at 30 °C. Plasmids were purified from picked colonies with E.Z.N.A. miniprep kit (Omega), and sequence-confirmed (Northwestern Sequencing Core).

Plasmid pEVOL-pAzF, a gift from Peter Schultz (Addgene plasmid # 31186) [261], and the sequence-verified plasmid of each ribosome-*sf-gfp* construct were co-transformed into MCJ.1217 cells and plated on LB agar plates supplemented with 50 μg ml^{-1} carbenicillin and 34 μg ml^{-1} Cm.

Six colonies each were picked and grown to saturation at 37 °C in LB supplemented with 50 μg ml^{-1} carbenicillin and 34 μg ml^{-1} Cm. Fresh LB supplemented with 50 μg ml^{-1} carbenicillin, 34 μg ml^{-1} Cm, 0.2% w/v arabinose, 1 mM IPTG, and 1 mM *p*-azido-L-phenylalanine was inoculated with 1/50 volume saturated culture and grown at 37 °C for 18 hours in the Biotek Synergy H1 plate reader with linear shaking at 2 mm. OD_{600} and fluorescence (485 nm/528 nm excitation/emission) was monitored.

4.3.12 Chemical probing of the structure of the Ribo-T tethers

Ribo-T v1 and Ribo-T v2 were isolated from the exponentially-growing E. coli SQ171fg cultures [175]. Specifically, cells expressing Ribo-T v1 or Ribo-T v2 were grown overnight at 37 °C in LB medium supplemented with 50 μg ml^{-1} ampicillin and 25 μg ml^{-1} spectinomycin. The cultures were diluted 1:100 into 1 L of fresh LB media supplemented with the same antibiotics and grown with vigorous shaking until optical density reached $A_{600} = 0.5$. Cells were collected by centrifugation for 20 min at 4000 rpm (4°C) in JA-10 rotor (Beckman) and stored at -80 °C. Cell pellets were resuspended in 20 ml of the buffer 10 mM HEPES-KOH, pH 7.6, 50 mM KCl, 10 mM $Mg(OAc)_2$, 7 mM β-mercaptoethanol and lysed in EmulsiFlex-C3 homogenizer (AVESTIN Inc) at 15000 psi for 5 min. Lysate was clarified by centrifugation for 30 min at 20,000 x g (4 °C) in JA-25.50 rotor (Beckman). After adding $(NH_4)_2SO_4$ to 1.5 M, tubes were centrifuged for 1 h at 20,000 x g (4°C) in JA-25.50 rotor (Beckman). The Ribo-T-containing supernatant was filtered through the 0.22-μm ∅ 30 mm polyethersulfone (PES) membrane filter, (CELLTREAT scientific products) and loaded on the 5 ml HiTrap Butyl FF column (GE Healthcare Life Sciences) in the buffer 20 mM HEPES-KOH, pH 7.6, 10 mM $Mg(OAc)_2$, 7 mM β-mercaptoethanol, 1.5 M $(NH_4)_2SO_4$. The column was washed with 25 ml of 20 mM HEPES-KOH, pH 7.6, 10 mM

$Mg(OAc)_2$, 7 mM β-mercaptoethanol, 1.2 M $(NH_4)_2SO_4$, and Ribo-T were eluted with the buffer 20 mM HEPES-KOH, pH 7.6, 10 mM $Mg(OAc)_2$, 7 mM β-mercaptoethanol, 0.75 M $(NH_4)_2SO_4$. Eluate fractions containing Ribo-T were pooled together and loaded over 16 ml of 30% sucrose cushion prepared in the buffer 20 mM HEPES-KOH, pH 7.6, 10 mM $Mg(OAc)_2$, 30 mM NH_4Cl, 7 mM β-mercaptoethanol. Ribosomes were pelleted by centrifugation at 36,000 rpm for 18 h at 4°C in the Type 70 Ti rotor (Beckman). Ribosome pellets were resuspended in the storage buffer (20 mM HEPES-KOH pH 7.6, 30 mM KCl, 6 mM $Mg(OAc)_2$, 7 mM β-mercaptoethanol) and stored at -80 °C.

Modification of Ribo-T with dimethylsulfate (DMS) was carried out in the final volume of 50 µl of the buffer 80 mM HEPES/KOH pH 7.6, 10 mM $MgCl_2$, 100 mM NH_4Cl; containing Ribo-T at the concentration of 0.2 µM. The modification reaction was initiated by addition of 2 µl of DMS (diluted 1:10 v/v in ethanol) to the Ribo-T solution. Reactions were incubated for 10 min at 37 °C and quenched by addition of 50 µl of stop buffer (300 mM NaAc, pH 5.5, 500 mM β-mercaptomethanol) and 300 µl ethanol.

rRNA was isolated by phenol-chloroform extraction and used as a template for primer extension reactions, employing primer L2904 with the AAGGTTAAGCCTCACGG for the T1 linker and primer S1516 with the CCCTACGGTTACCTTGTTACG for the T2 linker.

4.3.13 RNA structure modeling

RNA structure prediction and analysis software (RNAStructure)[262] was used to compare the secondary structure and hybrid free energies of the Ribo-T v2 tethers. Specifically, the bifold web server was used to compare the hybrid free energy folds between the two sequences of RNA, also allowing potential intramolecular base pairing interactions. Default parameters of 5%

maximum energy difference, maximum loop size of 30 nucleotides, and a temperature of 310.15 K were set before query submission. Structures with the lowest hybrid free energy were selected for comparison across library members.

4.3.14 Protein secondary structure map generation

Protein secondary structure maps were generated using STRIDE [263], a web server for secondary structure assignment. PDB identifiers for each protein were input to the webserver from RCSB PDB. Visual outputs were produced from each protein. The following PDB IDs were used: 1EMA [https://www.ncbi.nlm.nih.gov/pubmed/8703075], 3CLA [https://www.ncbi.nlm.nih.gov/pubmed/2187098], 3Q3E [https://www.ncbi.nlm.nih.gov/pubmed/21908603], and 1JYX [https://www.ncbi.nlm.nih.gov/pubmed/11732897].

4.4 Results

4.4.1 Tether optimization improves growth of Ribo-T cells

We first sought to improve Ribo-T function by optimizing the tether for length and sequence composition (Figure 4.2 a,b). The original Ribo-T's (Ribo-T v1) 9-adenine tether T1 connects the 3' 16S rRNA residue G1453 of helix 44 (h44) to the 5' 23S rRNA C2858 of helix 101 (H101), and a 8-adenine tether T2 links G2857 of H101 to G1454 of h44 (Figure 2a). Our initial choice of these oligo(A) tethers for Ribo-T was based on the simplicity of the linker sequence and its presumed resistance to the action of cellular nucleases [175]. We wondered if replacing unpaired linkers with sequences capable of base-pairing with each other and forming a double stranded RNA stem would be beneficial for Ribo-T stability and functionality. To test this, we designed four libraries of T1 and T2 tethers at the H101/h44 subunit connection point (Figure

4.2b). Libraries 1 and 2 explore tether length in a paired and unpaired format, respectively, without the apex loop remnants present in our original library design [175]. Specifically, library 1 explores tether length with potential base pairing using a 7A-20A T1 tether paired with a 7U-20U T2 tether (for a total library size of 196 members). Library 2 explores a dual poly(A) tether ranging from 7A-20A (196 members). Libraries 3 and 4 explore tether sequence with fixed length of the published pRibo-T tether [175]. Library 3 keeps the apex loop remnants of the original Ribo-T sequence for an 8N/9N randomized library of $1.7x10^{10}$ members, while library 4 fully randomizes the h44-tether-H101 structure for a 15N/10N randomized library of $1.1x10^{15}$ members, although the entire sequence space was not accessed experimentally because of transformation limitations.

Following library construction (Supplementary Figure 4.1), the resulting libraries were individually transformed into the *Escherichia coli* SQ171fg strain [175], which was evolved from the SQ171 strain [66] that lacks chromosomal rRNA alleles and survives on the pCSacB plasmid that carries the wt *rrnB* operon and the tRNA67 plasmid that carries missing tRNA genes. The pCSacB plasmid also contains a counter selectable marker *sacB* gene, that confers sensitivity to sucrose. Distinct from the SQ171 strain, the SQ171fg strain contains mutations that were previously shown to improve the growth of the Ribo-T cells [175]. The Ribo-T 23S rRNA in each library contains an A2058G mutation, conferring resistance to erythromycin that facilitates the selection of cells expressing functional Ribo-T. Colonies grew from all libraries in the presence of sucrose (indicating the loss of the pCSacB plasmid) and erythromycin, demonstrating full support of the cellular protein synthesis by tethered Ribo-T expressed from the plasmid (Figure 4.2c). Agarose gel electrophoresis of total RNA of a sampling of colonies from each library show the expected dominant Ribo-T size RNA corresponding to the 16S–23S chimera instead of the individual 16S

and 23S bands, confirming no significant wild-type ribosome contamination or tether cleavage (Supplementary Figure 4.2). Individual colonies (~50-100) were picked from each library (biasing towards bigger colonies), tethers were sequenced, and growth rates were determined (Figure 4.2d). While viable clones supported by intact tethered ribosomes were isolated from each library (Supplementary Figure 4.2), Library 4 was most successful in yielding clones with improved growth rates compared to pRibo-T v1 (Figure 4.2d).

We next carried out additional evolutionary experiments to let the cells with the top 15 most improved tether sequences that emerged from this selection compete in liquid culture. Specifically, the top 15 strains (Figure 4.2d, L4-1 through L4-13) were individually grown in separate liquid cultures, combined at equal OD_{600} in co-culture, in triplicate, and passaged for three days. Between each passage, both the bulk populations and individual resultant colonies from plated cultures were sequenced and analyzed (Supplementary Figure 4.3). After 3 passaging days, all 3 cultures converged to sequence L4-7, which we term Ribo-T v2 (Figure 4.3a).

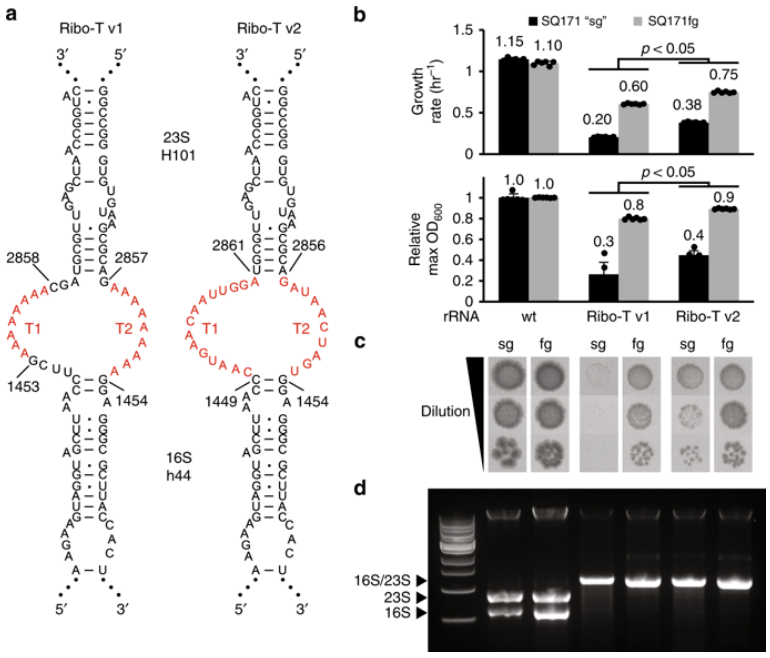

Figure 4.3 Optimizing tether sequence improves performance. a. Ribo-T v1: previously published tether sequence. Ribo-T v2: fastest growing and most frequent selected tether sequence. b. Growth rate and max OD_{600} of SQ171 slow growing (sg) and SQ171 and fast growing (fg) cells growing with pAM552 (wild-type *rrnb* operon), pRibo-T v1 and pRibo-T v2 (n=6; paired t-test [two-sided], $p<0.05$). Error bars = 1 SD. c. Spot plated SQ171 and SQ171fg cells growing with pAM552, pRibo-T v1 and pRibo-T v2 imaged after 48 hours at 37 °C. d. Total RNA extraction from SQ171 and SQ171fg cells growing with pAM552, pRibo-T v1 and pRibo-T v2.

In both liquid culture growth (Figure 4.3b) and plate growth assays (Figure 4.3c), cells supported exclusively by pRibo-T v2 outperform pRibo-T v1 in both SQ171 and SQ171fg strains. Specifically, in the SQ171fg strain, the pRibo-T v2 plasmid improves growth rate by 24% and the maximum OD_{600} in LB media by 12% as compared to the pRibo-T plasmid (n=6, paired t-test [two-sided], $p<0.05$). The benefits are more pronounced in the original SQ171 strain, where growth rate improves by 86%, and max OD_{600} by 70% as compared to pRibo-T (n=6, paired t-test [two-sided], $p<0.05$). The growth curves also highlight a significantly reduced lag time in cell growth for Ribo-T v2 cells versus Ribo-T v1 cells in both SQ171 and SQ171fg strains

(Supplementary Figure 4.4). Agarose gel electrophoresis of total RNA extracted from cells supported by pRibo-T v2 plasmids show the expected 16S-23S sized RNA, and the loss of individual 16S and 23S rRNA bands (Figure 4.3d).

We next tested if the Ribo-T v2 growth improvement properties were robust, by comparing growth relative to Ribo-T v1 in different strains (*i.e.,* SQ171, SQ171fg, POP2136), at various growth temperatures (30°C, 37°C, and 42°C) and different media (Supplementary Figure 4.5). We observed appreciable improvements in each case. The advantage of Ribo-T v2 was especially pronounced at 30 °C in M9-casamino acids (M9CA) minimal media with a 78% and 69% improvement, respectively, in final max OD and average doubling time over Ribo-T v1 (Supplementary Figure 4.5e and 4.5f). Since the Ribo-T v2 design showed superior growth characteristics, remained uncleaved, and outperformed other tether sequences in a liquid culture competition, this construct was selected for future experiments.

While we do not have a simple explanation for why the newly selected tethers improve the growth rate of Ribo-T v2 cells relative to Ribo-T v1, it may be attributed to the possible partial pairing of the new tethers. Specifically, chemical probing and modeling of the secondary structure [262] suggest that a segment of the tethers may form a base-paired duplex (Supplementary Figure 4.6). Conceivably, the structure of the improved tethers may either facilitate the Ribo-T v2 assembly, which as we know is one of the main limiting properties of the original Ribo-T design [214] or may better facilitate the relative movement of the tethered subunits during initiation, elongation of termination steps of translation.

4.4.2 Improvement of Ribo-T orthogonal function

After selecting optimized tethers, we sought to improve the orthogonality of the tethered ribosome system. Orthogonal function of Ribo-T is achieved by altering the mRNA Shine-Dalgarno (SD) sequence and the corresponding anti-Shine-Dalgarno (ASD) sequence of the 16S rRNA. In this way, a specialized pool of orthogonal Ribo-T (oRibo-T) is created that exclusively translates the cognate mRNA and in principle, should be functionally isolated from the pool of wild-type mRNA and ribosomes. Our oRibo-T system [175] utilized a modified version of a previously developed orthogonal 30S subunit system [249], not one developed in the Ribo-T context. We hypothesized that because initiation with Ribo-T is limiting [175,214], optimizing the SD/ASD pairing could improve orthogonal system functionality.

The goal of this effort was to improve orthogonal protein expression by oRibo-T v2, while minimizing cross-talk of the orthogonal mRNA with wild-type ribosomes. To this end, we used a robust directed evolution approach [249] to select highly functional and orthogonal Ribo-T v2/mRNA pairs (Figure 4.4). Specifically, a fusion of the *cat* and *upp* genes (Supplementary Figure 4.7a) enables both a positive and a negative selection from a single gene product: chloramphenicol acetyltransferase encoded in the *cat* gene confers resistance to chloramphenicol (Cm), whereas the fused *upp* gene codes for uracil phosphoribosyltranferase causing cell death in the presence of 5-fluorouracil (5-FU) (Supplementary Figure 4.8).

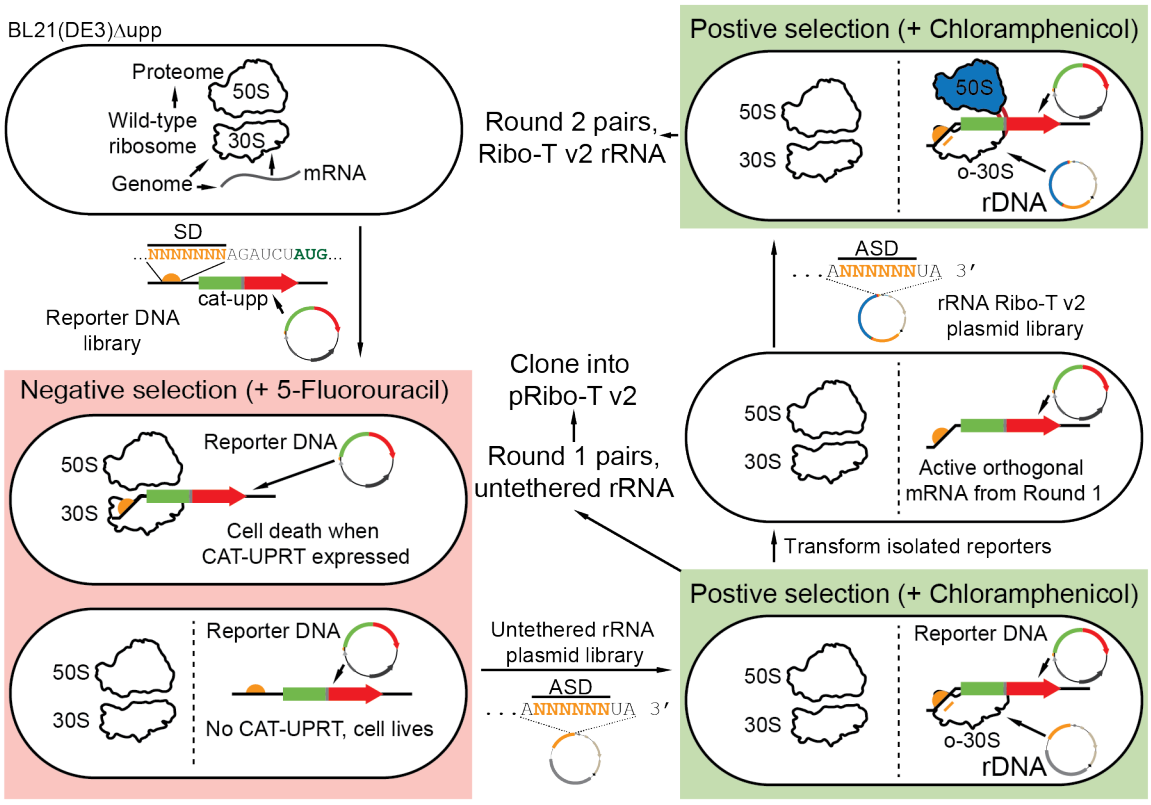

Figure 4.4 Improving orthogonal pairs. Selection scheme to optimize orthogonal Shine-Dalgarno (SD) and anti-Shine-Dalgarno (ASD) pairs in untethered and tethered context.

For the negative selection step, the wild-type SD sequence (5'-AAGGAGG-3') for the *cat-upp* gene on plasmid plpp5-catupp-p15A (Figure 4.4, Supplementary Figure 4.7a) was entirely randomized. We then transformed the plasmid library into BL21(DE3)Δupp cells and plated on M9 minimal media agar plates supplemented with 10 μg ml^{-1} 5-FU. Surviving cells produce mRNA that is not efficiently translated by endogenous ribosomes (desired outcome), or have non-functional plasmids. In the initial attempts of the subsequent positive selection, we had difficulty selecting robust orthogonal SD/ASD pairs from this o-SD mRNA pool with a randomized ASD-Ribo-T library directly. Therefore, we performed a first round of positive selection using untethered ribosomes with the small subunit carrying randomized ASD in order to limit the o-

mRNA sequence space to just orthogonal and sufficiently active o-mRNA sequences. Specifically, the 16S rRNA ASD sequence of plasmid-based untethered ribosomes (Supplementary Figure 4.7b) was randomized, the plasmids were transformed into the surviving cells from our negative selection, and then plated on LB-agar plates in the presence of 100 μg ml^{-1} Cm. Surviving colonies were picked, and plasmids were isolated and sequenced (Round 1, Supplementary Figure 9b).

To identify top performing o-mRNAs, we evaluated the round 1 selected SD/ASD pairs for overall reporter expression levels and assessed the extent of cross-talk with wild-type. This initial characterization of orthogonal SD/ASD pair activity was performed using a Cm-resistance assay and the *cat-upp* reporter plasmids. To test overall activity, each set of cognate o-mRNA and o-16S rRNA plasmids was added to the same cells and resistance to Cm assessed. Additionally, to measure orthogonality of the corresponding mRNAs with the wild-type ribosome pool (*i.e.,* how much cross-talk exists between wild-type ribosomes and our selected orthogonal mRNAs), each orthogonal mRNA construct was independently co-transformed into fresh BL21(DE3)Δupp cells with plasmid coding for wild-type ribosomes (pAM552, Supplementary Figure 4.7b). Round 1 strains were plated on a range of Cm concentrations (0, 0.5, 1, 2.5, 5, 10, 20, 40, 60, 80, 100, 200, 300, 400 and 500 μg ml^{-1}), and maximum growth concentrations noted (Supplementary Figure 4.9a). Evolved pairs had increased cognate pair activity (black bars) well above the background expression of the o-mRNA by wild-type ribosomes (white bars). Furthermore, orthogonal pair activity was significantly increased over the previous orthogonal system [175] (pAM552o/A, Supplementary Figure 4.9).

We used a set of 14 best-performing orthogonal mRNAs for a second round of positive selection with a library of Ribo-T v2 with the ASD sequence randomized. First, the active and

orthogonal mRNA (o-mRNA B-P, Supplementary Figure 4.9b) were isolated, pooled and transformed into the BL21(DE3)Δupp strain. Then, the ASD sequence on pRibo-T v2 plasmid was randomized, transformed into BL21(DE3)Δupp containing the top performing orthogonal mRNAs, and plated on LB-agar plates supplemented with 100 μg ml^{-1} Cm (Figure 4.4). Surviving colonies were picked, and plasmids were isolated and sequenced. Top performing pairs, aligned using the ribosome binding site (RBS) calculator [264,265], are shown in Figure 5a. The alignments show that while the selected orthogonal SD/ASD pairs are different from wild-type sequences, they have high complementarity between themselves. Our orthogonal Ribo-T constructs with improved v2 tethers are named pORTx.y, where x is a number indicating the orthogonal ASD sequence (1-9), and y is a letter indicating the corresponding cognate SD sequence (A-E). Corresponding rRNA plasmids with untethered ribosomes are named pOx.y.

4.4.3 Evaluation of evolved orthogonal pairs

With improved orthogonal Ribo-T v2/mRNA pairs in hand, we assessed performance with two key metrics: i) the overall activity and ii) the orthogonality to wild-type ribosomes. Pair activity and orthogonality were measured with two protein expression assays: fluorescent protein expression and antibiotic resistance. These two assays were chosen to validate and demonstrate that these orthogonal Ribo-T v2 exhibit comparable relative orthogonal expression regardless of the protein they express. Importantly, a metric for quantifying orthogonality is critical because it segregates the activity of oRibo-T v2 from that of wild-type ribosomes, and normalizes orthogonality across the two different assays. Percent orthogonality is calculated as:

$$\%\ \text{orthogonality} = \frac{A_{pair} - A_{mRNA}}{A_{pair}} * 100 \quad (1)$$

Where A_{pair} is the activity of the orthogonal pair (sfGFP fluorescence divided by OD_{600} for the fluorescent protein expression assay, or half maximal inhibitory concentration (IC_{50}) for the CAT assay), and A_{mRNA} is the activity of just the orthogonal mRNA expressed without the cognate orthogonal ribosome (*i.e.,* the crosstalk with wild-type ribosomes). The extent of orthogonality (%) is shown below each pair in the activity plots in Figure 5. With this metric, a higher percentage value indicates a lower background expression of o-mRNA in the absence of cognate oRibo-T v2 as compared to the expression when the cognate oRibo-T v2 is present.

For evaluation of selected orthogonal pairs, SD variants were cloned into vectors containing the *sf-gfp* and *cat* genes, respectively. ASD variants were freshly cloned into the pRibo-T v2 plasmid. Plasmid pairs were transformed into a naïve BL21(DE3)Δupp strain for testing. Expression of sfGFP was measured as final fluorescence normalized by the final OD_{600} reading (Figure 4.5b) and activity of CAT was evaluated as IC_{50} (Figure 4.5c). Of note, pair activity is improved in both sfGFP and CAT assays over the original published oRibo-T system [175] (noted as v1), as well as the published v1 orthogonal pair cloned with the optimized v2 tether sequences (noted as 1.A). We observed that some pairs achieved high sfGFP expression (*e.g.,* pORT3.C, Figure 4.5b), other pairs conferred particularly strong resistance to Cm (*e.g.,* pORT7.D, Figure 4.5c), some pairs achieved high orthogonality (*e.g.,* pORT3.B, Figures 4.5b and 4.5c), some pairs had moderate activity but poor orthogonality (*e.g.,* pORT4.D, pORT8.E, Figures 4.5b and 4.5c), and some pairs achieved a balance of high activity and orthogonality *e.g.,* pORT2.B, pORT3.B, Figures 4.5b and 4.5c). When considering both assays, and metrics of pair activity and orthogonality, we selected o-mRNA B (oSD: 5'-CAACCAC) paired with o-ASD #2 (5'-

UGUGGU) (selected in Round 1 in untethered context), and o-ASD #3 (5'-CUGUGG) (selected in Round 2 in v2 tether context).

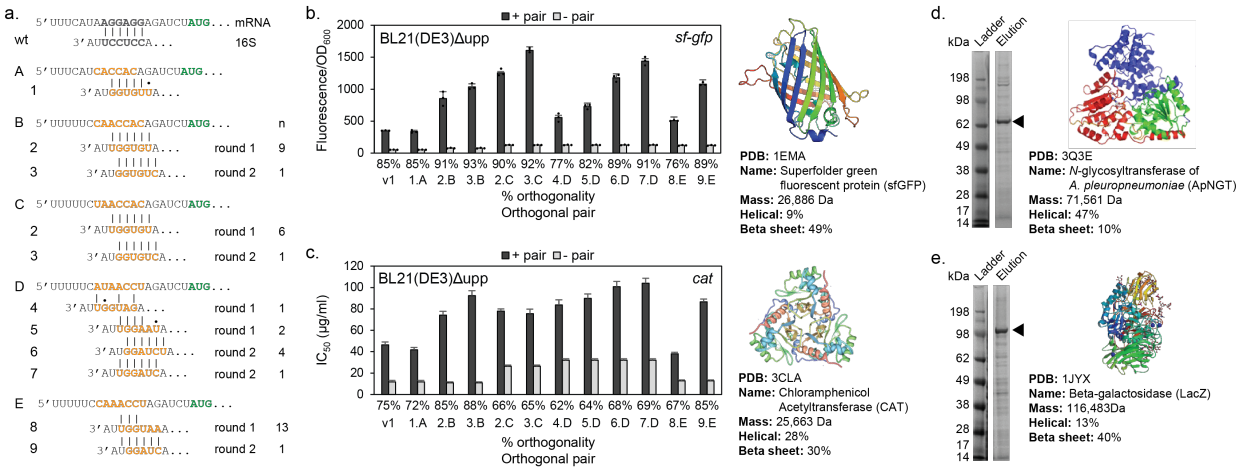

Figure 4.5 Selected orthogonal pair sequences and function in Ribo-T v2. (a) Top evolved orthogonal mRNA and 16S with predicted pairing. Selection round is noted by round 1 or round 2 to the right of each pair. n denotes number of isolated members with that sequence from the selection. (b-e) Orthogonal pair notation: Original orthogonal Ribo-T system denoted by v1, and x.y where x is o16S number and y is o-mRNA letter (pORTx.y plasmid name format). (b) Orthogonal expression of super folder green fluorescent protein (*sf-gfp*) in BL21(DE3)Δupp. + pair: both o-rRNA and o-mRNA expressed, - pair: just o-mRNA expressed without cognate o-rRNA. Percent orthogonality is shown below column labels. A higher percentage value is desired, indicating a lower background expression of o-mRNA as compared to the expression with the cognate orthogonal rRNA. Error bars = 1 SD of n=3 independent experiments. The protein's structure and details are listed to the right of the graph. (c) Orthogonal expression of Cm acetyltransferase (*cat*) in BL21(DE3)Δupp. Error bars = 1 standard error in IC_{50} curve fitting. The protein's structure and details are listed to the right of the graph. (d) Orthogonal expression of *N*-glycosyltransferase of *A. pleuropneumoniae* (*ApNGT*) in BL21(DE3). The protein's structure and details are listed to the right of the graph. (e) Orthogonal expression of Beta-galactosidase (LacZ) in BL21(DE3). The protein's structure and details are listed to the right of the graph.

To directly compare performance of the newly selected orthogonal pairs against our original orthogonal pair [175], we cloned the previous o-ASD sequence into the Ribo-T v2 plasmid to generate pORT1, and the cognate orthogonal SD sequence into the *sf-gfp* and *cat* reporter plasmids to generate plpp5.A.gfp and plpp5.A.cat (Figure 4.5a). For plasmids pORT2 and pORT3

paired with orthogonal GFP reporter B (plpp5.B.gfp), we observed activity increases of 154% and 208%, respectively, compared to pORT1. Percent orthogonality also increased by 6% and 8% (n=6, paired t-test [two-sided], $p<0.05$), respectively (Figure 4.5b). For plasmids pORT2 and pORT3 paired with orthogonal *cat* reporter B (plpp5.B.cat), pair activity increased 77% and 121% over pORT1, respectively. Percent orthogonality increased 13% (for 2.B) and 16% (for 3.B) over pORT1, respectively (Figure 4.5c). While the orthogonal GFP reporter C (plpp5.C.gfp) had higher functionality than the orthogonal GFP reporter B (plpp5.B.gfp) with pORT2 and pORT3, its orthogonality was lower than that of the reporter B (Figures 4.5b and 4.5c). The new mRNA/oRibo-T pairs (o-mRNA B: 5'-CAACCAC; o-ASD #3: 5'-CUGUGG) are poised to expand the versatility of the fully orthogonal ribosome–mRNA system.

4.4.4 Orthogonal pair activity in other *E. coli* strains

To test system versatility in a wide range of strains, top performing plasmid pairs for the sfGFP reporter set were next transformed into BL21 Star (DE3) (Invitrogen) and a variant of the fully recoded C321.ΔA strain [178,258], MCJ1217. These strains provide benefits for non-canonical amino acid incorporation using amber suppression and we recently showed that C321.ΔA could be coupled with extensively engineered synthetases for multi-site incorporation of up to 30 ncAAs into a single biopolymer *in vivo* [266] and developed for cell-free protein synthesis applications as well [178-180,267]. Following transformation, we evaluated the ability of our top performing oRibo-T v2/o-mRNA pairs to express sfGFP (Supplementary Figure 4.10a). General trends observed in the BL21(DE3)Δupp strain hold for these additional strains: pORT2.B, pORT3.B, pORT2.C and pORT3.C sets perform better than the original pair (>200% of pORT1 expression under similar

conditions), with maintained high orthogonality. The best performing orthogonal pairs similarly benefitted specialized 30S subunits in a non-tethered context (Supplementary Figure 4.11).

4.4.5 Synergistic effect of evolved tethers and orthogonal pairs

We next set out to study the effects of improved tethers and orthogonal pairs on the oRibo-T system performance. To do this, select orthogonal ASD sequences were cloned into both our improved oRibo-T v2 plasmid as well as our original published oRibo-T v1 (with tether sequences 9A/8A) [175]. Using both our orthogonal sfGFP and CAT assays, we measured the activity (fluorescence for sfGFP, and IC_{50} for CAT) of our orthogonal pairs in the context of either Ribo-T v1 or v2 tethers. In our sfGFP assay, we observed improvements in activity and orthogonality for Ribo-T v2 when combined with every orthogonal pair. Specifically, v2 tethers and improved orthogonal pairs worked synergistically to improve orthogonal function over the v1 tethers by up to 55% (Supplementary Figure 4.12a). The CAT assay did not show significant difference between v1 and v2 tethers (Supplementary Figure 4.12b), presumably because of the less sensitive assay range compared to the sfGFP fluorescence assay.

To further demonstrate the utility of the oRibo-T v2 system, we expressed additional recombinant proteins aiming to represent a diverse range of protein sizes, structures, and functions. Specifically, we cloned *E. coli* β-galactosidase (LacZ) and *N*-glycosyltransferase of porcine pathogen *A. pleuropneumoniae* (ApNGT) into our *in vivo* orthogonal reporter construct (plpp5.B). We then purified the encoded proteins, and compared their expression across oRibo-T v2 and oRibo-T v1 (Figure 4.5d,e and Supplementary Figure 4.10b,c,d). Importantly, cells carrying oRibo-T v2 had a 37% higher expression of LacZ and a 22% higher expression of ApNGT over oRibo-T v1 ($n=3$, paired t-test [two-sided], $p<0.05$). These results demonstrate Ribo-T v2's utility

in producing a variety of proteins of various sizes (25 kDa to 116 kDa), structural compositions (9%-47% alpha helical and 10%-49% beta sheets), and functions (fluorescence, antibiotic resistance, hydrolysis, and glycosylation).

4.4.6 Incorporation of non-canonical amino acids by Ribo-T

Engineering the translation apparatus is a key emerging opportunity in synthetic biology [268-270]. One of the central reasons to develop an orthogonal Ribo-T system is the possibility of selecting otherwise dominantly lethal rRNA mutations in the peptidyl transferase center that facilitate the translation of new abiological polymers made with the use of an expanded genetic code [116,271]. Such efforts require that the Ribo-T platform is compatible with orthogonal ncAA incorporation machinery and, up to now, compatibility has yet to be shown in the Ribo-T system, and multiple ncAA incorporations with a tethered o-ribosome has yet to be achieved.

We therefore tested whether oRiboT is compatible with multiple site-specific ncAA incorporation into proteins. Specifically, we assessed the ability of orthogonal Ribo-T v2 (pORT3) to site-specifically incorporate *p*-azido-L-phenylalanine (pAzF) into sfGFP, using a previously reported orthogonal transfer RNA (tRNA) and aminoacyl-tRNA synthetase (aaRS) pair from *Methanocaldococcus jannaschii* [261] (henceforth referred to as pAzFRS). Importantly, the idea was not to engineer oRibo-T to be better than a natural ribosome at incorporating pAzF, which is known to be incorporated efficiently, but rather to show that oRibo-T and the pAzF orthogonal translation system were able to cooperate in producing protein(s) with multiple ncAAs.

To minimize plasmid requirements for ncAA incorporation, we first combined the oRibo-T v2 rRNA and the reporter gene on one plasmid. Since relative directional orientation of the two expression cassettes from a single plasmid can have a significant impact on system performance

[272-274], we built and tested combined rRNA/mRNA plasmids in both the forward and reverse directions (Supplementary Figure 4.13a). While pORT3.B.gfp forward and reverse constructs had similar overall expression, the growth characteristics of the reverse orientation was significantly better than the forward orientation (Supplementary Figure 4.13b, graph inset), and so this orientation was selected for future experiments.

We then tested ncAA incorporation. The genomically-recoded organism derived from C321.ΔA (MCJ.1217) lacking UAG stop codons was co-transformed with our combined reporter gene and an orthogonal translation system plasmid containing an aaRS:tRNA pair previously engineered for incorporation of pAzF [261]. We quantitatively assessed the incorporation of pAzF into sfGFP variants with 1 or 5 TAG codons at amino acid positions D190 (1 TAG) or D36, K101, E132, D190 and E213 (5 TAG) (Figure 4.6a, Supplementary Figure 4.13c). Cells containing plasmids encoding for orthogonal Ribo-T with aSD sequence 3 and orthogonal sfGFP message B containing 1 TAG (pORT3B.gfp1TAG) or 5 TAG (pORT3B.gfp5TAG) were grown in LB media supplemented with pAzF. Upon analyzing fluorescence, we found oRibo-T v2 to be successful in translating the *sf-gfp* gene containing not only 1 TAG but even 5 internal TAG codons with expression levels >6-fold and >10-fold above background, respectively (Figure 4.6b). The expression levels are statistically significant (paired t-test [two-sided], $p<0.05$) and in line with previously reported values in the literature for this system configuration [275]. Similar expression was observed with the untethered orthogonal ribosome system with plasmids pO2B.gfp1TAG and pO2B.gfp5TAG (Supplementary Figure 4.13d). Our results highlight the effective utility of our combined plasmid design for incorporation of ncAAs. Furthermore, our work demonstrates a key proof-of-concept result that confirms compatibility and utility of a Ribo-T v2-based orthogonal

system with widely-used and standardized orthogonal components [178,275,276] for future ncAA incorporation work.

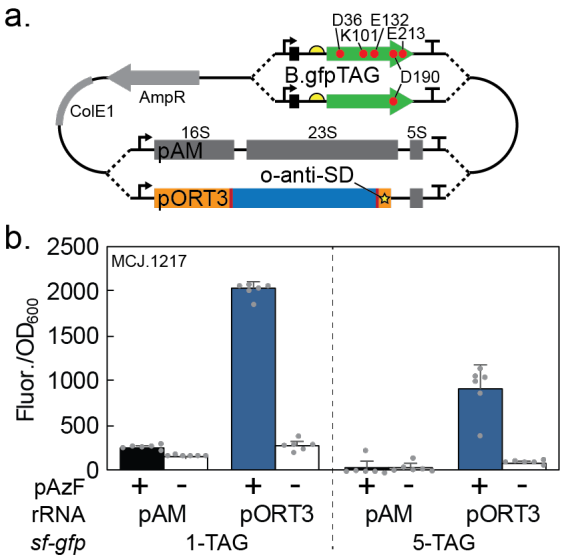

Figure 4.6 Incorporation of ncAA p-azido-L-phenylalanine (pAzF) by orthogonal Ribo-T. (a) Combined rRNA and *sf-gfp* plasmid with *sf-gfp* gene is replaced with a 1TAG or 5TAG version to create pORT3B.gfp1TAG and pORT3B.gfp5TAG (orthogonal Ribo-T with aSD sequence 3 and orthogonal sfGFP message B containing 1 TAG or 5 TAG, respectively). Wild-type *rrnb* operon was cloned as a negative control for background orthogonal expression (pAM.B.gfp1TAG and pAM.B.gfp5TAG). (b) Expression of *sf-gfp* with 1TAG or 5TAG in C321.ΔA derived strain MCJ.1217 (C321.ΔA.mutS^{+}.Δλred.Δupp), in the presence of (+) or absence of (-) pAzF. Error bars = 1 SD of n=6 independent experiments.

4.5 Discussion

Here, we present significant improvements to the original Ribo-T platform. This second-generation design was developed using tether libraries varying in both the length and composition of the tether sequence. We identified several sequences at the h44/H101 junction capable of supporting robust cell growth with the construct carrying T1 (CAATGAACAATTGGA) and T2 (GATAACTAGT) being the winning variant. The new Ribo-T v2 system exhibits up to an 86% improvement in growth rate and 70% improvement in maximum OD_{600} (in SQ171 strain), as

compared to the original Ribo-T v1. Of note, the improvement in tether design was insufficient to bring the growth rate of the Ribo-T v2 cells to that of wild type cells. We believe this reflects a fundamental limitation of this Ribo-T architecture, which is based on insertion of a circularly permutated 23S rRNA into a 16S rRNA helix at H101 and h44. The unusual structure and transcription order of the rRNA segments in Ribo-T causes notable assembly defects [214]. We are not sure whether it is the circular permutation of the large subunit rRNA or disruption of the continuity of the small subunit rRNA that are the primary cause of the assembly problems. However, in spite of assembly limitations, Ribo-T v2 has marked improvements over the original Ribo-T variant. Furthermore, after the selection of enhanced orthogonal Ribo-T v2/mRNA pairs, orthogonal Ribo-T v2 (pORT3) exhibits a ~200% increase in activity for sfGFP expression and also improved orthogonality compared to our original orthogonal system [175].

The improvements presented here to the Ribo-T platform significantly enhance the usefulness of the system for biochemical assays (*e.g.,* faster growth for RNA extractions, and higher density cultures for increased preparation of Ribo-T v2 variants for *in vitro* utilization), and applications. Specifically, these improvements allowed us to demonstrate the usefulness of the orthogonal mRNA-Ribo-T v2 system for two different applications. We demonstrated that orthogonal Ribo-T v2 is capable of synthesizing a range of diverse proteins of different sizes, structures, and functions with enhanced efficiency over Ribo-T v1. Second, as a proof of concept, we demonstrated for the first time that oRibo-T can be leveraged for the site-specific incorporation of multiple ncAAs into proteins. We showed successful Ribo-T mediated incorporation of up to 5 pAzF residues with >10-fold expression above background.

Looking forward, the new Ribo-T v2 is expected to become a versatile tool for many biotechnology, engineering, and basic science applications. These applications and opportunities have sparked enthusiasm, resulting in parallel work featuring a conceptually similar design of an orthogonal stapled ribosomes [215,216]. Although the stapled ribosomes leveraged our foundational circular permutation and helix connections found in the Ribo-T design (H101 and h44)[175,277], recently reported improvements to the initial stapled system yielded a strain carrying 34 mutations within the evolved strain [24], which leaves some uncertainty about portability of that system. Our Ribo-T v2 construct was originally developed in a widely used strain [66], and is portable and functional in several other strains without extensive strain modifications. These attributes make our orthogonal Ribo-T v2 system robust for a variety of applications and studies. This includes modifying the catalytic capacity of the ribosome for improved incorporation of ncAAs such as backbone extended monomers (*e.g.,* β-, D-, or γ- amino acids) [133,213] into polypeptides and biopolymers, probing single and multi-mutations in highly conserved rRNA nucleotides, translation of problematic protein sequences, and the creation of an orthogonal central dogma, which may insulate genetic programs from host regulation and allow expansion of the roles of these processes within the cell [218].

4.6 Acknowledgements and contributions

The authors would like to thank Professor Peter G. Schultz for providing the pEVOL plasmid. We thank Paul D. Carlson for helpful discussions and comments on this manuscript. This work was supported by the Human Frontiers Science Program (RGP0015/2017), the National Science Foundation (MCB-1716766), the David and Lucile Packard Foundation, the Chicago

Biomedical Consortium with support from the Searle Funds at the Chicago Community Trust, and the Dreyfus Teacher-Scholar Program.

Many thanks to Dr. Erik D. Carlson for conceiving this study with Dr. Michael Jewett. Dr. Erik Carlson wrote the paper with me, and Dr. Michael Jewett. Thank you to Kim Hoang, Teresa Szal, Emm Fulk, and Do Soon Kim for their experimental additions to the manuscript. And many thanks to Dr. Shura Mankin and Nora Vasquez-Laslop for their help in designing experiments, overlooking aspects of the project, and brainstorming with the team.

4.7 Patent information

Jewett, M.C.; Carlson, E.D.; d'Aquino, A.E.; Kim, D.S., Ribosomes with Tethered Subunits. **2016**. *US Patent Application Serial No. 15/363,828*.

4.8 Supplementary figures and tables

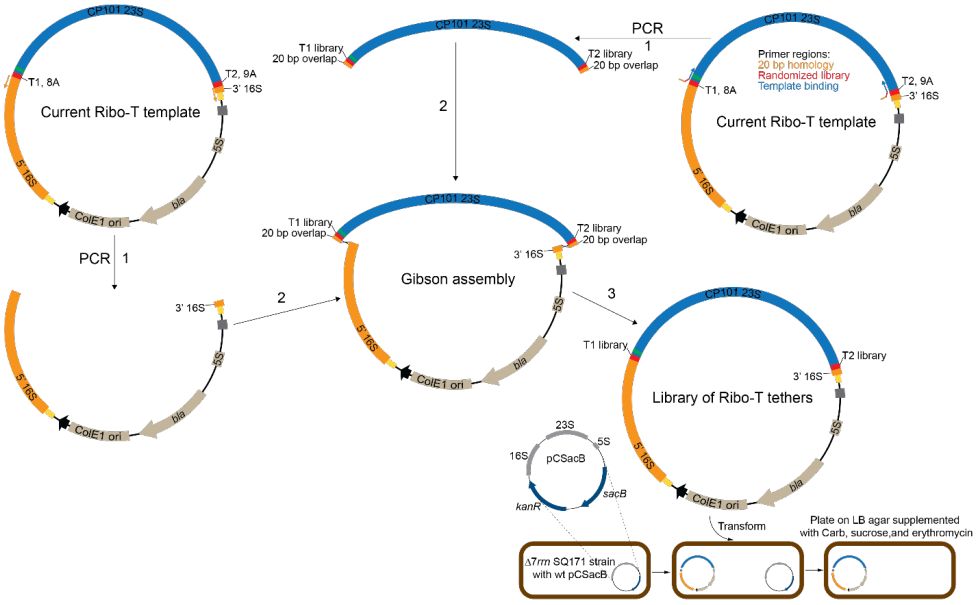

Supplementary Figure 4.1. Library construction and selection strategy for tether optimization.

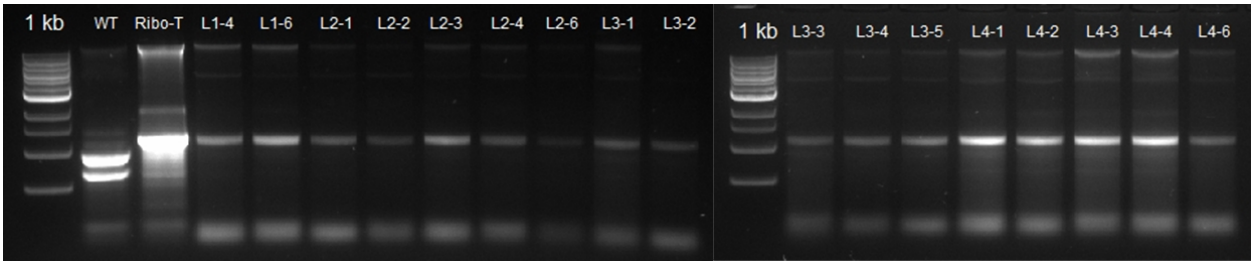

Supplementary Figure 4.2. Total RNA gel of selected library members. WT: wildtype ribosomes extracted from SQ171 cells with pAM552 plasmid. Sample names are organized as LX-Y; where X is the library number (1-4), and Y is a clone number from that library.

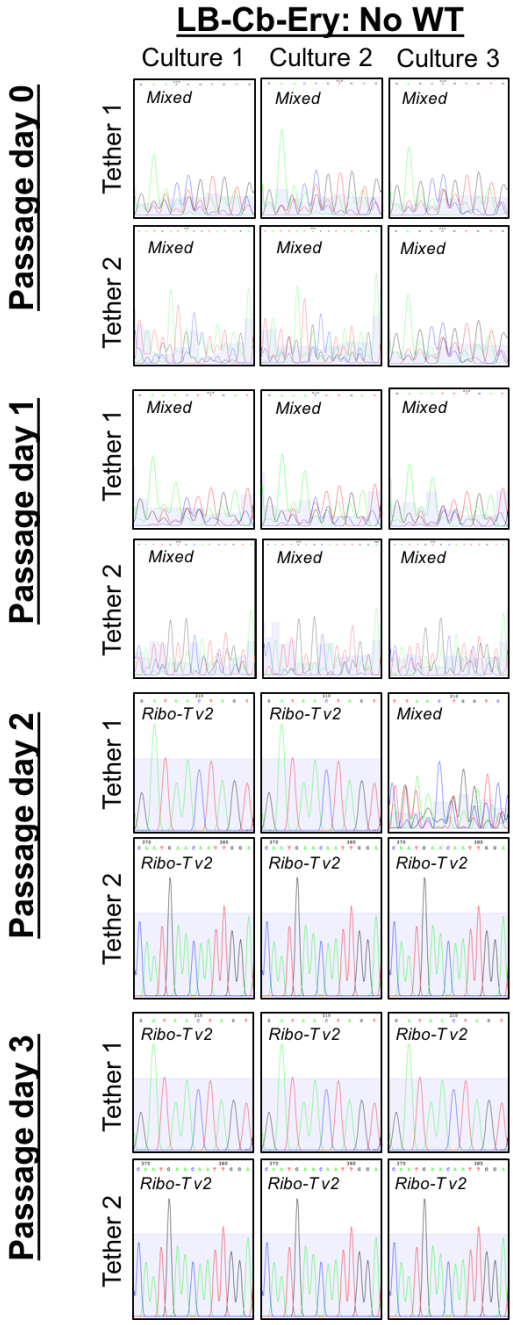

Supplementary Figure 4.3 Liquid culture enrichment and competition assay shows Ribo-T v2 as the dominant genotype following multiple generations of growth. The top 15 Ribo-T winners identified were co-cultured in triplicate and passaged for 3 days. Between each passage, the bulk populations from the culture were sequenced and analyzed.

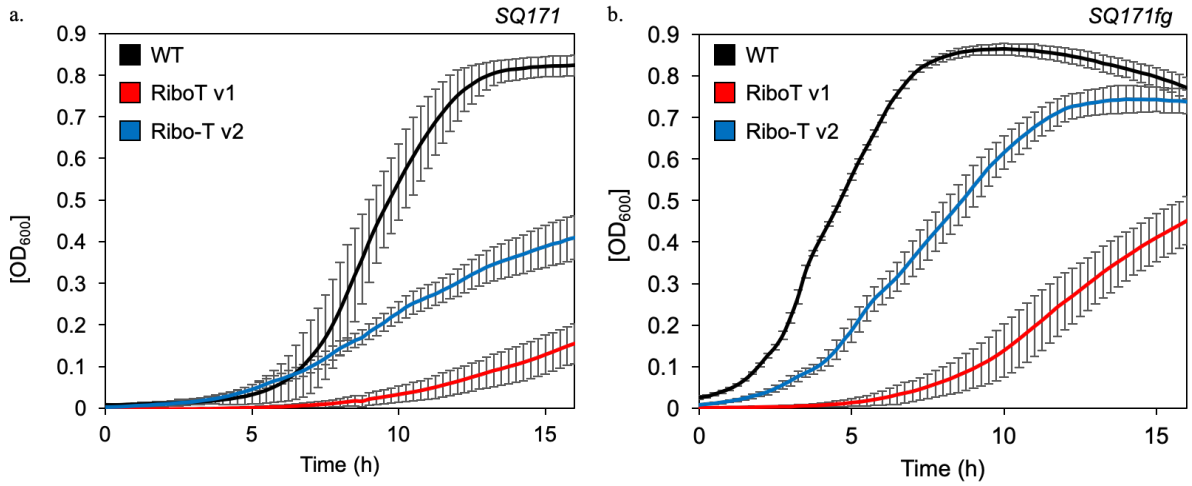

Supplementary Figure 4.4 Ribo-T v2 improvements enhance growth of SQ171 and SQ171fg cells in which Ribo-T replaces wild-type ribosomes. Growth curves of (a) SQ171 cells (Error bars = 1 SD; n=5). and (b) SQ171fg cells (Error bars = 1 SD; n=3) transformed with pAM552 DNA (wild-type, black), or Ribo-T v1 (blue) or Ribo-T v2 (green).

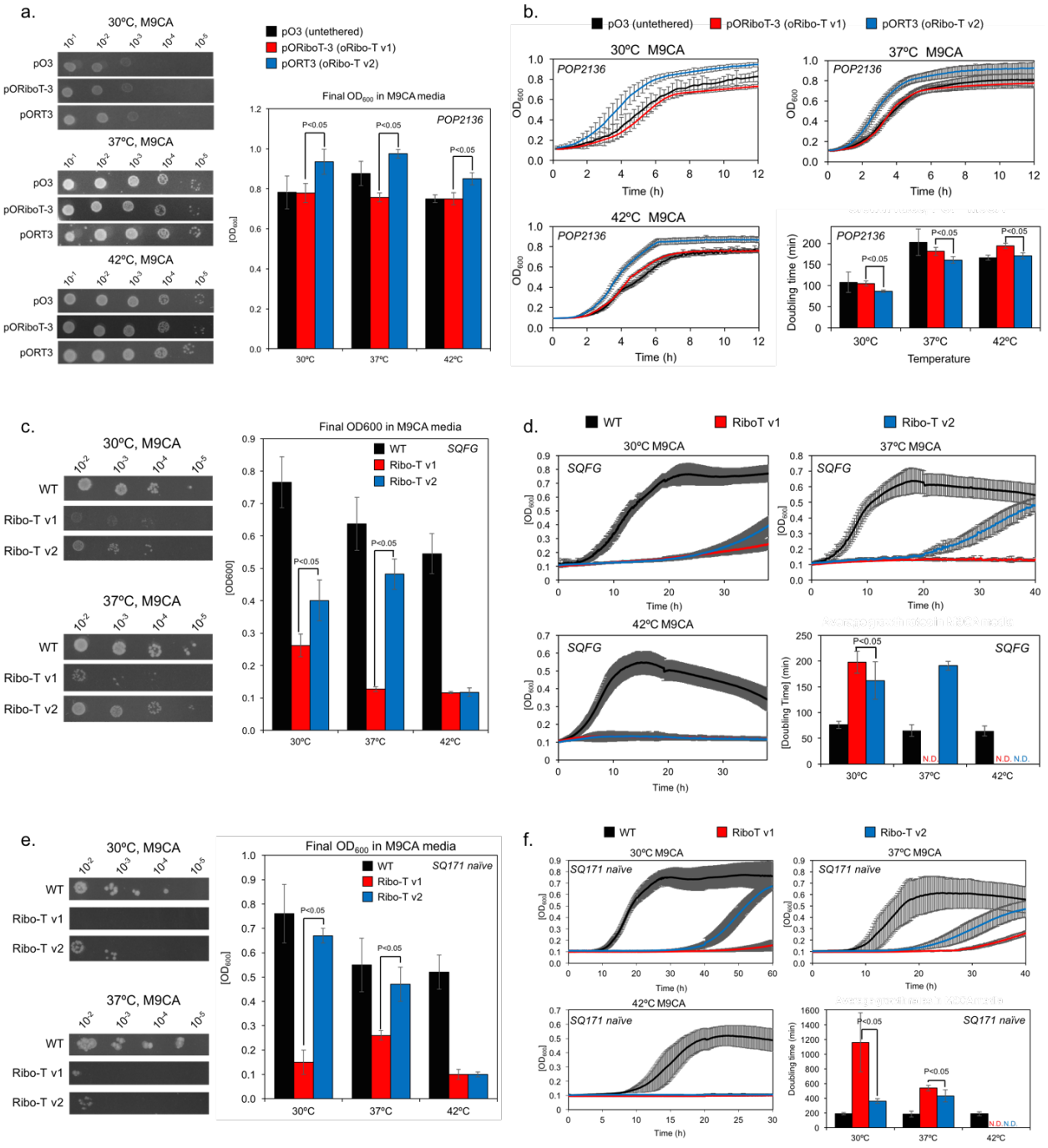

Supplementary Figure 4.5 Ribo-T v2 enhances cell fitness as compared to Ribo-T v1 when grown on minimal media (M9 casamino acids, M9CA) at various temperatures in different cell backgrounds. (a) Orthogonal and non-orthogonal untethered ribosomes, Ribo-T v1, and Ribo-T v2, were grown in and on M9CA media in a-b. POP cells (n=6-8), c-d. SQ171fg cells (n=5-6), and e-f. SQ171 cells (n=6). Final OD_{600} and doubling times were analyzed. Error bars = 1 SD.

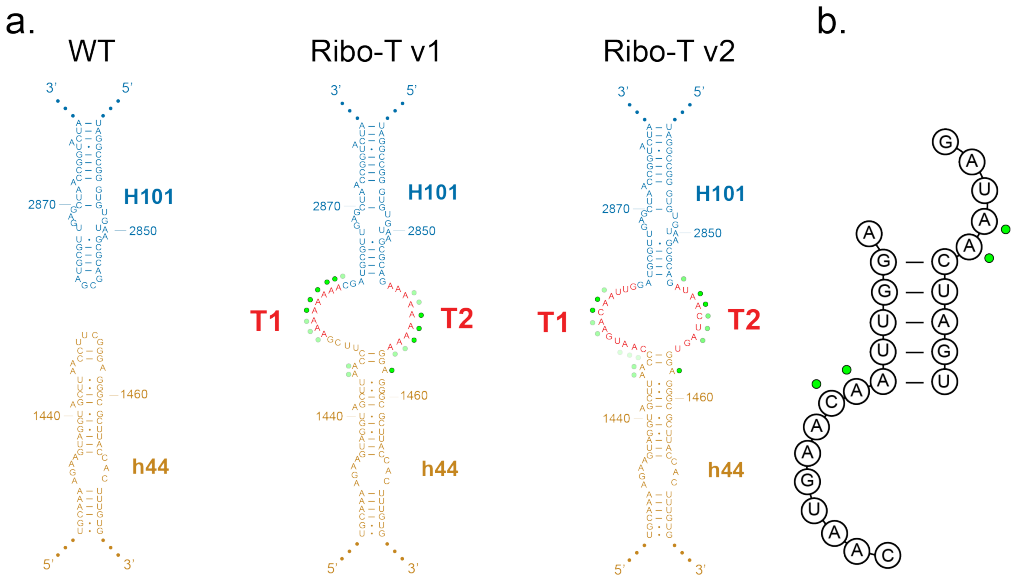

Supplementary Figure 4.6 Chemical probing and prediction of the structure of the Ribo-T v2 linkers. (a) The diagrams represent the structures of helices H101 and h44 in wild-type ribosomes (left), Ribo-T v1 (middle), and Ribo-T v2 (right), with the nucleotide accessible to the dimethyl sulfate (DMS modification indicated by green dots). Highly accessible residues are indicated by brightly-colored dots. (b) The predicted secondary structure formed by the Ribo-T v2 tethers with the nucleotides most accessible for DMS modifications indicated.

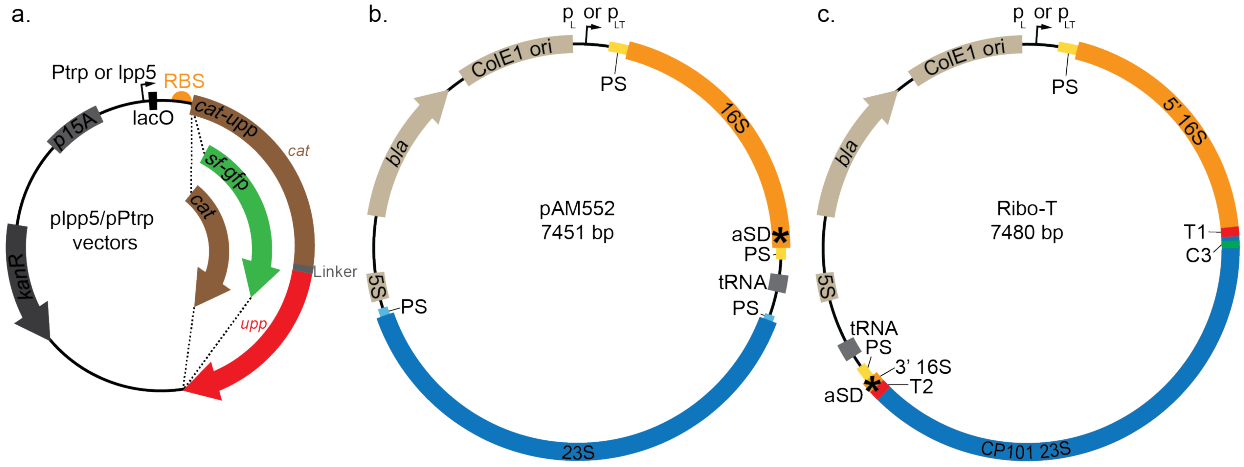

Supplementary Figure 4.7 Reporter plasmid and ribosome plasmid maps. (a) Reporter plasmid with Ptrp or lpp5 promoter, and chloramphenicol acetyltransferase-uracil phosphoribosyltransferase (*cat-upp*), super folder green fluorescent protein (*sf-gfp*) (reporter plasmid: plpp5.gfp), or *cat* gene (reporter plasmid: plpp5.cat). Plasmid contains kanamycin resistance and p15A origin of replication. (b) Plasmid coding for untethered ribosomal RNA (rRNA) from *rrnb* operon, with either p_L promoter or p_{LT} promoter for orthogonal expression. Plasmid contains ampicillin resistance gene lactamase, and ColE1 origin of replication. rRNA processing stems (PS) and anti-Shine-Dalgarno (aSD) sites indicated. (c) Plasmid coding for tethered ribosome Ribo-T. 5' tether 1 (T1) and 3' tether 2 (T2), and 23S circular permutation connecting piece C3 noted (plasmid name: pRibo-T vX; where X is either 1 or 2).

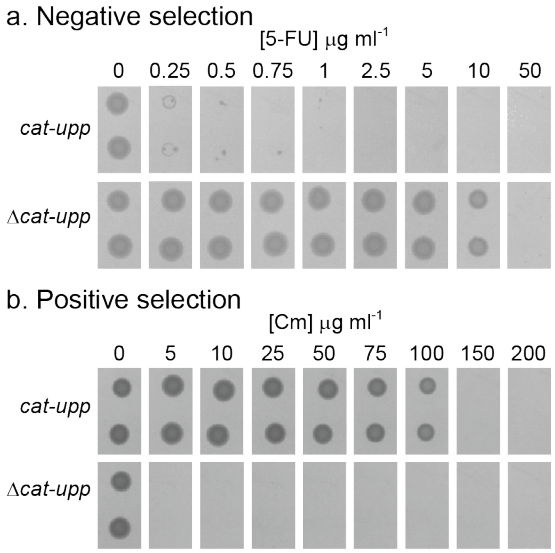

Supplementary Figure 4.8 Combined positive and negative selection scheme for evolving new orthogonal Shine-Dalgarno/anti-Shine-Dalgarno pairs. (a) BL21(DE3)Δupp cells with pPtrp-catupp-p15A and *cat-upp* expressed die in the presence of 5-Fluorouracil. (b) BL21(DE3)Δupp cells with pPtrp-catupp-p15A and *cat-upp* expressed gain resistance to the antibiotic chloramphenicol. Plates shown are representative of at least 3 independent experiments.

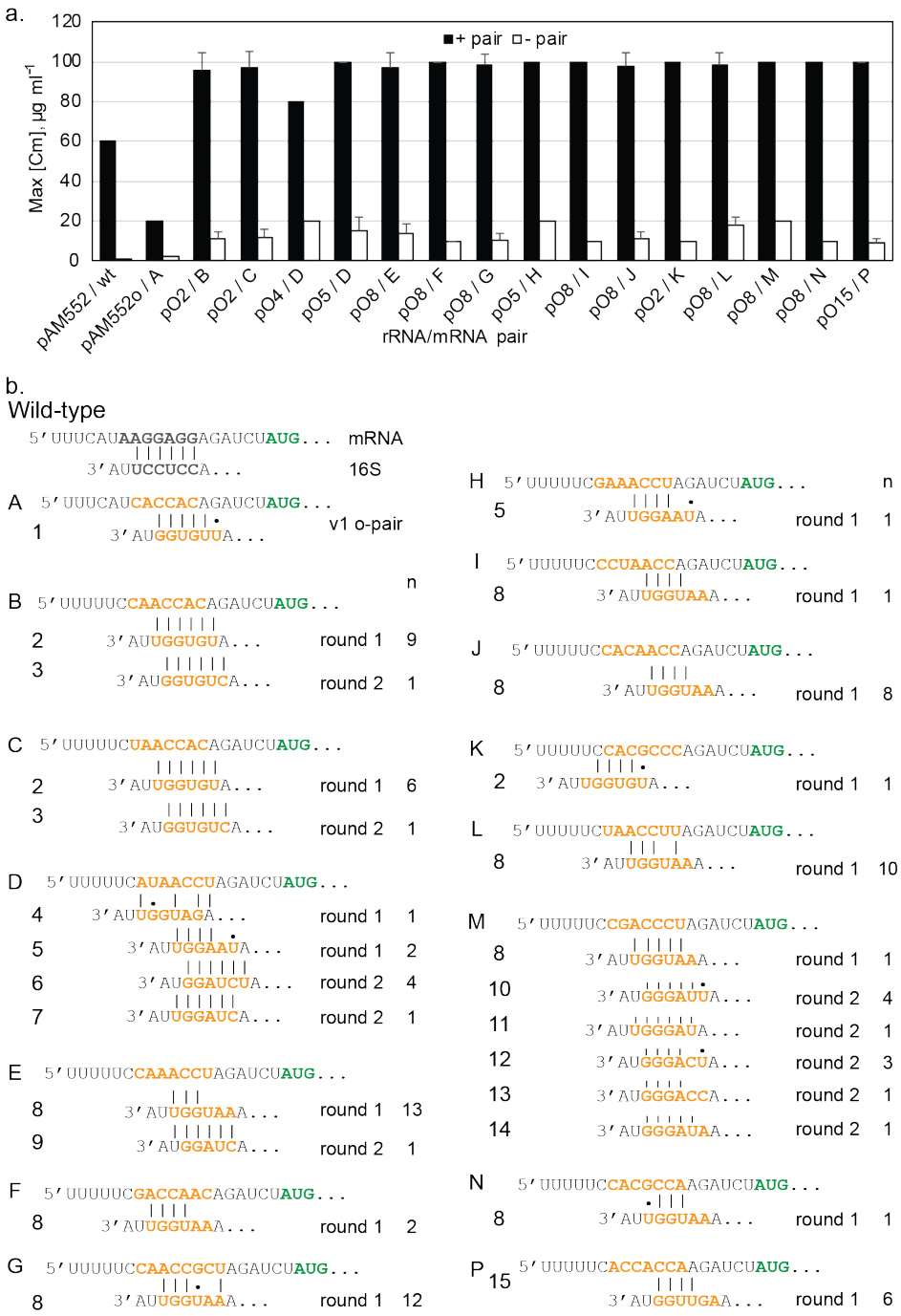

Supplementary Figure 4.9 Evolved orthogonal pairs. (a) Activity testing of untethered orthogonal ribosomes and mRNA following first round of positive selection. Controls: pAM552/wt: wild-type SD expression. pAM552o/A, original orthogonal system in untethered context. (b) Selected Shine-Dalgarno (SD) and anti-SD sequences. Round of selection and number of colonies (n) noted for each pair sequence. Orthogonal mRNA SD sequence is labeled with letters, and orthogonal 16S aSD sequence is labeled with numbers. Pair 1A is the previously published orthogonal pair noted as "v1 o-pair" [175]. Error bars = 1 SD for pairs possessing n>1 colonies.

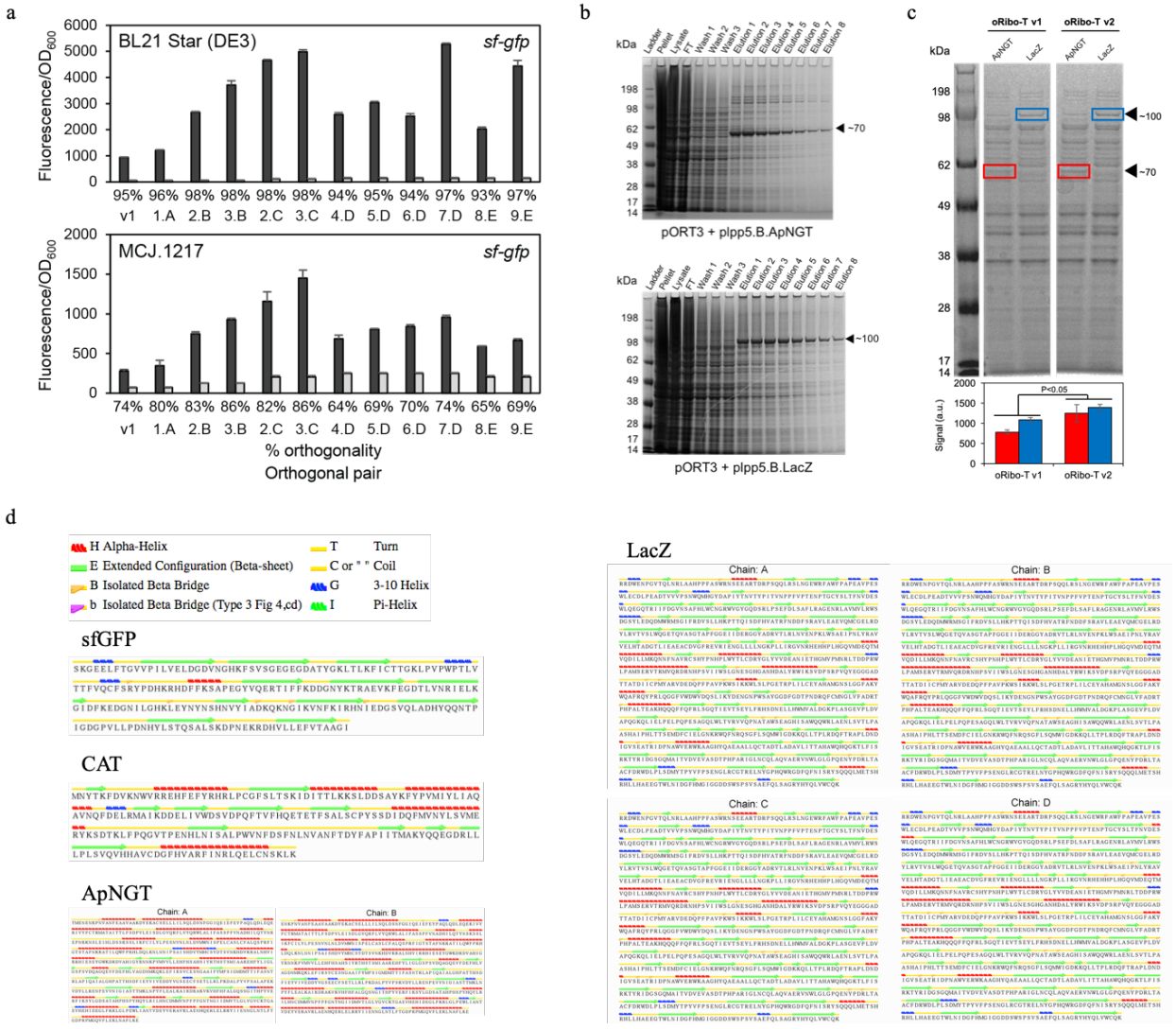

Supplementary Figure 4.10 Orthogonal Ribo-T v2 is capable of synthesizing diverse proteins of different sizes, compositions, and functions. (a) Orthogonal expression of *sf-gfp* in BL21 Star (DE3) strain (top panel). Orthogonal expression of *sf-gfp* in C321.ΔA derived strain MCJ.1217 (bottom panel). MCJ1217 (C321.ΔA.mutS^{+}.Δλred.Δupp) is a variant of the fully recoded C321.ΔA strain [178,258], and provides benefits for non-canonical amino acid incorporation using amber suppression. (b) SDS PAGE gels of the expression and purification of non-model proteins. (c) SDS-PAGE expression gel comparison between oRibo-T v1 and oRibo-T v2. oRibo-T v2 had a 37% improved expression level of LacZ (n=3, paired t-test, 2 df) and a 22% improved expression level of ApNGT (n=3, paired t-test, 2 df) over oRibo-T v1. Error bars = 1 SD. Gel is representative of three independent replicates (n=3). (d) The secondary structure maps of each protein.

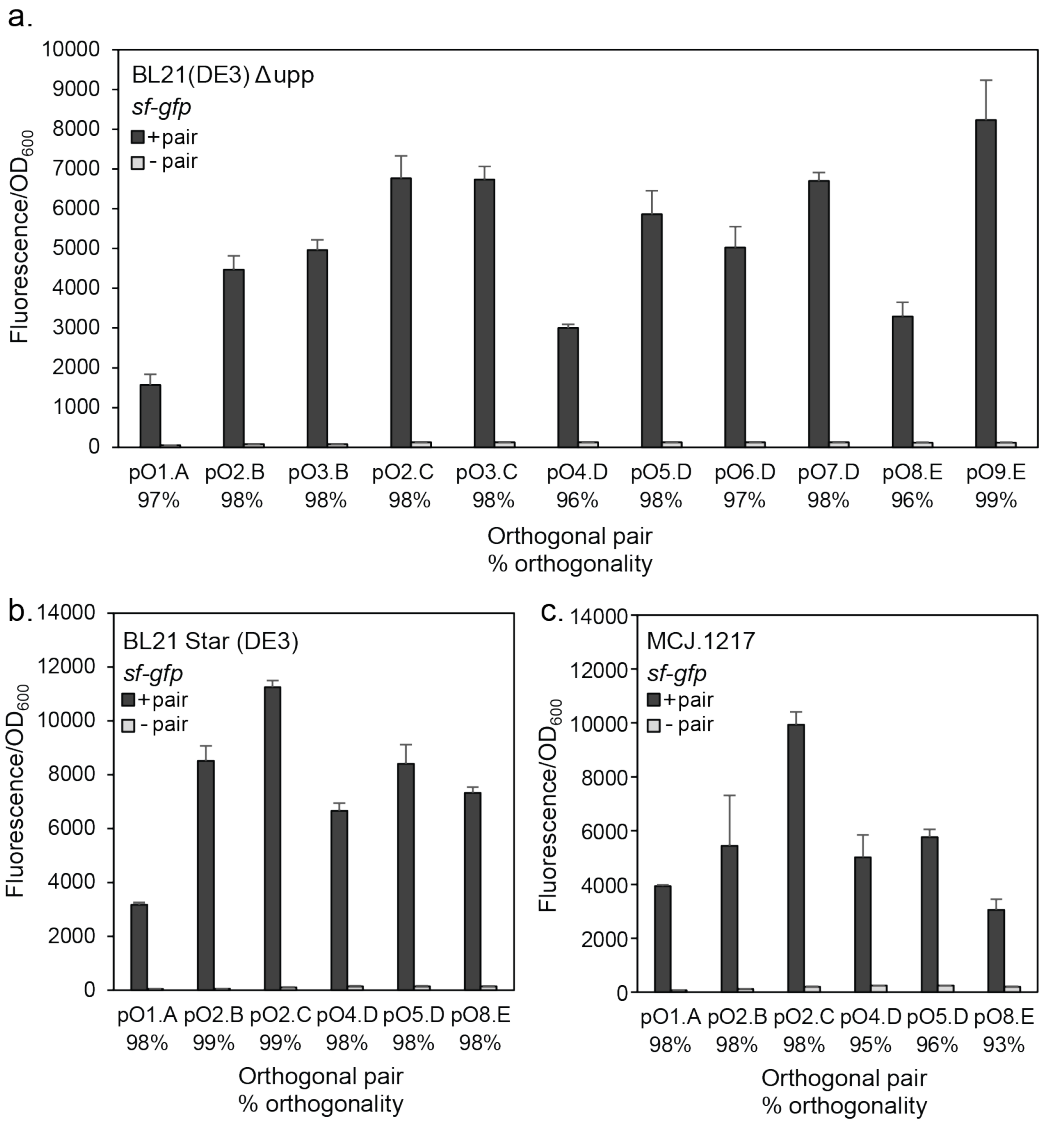

Supplementary Figure 4.11 (a) Orthogonal pair activity in untethered ribosomes in BL21(DE3)Δupp strain. (b) Orthogonal pair activity in untethered ribosomes in BL21 Star (DE3) and (c) recoded TAG-less strain MCJ.1217 (C321.ΔA.mutS^{+}.Δλred.Δupp). Error bars = 1 SD.

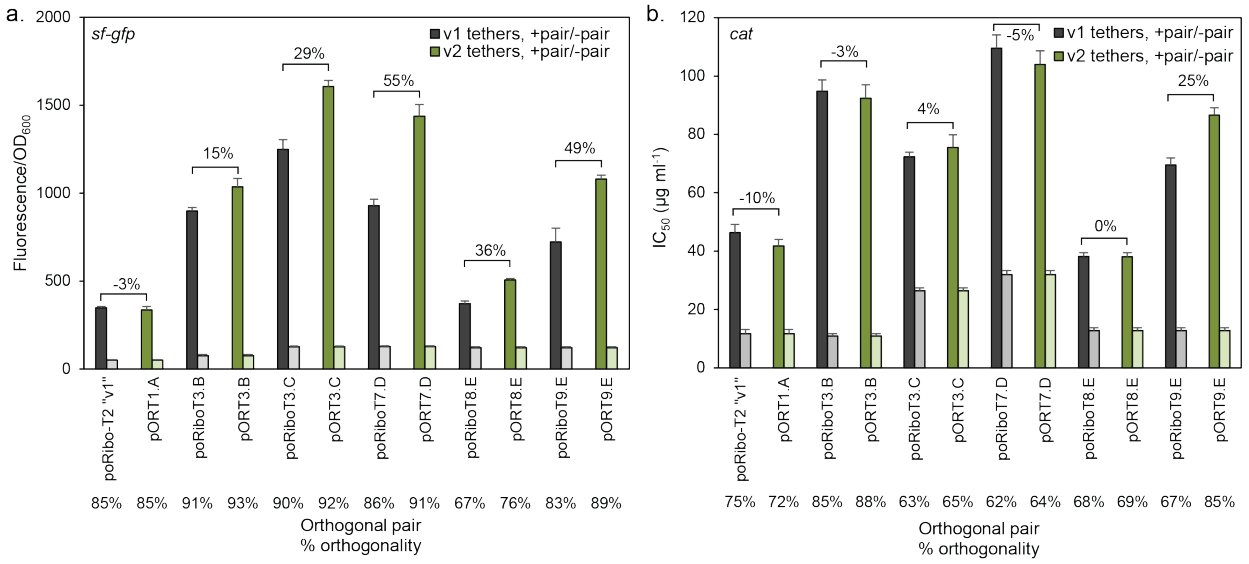

Supplementary Figure 4.12 Comparison between original published tether (v1) and improved v2 tether with a) *sf-gfp* and b) *cat* reporters. poRibo-T2 is the original orthogonal Ribo-T as published. poRiboT*x.y* contain v1 tethers and pORT*x.y* contain v2 tethers, where *x* indicates rRNA anti-Shine Dalgarno (ASD) species and *y* indicates the cognate mRNA SD species. The bars with corresponding percent values above each set of data represents the percent improvement of the orthogonal pairs with v2 tethers vs. v1 tethers. Error bars = 1 SD.

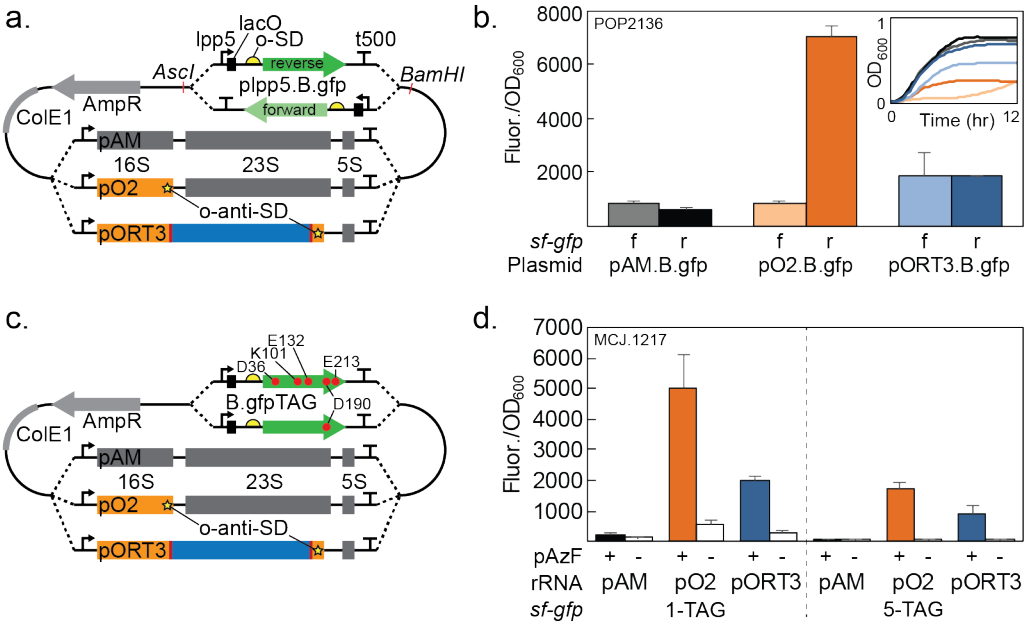

Supplementary Figure 4.13 Incorporation of non-canonical amino acid p-azidophenylalanine (pAzF) by orthogonal ribosomes. (a) Combined rRNA and sfGFP reporter plasmid system. The orthogonal reporter sfGFP is inserted in the forward (light green) and reverse (dark green) direction relative to the *rrn* operon. (b) Expression of orthogonal *sf-gfp* from a combined plasmid in POP2136. Representative ribosome constructs include pAM = wild-type untethered ribosomes, pO2 = orthogonal untethered ribosomes possessing optimized aSD sequence 2 (3'-UGGUGU), and pORT3 = orthogonal Ribo-T possessing optimized aSD sequence 3 (3'-GGUGUC). Each construct was combined with the orthogonal sfGFP reporter B (5'-CAACCAC) in the forward (f) or reverse (r) orientation. Fluorescence is normalized by OD_{600} and is the average of at least 3 independent colonies. Error bars = 1 SD. (c) Combined rRNA and *sf-gfp* plasmid with reverse orientation. For amber suppression, the *sf-gfp* gene is replaced with a 1TAG or 5TAG version as noted. (d) Expression of *sf-gfp* with 1TAG or 5TAG in C321.ΔA.mutS^{+}.Δλred.Δupp (MCJ.1217), in the presence of pAzF (+) or absence of pAzF (-). Fluorescence is normalized by OD_{600} and is the average of at least 3 independent colonies. Error bars = 1 SD.

Supplementary Table 4.1 Primers used for the construction of Ribo-T tether libraries and gBlocks used in cloning steps.

Primer name	Sequence, 5'-3'
RiboTbb-f	GGAGGGCGCTTACCACTTTG
RiboTbb-r	GGTTAAGCTACCTACTTCTTTTG
T1-A7-f	AAGAAGTAGGTAGCTTAACCAAAAAAATGCGTTGAGCTAAC
T1-A8-f	AAGAAGTAGGTAGCTTAACCAAAAAAAATGCGTTGAGCTAAC
T1-A9-f	AAGAAGTAGGTAGCTTAACCAAAAAAAAATGCGTTGAGCTAAC
T1-A10-f	AAGAAGTAGGTAGCTTAACCAAAAAAAAAATGCGTTGAGCTAAC
T1-A11-f	AAGAAGTAGGTAGCTTAACCAAAAAAAAAAATGCGTTGAGCTAAC
T1-A12-f	AAGAAGTAGGTAGCTTAACCAAAAAAAAAAAATGCGTTGAGCTAAC
T1-A13-f	AAGAAGTAGGTAGCTTAACCAAAAAAAAAAAAATGCGTTGAGCTAAC
T1-A14-f	AAGAAGTAGGTAGCTTAACCAAAAAAAAAAAAAATGCGTTGAGCTAAC
T1-A15-f	AAGAAGTAGGTAGCTTAACCAAAAAAAAAAAAAAATGCGTTGAGCTAAC
T1-A16-f	AAGAAGTAGGTAGCTTAACCAAAAAAAAAAAAAAAATGCGTTGAGCTAAC
T1-A17-f	AAGAAGTAGGTAGCTTAACCAAAAAAAAAAAAAAAAATGCGTTGAGCTAAC
T1-A18-f	AAGAAGTAGGTAGCTTAACCAAAAAAAAAAAAAAAAAATGCGTTGAGCTAAC
T1-A19-f	AAGAAGTAGGTAGCTTAACCAAAAAAAAAAAAAAAAAAATGCGTTGAGCTAAC
T1-A20-f	AAGAAGTAGGTAGCTTAACCAAAAAAAAAAAAAAAAAAAATGCGTTGAGCTAAC
T2-T7-r	CAAAGTGGTAAGCGCCCTCCAAAAAAATGCGCTTACACAC
T2-T8-r	CAAAGTGGTAAGCGCCCTCCAAAAAAAATGCGCTTACACAC
T2-T9-r	CAAAGTGGTAAGCGCCCTCCAAAAAAAAATGCGCTTACACAC
T2-T10-r	CAAAGTGGTAAGCGCCCTCCAAAAAAAAAATGCGCTTACACAC
T2-T11-r	CAAAGTGGTAAGCGCCCTCCAAAAAAAAAAATGCGCTTACACAC
T2-T12-r	CAAAGTGGTAAGCGCCCTCCAAAAAAAAAAAATGCGCTTACACAC
T2-T13-r	CAAAGTGGTAAGCGCCCTCCAAAAAAAAAAAAATGCGCTTACACAC
T2-T14-r	CAAAGTGGTAAGCGCCCTCCAAAAAAAAAAAAAATGCGCTTACACAC
T2-T15-r	CAAAGTGGTAAGCGCCCTCCAAAAAAAAAAAAAAATGCGCTTACACAC
T2-T16-r	CAAAGTGGTAAGCGCCCTCCAAAAAAAAAAAAAAAATGCGCTTACACAC
T2-T17-r	CAAAGTGGTAAGCGCCCTCCAAAAAAAAAAAAAAAAATGCGCTTACACAC
T2-T18-r	CAAAGTGGTAAGCGCCCTCCAAAAAAAAAAAAAAAAAATGCGCTTACACAC
T2-T19-r	CAAAGTGGTAAGCGCCCTCCAAAAAAAAAAAAAAAAAAATGCGCTTACACAC
T2-T20-r	CAAAGTGGTAAGCGCCCTCCAAAAAAAAAAAAAAAAAAAATGCGCTTACACAC
T2-A7-r	CAAAGTGGTAAGCGCCCTCCTTTTTTTTGCGCTTACACAC
T2-A8-r	CAAAGTGGTAAGCGCCCTCCTTTTTTTTTGCGCTTACACAC
T2-A9-r	CAAAGTGGTAAGCGCCCTCCTTTTTTTTTTGCGCTTACACAC
T2-A10-r	CAAAGTGGTAAGCGCCCTCCTTTTTTTTTTTGCGCTTACACAC
T2-A11-r	CAAAGTGGTAAGCGCCCTCCTTTTTTTTTTTTGCGCTTACACAC
T2-A12-r	CAAAGTGGTAAGCGCCCTCCTTTTTTTTTTTTTGCGCTTACACAC
T2-A13-r	CAAAGTGGTAAGCGCCCTCCTTTTTTTTTTTTTTGCGCTTACACAC
T2-A14-r	CAAAGTGGTAAGCGCCCTCCTTTTTTTTTTTTTTTGCGCTTACACAC

T2-A15-r	CAAAGTGGTAAGCGCCCTCCTTTTTTTTTTTTTTTTGCGCTTACACAC
T2-A16-r	CAAAGTGGTAAGCGCCCTCCTTTTTTTTTTTTTTTTTGCGCTTACACAC
T2-A17-r	CAAAGTGGTAAGCGCCCTCCTTTTTTTTTTTTTTTTTTGCGCTTACACAC
T2-A18-r	CAAAGTGGTAAGCGCCCTCCTTTTTTTTTTTTTTTTTTTGCGCTTACACAC
T2-A19-r	CAAAGTGGTAAGCGCCCTCCTTTTTTTTTTTTTTTTTTTTGCGCTTACACAC
T2-A20-r	CAAAGTGGTAAGCGCCCTCCTTTTTTTTTTTTTTTTTTTTTGCGCTTACACAC
T1-8N-f	AAGAAGTAGGTAGCTTAACCTTCGNNNNNNNNCGATGCGTTGAGCTAAC
T2-9N-r	CAAAGTGGTAAGCGCCCTCCGNNNNNNNNNTGCGCTTACACAC
T1-15N-f	AAGAAGTAGGTAGCTTAACCNNNNNNNNNNNNNNNTGCGTTGAGCTAAC
T2-10N-r	CAAAGTGGTAAGCGCCCTCCNNNNNNNNNNTGCGCTTACACAC
p15A gBlock	GATGGCCTTTTTGCGTTTCTACAGAGCGTCAGACCCCTTAATAAGATGATCTTCTTG AGATCGTTTTGGTCTGCGCGTAATCTCTTGCTCTGAAAACGAAAAAACCGCCTTGC AGGGCGGTTTTTCGAAGGTTCTCTGAGCTACCAACTCTTTGAACCGAGGTAACTGG CTTGGAGGAGCGCAGTCACCAAAACTTGTCCTTTCAGTTTAGCCTTAACCGGCGCA TGACTTCAAGACTAACTCCTCTAAATCAATTACCAGTGGCTGCTGCCAGTGGTGCTT TTGCATGTCTTTCCGGGTTGGACTCAAGACGATAGTTACCGGATAAGGCGCAGCGG TCGGACTGAACGGGGGGTTCGTGCATACAGTCCAGCTTGGAGCGAACTGCCTACCC GGAACTGAGTGTCAGGCGTGGAATGAGACAAACGCGGCCATAACAGCGGAATGAC ACCGGTAAACCGAAAGGCAGGAACAGGAGAGCGCACGAGGGAGCCGCCAGGGGG AAACGCCTGGTATCTTTATAGTCCTGTCGGGTTTCGCCACCACTGATTTGAGCGTCA GATTTCGTGATGCTTGTCAGGGGGGCGGAGCCTATGGAAAAACGGCTTTGCCGCGG CCCTCTCGGATCTGTATGGTGCACTCTCAG
lpp5-oRBS	GAGACACAACGTGGCTTTCCATCAAAAAAATATTGACAACATAAAAAACTTTGTGT TATACTTGTGGAATTGTGAGCGGATAACAATTCTATATCTGTTATTTTTTCACACCA CAGATCTATGGAGAAAAAAATCACTGGATATACCACCGTTG

CHAPTER 5

Studying computationally designed ribosome variants *in vivo* and *in vitro*

The work presented in this chapter is based upon work published in part in:

Yesselman, J. D.; Eiler, D.; Carlson, E. D.; Gotrik, M.R.; d'Aquino, A.E.; Ooms, A.N.; Kladwang, W.; Carlson, P.D.; Shi, X.; Costantino, D.A.; Herschlag, D.; Lucks, J.B.; Jewett, M.C.; Kieft, J.S.; Das, R. Computational design of three-dimensional RNA structure and function. *Nat. Nanotechnol*. **2019**, *14*, 866–873. DOI: 10.1038/s41565-019-0517-8.

5.1 Abstract

RNA nanotechnology and ribosome engineering seek to create nanoscale machines by repurposing natural and well-studied RNA modules. Current ribosome engineering efforts, for example, are slowed by the need for human intuition during three-dimensional structural design. Two possible ways to overcome this obstacle is to: (1) leverage RNA folding algorithms to computationally predict stable RNA structures, (2) use well-studied RNA motifs directly as a part of ribosome design and engineering efforts. Here we demonstrate a proof of concept through the design, synthesis, and characterization of tethered ribosome structures possessing RNA motifs within their tethers. One such tethered ribosome structure is designed computationally by an algorithm called RNAMake, and the second set of tethered ribosome structures are designed using well-known and studied RNA motifs.

5.2 Introduction

RNA-based nanotechnology is an emerging field that harnesses RNA's unique structural properties to create new nanostructures and machines [278]. More so than for other biomolecules, the RNA tertiary structure is composed of discrete and recurring components known as tertiary motifs [279]. Along with the helices that they interconnect, many of these structural motifs are highly modular, in that they each fold into well-defined three-dimensional structures in a broad range of contexts [280]. In previous work, through modelling and computational tools, these motifs have been demonstrated and used to assemble new polyhedral, sheets, and cargo-carrying nanoparticles for biomedical use [281-283]. Despite these advancements, the field is currently hindered by the current requirement for human intuition during three-dimensional structural design.

One way to overcome this hinderance is to computationally design three-dimensional RNA structures. The Das lab at Stanford has approached this problem with an algorithm they developed, called RNAMake [284]. RNAMake uses a 3D motif library drawn from all unique, publicly deposited crystallographic RNA structures and an efficient algorithm to discover combinations of these motifs and helices that solve the RNA motif pathfinding problem. The pathfinding algorithm assembles canonical helical segments that range from 1 to 22 base pairs with these non-canonical structural motifs, step-by-step in a depth-first search. The canonical helical segments are idealized and sequence invariant [285]; after completion of the 3D structural designs, they are filled in with sequences that best match the target secondary structure and minimize alternative secondary structures [286].

Efforts to select engineered ribosomes with messenger RNA decoding, polypeptide synthesis and protein excretion functions optimized for new substrates might be dramatically accelerated through the design of integrated ribosomes. An important step towards this goal involves tethering the two 23S and 16S ribosomal RNAs (rRNAs) of the ribosome into a single RNA strand that supports *E. coli* growth [175,277,287]. RNAMake 3D designs for the tether require solving the RNA motif pathfinding problem over >100Å distances and avoiding steric collisions with the ribosome's RNA and protein components. Even after the identification of appropriate helix end-points, this difficult design challenge previously took more than a year to solve using *in vivo* assays based on trial-and-error refinement [175,277,287].

Based on our published tethered ribosome construct, here we have designed (using both RNAMake and published aptamers), built, and tested a variety of tethered ribosomes with functional tethers. In our work, we have successfully built and characterized a library of tethered

ribosomes which are capable of sustaining the life of the cell, remaining tethered, and maintaining a sustainable growth rate. Importantly, a subset of our designs possesses tether sequences with potentially functional capabilities. In this chapter, we demonstrate two approaches for designing RNA nanomachine components: First, using a computational method called RNAMake, we develop structured tethers that integrate 16S and 23S ribosomal RNAs that remain uncleaved by ribonucleases and assemble onto messenger RNA. Second, we use well-studied RNA aptamers to tether 16S and 23S ribosomal RNAs. Future work will involve further characterizing these capabilities. Our current work represents an in-depth investigation of permissible tether designs which will aid in the assembly of ribosome tether design rules. Furthermore, our designs will inform both the basic and synthetic biology fields by highlighting permissible and functional designs for connecting large macromolecular complexes.

5.3 Materials and methods

5.3.1 Design of ribosome tether constructs

For RNAMake ribosome tether designs, PDB coordinates 3R8T and 4GD2 for the 50S and 30S ribosomal subunits structures were used, respectively. From the 50S coordinates we removed residues A2854-A2863, and from the 30S, we removed residues A1445-A1457. Due to the large size we had to generate an RNAMake motif graph file to parse the structures into a format easier for RNAMake to read on command line.

5.3.2 Construction and experimental testing of ribosome tether constructs

The designed tethers were cloned into plasmid pRibo-T-A2058G. The backbone was generated for each design using forward (f) and reverse (r) primer pairs (noted with “bb”) in Supplementary Table 5.1 in separate PCR reactions using plasmid pRibo-T as a template, Phusion

polymerase (NEB), and 3% DMSO. PCR cycling was as follows: 98 °C for 3 min; 25 cycles of 98 °C for 30 sec, 55 °C for 30 sec, 72 °C for 2 min; and 72 °C for 10 min. Circularly permuted 23S ribosomal RNA (rRNA) was generated with forward and reverse primer pairs (noted with "23S" in Supplementary Table 5.1), the pRibo-T template, and the same PCR conditions as described above. Each PCR reaction was purified by gel extraction from a 0.7% agarose gel with an E.Z.N.A. gel extraction kit (Omega). Each purified backbone (50 ng) was assembled with the respective 23S insert in 3-fold molar excess using Gibson assembly. Assembly reactions were transformed into POP2136 cells, and the cells were grown at 30 °C overnight. Colonies were picked and plasmids were isolated using an E.Z.N.A. miniprep kit (Omega) and confirmed with full plasmid sequencing by ACGT, Inc.

5.3.3 *In vivo* replacement of the wild-type ribosome by tethered ribosome variants

Each purified plasmid (100 ng) was separately transformed into electrocompetent SQ171fg cells containing pCSacB. Cells were recovered in 1 mL of SOC media at 37 °C with shaking for 1 hour. Fresh SOC (1.85 mL) supplemented with 50 μg/mL carbenicillin and 0.25% sucrose was inoculated with 250 μL of recovered cells and incubated overnight at 37 °C with shaking. Cultures (10% and 90%) were plated on LB agar plates supplemented with 50 μg/mL carbenicillin, 5% sucrose and 1 mg/mL erythromycin and incubated at 37 °C. After 48 hours with no visible colonies, the plates were replica plated onto fresh LB agar plates supplemented with 50 μg/mL carbenicillin, 5% sucrose and 1 mg/mL erythromycin and incubated at 37 °C. After 72 additional hours, colonies appeared on the plate containing RM-Tether design 4. Eight colonies were streaked onto LB agar supplemented with 50 μg/mL carbenicillin and 1 mg/mL erythromycin and LB agar supplemented with 30 μg/mL kanamycin (to confirm loss of the pCSacB plasmid) and were also

used to inoculate 5 mL of LB supplemented with 50 μg/mL carbenicillin and 1 mg/mL erythromycin. Plates were incubated at 37 °C, and cultures were incubated at 37 °C with shaking. The OD600 of the cultures was tracked to generate growth curves (Biochrom Libra S4 spectrophotometer). After 5 days at 37 °C, total RNA was extracted using an RNA extraction kit from Qiagen. Total RNA was analyzed by gel electrophoresis on a 1% agarose gel with GelRed. Total plasmid was extracted from saturated 5 mL cultures with an E.Z.N.A. miniprep kit (Omega) and sequenced to confirm the correct RM-Tether design 4 sequence.

5.3.4 *In vitro* construction, testing, and characterization of ribosomes

For in vitro characterization of ribosomes, all constructs (wild type, Ribo-T v1.0, and RMTether 4) were cloned to be under control of a T7 promoter. The T7 promoter was introduced into primers, and amplified using the wild type, Ribo-T v1.0, and RM-Tether 4 plasmids as templates for PCR amplification. PCR products were blunt end ligated, transformed into DH5α *E. coli* cells using electroporation, and plated onto LBagar/ampicillin plates at 37°C. Plasmid was recovered from resulting clones and sequence confirmed. *In vitro* ribosome synthesis, assembly, and translation (iSAT) reactions were set-up as previously described [51]. Briefly, eight 15 μL reactions were prepared and incubated for 2 hours at 37 °C, then pooled together. Sucrose gradients were prepared from buffer C (10 mM Tris-OAc (pH = 7.5 at 4 °C), 60 mM NH4Cl, 7.5 mM Mg(OAc)2, 0.5 mM EDTA, 2 mM DTT) with 10 and 40% sucrose in SW41 polycarbonate tubes using a Biocomp Gradient Master. Gradients were placed in SW41 buckets and chilled to 4 °C. 120 μL of pooled iSAT reactions were loaded onto the gradients. The gradients were ultra-centrifuged at 22,500 rpm for 17 hours at 4 °C, using an Optima L-80 XP ultracentrifuge (Beckman-Coulter) at medium acceleration and braking (setting of 5 for each). Gradients were

analyzed with a BR-188 density gradient fractionation system (Brandel) by pushing 60% sucrose into the gradient at 0.75 mL/min (at normal speed). Traces of A_{254} readings versus elution volumes were obtained for each gradient. Gradient fractions were collected and analysed for rRNA content by gel electrophoresis in 1% agarose and imaged in a GelDoc Imager (Bio-Rad). Ribosome profile peaks were identified based on the rRNA content as representing 30S or 50S subunits, 70S ribosomes, or polysomes. 23 Fractions containing 70S ribosomes and polysomes were collected and pooled. These fractions were recovered as previously described, with pelleted iSAT ribosomes resuspended in iSAT buffer, aliquoted, and flash-frozen. These pelleted fractions were re-run on a 1% agarose gel and imaged in a GelDoc to confirm tethering in monosome and polysome peaks.

5.3.5 Selecting tether mutants, evaluating growth rate and analyzing tethers

Colonies that appeared after incubation of plates at 37°C were inoculated in a Costar flat bottom 96-well plate containing 100 µL of LB supplemented with 50 µg mL^{-1} carbenicillin and 1 mg mL^{-1} erythromycin. Growth rates were monitored at 37°C in a BioTek microplate reader. Absorbance at 600 nm was read every 10 minutes (continuous linear shaking with a 2-mm amplitude). Doubling times were calculated from the growth curve readings during logarithmic growth as determined by regression.

The fastest growing tether mutants were inoculated in 2 mL LB supplemented with 50 µg mL^{-1} carbenicillin, 5% sucrose and 1 mg ml^{-1} erythromycin and grown for 24–48 hr. Plasmids were isolated from clones and tethers were sequenced (ACGT Inc.). Tether composition was analyzed by sequencing with primers 5'- GCTGTCGTCAGCTCGTGTTG-3' for T1 site and 5'-CTGGAGAACTGAGGGG-3' for T2 site.

5.3.6 Total RNA analysis of tethered ribosomes

Successful replacement of the wild type of pCSacB plasmid with the pRibo-T plasmids carrying the various tethered constructs was confirmed via total RNA extraction. Total RNA was extracted from these clones using RNeasy Mini Kit (Qiagen) and analyzed by agarose gel electrophoresis.

5.4 Results

5.4.1 Characterizing computationally designed tethered ribosomes

The ribosome is a ribonucleoprotein machine dominated by two extensive RNA subunits, the 16S and 23S rRNAs. In previous work, we constructed a tethered ribosome called Ribo-T in which the large and small subunit rRNAs were connected by an RNA tether to form a single subunit ribosome [175]. In that work, the major bottleneck involved more than a year of numerous trial-and-error iterations to identify RNA tethers that were not cleaved by ribonucleases *in vivo* when wild-type ribosomes were replaced in the Squires strain of *E. coli*. The Squires strain cells lack genetic rRNA alleles, surviving off plasmids that can be exchanged using positive and negative selections [66]. Early failure rounds that involved ribosomes from our and other studies are shown in Figure 5.1a,b and the success with Ribo-T in Figure 5.1c Nevertheless, the current tethers in Ribo-T are unstructured and unlikely to remain stable if other modules are incorporated (Figure 5.1c). We hypothesized that an automated design by the RNAMake algorithm [284] might give structured, chemically stable tethers for this design problem.

The RNAMake algorithm generated 100 designs (RM-Tethers), which contained either four or five non-canonical structural motifs each, to tether the H101 helix on a circularly permuted 23S rRNA to the h44 helix on the 16S rRNA. Of the nine diverse solutions we tested (RM-Tether

1–9), DNA templates for seven could be synthesized, and the transformation of these DNA templates into the Squires strain allowed us to assay whether the RNAMake designs could replace wild-type ribosomes deleted from growing bacteria (Supplementary Table 5.2). One of these seven constructs, RM-Tether 4, led to the viable growth of bacterial colonies. DNA sequencing confirmed that these colonies harbored the correct RM-Tether 4 plasmid; and RNA electrophoresis confirmed the presence of a single dominant RNA species with the same length as Ribo-T, with no detectable products that corresponded to separate 16S or 23S rRNA lengths or other cleavage products (Figure 5.1d). Although the growth rate of this strain was slow (Figure 5.2), we were able to confirm independently that the ribosomes loaded on messenger RNA *in vitro*, using integrated synthesis, assembly, and translation (iSAT) in ribosome-free S150 extracts. Similar to Ribo-T, we detected 70S/monosome and polysomes (and no 30S or 50S subunits) by separation of the iSAT-prepared RM-Tether 4 ribosomes on a sucrose gradient (Figure 5.1e). Electrophoresis of the polysome fraction confirmed that it contained an uncleaved rRNA the same size as Ribo-T (Figure 5.1f). In addition, SHAPE-Seq mapping on this rRNA confirmed that the RM-Tether 4 can be reverse transcribed from one ribosomal subunit to the other across both strands of the tether and highlights a chemical reactivity profile consistent with the design, with one region of flexibility around the middle junction. Taken together, these data demonstrate that RNAMake-designed ribosomes with structured, chemically stable tethers can replace wild-type ribosomes *in vivo* and more than one such ribosome can be loaded onto a single message in vitro. RNAMake obviates the repeated rounds of trial and error that were previously required to achieve these design goals.

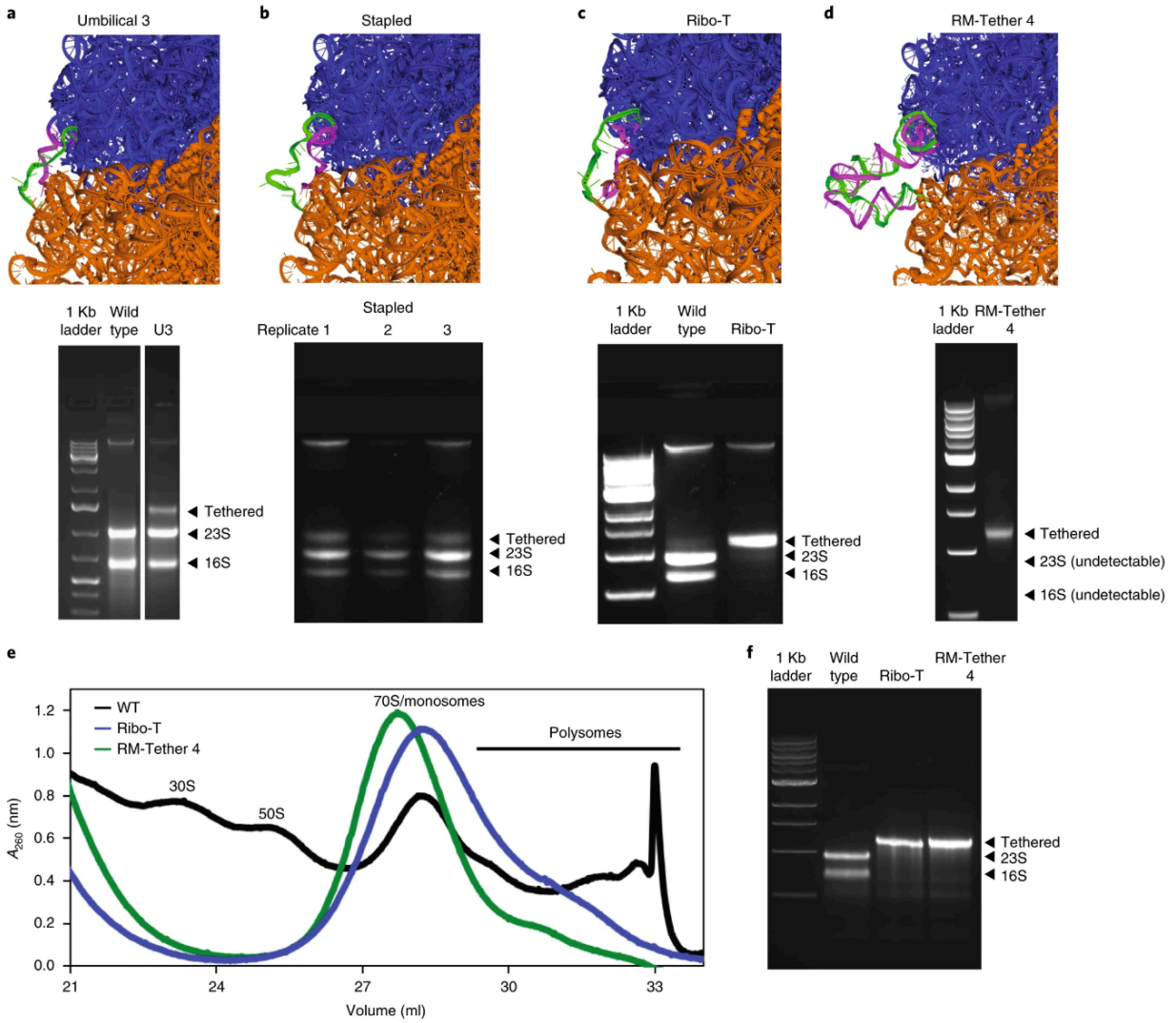

Figure 5.1 (a–d) Modelling (top panels) of tethers (green and magenta strands) that connect 16S and 23S rRNA into a single rRNA, and agarose gel electrophoresis (bottom panels) of RNA extracted from *E. coli* (Squires strain) in which wild-type ribosomes were completely replaced with the designed molecules (top): an early U3 tether (Umbilical 3) designed by the Jewett lab, cleaved into two bands in vivo (a), a stapled ribosomes developed by a separate group (three replicates shown), also cleaved in this plasmid context and strain *in vivo* (b), the successful Ribo-T design developed after a year of manual trial and error to withstand cleavage in vivo (c) and RM-Tether 4, a design automatically generated by RNAMake, which also presents as a single band *in vivo* (d). (e) Sucrose gradient fractionation prepared from in vitro iSAT reactions that express wild-type ribosomes, Ribo-T version 1.0 and RM-Tether 4. Peaks correspond to small subunits (30S), large subunits (50S), monosomes/70S and polysomes (standard assignments of the peaks are given in, for example, Underwood et al.). (f) Agarose electrophoresis analysis confirms that the polysome fraction of **e** is composed of tethered ribosomes. Full gels are given in Figure 5.2.

To test RNAMake's accuracy in designing functional RNAs, each RM-Tether design (Supplementary Figure 5.1) was cloned into the pRibo-T plasmid and used to replace the wild-type ribosomal rRNA plasmid in the SQ171fg strain. After 48 hours at 37 °C, no colonies were visible on the plates. Fresh plates were replica plated and incubated for a further 72 hours at 37°C, after which colonies appeared on the plate for RM-Tether design 4. Eight colonies were picked and checked for the loss of the wild-type rRNA plasmid. Growth curves were generated in liquid culture at 37°C (Figure 5.2d). These constructs exhibited doubling times of 1.5 ± 0.8 days and a maximum OD600 of 0.7 ± 0.3 (Figure 5.2d). While slower than wild-type *E. coli*, the first successful version of Ribo-T was also slower growing before mutational optimization. After five days of growth, total RNA was extracted and analyzed by gel electrophoresis. Seven of the eight clones showed a clean Ribo-T-sized band and no detectable wild-type 23S and 16S rRNA bands (Figure 5.2e), indicating the formation of stable tethered ribosomes, as previously demonstrated for Ribo-T.

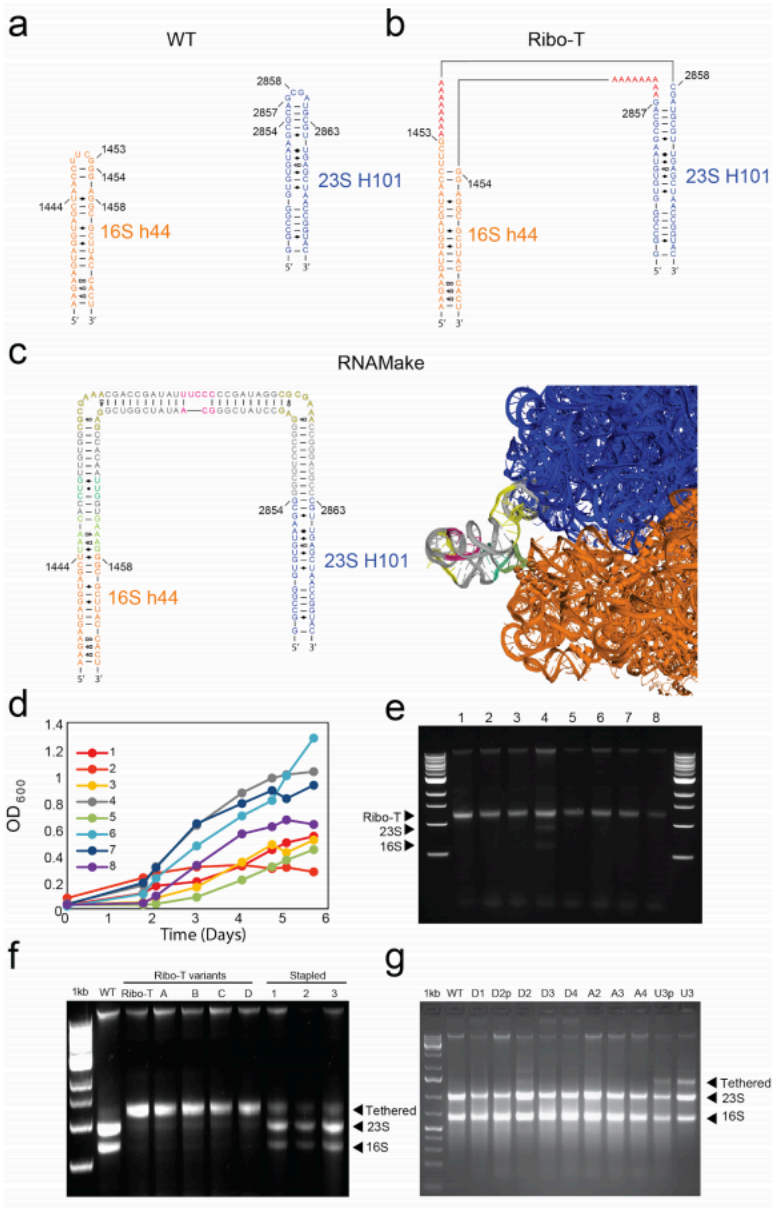

Figure 5.2 Secondary structure comparison and full gels for ribosome tethering studies (a) Secondary structure of 16S helix 44 (h44) and wild-type 23S helix 101 (H101). (b) Published Ribo-T secondary structure. (c) (left) Secondary structure of RM-Tether 4 designed with RNAMake. Each motif is colored as in the 3D structure model (right). (d) Culture density of *E. coli* cells containing RNAMake RM-Tether design 4. (e) Gel assay of 8 distinct colonies, verifying the RNAMake-designed Ribo-T. In one case, lane 4, we observed very faint 16S and 23S-like rRNA bands, possibly reflecting linker cleavage either in the cell or during ribosome isolation. (f) Agarose gel electrophoresis of RNA extracted from E. coli (Squires strain SQ171fg) in which wild type ribosomes were completely replaced with the indicated ribosomes. The double band under the wild type lane indicates the 16S and 23S rRNA in the two separate subunits of the ribosome.

The Ribo-T lane represents the original Ribo-T construct published by Orelle *et al*. The Ribo-T variants (a-d) represent tether variants of Ribo-T (unpublished data from the Jewett lab) that remain tethered, and the stapled ribosomes represent tethers generated from published work by Fried, *et al*. In our system and constructs, stapled tethers do not maintain a single-subunit entity, resulting in a 3-band pattern. (g) U3 tether (Umbilical 3) designed by the Jewett lab, presents as three bands in vivo (last lane).

5.4.2 Characterizing ribosomes with RNA aptamer tethers

As an alternative to computationally designed tethers, we sought to construct tethered ribosomes possessing RNA aptamers found in nature, specifically the MS2 aptamer (Figure 5.3) [288]. In addition to being well-studied, previously published, and found in nature; these RNA aptamer tethers have the potential to introduce functionality into the RNA tethers of a ribosome. This functionality may include protein binding, small molecule binding, sequestering substrates, fluorescence, and more. As a proof of concept that the large and small subunits of a ribosome may be tethered by a well-studied RNA aptamer, we sought to build MS2-Ribo-T constructs and characterize them (Figure 5.3).

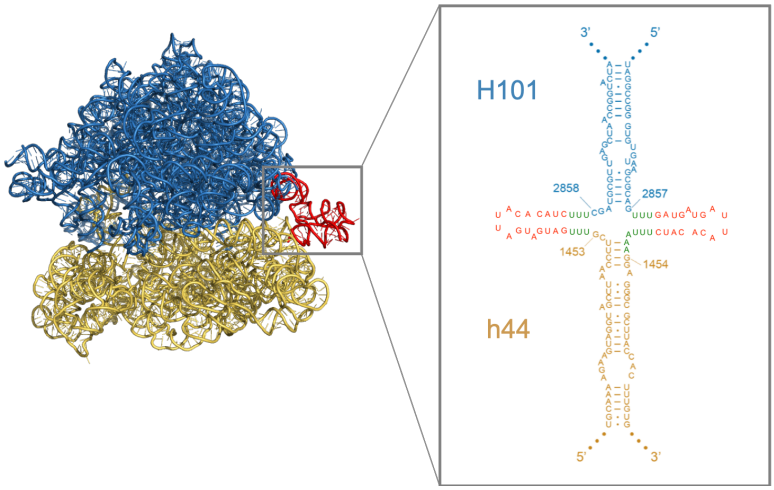

Figure 5.3 MS2 tethered ribosome design, with an MS2 RNA aptamer linking H101 and h44 of the large and small subunits, respectively.

To test the MS2-Ribo-T designs, a series of MS2-Ribo-T designs, carrying different variations of the MS2 aptamer within the tethers, were cloned into the pRibo-T plasmid and used to replace the wild-type ribosomal rRNA plasmid in the SQ171fg strain. Additionally, we included various linker spacers or no linker spacers between the ribosomal helices and the tethers, to observe the impact of extra structure. As a first proof of concept, we constructed and tested two simple MS2-Ribo-T sequence constructs, each with and without linker spacers. Clones were sequence confirmed in POP2136 cells, and subsequently confirmed in the Squires strain [66]. We found that across the two sets, those with short linker spacers were able to grow and sustain the life of the cell, while those without the linker spacers did not grow. Furthermore, those with the MS2 aptamer and linker spacers remained uncleaved in the cell, maintaining a fully tethered state (Figure 5.4).

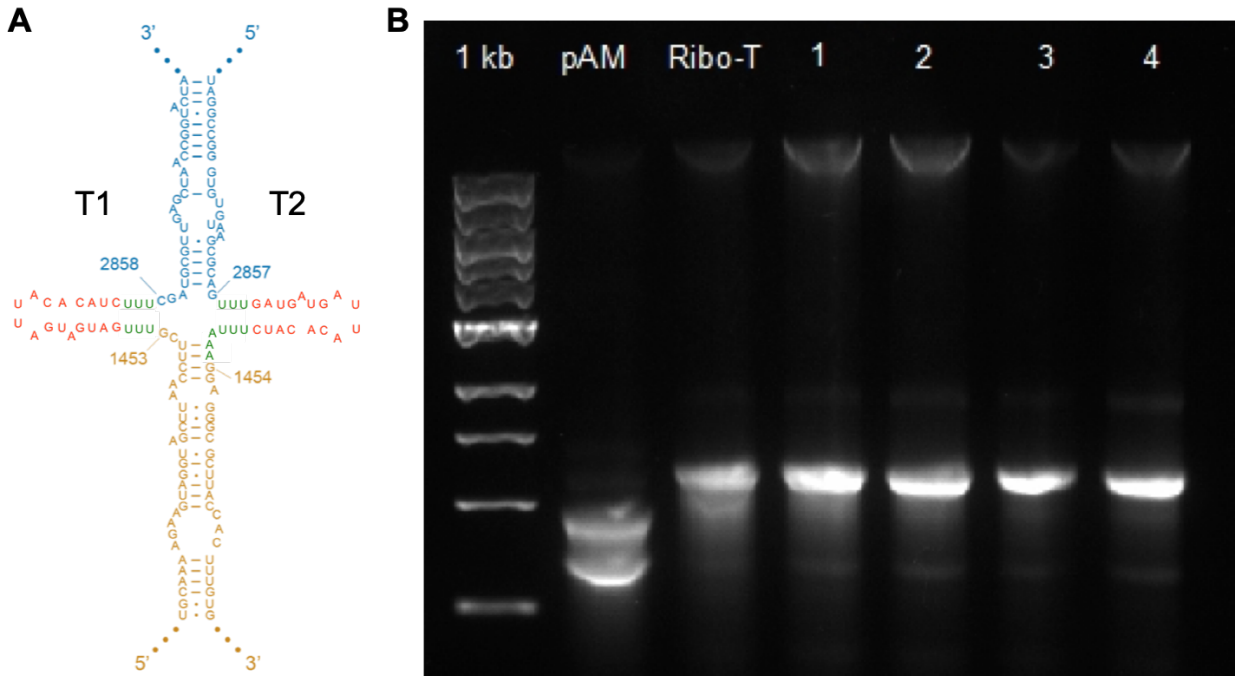

Figure 5.4 Initial MS2-Ribo-T constructs either possessing or lacking linker spacers were tested in the Squires strain. (a) The secondary structure of the MS2-Ribo-T construct with linker spacers that was successful in maintaining the life of the cell. Tether sequences are as follows: T1=

TTTGATGAGGAATTACCCATCTTT; T2= TTTGATGAGGATTACCCATCTTTAAA. (b) RNA extraction gel demonstrating that MS2-Ribo-T constructs possessing linker spacers are capable of maintaining their tethered identities after introduction into the Squires strain.

Next, we compared MS2-Ribo-T constructs that possessed similar MS2 aptamer sequences, but with one possessing an extra nucleotide insertion (v1.0) versus one lacking the extra insertion (v3.0). This would help demonstrate the impacts of breaking up or altering a small piece of the functional RNA sequence for the purpose of tuning or changing the accessibility or functionality of the tethers. Additionally, we again tested these constructs with and without linker spacers. We found that small single nucleotide changes in the tether did no substantially change the functionality and growth of cells living on the MS2-Ribo-T constructs, and both constructs remained fully tethered (Figure 5.5 a,b,c). When testing the constructs lacking the linker spacers, again, we saw poor functionality (slow growth rates or no growth at all), and also observed tether cleavage (Figure 5.5 a,b,c).

Growth curves were generated in liquid culture at 37°C (Figure 5.5 b,d). These constructs exhibited doubling times of 240-270 min and a maximum OD600 of ~0.5-0.6 (Figure 5.5 b,d). While slower than wild-type *E. coli*, the first successful version of Ribo-T was also slower growing before mutational optimization.

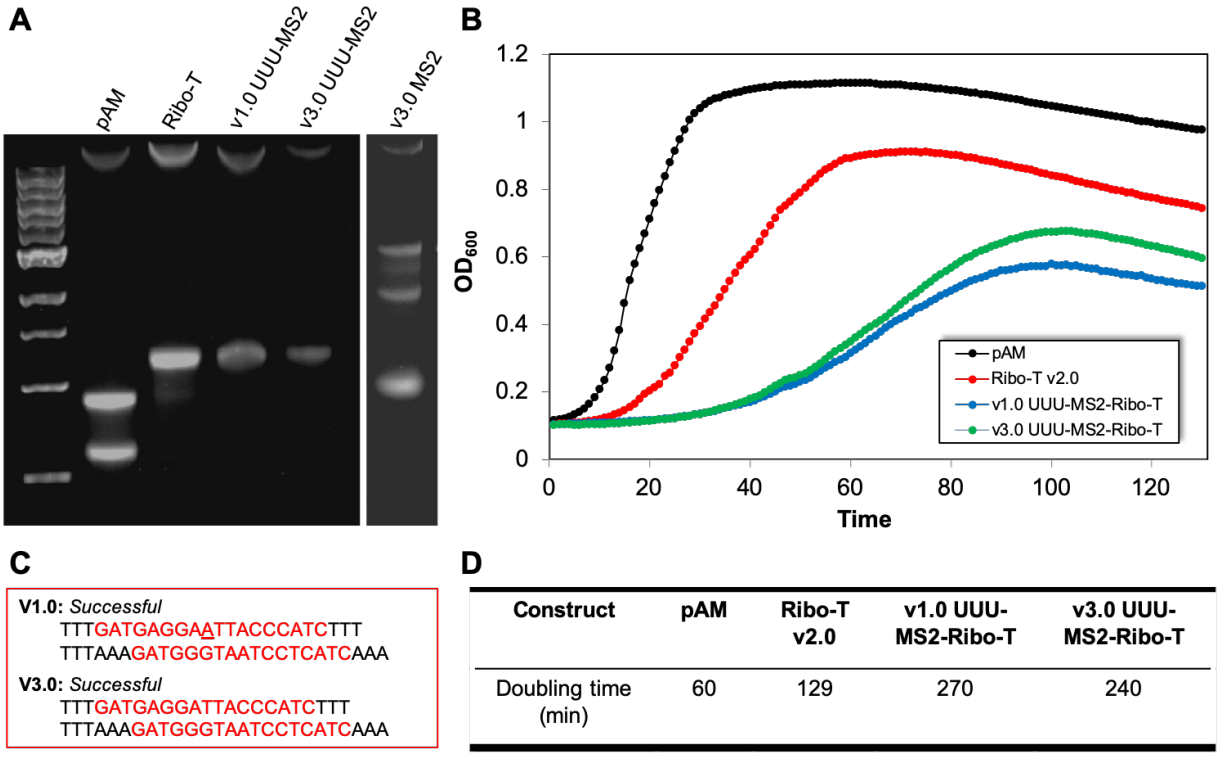

Construct	pAM	Ribo-T v2.0	v1.0 UUU-MS2-Ribo-T	v3.0 UUU-MS2-Ribo-T
Doubling time (min)	60	129	270	240

Figure 5.5 The impact of MS2 tether composition on doubling time. (a) RNA gels of the various MS2-Ribo-T constructs. (b) Growth curves of the MS2-Ribo-T constructs as well as wild-type and Ribo-T controls. (c)

Finally, as a last step towards generating design rules for the design and synthesis of functional RNA aptamer tethers, we designed, built, and characterized a diverse array of RNA aptamer tethers (Supplementary Table 5.3). These tethers each had different MS2 variant sequences as well as varied linker spacer sequences and lengths (Supplementary Table 5.3). One also included a double MS2 aptamer with a short dividing spacer sequence in between (Ribo-Switch 10). We characterized their growth rates, as well as their ability to remain tethered in a living cell (Figure 5.6). Interestingly, we found that in every case, these MS2-Ribo-T variants were capable of maintaining the life of *E. coli* cells while still maintaining their tethered identities (Figure 5.6).

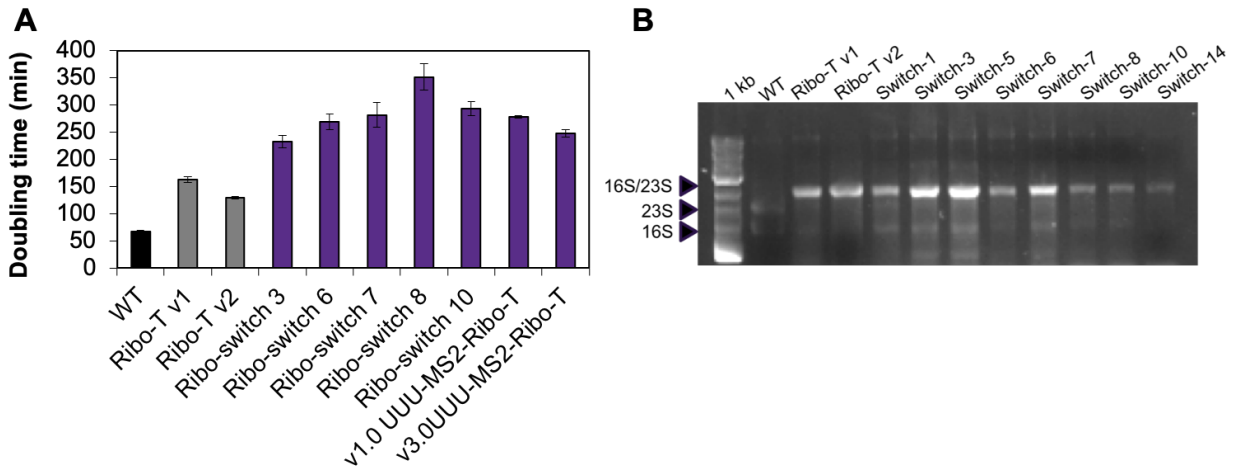

Figure 5.6 (a) Doubling time characterization of MS2-Ribo-T library members; and (b) RNA gel confirmation of tethered identities in living Squires strain *E. coli* cells.

5.5 Discussion

As RNA nanotechnology seeks to create artificial molecules closer in sophistication to natural RNA molecules, the design of tertiary structures that are as complex, asymmetric and diverse as natural RNAs becomes an important goal. Here, we hypothesized that designing complex RNA tertiary structures might be reduced to both instances of a single RNA motif pathfinding problem as well as nature's repertoire of RNA aptamers. In this vein, we used (1) the algorithm RNAMake to solve the pathfinding task and generate computationally designed tethers, and (2) used well-studied RNA aptamers that are found in nature. For the problem of tethering *E. coli* 16S and 23S rRNAs into a single RNA molecule, one of nine RNAMake-designed molecules replaced ribosomes *in vivo* and was confirmed to translate in polysomes in cell-free translation reactions. Additionally, MS2 aptamer variants, which are found in nature, were also successfully in replacing wild-type ribosomes in cells without cleavage.

The RNAMake algorithm achieved its design objectives in a single round of tests that involved the parallel synthesis of rRNA tether constructs, without further trial-and-error iteration.

Importantly, as RNAMake is applied to more problems, we expect its success rate to improve further. Accumulating knowledge as to which structural motifs recur in successful versus failing designs may allow an empirical scoring for the modularity of each motif; inferences for some motifs, such as A–A mismatches, are already possible. Additionally, the incorporation of more diverse motifs may allow an improved design of such machines as the ribosome. Furthermore, natural structured RNAs often contain configurations that may be used effectively for tethering ribosomal subunits, such as MS2 aptamers. Finally, we expect RNAMake's computational design approach to be complementary to library selection, using RNA structures found in nature, as well as high-throughput screening methods, especially for larger problems that require numerous non-canonical motifs.

5.6 Acknowledgements and contributions

Dr. Rhiju Das and Dr. Joseph D. Yesselman conceived the study. Dr. Joseph D. Yesselman developed RNAMake and generated the models and sequences used throughout the study. Alexandra N. Ooms, Wipapat Kladwang and Dr. Joseph D. Yesselman performed the chemical mapping, titrations and native gel assays for miniTTR constructs. Xuesong Shi and Daniel Herschlag designed and performed the SAXS on miniTTR 2 and 6. D.E. solved the miniTTR crystal structure assisted by David A. Costantino and Jeffrey S. Kieft in preparing the RNA and analysis. Erik D. Carlson, Anne E. d'Aquino and Michael C. Jewett made and tested the RNAMake-designed ribosomes. Paul D. Carlson and Julius B. Lucks carried out the SHAPE-seq and in vivo tests of Spinach-TTRs. Michael R. Gotrik performed fluorescence and lysate experiments on Spinach-TTRs. Dr. Rhiju Das and Dr. Joseph D. Yesselman wrote the paper, with

participation by all the authors. Kim Hoang and Alysse DeFoe aided in the cloning and construction of the MS2-Ribo-T variants, as well as their characterization in the Squires strain.

5.7 Supplementary figures and tables

Supplementary Table 5.1 Ribosome tether primers for pRibo-T template.

Primer Name	Primer
RM_tether-1-bb-r	GTCTTAGATCGAAATCCTCGGCACGGACCTGTTGCTCAGCTACCTACTTCTTTTGC
RM_tether-1-bb-f	TGACGGATCGAAATCCGTTTGACGCACGGCCTGGCGGCGCTTACCACTTTGTG
RM_tether-1-23S-f	CGAGGATTTCGATCTAAGACAGTATGGGGCCCCGTTGAGCTAACCGGTACTAATG
RM_tether-1-23S-r	AAACGGATTTCGATCCGTCATTGTATGGGGCCCCGCTTACACACCCGGCCTATC
RM_tether-2-bb-r	CCCCGGCCGTGGATCCCGTTCACAGCCACACGGCCCTGTAGCTACCTACTTCTTTTGC
RM_tether-2-bb-f	GCCCCGAAGCCGTGGATCCCGGGAGCCACGTGGCTGGCCTGTGGCGCTTACCACTTTGTG
RM_tether-2-23S-f	AACGGGATCCACGGCCGGGGCCGAGGTGGGGGGCCCCGTTGAGCTAACCGGTACTAATG
RM_tether-2-23S-r	GGGATCCACGGCTTCGGGGCGTCAAACGGTGGGGGGCCCCGCTTACACACCCGGCCTATC
RM_tether-3-bb-r	TCGAATGTTACGTCCATGATCTCCCTACCCGCTAGGAGCTACCTACTTCTTTTGC
RM_tether-3-bb-f	ATCGAATGCCCGTCCATGATCTGTGAACTACCCGCTAGAAGGGCGCTTACCACTTTGTG
RM_tether-3-23S-f	ATCATGGACGTAACATTCGATCCGAGGGGGGGGGACCGTTGAGCTAACCGGTACTAATG
RM_tether-3-23S-r	ATCATGGACGGGCATTCGATCGTCAAACGGGGGGGGGACCGCTTACACACCCGGCCTATC
RM_tether-4-bb-r	TCGGGGGAAATATCGGTCGTTTCGCGCCACAACAGGTGTTAAGCTACCTACTTCTTTTGC
RM_tether-4-bb-f	TATCGGGCAATATCGGTCGGAGCCACAATTGGTGAAAGGGCGCTTACCACTTTGTG
RM_tether-4-23S-f	ACGACCGATATTTCCCCCGATATGGCGCGAAACCGGGACGCCCGTTGAGCTAACCGGTACTAATG
RM_tether-4-23S-r	CCGACCGATATTGCCCGATATGGCTCCCGGGACGCCCGCTTACACACCCGGCCTATC
RM_tether-5-bb-r	GAATATAATCCCATACGTACGAGTTAGTAGTTCGCCTACAGAGCTACCTACTTCTTTTGC
RM_tether-5-bb-f	TATATCGAATATAATCCCATACGCAAATTAGCGCCTATTGGGCGCTTACCACTTTGTG
RM_tether-5-23S-f	GTACGTATGGGATTATATTCGATATATGGACCTATGGACCCCCGTTGAGCTAACCGGTACTAATG
RM_tether-5-23S-r	ATGGGATTATATTCGATATACTTCCATCCTATGGACCCCCGCTTACACACCCGGCCTATC
RM_tether-6-bb-r	CTGACGGGTACCATCGGCCCCCCTCCCTGGACGCCCTAGAGCTACCTACTTCTTTTGC
RM_tether-6-bb-f	GACGAACACCATCGGCCCCCCTGTGAACTGGCGCTGGCCTAGGGCGCTTACCACTTTGTG
RM_tether-6-23S-f	GGGCCGATGGTACCCGTCAGGGAGATGGGGGGCCCCGTTGAGCTAACCGGTACTAATG

RM_tether-6-23S-r	GGGGGCCGATGGTGTTCGTCAGTTCACAGATGGGGGGCCCCGCTTACACACCCGGCCTATC
RM_tether-8-bb-r	TTAGTATCTCCTGTGACGCCCTACGTACGAGTCAGACAGCTACCTACTTCTTTTGC
RM_tether-8-bb-f	GGTATCCGAGCTGTGACGCTGGCCTACGCAAATCAGCGGCGCTTACCACTTTGTG
RM_tether-8-23S-f	GGCGTCACAGGAGATACTAAGACAGAATATACCCCCCGTTGAGCTAACCGGTACTAATG
RM_tether-8-23S-r	AGCGTCACAGCTCGGATACCGTCATTGAATATACCCCCCGCTTACACACCCGGCCTATC

Supplementary Table 5.2 Ribosome tether sequences from RNAMake.

Design	Sequence
RM_Tether 1	GCGGCCGCGATCTCTCACCTACCAAACAATGCCCCCCTGCAAAAAATAAATTCATATAAAAAACATACAGATAACCATCTGCGGTGATAA ATTATCTCTGGCGGTGTTGACATAAATACCACTGGCGGTGATACTGAGCACGGGTACCGGCCGCTGAGAAAAAGCGAAGCGGCACTGCTC TTTAACAATTTATCAGACAATCTGTGTGGGCACTCGAAGATACGGATTCTTAACGTCGCAAGACGAAAAATGAATACCAAGTCTCAAGAG TGAACACGTAATTCATTACGAAGTTTAATTCTTTGAGCGTCAAACTTTTAAATTGAAGAGTTTGATCATGGCTCAGATTGAACGCTGGCG GCAGGCCTAACACATGCAAGTCGAACGGTAACAGGAAGAAGCTTGCTTCTTTGCTGACGAGTGGCGGACGGGTGAGTAATGTCTGGGAAA CTGCCTGATGGAGGGGGATAACTACTGGAAACGGTAGCTAATACCGCATAACGTCGCAAGACCAAAGAGGGGGACCTTCGGGCCTCTTGC CATCGGATGTGCCCAGATGGGATTAGCTAGTAGGTGGGGTAACGGCTCACCTAGGCGACGATCCCTAGCTGGTCTGAGAGGATGACCAGC CACACTGGAACTGAGACACGGTCCAGACTCCTACGGGAGGCAGCAGTGGGGAATATTGCACAATGGGCGCAAGCCTGATGCAGCCATGCC GCGTGTATGAAGAAGGCCTTCGGGTTGTAAAGTACTTTCAGCGGGGAGGAAGGGAGTAAAGTTAATACCTTTGCTCATTGACGTTACCCG CAGAAGAAGCACCGGCTAACTCCGTGCCAGCAGCCGCGGTAATACGGAGGGTGCAAGCGTTAATCGGAATTACTGGGCGTAAAGCGCACG CAGGCGGTTTGTTAAGTCAGATGTGAAATCCCCGGGCTCAACCTGGGAACTGCATCTGATACTGGCAAGCTTGAGTCTCGTAGAGGGGGG TAGAATTCCAGGTGTAGCGGTGAAATGCGTAGAGATCTGGAGGAATACCGGTGGCGAAGGCGGCCCCCTGGACGAAGACTGACGCTCAGG TGCGAAAGCGTGGGGAGCAAACAGGATTAGATACCCTGGTAGTCCACGCCGTAAACGATGTCGACTTGGAGGTTGTGCCCTTGAGGCGTG GCTTCCGGAGCTAACGCGTTAAGTCGACCGCCTGGGGAGTACGGCCGCAAGGTTAAAACTCAAATGAATTGACGGGGGCCCGCACAAGCG GTGGAGCATGTGGTTTAATTCGATGCAACGCGAAGAACCTTACCTGGTCTTGACATCCACGGAAGTTTTCAGAGATGAGAATGTGCCTTC GGGAACCGTGAGACAGGTGCTGCATGGCTGTCGTCAGCTCGTGTTGTGAAATGTTGGGTTAAGTCCCGCAACGAGCGCAACCCTTATCCT TTGTTGCCAGCGGTCCGGCCGGGAACTCAAAGGAGACTGCCAGTGATAAACTGGAGGAAGGTGGGGATGACGTCAAGTCATCATGGCCCT TACGACCAGGGCTACACACGTGCTACAATGGCGCATACAAAGAGAAGCGACCTCGCGAGAGCAAGCGGACCTCATAAAGTGCGTCGTAGT CCGGATTGGAGTCTGCAACTCGACTCCATGAAGTCGGAATCGCTAGTAATCGTGGATCAGAATGCCACGGTGAATACGTTCCCGGGCCTT GTACACACCGCCCGTCACACCATGGGAGTGGGTTGCAAAAGAAGTAGGTAGCTGAGCAACAGGTCCGTGCCGAGGATTTCGATCTAAGAC AGTATGGGGCCCCGTTGAGCTAACCGGTACTAATGAACCGTGAGGCTTAACCGAGAGGTTAAGCGACTAAGCGTACACGGTGGATGCCCT GGCAGTCAGAGGCGATGAAGGACGTGCTAATCTGCGATAAGCGTCGGTAAGGTGATATGAACCGTTATAACCGGCGATTTCCGAATGGGG AAACCCAGTGTGTTTCGACACACTATCATTAACTGAATCCATAGGTTAATGAGGCGAACCGGGGGAACTGAAACATCTAAGTACCCCGAG GAAAAGAAATCAACCGAGATTCCCCCAGTAGCGGCGAGCGAACGGGGAGCAGCCCAGAGCCTGAATCAGTGTGTGTGTTAGTGGAAGCGT CTGGAAAGGCGCGCGATACAGGGTGACAGCCCCGTACACAAAAATGCACATGCTGTGAGCTCGATGAGTAGGGCGGGACACGTGGTATCC TGTCTGAATATGGGGGGACCATCCTCCAAGGCTAAATACTCCTGACTGACCGATAGTGAACCAGTACCGTGAGGGAAAGGCGAAAAGAAC CCCGGCGAGGGGAGTGAAAAAGAACCTGAAACCGTGTACGTACAAGCAGTGGGAGCACGCTTAGGCGTGTGACTGCGTACCTTTTGTATA ATGGGTCAGCGACTTATATTCTGTAGCAAGGTTAACCGAATAGGGGAGCCGAAGGGAAACCGAGTCTTAACTGGGCGTTAAGTTGCAGGG TATAGACCCGAAACCCGGTGATCTAGCCATGGGCAGGTTGAAGGTTGGGTAACACTAACTGGAGGACCGAACCGACTAATGTTGAAAAAT TAGCGGATGACTTGTGGCTGGGGGTGAAAGGCCAATCAAACCGGGAGATAGCTGGTTCTCCCCGAAAGCTATTTAGGTAGCGCCTCGTGA ATTCATCTCCGGGGGTAGAGCACTGTTTCGGCAAGGGGGTCATCCCGACTTACCAACCCGATGCAAACTGCGAATACCGGAGAATGTTAT CACGGGAGACACACGGCGGGTGCTAACGTCCGTCGTGAAGAGGGAAACAACCCAGACCGCCAGCTAAGGTCCCAAAGTCATGGTTAAGTG GGAAACGATGTGGGAAGGCCCAGACAGCCAGGATGTTGGCTTAGAAGCAGCCATCATTTAAAGAAAGCGTAATAGCTCACTGGTCGAGTC GGCCTGCGCGGAAGATGTAACGGGGCTAAACCATGCACCGAAGCTGCGGCAGCGACGCTTATGCGTTGTTGGGTAGGGGAGCGTTCTGTA AGCCTGCGAAGGTGTGCTGTGAGGCATGCTGGAGGTATCAGAAGTGCGAATGCTGACATAAGTAACGATAAAGCGGGTGAAAAGCCCGCT CGCCGGAAGACCAAGGGTTCCTGTCCAACGTTAATCGGGGCAGGGTGAGTCGACCCCTAAGGCGAGGCCGAAAGGCGTAGTCGATGGGAA ACAGGTTAATATTCCTGTACTTGGTGTTACTGCGAAGGGGGACGGAGAAGGCTATGTTGGCCGGGCGACGGTTGTCCCGGTTTAAGCGT GTAGGCTGGTTTTCCAGGCAAATCCGGAAAATCAAGGCTGAGGCGTGATGACGAGGCACTACGGTGCTGAAGCAACAAATGCCCTGCTTC CAGGAAAAGCCTCTAAGCATCAGGTAACATCAAATCGTACCCCAAACCGACACAGGTGGTCAGGTAGAGAATACCAAGGCGCTTGAGAGA ACTCGGGTGAAGGAACTAGGCAAAATGGTGCCGTAACTTCGGGAGAAGGCACGCTGATATGTAGGTGAGGTCCCTCGCGGATGGAGCTGA AATCAGTCGAAGATACCAGCTGGCTGCAACTGTTTATTAAAAACACAGCACTGTGCAAACACGAAAGTGGACGTATACGGTGTGACGCCT GCCCGGTGCCGGAAGGTTAATTGATGGGGTTAGCGCAAGCGAAGCTCTTGATCGAAGCCCCGGTAAACGGCGGCCGTAACTATAACGGTC CTAAGGTAGCGAAATTCCTTGTCGGGTAAGTTCCGACCTGCACGAATGGCGTAATGATGGCCAGGCTGTCTCCACCCGAGACTCAGTGAA ATTGAACTCGCTGTGAAGATGCAGTGTACCCGCGGCAAGACGGAAAGACCCCGTGAACCTTTACTATAGCTTGACACTGAACATTGAGCC TTGATGTGTAGGATAGGTGGGAGGCTTTGAAGTGTGGACGCCAGTCTGCATGGAGCCGACCTTGAAATACCACCCTTTAATGTTTGATGT TCTAACGTTGACCCGTAATCCGGGTTGCGGACAGTGTCTGGTGGGTAGTTTGACTGGGGCGGTCTCCTCCTAAAGAGTAACGGAGGAGCA CGAAGGTTGGCTAATCCTGGTCGGACATCAGGAGGTTAGTGCAATGGCATAAGCCAGCTTGACTGCGAGCGTGACGGCGCGAGCAGGTGC GAAAGCAGGTCATAGTGATCCGGTGGTTCTGAATGGAAGGGCCATCGCTCAACGGATAAAAGGTACTCCGGGGATAACAGGCTGATACCG

CCCAAGAGTTCATATCGACGGCGGTGTTTGGCACCTCGATGTCGGCTCATCACATCCTGGGGCTGAAGTAGGTCCCAAGGGTATGGCTGT
TCGCCATTTAAAGTGGTACGCGAGCTGGGTTTAGAACGTCGTGAGACAGTTCGGTCCCTATCTGCCGTGGGCGCTGGAGAACTGAGGGGG
GCTGCTCCTAGTACGAGAGGACCGGAGTGGACGCATCACTGGTGTTCGGGTTGTCATGCCAATGGCACTGCCCGGTAGCTAAATGCGGAA
GAGATAAGTGCTGAAAGCATCTAAGCACGAAACTTGCCCCGAGATGAGTTCTCCCTGACCCTTTAAGGGTCCTGAAGGAACGTTGAAGAC
GACGACGTTGATAGGCCGGGTGTGTAAGCGGGGCCCCATACAATGACGGATCGAAATCCGTTTGACGCACGGCCTGGCGGCGCTTACCAC
TTTGTGATTCATGACTGGGGTGAAGTCGTAACAAGGTAACCGTAGGGGAACCTGCGGTTGGATCACCTCCTTACCTTAAAGAAGCGTACT
TTGTAGTGCTCACACAGATTGTCTGATAGAAAGTGAAAAGCAAGGCGTTTACGCGTTGGGAGTGAGGCTGAAGAGAATAAGGCCGTTCGC
TTTCTATTAATGAAAGCTCACCCTACACGAAAATATCACGCAACGCGTGATAAGCAATTTTCGTGTCCCCTTCGTCTAGAGGCCCAGGAC
ACCGCCCTTTCACGGCGGTAACAGGGGTTCGAATCCCCTAGGGGACGCCACTTGCTGGTTTGTGAGTGAAAGTCGCCGACCTTAATATCT
CAAAACTCATCTTCGGGTGATGTTTGAGATATTTGCTCTTTAAAAATCTGGATCAAGCTGAAAATTGAAACACTGAACAACGAGAGTTGT
TCGTGAGTCTCTCAAATTTTCGCAACACGATGATGAATCGAAAGAAACATCTTCGGGTTGTGAGCTTAAGCTTACAACGCCGAAGCTGTT
TTGGCGGATGAGAGAAGATTTTCAGCCTGATACAGATTAAATCAGAACGCAGAAGCGGTCTGATAAAACAGAATTTGCCTGGCGGCAGTA
GCGCGGTGGTCCCACCTGACCCCATGCCGAACTCAGAAGTGAAACGCCGTAGCGCCGATGGTAGTGTGGGGTCTCCCCATGCGAGAGTAG
GGAACTGCCAGGCATCAAATAAAACGAAAGGCTCAGTCGAAAGACTGGGCCTTTCGTTTTATCTGTTGTTTGTCGGTGAACGCTCTCCTG
AGTAGGACAAATCCGCCGGGAGCGGATTTGAACGTTGCGAAGCAACGGCCCGGAGGGTGGCGGGCAGGACGCCCGCCATAAACTGCCAGG
CATCAAATTAAGCAGAAGGCCATCCTGACGGATGGCCTTTTTGCGTTTCTACAAACTCTTCCTGTCGTCATATCTACAAGCCGGCGCGCC
GGGAAATGTGCGCGGAACCCCTATTTGTTTATTTTTCTAAATACATTCAAATATGTATCCGCTCATGAGACAATAACCCTGATAAATGCT
TCAATAATATTGAAAAAGGAAGAGTATGAGTATTCAACATTTCCGTGTCGCCCTTATTCCCTTTTTTGCGGCATTTTGCCTTCCTGTTTT
TGCTCACCCAGAAACGCTGGTGAAAGTAAAAGATGCTGAAGATCAGTTGGGTGCACGAGTGGGTTACATCGAACTGGATCTCAACAGCGG
TAAGATCCTTGAGAGTTTTCGCCCCGAAGAACGTTTTCCAATGATGAGCACTTTTAAAGTTCTGCTATGTGGCGCGGTATTATCCCGTGT
TGACGCCGGGCAAGAGCAACTCGGTCGCCGCATACACTATTCTCAGAATGACTTGGTTGAGTACTCACCAGTCACAGAAAAGCATCTTAC
GGATGGCATGACAGTAAGAGAATTATGCAGTGCTGCAATAACCATGAGTGATAACACTGCGGCCAACTTACTTCTGACAACGATCGGAGG
ACCGAAGGAGCTAACCGCTTTTTTGCACAACATGGGGGATCATGTAACTCGCCTTGATCGTTGGGAACCGGAGCTGAATGAAGCCATACC
AAACGACGAGCGTGACACCACGATGCCTGCAGCAATGGCAACAACGTTGCGCAAACTATTAACTGGCGAACTACTTACTCTAGCTTCCCG
GCAACAATTAATAGACTGGATGGAGGCGGATAAAGTTGCAGGACCACTTCTGCGCTCGGCCCTTCCGGCTAGCTGGTTTATTGCTGATAA
ATCTGGAGCCGGTGAGCGTGGGTCTCGCGGTATCATTGCAGCACTGGGGCCAGATGGTAAGCCCTCCCGTATCGTAGTTATCTACACGAC
GGGGAGTCAGGCAACTATGGATGAACGAAATAGACAGATCGCTGAGATAGGTGCCTCACTGATTAAGCATTGGTAACTGCAGACCAAGTT
TACTCATATATACTTTAGATTGATTTAAAACTTCATTTTTAATTTAAAAGGATCTAGGTGAAGATCCTTTTTGATAATCTCATGACCAAA
ATCCCTTAACGTGAGTTTTCGTTCCACTGAGCGTCAGACCCCGTAGAAAAGATCAAAGGATCTTCTTGAGATCCTTTTTTTCTGCGCGTA
ATCTGCTGCTTGCAAACAAAAAAACCACCGCTACCAGCGGTGGTTTGTTTGCCGGATCAAGAGCTACCAACTCTTTTTCCGAAGGTAACT
GGCTTCAGCAGAGCGCAGATACCAAATACTGTCCTTCTAGTGTAGCCGTAGTTAGGCCACCACTTCAAGAACTCTGTAGCACCGCCTACA
TACCTCGCTCTGCTAATCCTGTTACCAGTGGCTGCTGCCAGTGGCGATAAGTCGTGTCTTACCGGGTTGGACTCAAGACGATAGTTACCG
GATAAGGCGCAGCGGTCGGGCTGAACGGGGGGTTCGTGCACACAGCCCAGCTTGGAGCGAACGACCTACACCGAACTGAGATACCTACAG
CGTGAGCTATGAGAAAGCGCCACGCTTCCCGAAGGGAGAAAGGCGGACAGGTATCCGGTAAGCGGCAGGGTCGGAACAGGAGAGCGCACG
AGGGAGCTTCCAGGGGGAAACGCCTGGTATCTTTATAGTCCTGTCGGGTTTCGCCACCTCTGACTTGAGCGTCGATTTTTGTGATGCTCG
TCAGGGGGGCGGAGCCTATGGAAAAACGCCAGCAACGCGGCCTTTTTACGGTTCCTGGCCTTTTGCTGG

RM_Tether 2	GCGGCCGCGATCTCTCACCTACCAAACAATGCCCCCCTGCAAAAAATAAATTCATATAAAAAACATACAGATAACCATCTGCGGTGATAA ATTATCTCTGGCGGTGTTGACATAAATACCACTGGCGGTGATACTGAGCACGGGTACCGGCCGCTGAGAAAAAGCGAAGCGGCACTGCTC TTTAACAATTTATCAGACAATCTGTGTGGGCACTCGAAGATACGGATTCTTAACGTCGCAAGACGAAAAATGAATACCAAGTCTCAAGAG TGAACACGTAATTCATTACGAAGTTTAATTCTTTGAGCGTCAAACTTTTAAATTGAAGAGTTTGATCATGGCTCAGATTGAACGCTGGCG GCAGGCCTAACACATGCAAGTCGAACGGTAACAGGAAGAAGCTTGCTTCTTTGCTGACGAGTGGCGGACGGGTGAGTAATGTCTGGGAAA CTGCCTGATGGAGGGGGATAACTACTGGAAACGGTAGCTAATACCGCATAACGTCGCAAGACCAAAGAGGGGGACCTTCGGGCCTCTTGC CATCGGATGTGCCCAGATGGGATTAGCTAGTAGGTGGGGTAACGGCTCACCTAGGCGACGATCCCTAGCTGGTCTGAGAGGATGACCAGC CACACTGGAACTGAGACACGGTCCAGACTCCTACGGGAGGCAGCAGTGGGGAATATTGCACAATGGGCGCAAGCCTGATGCAGCCATGCC GCGTGTATGAAGAAGGCCTTCGGGTTGTAAAGTACTTTCAGCGGGGAGGAAGGGAGTAAAGTTAATACCTTTGCTCATTGACGTTACCCG CAGAAGAAGCACCGGCTAACTCCGTGCCAGCAGCCGCGGTAATACGGAGGGTGCAAGCGTTAATCGGAATTACTGGGCGTAAAGCGCACG CAGGCGGTTTGTTAAGTCAGATGTGAAATCCCCGGGCTCAACCTGGGAACTGCATCTGATACTGGCAAGCTTGAGTCTCGTAGAGGGGGG TAGAATTCCAGGTGTAGCGGTGAAATGCGTAGAGATCTGGAGGAATACCGGTGGCGAAGGCGGCCCCCTGGACGAAGACTGACGCTCAGG TGCGAAAGCGTGGGGAGCAAACAGGATTAGATACCCTGGTAGTCCACGCCGTAAACGATGTCGACTTGGAGGTTGTGCCCTTGAGGCGTG GCTTCCGGAGCTAACGCGTTAAGTCGACCGCCTGGGGAGTACGGCCGCAAGGTTAAAACTCAAATGAATTGACGGGGGCCCGCACAAGCG GTGGAGCATGTGGTTTAATTCGATGCAACGCGAAGAACCTTACCTGGTCTTGACATCCACGGAAGTTTTCAGAGATGAGAATGTGCCTTC GGGAACCGTGAGACAGGTGCTGCATGGCTGTCGTCAGCTCGTGTTGTGAAATGTTGGGTTAAGTCCCGCAACGAGCGCAACCCTTATCCT TTGTTGCCAGCGGTCCGGCCGGGAACTCAAAGGAGACTGCCAGTGATAAACTGGAGGAAGGTGGGGATGACGTCAAGTCATCATGGCCCT TACGACCAGGGCTACACACGTGCTACAATGGCGCATACAAAGAGAAGCGACCTCGCGAGAGCAAGCGGACCTCATAAAGTGCGTCGTAGT CCGGATTGGAGTCTGCAACTCGACTCCATGAAGTCGGAATCGCTAGTAATCGTGGATCAGAATGCCACGGTGAATACGTTCCCGGGCCTT GTACACACCGCCCGTCACACCATGGGAGTGGGTTGCAAAAGAAGTAGGTAGCTACAGGGCCGUGUGGCUGUGAACGGGAUCCACGGCCGG GGCCGAGGUGGGGGGCCCCGTTGAGCTAACCGGTACTAATGAACCGTGAGGCTTAACCGAGAGGTTAAGCGACTAAGCGTACACGGTGGA TGCCCTGGCAGTCAGAGGCGATGAAGGACGTGCTAATCTGCGATAAGCGTCGGTAAGGTGATATGAACCGTTATAACCGGCGATTTCCGA ATGGGGAAACCCAGTGTGTTTCGACACACTATCATTAACTGAATCCATAGGTTAATGAGGCGAACCGGGGGAACTGAAACATCTAAGTAC CCCGAGGAAAAGAAATCAACCGAGATTCCCCCAGTAGCGGCGAGCGAACGGGGAGCAGCCCAGAGCCTGAATCAGTGTGTGTGTTAGTGG AAGCGTCTGGAAAGGCGCGCGATACAGGGTGACAGCCCCGTACACAAAAATGCACATGCTGTGAGCTCGATGAGTAGGGCGGGACACGTG GTATCCTGTCTGAATATGGGGGGACCATCCTCCAAGGCTAAATACTCCTGACTGACCGATAGTGAACCAGTACCGTGAGGGAAAGGCGAA AAGAACCCCGGCGAGGGGAGTGAAAAAGAACCTGAAACCGTGTACGTACAAGCAGTGGGAGCACGCTTAGGCGTGTGACTGCGTACCTTT TGTATAATGGGTCAGCGACTTATATTCTGTAGCAAGGTTAACCGAATAGGGGAGCCGAAGGGAAACCGAGTCTTAACTGGGCGTTAAGTT GCAGGGTATAGACCCGAAACCCGGTGATCTAGCCATGGGCAGGTTGAAGGTTGGGTAACACTAACTGGAGGACCGAACCGACTAATGTTG AAAAATTAGCGGATGACTTGTGGCTGGGGGTGAAAGGCCAATCAAACCGGGAGATAGCTGGTTCTCCCCGAAAGCTATTTAGGTAGCGCC TCGTGAATTCATCTCCGGGGGTAGAGCACTGTTTCGGCAAGGGGGTCATCCCGACTTACCAACCCGATGCAAACTGCGAATACCGGAGAA TGTTATCACGGGAGACACACGGCGGGTGCTAACGTCCGTCGTGAAGAGGGAAACAACCCAGACCGCCAGCTAAGGTCCCAAAGTCATGGT TAAGTGGGAAACGATGTGGGAAGGCCCAGACAGCCAGGATGTTGGCTTAGAAGCAGCCATCATTTAAAGAAAGCGTAATAGCTCACTGGT CGAGTCGGCCTGCGCGGAAGATGTAACGGGGCTAAACCATGCACCGAAGCTGCGGCAGCGACGCTTATGCGTTGTTGGGTAGGGGAGCGT TCTGTAAGCCTGCGAAGGTGTGCTGTGAGGCATGCTGGAGGTATCAGAAGTGCGAATGCTGACATAAGTAACGATAAAGCGGGTGAAAAG CCCGCTCGCCGGAAGACCAAGGGTTCCTGTCCAACGTTAATCGGGGCAGGGTGAGTCGACCCCTAAGGCGAGGCCGAAAGGCGTAGTCGA TGGGAAACAGGTTAATATTCCTGTACTTGGTGTTACTGCGAAGGGGGGACGGAGAAGGCTATGTTGGCCGGGCGACGGTTGTCCCGGTTT AAGCGTGTAGGCTGGTTTTCCAGGCAAATCCGGAAAATCAAGGCTGAGGCGTGATGACGAGGCACTACGGTGCTGAAGCAACAAATGCCC TGCTTCCAGGAAAAGCCTCTAAGCATCAGGTAACATCAAATCGTACCCCAAACCGACACAGGTGGTCAGGTAGAGAATACCAAGGCGCTT GAGAGAACTCGGGTGAAGGAACTAGGCAAAATGGTGCCGTAACTTCGGGAGAAGGCACGCTGATATGTAGGTGAGGTCCCTCGCGGATGG AGCTGAAATCAGTCGAAGATACCAGCTGGCTGCAACTGTTTATTAAAAACACAGCACTGTGCAAACACGAAAGTGGACGTATACGGTGTG ACGCCTGCCCGGTGCCGGAAGGTTAATTGATGGGGTTAGCGCAAGCGAAGCTCTTGATCGAAGCCCCGGTAAACGGCGGCCGTAACTATA ACGGTCCTAAGGTAGCGAAATTCCTTGTCGGGTAAGTTCCGACCTGCACGAATGGCGTAATGATGGCCAGGCTGTCTCCACCCGAGACTC AGTGAAATTGAACTCGCTGTGAAGATGCAGTGTACCCGCGGCAAGACGGAAAGACCCCGTGAACCTTTACTATAGCTTGACACTGAACAT TGAGCCTTGATGTGTAGGATAGGTGGGAGGCTTTGAAGTGTGGACGCCAGTCTGCATGGAGCCGACCTTGAAATACCACCCTTTAATGTT TGATGTTCTAACGTTGACCCGTAATCCGGGTTGCGGACAGTGTCTGGTGGGTAGTTTGACTGGGGCGGTCTCCTCCTAAAGAGTAACGGA GGAGCACGAAGGTTGGCTAATCCTGGTCGGACATCAGGAGGTTAGTGCAATGGCATAAGCCAGCTTGACTGCGAGCGTGACGGCGCGAGC AGGTGCGAAAGCAGGTCATAGTGATCCGGTGGTTCTGAATGGAAGGGCCATCGCTCAACGGATAAAAGGTACTCCGGGGATAACAGGCTG ATACCGCCCAAGAGTTCATATCGACGGCGGTGTTTGGCACCTCGATGTCGGCTCATCACATCCTGGGGCTGAAGTAGGTCCCAAGGGTAT GGCTGTTCGCCATTTAAAGTGGTACGCGAGCTGGGTTTAGAACGTCGTGAGACAGTTCGGTCCCTATCTGCCGTGGGCGCTGGAGAACTG AGGGGGGCTGCTCCTAGTACGAGAGGACCGGAGTGGACGCATCACTGGTGTTCGGGTTGTCATGCCAATGGCACTGCCCGGTAGCTAAAT GCGGAAGAGATAAGTGCTGAAAGCATCTAAGCACGAAACTTGCCCCGAGATGAGTTCTCCCTGACCCTTTAAGGGTCCTGAAGGAACGTT GAAGACGACGACGTTGATAGGCCGGGTGTGTAAGCGGGGCCCCCCACCGUUUGACGCCCCGAAGCCGUGGAUCCCGGGAGCCACGUGGCU GGCCUGUCGGCGCTTACCACTTTGTGATTCATGACTGGGGTGAAGTCGTAACAAGGTAACCGTAGGGGAACCTGCGGTTGGATCACCTCC TTACCTTAAAGAAGCGTACTTTGTAGTGCTCACACAGATTGTCTGATAGAAAGTGAAAAGCAAGGCGTTTACGCGTTGGGAGTGAGGCTG AAGAGAATAAGGCCGTTCGCTTTCTATTAATGAAAGCTCACCCTACACGAAAATATCACGCAACGCGTGATAAGCAATTTTCGTGTCCCC TTCGTCTAGAGGCCCAGGACACCGCCCTTTCACGGCGGTAACAGGGGTTCGAATCCCCTAGGGGACGCCACTTGCTGGTTTGTGAGTGAA AGTCGCCGACCTTAATATCTCAAAACTCATCTTCGGGTGATGTTTGAGATATTTGCTCTTTAAAAATCTGGATCAAGCTGAAAATTGAAA CACTGAACAACGAGAGTTGTTCGTGAGTCTCTCAAATTTTCGCAACACGATGATGAATCGAAAGAAACATCTTCGGGTTGTGAGCTTAAG CTTACAACGCCGAAGCTGTTTTGGCGGATGAGAGAAGATTTTCAGCCTGATACAGATTAAATCAGAACGCAGAAGCGGTCTGATAAAACA GAATTTGCCTGGCGGCAGTAGCGCGGTGGTCCCACCTGACCCCATGCCGAACTCAGAAGTGAAACGCCGTAGCGCCGATGGTAGTGTGGG GTCTCCCCATGCGAGAGTAGGGAACTGCCAGGCATCAAATAAAACGAAAGGCTCAGTCGAAAGACTGGGCCTTTCGTTTTATCTGTTGTT TGTCGGTGAACGCTCTCCTGAGTAGGACAAATCCGCCGGGAGCGGATTTGAACGTTGCGAAGCAACGGCCCGGAGGGTGGCGGGCAGGAC GCCCGCCATAAACTGCCAGGCATCAAATTAAGCAGAAGGCCATCCTGACGGATGGCCTTTTTGCGTTTCTACAAACTCTTCCTGTCGTCA TATCTACAAGCCGGCGCGCCGGGAAATGTGCGCGGAACCCCTATTTGTTTATTTTTCTAAATACATTCAAATATGTATCCGCTCATGAGA CAATAACCCTGATAAATGCTTCAATAATATTGAAAAAGGAAGAGTATGAGTATTCAACATTTCCGTGTCGCCCTTATTCCCTTTTTTGCG GCATTTTGCCTTCCTGTTTTTGCTCACCCAGAAACGCTGGTGAAAGTAAAAGATGCTGAAGATCAGTTGGGTGCACGAGTGGGTTACATC GAACTGGATCTCAACAGCGGTAAGATCCTTGAGAGTTTTCGCCCCGAAGAACGTTTTCCAATGATGAGCACTTTTAAAGTTCTGCTATGT

GGCGCGGTATTATCCCGTGTTGACGCCGGGCAAGAGCAACTCGGTCGCCGCATACACTATTCTCAGAATGACTTGGTTGAGTACTCACCA
GTCACAGAAAAGCATCTTACGGATGGCATGACAGTAAGAGAATTATGCAGTGCTGCAATAACCATGAGTGATAACACTGCGGCCAACTTA
CTTCTGACAACGATCGGAGGACCGAAGGAGCTAACCGCTTTTTTGCACAACATGGGGGATCATGTAACTCGCCTTGATCGTTGGGAACCG
GAGCTGAATGAAGCCATACCAAACGACGAGCGTGACACCACGATGCCTGCAGCAATGGCAACAACGTTGCGCAAACTATTAACTGGCGAA
CTACTTACTCTAGCTTCCCGGCAACAATTAATAGACTGGATGGAGGCGGATAAAGTTGCAGGACCACTTCTGCGCTCGGCCCTTCCGGCT
AGCTGGTTTATTGCTGATAAATCTGGAGCCGGTGAGCGTGGGTCTCGCGGTATCATTGCAGCACTGGGGCCAGATGGTAAGCCCTCCCGT
ATCGTAGTTATCTACACGACGGGGAGTCAGGCAACTATGGATGAACGAAATAGACAGATCGCTGAGATAGGTGCCTCACTGATTAAGCAT
TGGTAACTGCAGACCAAGTTTACTCATATATACTTTAGATTGATTTAAAACTTCATTTTTAATTTAAAAGGATCTAGGTGAAGATCCTTT
TTGATAATCTCATGACCAAAATCCCTTAACGTGAGTTTTCGTTCCACTGAGCGTCAGACCCCGTAGAAAAGATCAAAGGATCTTCTTGAG
ATCCTTTTTTTTCTGCGCGTAATCTGCTGCTTGCAAACAAAAAAACCACCGCTACCAGCGGTGGTTTGTTTGCCGGATCAAGAGCTACCAA
CTCTTTTTCCGAAGGTAACTGGCTTCAGCAGAGCGCAGATACCAAATACTGTCCTTCTAGTGTAGCCGTAGTTAGGCCACCACTTCAAGA
ACTCTGTAGCACCGCCTACATACCTCGCTCTGCTAATCCTGTTACCAGTGGCTGCTGCCAGTGGCGATAAGTCGTGTCTTACCGGGTTGG
ACTCAAGACGATAGTTACCGGATAAGGCGCAGCGGTCGGGCTGAACGGGGGGTTCGTGCACACAGCCCAGCTTGGAGCGAACGACCTACA
CCGAACTGAGATACCTACAGCGTGAGCTATGAGAAAGCGCCACGCTTCCCGAAGGGAGAAAGGCGGACAGGTATCCGGTAAGCGGCAGGG
TCGGAACAGGAGAGCGCACGAGGGAGCTTCCAGGGGGAAACGCCTGGTATCTTTATAGTCCTGTCGGGTTTCGCCACCTCTGACTTGAGC
GTCGATTTTTGTGATGCTCGTCAGGGGGGCGGAGCCTATGGAAAAACGCCAGCAACGCGGCCTTTTTACGGTTCCTGGCCTTTTGCTGG


RM
_T
eth
er
3

CGGTATTATCCCGTGTTGACGCCGGGCAAGAGCAACTCGGTCGCCGCATACACTATTCTCAGAATGACTTGGTTGAGTACTCACCAGTCA
CAGAAAAGCATCTTACGGATGGCATGACAGTAAGAGAATTATGCAGTGCTGCAATAACCATGAGTGATAACACTGCGGCCAACTTACTTC
TGACAACGATCGGAGGACCGAAGGAGCTAACCGCTTTTTTGCACAACATGGGGGATCATGTAACTCGCCTTGATCGTTGGGAACCGGAGC
TGAATGAAGCCATACCAAACGACGAGCGTGACACCACGATGCCTGCAGCAATGGCAACAACGTTGCGCAAACTATTAACTGGCGAACTAC
TTACTCTAGCTTCCCGGCAACAATTAATAGACTGGATGGAGGCGGATAAAGTTGCAGGACCACTTCTGCGCTCGGCCCTTCCGGCTAGCT
GGTTTATTGCTGATAAATCTGGAGCCGGTGAGCGTGGGTCTCGCGGTATCATTGCAGCACTGGGGCCAGATGGTAAGCCCTCCCGTATCG
TAGTTATCTACACGACGGGGAGTCAGGCAACTATGGATGAACGAAATAGACAGATCGCTGAGATAGGTGCCTCACTGATTAAGCATTGGT
AACTGCAGACCAAGTTTACTCATATATACTTTAGATTGATTTAAAACTTCATTTTTAATTTAAAAGGATCTAGGTGAAGATCCTTTTTGA
TAATCTCATGACCAAAATCCCTTAACGTGAGTTTTCGTTCCACTGAGCGTCAGACCCCGTAGAAAAGATCAAAGGATCTTCTTGAGATCC
TTTTTTTCTGCGCGTAATCTGCTGCTTGCAAACAAAAAAACCACCGCTACCAGCGGTGGTTTGTTTGCCGGATCAAGAGCTACCAACTCT
TTTTCCGAAGGTAACTGGCTTCAGCAGAGCGCAGATACCAAATACTGTCCTTCTAGTGTAGCCGTAGTTAGGCCACCACTTCAAGAACTC
TGTAGCACCGCCTACATACCTCGCTCTGCTAATCCTGTTACCAGTGGCTGCTGCCAGTGGCGATAAGTCGTGTCTTACCGGGTTGGACTC
AAGACGATAGTTACCGGATAAGGCGCAGCGGTCGGGCTGAACGGGGGGTTCGTGCACACAGCCCAGCTTGGAGCGAACGACCTACACCGA
ACTGAGATACCTACAGCGTGAGCTATGAGAAAGCGCCACGCTTCCCGAAGGGAGAAAGGCGGACAGGTATCCGGTAAGCGGCAGGGTCGG
AACAGGAGAGCGCACGAGGGAGCTTCCAGGGGGAAACGCCTGGTATCTTTATAGTCCTGTCGGGTTTCGCCACCTCTGACTTGAGCGTCG
ATTTTTGTGATGCTCGTCAGGGGGGCGGAGCCTATGGAAAAACGCCAGCAACGCGGCCTTTTTACGGTTCCTGGCCTTTTGCTGG

RM_Tether 4	GCGGCCGCGATCTCTCACCTACCAAACAATGCCCCCCTGCAAAAAATAAATTCATATAAAAAACATACAGATAACCATCTGCGGTGATAA ATTATCTCTGGCGGTGTTGACATAAATACCACTGGCGGTGATACTGAGCACGGGTACCGGCCGCTGAGAAAAAGCGAAGCGGCACTGCTC TTTAACAATTTATCAGACAATCTGTGTGGGCACTCGAAGATACGGATTCTTAACGTCGCAAGACGAAAAATGAATACCAAGTCTCAAGAG TGAACACGTAATTCATTACGAAGTTTAATTCTTTGAGCGTCAAACTTTTAAATTGAAGAGTTTGATCATGGCTCAGATTGAACGCTGGCG GCAGGCCTAACACATGCAAGTCGAACGGTAACAGGAAGAAGCTTGCTTCTTTGCTGACGAGTGGCGGACGGGTGAGTAATGTCTGGGAAA CTGCCTGATGGAGGGGGATAACTACTGGAAACGGTAGCTAATACCGCATAACGTCGCAAGACCAAAGAGGGGGACCTTCGGGCCTCTTGC CATCGGATGTGCCCAGATGGGATTAGCTAGTAGGTGGGGTAACGGCTCACCTAGGCGACGATCCCTAGCTGGTCTGAGAGGATGACCAGC CACACTGGAACTGAGACACGGTCCAGACTCCTACGGGAGGCAGCAGTGGGGAATATTGCACAATGGGCGCAAGCCTGATGCAGCCATGCC GCGTGTATGAAGAAGGCCTTCGGGTTGTAAAGTACTTTCAGCGGGGAGGAAGGGAGTAAAGTTAATACCTTTGCTCATTGACGTTACCCG CAGAAGAAGCACCGGCTAACTCCGTGCCAGCAGCCGCGGTAATACGGAGGGTGCAAGCGTTAATCGGAATTACTGGGCGTAAAGCGCACG CAGGCGGTTTGTTAAGTCAGATGTGAAATCCCCGGGCTCAACCTGGGAACTGCATCTGATACTGGCAAGCTTGAGTCTCGTAGAGGGGGG TAGAATTCCAGGTGTAGCGGTGAAATGCGTAGAGATCTGGAGGAATACCGGTGGCGAAGGCGGCCCCCTGGACGAAGACTGACGCTCAGG TGCGAAAGCGTGGGGAGCAAACAGGATTAGATACCCTGGTAGTCCACGCCGTAAACGATGTCGACTTGGAGGTTGTGCCCTTGAGGCGTG GCTTCCGGAGCTAACGCGTTAAGTCGACCGCCTGGGGAGTACGGCCGCAAGGTTAAAACTCAAATGAATTGACGGGGGCCCGCACAAGCG GTGGAGCATGTGGTTTAATTCGATGCAACGCGAAGAACCTTACCTGGTCTTGACATCCACGGAAGTTTTCAGAGATGAGAATGTGCCTTC GGGAACCGTGAGACAGGTGCTGCATGGCTGTCGTCAGCTCGTGTTGTGAAATGTTGGGTTAAGTCCCGCAACGAGCGCAACCCTTATCCT TTGTTGCCAGCGGTCCGGCCGGGAACTCAAAGGAGACTGCCAGTGATAAACTGGAGGAAGGTGGGGATGACGTCAAGTCATCATGGCCCT TACGACCAGGGCTACACACGTGCTACAATGGCGCATACAAAGAGAAGCGACCTCGCGAGAGCAAGCGGACCTCATAAAGTGCGTCGTAGT CCGGATTGGAGTCTGCAACTCGACTCCATGAAGTCGGAATCGCTAGTAATCGTGGATCAGAATGCCACGGTGAATACGTTCCCGGGCCTT GTACACACCGCCCGTCACACCATGGGAGTGGGTTGCAAAAGAAGTAGGTAGCTUAACACCUGUUGUGGCGCGAAACGACCGAUAUUUCCC CCGAUAUGGCGCGAAACCGGGACGCCCGTTGAGCTAACCGGTACTAATGAACCGTGAGGCTTAACCGAGAGGTTAAGCGACTAAGCGTAC ACGGTGGATGCCCTGGCAGTCAGAGGCGATGAAGGACGTGCTAATCTGCGATAAGCGTCGGTAAGGTGATATGAACCGTTATAACCGGCG ATTTCCGAATGGGGAAACCCAGTGTGTTTCGACACACTATCATTAACTGAATCCATAGGTTAATGAGGCGAACCGGGGGAACTGAAACAT CTAAGTACCCCGAGGAAAAGAAATCAACCGAGATTCCCCCAGTAGCGGCGAGCGAACGGGGAGCAGCCCAGAGCCTGAATCAGTGTGTGT GTTAGTGGAAGCGTCTGGAAAGGCGCGCGATACAGGGTGACAGCCCCGTACACAAAAATGCACATGCTGTGAGCTCGATGAGTAGGGCGG GACACGTGGTATCCTGTCTGAATATGGGGGGACCATCCTCCAAGGCTAAATACTCCTGACTGACCGATAGTGAACCAGTACCGTGAGGGA AAGGCGAAAAGAACCCCGGCGAGGGGAGTGAAAAAGAACCTGAAACCGTGTACGTACAAGCAGTGGGAGCACGCTTAGGCGTGTGACTGC GTACCTTTTGTATAATGGGTCAGCGACTTATATTCTGTAGCAAGGTTAACCGAATAGGGGAGCCGAAGGGAAACCGAGTCTTAACTGGGC GTTAAGTTGCAGGGTATAGACCCGAAACCCGGTGATCTAGCCATGGGCAGGTTGAAGGTTGGGTAACACTAACTGGAGGACCGAACCGAC TAATGTTGAAAAATTAGCGGATGACTTGTGGCTGGGGGTGAAAGGCCAATCAAACCGGGAGATAGCTGGTTCTCCCCGAAAGCTATTTAG GTAGCGCCTCGTGAATTCATCTCCGGGGGTAGAGCACTGTTTCGGCAAGGGGGTCATCCCGACTTACCAACCCGATGCAAACTGCGAATA CCGGAGAATGTTATCACGGGAGACACACGGCGGGTGCTAACGTCCGTCGTGAAGAGGGAAACAACCCAGACCGCCAGCTAAGGTCCCAAA GTCATGGTTAAGTGGGAAACGATGTGGGAAGGCCCAGACAGCCAGGATGTTGGCTTAGAAGCAGCCATCATTTAAAGAAAGCGTAATAGC TCACTGGTCGAGTCGGCCTGCGCGGAAGATGTAACGGGGCTAAACCATGCACCGAAGCTGCGGCAGCGACGCTTATGCGTTGTTGGGTAG GGGAGCGTTCTGTAAGCCTGCGAAGGTGTGCTGTGAGGCATGCTGGAGGTATCAGAAGTGCGAATGCTGACATAAGTAACGATAAAGCGG GTGAAAAGCCCGCTCGCCGGAAGACCAAGGGTTCCTGTCCAACGTTAATCGGGGCAGGGTGAGTCGACCCCTAAGGCGAGGCCGAAAGGC GTAGTCGATGGGAAACAGGTTAATATTCCTGTACTTGGTGTTACTGCGAAGGGGGGACGGAGAAGGCTATGTTGGCCGGGCGACGGTTGT CCCGGTTTAAGCGTGTAGGCTGGTTTTCCAGGCAAATCCGGAAAATCAAGGCTGAGGCGTGATGACGAGGCACTACGGTGCTGAAGCAAC AAATGCCCTGCTTCCAGGAAAAGCCTCTAAGCATCAGGTAACATCAAATCGTACCCCAAACCGACACAGGTGGTCAGGTAGAGAATACCA AGGCGCTTGAGAGAACTCGGGTGAAGGAACTAGGCAAAATGGTGCCGTAACTTCGGGAGAAGGCACGCTGATATGTAGGTGAGGTCCCTC GCGGATGGAGCTGAAATCAGTCGAAGATACCAGCTGGCTGCAACTGTTTATTAAAAACACAGCACTGTGCAAACACGAAAGTGGACGTAT ACGGTGTGACGCCTGCCCGGTGCCGGAAGGTTAATTGATGGGGTTAGCGCAAGCGAAGCTCTTGATCGAAGCCCCGGTAAACGGCGGCCG TAACTATAACGGTCCTAAGGTAGCGAAATTCCTTGTCGGGTAAGTTCCGACCTGCACGAATGGCGTAATGATGGCCAGGCTGTCTCCACC CGAGACTCAGTGAAATTGAACTCGCTGTGAAGATGCAGTGTACCCGCGGCAAGACGGAAAGACCCCGTGAACCTTTACTATAGCTTGACA CTGAACATTGAGCCTTGATGTGTAGGATAGGTGGGAGGCTTTGAAGTGTGGACGCCAGTCTGCATGGAGCCGACCTTGAAATACCACCCT TTAATGTTTGATGTTCTAACGTTGACCCGTAATCCGGGTTGCGGACAGTGTCTGGTGGGTAGTTTGACTGGGGCGGTCTCCTCCTAAAGA GTAACGGAGGAGCACGAAGGTTGGCTAATCCTGGTCGGACATCAGGAGGTTAGTGCAATGGCATAAGCCAGCTTGACTGCGAGCGTGACG GCGCGAGCAGGTGCGAAAGCAGGTCATAGTGATCCGGTGGTTCTGAATGGAAGGGCCATCGCTCAACGGATAAAAGGTACTCCGGGGATA ACAGGCTGATACCGCCCAAGAGTTCATATCGACGGCGGTGTTTGGCACCTCGATGTCGGCTCATCACATCCTGGGGCTGAAGTAGGTCCC AAGGGTATGGCTGTTCGCCATTTAAAGTGGTACGCGAGCTGGGTTTAGAACGTCGTGAGACAGTTCGGTCCCTATCTGCCGTGGGCGCTG GAGAACTGAGGGGGGCTGCTCCTAGTACGAGAGGACCGGAGTGGACGCATCACTGGTGTTCGGGTTGTCATGCCAATGGCACTGCCCGGT AGCTAAATGCGGAAGAGATAAGTGCTGAAAGCATCTAAGCACGAAACTTGCCCCGAGATGAGTTCTCCCTGACCCTTTAAGGGTCCTGAA GGAACGTTGAAGACGACGACGTTGATAGGCCGGGTGTGTAAGCGGGCGUCCCGGGAGCCAUAUCGGGCAAUAUCGGUCGGAGCCACAAUU GGUGAAAGCGGCGCTTACCACTTTGTGATTCATGACTGGGGTGAAGTCGTAACAAGGTAACCGTAGGGGAACCTGCGGTTGGATCACCTC CTTACCTTAAAGAAGCGTACTTTGTAGTGCTCACACAGATTGTCTGATAGAAAGTGAAAAGCAAGGCGTTTACGCGTTGGGAGTGAGGCT GAAGAGAATAAGGCCGTTCGCTTTCTATTAATGAAAGCTCACCCTACACGAAAATATCACGCAACGCGTGATAAGCAATTTTCGTGTCCC CTTCGTCTAGAGGCCCAGGACACCGCCCTTTCACGGCGGTAACAGGGGTTCGAATCCCCTAGGGGACGCCACTTGCTGGTTTGTGAGTGA AAGTCGCCGACCTTAATATCTCAAAACTCATCTTCGGGTGATGTTTGAGATATTTGCTCTTTAAAAATCTGGATCAAGCTGAAAATTGAA ACACTGAACAACGAGAGTTGTTCGTGAGTCTCTCAAATTTTCGCAACACGATGATGAATCGAAAGAAACATCTTCGGGTTGTGAGCTTAA GCTTACAACGCCGAAGCTGTTTTGGCGGATGAGAGAAGATTTTCAGCCTGATACAGATTAAATCAGAACGCAGAAGCGGTCTGATAAAAC AGAATTTGCCTGGCGGCAGTAGCGCGGTGGTCCCACCTGACCCCATGCCGAACTCAGAAGTGAAACGCCGTAGCGCCGATGGTAGTGTGG GGTCTCCCCATGCGAGAGTAGGGAACTGCCAGGCATCAAATAAAACGAAAGGCTCAGTCGAAAGACTGGGCCTTTCGTTTTATCTGTTGT TTGTCGGTGAACGCTCTCCTGAGTAGGACAAATCCGCCGGGAGCGGATTTGAACGTTGCGAAGCAACGGCCCGGAGGGTGGCGGGCAGGA CGCCCGCCATAAACTGCCAGGCATCAAATTAAGCAGAAGGCCATCCTGACGGATGGCCTTTTTGCGTTTCTACAAACTCTTCCTGTCGTC ATATCTACAAGCCGGCGCGCCGGGAAATGTGCGCGGAACCCCTATTTGTTTATTTTTCTAAATACATTCAAATATGTATCCGCTCATGAG ACAATAACCCTGATAAATGCTTCAATAATATTGAAAAAGGAAGAGTATGAGTATTCAACATTTCCGTGTCGCCCTTATTCCCTTTTTTGC GGCATTTTGCCTTCCTGTTTTTGCTCACCCAGAAACGCTGGTGAAAGTAAAAGATGCTGAAGATCAGTTGGGTGCACGAGTGGGTTACAT CGAACTGGATCTCAACAGCGGTAAGATCCTTGAGAGTTTTCGCCCCGAAGAACGTTTTCCAATGATGAGCACTTTTAAAGTTCTGCTATG

TGGCGCGGTATTATCCCGTGTTGACGCCGGGCAAGAGCAACTCGGTCGCCGCATACACTATTCTCAGAATGACTTGGTTGAGTACTCACC
AGTCACAGAAAAGCATCTTACGGATGGCATGACAGTAAGAGAATTATGCAGTGCTGCAATAACCATGAGTGATAACACTGCGGCCAACTT
ACTTCTGACAACGATCGGAGGACCGAAGGAGCTAACCGCTTTTTTGCACAACATGGGGGATCATGTAACTCGCCTTGATCGTTGGGAACC
GGAGCTGAATGAAGCCATACCAAACGACGAGCGTGACACCACGATGCCTGCAGCAATGGCAACAACGTTGCGCAAACTATTAACTGGCGA
ACTACTTACTCTAGCTTCCCGGCAACAATTAATAGACTGGATGGAGGCGGATAAAGTTGCAGGACCACTTCTGCGCTCGGCCCTTCCGGC
TAGCTGGTTTATTGCTGATAAATCTGGAGCCGGTGAGCGTGGGTCTCGCGGTATCATTGCAGCACTGGGGCCAGATGGTAAGCCCTCCCG
TATCGTAGTTATCTACACGACGGGGAGTCAGGCAACTATGGATGAACGAAATAGACAGATCGCTGAGATAGGTGCCTCACTGATTAAGCA
TTGGTAACTGCAGACCAAGTTTACTCATATATACTTTAGATTGATTTAAAACTTCATTTTTAATTTAAAAGGATCTAGGTGAAGATCCTT
TTTGATAATCTCATGACCAAAATCCCTTAACGTGAGTTTTCGTTCCACTGAGCGTCAGACCCCGTAGAAAAGATCAAAGGATCTTCTTGA
GATCCTTTTTTTCTGCGCGTAATCTGCTGCTTGCAAACAAAAAAACCACCGCTACCAGCGGTGGTTTGTTTGCCGGATCAAGAGCTACCA
ACTCTTTTTCCGAAGGTAACTGGCTTCAGCAGAGCGCAGATACCAAATACTGTCCTTCTAGTGTAGCCGTAGTTAGGCCACCACTTCAAG
AACTCTGTAGCACCGCCTACATACCTCGCTCTGCTAATCCTGTTACCAGTGGCTGCTGCCAGTGGCGATAAGTCGTGTCTTACCGGGTTG
GACTCAAGACGATAGTTACCGGATAAGGCGCAGCGGTCGGGCTGAACGGGGGGTTCGTGCACACAGCCCAGCTTGGAGCGAACGACCTAC
ACCGAACTGAGATACCTACAGCGTGAGCTATGAGAAAGCGCCACGCTTCCCGAAGGGAGAAAGGCGGACAGGTATCCGGTAAGCGGCAGG
GTCGGAACAGGAGAGCGCACGAGGGAGCTTCCAGGGGGAAACGCCTGGTATCTTTATAGTCCTGTCGGGTTTCGCCACCTCTGACTTGAG
CGTCGATTTTTGTGATGCTCGTCAGGGGGGCGGAGCCTATGGAAAAACGCCAGCAACGCGGCCTTTTTACGGTTCCTGGCCTTTTGCTGG

RM_Tether 5	GCGGCCGCGATCTCTCACCTACCAAACAATGCCCCCCTGCAAAAAATAAATTCATATAAAAAACATACAGATAACCATCTGCGGTGATAA ATTATCTCTGGCGGTGTTGACATAAATACCACTGGCGGTGATACTGAGCACGGGTACCGGCCGCTGAGAAAAAGCGAAGCGGCACTGCTC TTTAACAATTTATCAGACAATCTGTGTGGGCACTCGAAGATACGGATTCTTAACGTCGCAAGACGAAAAATGAATACCAAGTCTCAAGAG TGAACACGTAATTCATTACGAAGTTTAATTCTTTGAGCGTCAAACTTTTAAATTGAAGAGTTTGATCATGGCTCAGATTGAACGCTGGCG GCAGGCCTAACACATGCAAGTCGAACGGTAACAGGAAGAAGCTTGCTTCTTTGCTGACGAGTGGCGGACGGGTGAGTAATGTCTGGGAAA CTGCCTGATGGAGGGGGATAACTACTGGAAACGGTAGCTAATACCGCATAACGTCGCAAGACCAAAGAGGGGGACCTTCGGGCCTCTTGC CATCGGATGTGCCCAGATGGGATTAGCTAGTAGGTGGGGTAACGGCTCACCTAGGCGACGATCCCTAGCTGGTCTGAGAGGATGACCAGC CACACTGGAACTGAGACACGGTCCAGACTCCTACGGGAGGCAGCAGTGGGGAATATTGCACAATGGGCGCAAGCCTGATGCAGCCATGCC GCGTGTATGAAGAAGGCCTTCGGGTTGTAAAGTACTTTCAGCGGGGAGGAAGGGAGTAAAGTTAATACCTTTGCTCATTGACGTTACCCG CAGAAGAAGCACCGGCTAACTCCGTGCCAGCAGCCGCGGTAATACGGAGGGTGCAAGCGTTAATCGGAATTACTGGGCGTAAAGCGCACG CAGGCGGTTTGTTAAGTCAGATGTGAAATCCCCGGGCTCAACCTGGGAACTGCATCTGATACTGGCAAGCTTGAGTCTCGTAGAGGGGGG TAGAATTCCAGGTGTAGCGGTGAAATGCGTAGAGATCTGGAGGAATACCGGTGGCGAAGGCGGCCCCCTGGACGAAGACTGACGCTCAGG TGCGAAAGCGTGGGGAGCAAACAGGATTAGATACCCTGGTAGTCCACGCCGTAAACGATGTCGACTTGGAGGTTGTGCCCTTGAGGCGTG GCTTCCGGAGCTAACGCGTTAAGTCGACCGCCTGGGGAGTACGGCCGCAAGGTTAAAACTCAAATGAATTGACGGGGGCCCGCACAAGCG GTGGAGCATGTGGTTTAATTCGATGCAACGCGAAGAACCTTACCTGGTCTTGACATCCACGGAAGTTTTCAGAGATGAGAATGTGCCTTC GGGAACCGTGAGACAGGTGCTGCATGGCTGTCGTCAGCTCGTGTTGTGAAATGTTGGGTTAAGTCCCGCAACGAGCGCAACCCTTATCCT TTGTTGCCAGCGGTCCGGCCGGGAACTCAAAGGAGACTGCCAGTGATAAACTGGAGGAAGGTGGGGATGACGTCAAGTCATCATGGCCCT TACGACCAGGGCTACACACGTGCTACAATGGCGCATACAAAGAGAAGCGACCTCGCGAGAGCAAGCGGACCTCATAAAGTGCGTCGTAGT CCGGATTGGAGTCTGCAACTCGACTCCATGAAGTCGGAATCGCTAGTAATCGTGGATCAGAATGCCACGGTGAATACGTTCCCGGGCCTT GTACACACCGCCCGTCACACCATGGGAGTGGGTTGCAAAAGAAGTAGGTAGCTCUGUAGGCGAACUACUAACUCGUACGUAUGGGAUUAU AUUCGAUAUAUGGACCUAUGGACCCCCGTTGAGCTAACCGGTACTAATGAACCGTGAGGCTTAACCGAGAGGTTAAGCGACTAAGCGTAC ACGGTGGATGCCCTGGCAGTCAGAGGCGATGAAGGACGTGCTAATCTGCGATAAGCGTCGGTAAGGTGATATGAACCGTTATAACCGGCG ATTTCCGAATGGGGAAACCCAGTGTGTTTCGACACACTATCATTAACTGAATCCATAGGTTAATGAGGCGAACCGGGGGAACTGAAACAT CTAAGTACCCCGAGGAAAAGAAATCAACCGAGATTCCCCCAGTAGCGGCGAGCGAACGGGGAGCAGCCCAGAGCCTGAATCAGTGTGTGT GTTAGTGGAAGCGTCTGGAAAGGCGCGCGATACAGGGTGACAGCCCCGTACACAAAAATGCACATGCTGTGAGCTCGATGAGTAGGGCGG GACACGTGGTATCCTGTCTGAATATGGGGGGACCATCCTCCAAGGCTAAATACTCCTGACTGACCGATAGTGAACCAGTACCGTGAGGGA AAGGCGAAAAGAACCCCGGCGAGGGGAGTGAAAAAGAACCTGAAACCGTGTACGTACAAGCAGTGGGAGCACGCTTAGGCGTGTGACTGC GTACCTTTTGTATAATGGGTCAGCGACTTATATTCTGTAGCAAGGTTAACCGAATAGGGGAGCCGAAGGGAAACCGAGTCTTAACTGGGC GTTAAGTTGCAGGGTATAGACCCGAAACCCGGTGATCTAGCCATGGGCAGGTTGAAGGTTGGGTAACACTAACTGGAGGACCGAACCGAC TAATGTTGAAAAATTAGCGGATGACTTGTGGCTGGGGGTGAAAGGCCAATCAAACCGGGAGATAGCTGGTTCTCCCCGAAAGCTATTTAG GTAGCGCCTCGTGAATTCATCTCCGGGGGTAGAGCACTGTTTCGGCAAGGGGGTCATCCCGACTTACCAACCCGATGCAAACTGCGAATA CCGGAGAATGTTATCACGGGAGACACACGGCGGGTGCTAACGTCCGTCGTGAAGAGGGAAACAACCCAGACCGCCAGCTAAGGTCCCAAA GTCATGGTTAAGTGGGAAACGATGTGGGAAGGCCCAGACAGCCAGGATGTTGGCTTAGAAGCAGCCATCATTTAAAGAAAGCGTAATAGC TCACTGGTCGAGTCGGCCTGCGCGGAAGATGTAACGGGGCTAAACCATGCACCGAAGCTGCGGCAGCGACGCTTATGCGTTGTTGGGTAG GGGAGCGTTCTGTAAGCCTGCGAAGGTGTGCTGTGAGGCATGCTGGAGGTATCAGAAGTGCGAATGCTGACATAAGTAACGATAAAGCGG GTGAAAAGCCCGCTCGCCGGAAGACCAAGGGTTCCTGTCCAACGTTAATCGGGGCAGGGTGAGTCGACCCCTAAGGCGAGGCCGAAAGGC GTAGTCGATGGGAAACAGGTTAATATTCCTGTACTTGGTGTTACTGCGAAGGGGGGACGGAGAAGGCTATGTTGGCCGGGCGACGGTTGT CCCGGTTTAAGCGTGTAGGCTGGTTTTCCAGGCAAATCCGGAAAATCAAGGCTGAGGCGTGATGACGAGGCACTACGGTGCTGAAGCAAC AAATGCCCTGCTTCCAGGAAAAGCCTCTAAGCATCAGGTAACATCAAATCGTACCCCAAACCGACACAGGTGGTCAGGTAGAGAATACCA AGGCGCTTGAGAGAACTCGGGTGAAGGAACTAGGCAAAATGGTGCCGTAACTTCGGGAGAAGGCACGCTGATATGTAGGTGAGGTCCCTC GCGGATGGAGCTGAAATCAGTCGAAGATACCAGCTGGCTGCAACTGTTTATTAAAAACACAGCACTGTGCAAACACGAAAGTGGACGTAT ACGGTGTGACGCCTGCCCGGTGCCGGAAGGTTAATTGATGGGGTTAGCGCAAGCGAAGCTCTTGATCGAAGCCCCGGTAAACGGCGGCCG TAACTATAACGGTCCTAAGGTAGCGAAATTCCTTGTCGGGTAAGTTCCGACCTGCACGAATGGCGTAATGATGGCCAGGCTGTCTCCACC CGAGACTCAGTGAAATTGAACTCGCTGTGAAGATGCAGTGTACCCGCGGCAAGACGGAAAGACCCCGTGAACCTTTACTATAGCTTGACA CTGAACATTGAGCCTTGATGTGTAGGATAGGTGGGAGGCTTTGAAGTGTGGACGCCAGTCTGCATGGAGCCGACCTTGAAATACCACCCT TTAATGTTTGATGTTCTAACGTTGACCCGTAATCCGGGTTGCGGACAGTGTCTGGTGGGTAGTTTGACTGGGGCGGTCTCCTCCTAAAGA GTAACGGAGGAGCACGAAGGTTGGCTAATCCTGGTCGGACATCAGGAGGTTAGTGCAATGGCATAAGCCAGCTTGACTGCGAGCGTGACG GCGCGAGCAGGTGCGAAAGCAGGTCATAGTGATCCGGTGGTTCTGAATGGAAGGGCCATCGCTCAACGGATAAAAGGTACTCCGGGGATA ACAGGCTGATACCGCCCAAGAGTTCATATCGACGGCGGTGTTTGGCACCTCGATGTCGGCTCATCACATCCTGGGGCTGAAGTAGGTCCC AAGGGTATGGCTGTTCGCCATTTAAAGTGGTACGCGAGCTGGGTTTAGAACGTCGTGAGACAGTTCGGTCCCTATCTGCCGTGGGCGCTG GAGAACTGAGGGGGGCTGCTCCTAGTACGAGAGGACCGGAGTGGACGCATCACTGGTGTTCGGGTTGTCATGCCAATGGCACTGCCCGGT AGCTAAATGCGGAAGAGATAAGTGCTGAAAGCATCTAAGCACGAAACTTGCCCCGAGATGAGTTCTCCCTGACCCTTTAAGGGTCCTGAA GGAACGTTGAAGACGACGACGTTGATAGGCCGGGTGTGTAAGCGGGGGUCCAUAGGAUGGAAGUAUAUCGAAUAUAAUCCCAUACGCAAA UUAGCGCCUAUUGCGGCGCTTACCACTTTGTGATTCATGACTGGGGTGAAGTCGTAACAAGGTAACCGTAGGGGAACCTGCGGTTGGATC ACCTCCTTACCTTAAAGAAGCGTACTTTGTAGTGCTCACACAGATTGTCTGATAGAAAGTGAAAAGCAAGGCGTTTACGCGTTGGGAGTG AGGCTGAAGAGAATAAGGCCGTTCGCTTTCTATTAATGAAAGCTCACCCTACACGAAAATATCACGCAACGCGTGATAAGCAATTTTCGT GTCCCCTTCGTCTAGAGGCCCAGGACACCGCCCTTTCACGGCGGTAACAGGGGTTCGAATCCCCTAGGGGACGCCACTTGCTGGTTTGTG AGTGAAAGTCGCCGACCTTAATATCTCAAAACTCATCTTCGGGTGATGTTTGAGATATTTGCTCTTTAAAAATCTGGATCAAGCTGAAAA TTGAAACACTGAACAACGAGAGTTGTTCGTGAGTCTCTCAAATTTTCGCAACACGATGATGAATCGAAAGAAACATCTTCGGGTTGTGAG CTTAAGCTTACAACGCCGAAGCTGTTTTGGCGGATGAGAGAAGATTTTCAGCCTGATACAGATTAAATCAGAACGCAGAAGCGGTCTGAT AAAACAGAATTTGCCTGGCGGCAGTAGCGCGGTGGTCCCACCTGACCCCATGCCGAACTCAGAAGTGAAACGCCGTAGCGCCGATGGTAG TGTGGGGTCTCCCCATGCGAGAGTAGGGAACTGCCAGGCATCAAATAAAACGAAAGGCTCAGTCGAAAGACTGGGCCTTTCGTTTTATCT GTTGTTTGTCGGTGAACGCTCTCCTGAGTAGGACAAATCCGCCGGGAGCGGATTTGAACGTTGCGAAGCAACGGCCCGGAGGGTGGCGGG CAGGACGCCCGCCATAAACTGCCAGGCATCAAATTAAGCAGAAGGCCATCCTGACGGATGGCCTTTTTGCGTTTCTACAAACTCTTCCTG TCGTCATATCTACAAGCCGGCGCGCCGGGAAATGTGCGCGGAACCCCTATTTGTTTATTTTTCTAAATACATTCAAATATGTATCCGCTC ATGAGACAATAACCCTGATAAATGCTTCAATAATATTGAAAAAGGAAGAGTATGAGTATTCAACATTTCCGTGTCGCCCTTATTCCCTTT TTTGCGGCATTTTGCCTTCCTGTTTTTGCTCACCCAGAAACGCTGGTGAAAGTAAAAGATGCTGAAGATCAGTTGGGTGCACGAGTGGGT TACATCGAACTGGATCTCAACAGCGGTAAGATCCTTGAGAGTTTTCGCCCCGAAGAACGTTTTCCAATGATGAGCACTTTTAAAGTTCTG

CTATGTGGCGCGGTATTATCCCGTGTTGACGCCGGGCAAGAGCAACTCGGTCGCCGCATACACTATTCTCAGAATGACTTGGTTGAGTAC
TCACCAGTCACAGAAAAGCATCTTACGGATGGCATGACAGTAAGAGAATTATGCAGTGCTGCAATAACCATGAGTGATAACACTGCGGCC
AACTTACTTCTGACAACGATCGGAGGACCGAAGGAGCTAACCGCTTTTTTGCACAACATGGGGGATCATGTAACTCGCCTTGATCGTTGG
GAACCGGAGCTGAATGAAGCCATACCAAACGACGAGCGTGACACCACGATGCCTGCAGCAATGGCAACAACGTTGCGCAAACTATTAACT
GGCGAACTACTTACTCTAGCTTCCCGGCAACAATTAATAGACTGGATGGAGGCGGATAAAGTTGCAGGACCACTTCTGCGCTCGGCCCTT
CCGGCTAGCTGGTTTATTGCTGATAAATCTGGAGCCGGTGAGCGTGGGTCTCGCGGTATCATTGCAGCACTGGGGCCAGATGGTAAGCCC
TCCCGTATCGTAGTTATCTACACGACGGGGAGTCAGGCAACTATGGATGAACGAAATAGACAGATCGCTGAGATAGGTGCCTCACTGATT
AAGCATTGGTAACTGCAGACCAAGTTTACTCATATATACTTTAGATTGATTTAAAACTTCATTTTTAATTTAAAAGGATCTAGGTGAAGA
TCCTTTTTGATAATCTCATGACCAAAATCCCTTAACGTGAGTTTTCGTTCCACTGAGCGTCAGACCCCGTAGAAAAGATCAAAGGATCTT
CTTGAGATCCTTTTTTTCTGCGCGTAATCTGCTGCTTGCAAACAAAAAAACCACCGCTACCAGCGGTGGTTTGTTTGCCGGATCAAGAGC
TACCAACTCTTTTTCCGAAGGTAACTGGCTTCAGCAGAGCGCAGATACCAAATACTGTCCTTCTAGTGTAGCCGTAGTTAGGCCACCACT
TCAAGAACTCTGTAGCACCGCCTACATACCTCGCTCTGCTAATCCTGTTACCAGTGGCTGCTGCCAGTGGCGATAAGTCGTGTCTTACCG
GGTTGGACTCAAGACGATAGTTACCGGATAAGGCGCAGCGGTCGGGCTGAACGGGGGGTTCGTGCACACAGCCCAGCTTGGAGCGAACGA
CCTACACCGAACTGAGATACCTACAGCGTGAGCTATGAGAAAGCGCCACGCTTCCCGAAGGGAGAAAGGCGGACAGGTATCCGGTAAGCG
GCAGGGTCGGAACAGGAGAGCGCACGAGGGAGCTTCCAGGGGGAAACGCCTGGTATCTTTATAGTCCTGTCGGGTTTCGCCACCTCTGAC
TTGAGCGTCGATTTTTGTGATGCTCGTCAGGGGGGCGGAGCCTATGGAAAAACGCCAGCAACGCGGCCTTTTTACGGTTCCTGGCCTTTT
GCTGG

RM_Tether 6

GCGGCCGCGATCTCTCACCTACCAAACAATGCCCCCCTGCAAAAAATAAATTCATATAAAAAACATACAGATAACCATCTGCGGTGATAA
ATTATCTCTGGCGGTGTTGACATAAATACCACTGGCGGTGATACTGAGCACGGGTACCGGCCGCTGAGAAAAAGCGAAGCGGCACTGCTC
TTTAACAATTTATCAGACAATCTGTGTGGGCACTCGAAGATACGGATTCTTAACGTCGCAAGACGAAAAATGAATACCAAGTCTCAAGAG
TGAACACGTAATTCATTACGAAGTTTAATTCTTTGAGCGTCAAACTTTTAAATTGAAGAGTTTGATCATGGCTCAGATTGAACGCTGGCG
GCAGGCCTAACACATGCAAGTCGAACGGTAACAGGAAGAAGCTTGCTTCTTTGCTGACGAGTGGCGGACGGGTGAGTAATGTCTGGGAAA
CTGCCTGATGGAGGGGGATAACTACTGGAAACGGTAGCTAATACCGCATAACGTCGCAAGACCAAAGAGGGGGACCTTCGGGCCTCTTGC
CATCGGATGTGCCCAGATGGGATTAGCTAGTAGGTGGGGTAACGGCTCACCTAGGCGACGATCCCTAGCTGGTCTGAGAGGATGACCAGC
CACACTGGAACTGAGACACGGTCCAGACTCCTACGGGAGGCAGCAGTGGGGAATATTGCACAATGGGCGCAAGCCTGATGCAGCCATGCC
GCGTGTATGAAGAAGGCCTTCGGGTTGTAAAGTACTTTCAGCGGGGAGGAAGGGAGTAAAGTTAATACCTTTGCTCATTGACGTTACCCG
CAGAAGAAGCACCGGCTAACTCCGTGCCAGCAGCCGCGGTAATACGGAGGGTGCAAGCGTTAATCGGAATTACTGGGCGTAAAGCGCACG
CAGGCGGTTTGTTAAGTCAGATGTGAAATCCCCGGGCTCAACCTGGGAACTGCATCTGATACTGGCAAGCTTGAGTCTCGTAGAGGGGGG
TAGAATTCCAGGTGTAGCGGTGAAATGCGTAGAGATCTGGAGGAATACCGGTGGCGAAGGCGGCCCCCTGGACGAAGACTGACGCTCAGG
TGCGAAAGCGTGGGGAGCAAACAGGATTAGATACCCTGGTAGTCCACGCCGTAAACGATGTCGACTTGGAGGTTGTGCCCTTGAGGCGTG
GCTTCCGGAGCTAACGCGTTAAGTCGACCGCCTGGGGAGTACGGCCGCAAGGTTAAAACTCAAATGAATTGACGGGGGCCCGCACAAGCG
GTGGAGCATGTGGTTTAATTCGATGCAACGCGAAGAACCTTACCTGGTCTTGACATCCACGGAAGTTTTCAGAGATGAGAATGTGCCTTC
GGGAACCGTGAGACAGGTGCTGCATGGCTGTCGTCAGCTCGTGTTGTGAAATGTTGGGTTAAGTCCCGCAACGAGCGCAACCCTTATCCT
TTGTTGCCAGCGGTCCGGCCGGGAACTCAAAGGAGACTGCCAGTGATAAACTGGAGGAAGGTGGGGATGACGTCAAGTCATCATGGCCCT
TACGACCAGGGCTACACACGTGCTACAATGGCGCATACAAAGAGAAGCGACCTCGCGAGAGCAAGCGGACCTCATAAAGTGCGTCGTAGT
CCGGATTGGAGTCTGCAACTCGACTCCATGAAGTCGGAATCGCTAGTAATCGTGGATCAGAATGCCACGGTGAATACGTTCCCGGGCCTT
GTACACACCGCCCGTCACACCATGGGAGTGGGTTGCAAAAGAAGTAGGTAGCTCUGUAGGCGAACUACUAACUCGUACGUAUGGGAUUAU
AUUCGAUAUAUGGACCUAUGGACCCCCGTTGAGCTAACCGGTACTAATGAACCGTGAGGCTTAACCGAGAGGTTAAGCGACTAAGCGTAC
ACGGTGGATGCCCTGGCAGTCAGAGGCGATGAAGGACGTGCTAATCTGCGATAAGCGTCGGTAAGGTGATATGAACCGTTATAACCGGCG
ATTTCCGAATGGGGAAACCCAGTGTGTTTCGACACACTATCATTAACTGAATCCATAGGTTAATGAGGCGAACCGGGGGAACTGAAACAT
CTAAGTACCCCGAGGAAAAGAAATCAACCGAGATTCCCCCAGTAGCGGCGAGCGAACGGGGAGCAGCCCAGAGCCTGAATCAGTGTGTGT
GTTAGTGGAAGCGTCTGGAAAGGCGCGCGATACAGGGTGACAGCCCCGTACACAAAAATGCACATGCTGTGAGCTCGATGAGTAGGGCGG
GACACGTGGTATCCTGTCTGAATATGGGGGGACCATCCTCCAAGGCTAAATACTCCTGACTGACCGATAGTGAACCAGTACCGTGAGGGA
AAGGCGAAAAGAACCCCGGCGAGGGGAGTGAAAAAGAACCTGAAACCGTGTACGTACAAGCAGTGGGAGCACGCTTAGGCGTGTGACTGC
GTACCTTTTGTATAATGGGTCAGCGACTTATATTCTGTAGCAAGGTTAACCGAATAGGGGAGCCGAAGGGAAACCGAGTCTTAACTGGGC
GTTAAGTTGCAGGGTATAGACCCGAAACCCGGTGATCTAGCCATGGGCAGGTTGAAGGTTGGGTAACACTAACTGGAGGACCGAACCGAC
TAATGTTGAAAAATTAGCGGATGACTTGTGGCTGGGGGTGAAAGGCCAATCAAACCGGGAGATAGCTGGTTCTCCCCGAAAGCTATTTAG
GTAGCGCCTCGTGAATTCATCTCCGGGGGTAGAGCACTGTTTCGGCAAGGGGGTCATCCCGACTTACCAACCCGATGCAAACTGCGAATA
CCGGAGAATGTTATCACGGGAGACACACGGCGGGTGCTAACGTCCGTCGTGAAGAGGGAAACAACCCAGACCGCCAGCTAAGGTCCCAAA
GTCATGGTTAAGTGGGAAACGATGTGGGAAGGCCCAGACAGCCAGGATGTTGGCTTAGAAGCAGCCATCATTTAAAGAAAGCGTAATAGC
TCACTGGTCGAGTCGGCCTGCGCGGAAGATGTAACGGGGCTAAACCATGCACCGAAGCTGCGGCAGCGACGCTTATGCGTTGTTGGGTAG
GGGAGCGTTCTGTAAGCCTGCGAAGGTGTGCTGTGAGGCATGCTGGAGGTATCAGAAGTGCGAATGCTGACATAAGTAACGATAAAGCGG
GTGAAAAGCCCGCTCGCCGGAAGACCAAGGGTTCCTGTCCAACGTTAATCGGGGCAGGGTGAGTCGACCCCTAAGGCGAGGCCGAAAGGC
GTAGTCGATGGGAAACAGGTTAATATTCCTGTACTTGGTGTTACTGCGAAGGGGGGACGGAGAAGGCTATGTTGGCCGGGCGACGGTTGT
CCCGGTTTAAGCGTGTAGGCTGGTTTTCCAGGCAAATCCGGAAAATCAAGGCTGAGGCGTGATGACGAGGCACTACGGTGCTGAAGCAAC
AAATGCCCTGCTTCCAGGAAAAGCCTCTAAGCATCAGGTAACATCAAATCGTACCCCAAACCGACACAGGTGGTCAGGTAGAGAATACCA
AGGCGCTTGAGAGAACTCGGGTGAAGGAACTAGGCAAAATGGTGCCGTAACTTCGGGAGAAGGCACGCTGATATGTAGGTGAGGTCCCTC
GCGGATGGAGCTGAAATCAGTCGAAGATACCAGCTGGCTGCAACTGTTTATTAAAAACACAGCACTGTGCAAACACGAAAGTGGACGTAT
ACGGTGTGACGCCTGCCCGGTGCCGGAAGGTTAATTGATGGGGTTAGCGCAAGCGAAGCTCTTGATCGAAGCCCCGGTAAACGGCGGCCG
TAACTATAACGGTCCTAAGGTAGCGAAATTCCTTGTCGGGTAAGTTCCGACCTGCACGAATGGCGTAATGATGGCCAGGCTGTCTCCACC
CGAGACTCAGTGAAATTGAACTCGCTGTGAAGATGCAGTGTACCCGCGGCAAGACGGAAAGACCCCGTGAACCTTTACTATAGCTTGACA
CTGAACATTGAGCCTTGATGTGTAGGATAGGTGGGAGGCTTTGAAGTGTGGACGCCAGTCTGCATGGAGCCGACCTTGAAATACCACCCT
TTAATGTTTGATGTTCTAACGTTGACCCGTAATCCGGGTTGCGGACAGTGTCTGGTGGGTAGTTTGACTGGGGCGGTCTCCTCCTAAAGA
GTAACGGAGGAGCACGAAGGTTGGCTAATCCTGGTCGGACATCAGGAGGTTAGTGCAATGGCATAAGCCAGCTTGACTGCGAGCGTGACG
GCGCGAGCAGGTGCGAAAGCAGGTCATAGTGATCCGGTGGTTCTGAATGGAAGGGCCATCGCTCAACGGATAAAAGGTACTCCGGGGATA
ACAGGCTGATACCGCCCAAGAGTTCATATCGACGGCGGTGTTTGGCACCTCGATGTCGGCTCATCACATCCTGGGGCTGAAGTAGGTCCC
AAGGGTATGGCTGTTCGCCATTTAAAGTGGTACGCGAGCTGGGTTTAGAACGTCGTGAGACAGTTCGGTCCCTATCTGCCGTGGGCGCTG
GAGAACTGAGGGGGGCTGCTCCTAGTACGAGAGGACCGGAGTGGACGCATCACTGGTGTTCGGGTTGTCATGCCAATGGCACTGCCCGGT
AGCTAAATGCGGAAGAGATAAGTGCTGAAAGCATCTAAGCACGAAACTTGCCCCGAGATGAGTTCTCCCTGACCCTTTAAGGGTCCTGAA
GGAACGTTGAAGACGACGACGTTGATAGGCCGGGTGTGTAAGCGGGGGUCCAUAGGAUGGAAGUAUAUCGAAUAUAAUCCCAUACGCAAA
UUAGCGCCUAUUGCGGCGCTTACCACTTTGTGATTCATGACTGGGGTGAAGTCGTAACAAGGTAACCGTAGGGGAACCTGCGGTTGGATC
ACCTCCTTACCTTAAAGAAGCGTACTTTGTAGTGCTCACACAGATTGTCTGATAGAAAGTGAAAAGCAAGGCGTTTACGCGTTGGGAGTG
AGGCTGAAGAGAATAAGGCCGTTCGCTTTCTATTAATGAAAGCTCACCCTACACGAAAATATCACGCAACGCGTGATAAGCAATTTTCGT
GTCCCCTTCGTCTAGAGGCCCAGGACACCGCCCTTTCACGGCGGTAACAGGGGTTCGAATCCCCTAGGGGACGCCACTTGCTGGTTTGTG
AGTGAAAGTCGCCGACCTTAATATCTCAAAACTCATCTTCGGGTGATGTTTGAGATATTTGCTCTTTAAAAATCTGGATCAAGCTGAAAA
TTGAAACACTGAACAACGAGAGTTGTTCGTGAGTCTCTCAAATTTTCGCAACACGATGATGAATCGAAAGAAACATCTTCGGGTTGTGAG
CTTAAGCTTACAACGCCGAAGCTGTTTTGGCGGATGAGAGAAGATTTTCAGCCTGATACAGATTAAATCAGAACGCAGAAGCGGTCTGAT
AAAACAGAATTTGCCTGGCGGCAGTAGCGCGGTGGTCCCACCTGACCCCATGCCGAACTCAGAAGTGAAACGCCGTAGCGCCGATGGTAG
TGTGGGGTCTCCCCATGCGAGAGTAGGGAACTGCCAGGCATCAAATAAAACGAAAGGCTCAGTCGAAAGACTGGGCCTTTCGTTTTATCT
GTTGTTTGTCGGTGAACGCTCTCCTGAGTAGGACAAATCCGCCGGGAGCGGATTTGAACGTTGCGAAGCAACGGCCCGGAGGGTGGCGGG
CAGGACGCCCGCCATAAACTGCCAGGCATCAAATTAAGCAGAAGGCCATCCTGACGGATGGCCTTTTGCGTTTCTACAAACTCTTCCTG
TCGTCATATCTACAAGCCGGCGCGCCGGGAAATGTGCGCGGAACCCCTATTTGTTTATTTTTCTAAATACATTCAAATATGTATCCGCTC
ATGAGACAATAACCCTGATAAATGCTTCAATAATATTGAAAAAGGAAGAGTATGAGTATTCAACATTTCCGTGTCGCCCTTATTCCCTTT
TTTGCGGCATTTTGCCTTCCTGTTTTTGCTCACCCAGAAACGCTGGTGAAAGTAAAAGATGCTGAAGATCAGTTGGGTGCACGAGTGGGT
TACATCGAACTGGATCTCAACAGCGGTAAGATCCTTGAGAGTTTTCGCCCCGAAGAACGTTTTCCAATGATGAGCACTTTTAAAGTTCTG

CTATGTGGCGCGGTATTATCCCGTGTTGACGCCGGGCAAGAGCAACTCGGTCGCCGCATACACTATTCTCAGAATGACTTGGTTGAGTAC
TCACCAGTCACAGAAAAGCATCTTACGGATGGCATGACAGTAAGAGAATTATGCAGTGCTGCAATAACCATGAGTGATAACACTGCGGCC
AACTTACTTCTGACAACGATCGGAGGACCGAAGGAGCTAACCGCTTTTTTGCACAACATGGGGGATCATGTAACTCGCCTTGATCGTTGG
GAACCGGAGCTGAATGAAGCCATACCAAACGACGAGCGTGACACCACGATGCCTGCAGCAATGGCAACAACGTTGCGCAAACTATTAACT
GGCGAACTACTTACTCTAGCTTCCCGGCAACAATTAATAGACTGGATGGAGGCGGATAAAGTTGCAGGACCACTTCTGCGCTCGGCCCTT
CCGGCTAGCTGGTTTATTGCTGATAAATCTGGAGCCGGTGAGCGTGGGTCTCGCGGTATCATTGCAGCACTGGGGCCAGATGGTAAGCCC
TCCCGTATCGTAGTTATCTACACGACGGGGAGTCAGGCAACTATGGATGAACGAAATAGACAGATCGCTGAGATAGGTGCCTCACTGATT
AAGCATTGGTAACTGCAGACCAAGTTTACTCATATATACTTTAGATTGATTTAAAACTTCATTTTTAATTTAAAAGGATCTAGGTGAAGA
TCCTTTTTGATAATCTCATGACCAAAATCCCTTAACGTGAGTTTTCGTTCCACTGAGCGTCAGACCCCGTAGAAAAGATCAAAGGATCTT
CTTGAGATCCTTTTTTTCTGCGCGTAATCTGCTGCTTGCAAACAAAAAAACCACCGCTACCAGCGGTGGTTTGTTTGCCGGATCAAGAGC
TACCAACTCTTTTTCCGAAGGTAACTGGCTTCAGCAGAGCGCAGATACCAAATACTGTCCTTCTAGTGTAGCCGTAGTTAGGCCACCACT
TCAAGAACTCTGTAGCACCGCCTACATACCTCGCTCTGCTAATCCTGTTACCAGTGGCTGCTGCCAGTGGCGATAAGTCGTGTCTTACCG
GGTTGGACTCAAGACGATAGTTACCGGATAAGGCGCAGCGGTCGGGCTGAACGGGGGGTTCGTGCACACAGCCCAGCTTGGAGCGAACGA
CCTACACCGAACTGAGATACCTACAGCGTGAGCTATGAGAAAGCGCCACGCTTCCCGAAGGGAGAAAGGCGGACAGGTATCCGGTAAGCG
GCAGGGTCGGAACAGGAGAGCGCACGAGGGAGCTTCCAGGGGGAAACGCCTGGTATCTTTATAGTCCTGTCGGGTTTCGCCACCTCTGAC
TTGAGCGTCGATTTTTGTGATGCTCGTCAGGGGGGCGGAGCCTATGGAAAAACGCCAGCAACGCGGCCTTTTTACGGTTCCTGGCCTTTT
GCTGG

RM_Tether 7	GCGGCCGCGATCTCTCACCTACCAAACAATGCCCCCCTGCAAAAAATAAATTCATATAAAAAACATACAGATAACCATCTGCGGTGATAA ATTATCTCTGGCGGTGTTGACATAAATACCACTGGCGGTGATACTGAGCACGGGTACCGGCCGCTGAGAAAAAGCGAAGCGGCACTGCTC TTTAACAATTTATCAGACAATCTGTGTGGGCACTCGAAGATACGGATTCTTAACGTCGCAAGACGAAAAATGAATACCAAGTCTCAAGAG TGAACACGTAATTCATTACGAAGTTTAATTCTTTGAGCGTCAAACTTTTAAATTGAAGAGTTTGATCATGGCTCAGATTGAACGCTGGCG GCAGGCCTAACACATGCAAGTCGAACGGTAACAGGAAGAAGCTTGCTTCTTTGCTGACGAGTGGCGGACGGGTGAGTAATGTCTGGGAAA CTGCCTGATGGAGGGGGATAACTACTGGAAACGGTAGCTAATACCGCATAACGTCGCAAGACCAAAGAGGGGGACCTTCGGGCCTCTTGC CATCGGATGTGCCCAGATGGGATTAGCTAGTAGGTGGGGTAACGGCTCACCTAGGCGACGATCCCTAGCTGGTCTGAGAGGATGACCAGC CACACTGGAACTGAGACACGGTCCAGACTCCTACGGGAGGCAGCAGTGGGGAATATTGCACAATGGGCGCAAGCCTGATGCAGCCATGCC GCGTGTATGAAGAAGGCCTTCGGGTTGTAAAGTACTTTCAGCGGGGAGGAAGGGAGTAAAGTTAATACCTTTGCTCATTGACGTTACCCG CAGAAGAAGCACCGGCTAACTCCGTGCCAGCAGCCGCGGTAATACGGAGGGTGCAAGCGTTAATCGGAATTACTGGGCGTAAAGCGCACG CAGGCGGTTTGTTAAGTCAGATGTGAAATCCCCGGGCTCAACCTGGGAACTGCATCTGATACTGGCAAGCTTGAGTCTCGTAGAGGGGGG TAGAATTCCAGGTGTAGCGGTGAAATGCGTAGAGATCTGGAGGAATACCGGTGGCGAAGGCGGCCCCCTGGACGAAGACTGACGCTCAGG TGCGAAAGCGTGGGGAGCAAACAGGATTAGATACCCTGGTAGTCCACGCCGTAAACGATGTCGACTTGGAGGTTGTGCCCTTGAGGCGTG GCTTCCGGAGCTAACGCGTTAAGTCGACCGCCTGGGGAGTACGGCCGCAAGGTTAAAACTCAAATGAATTGACGGGGGCCCGCACAAGCG GTGGAGCATGTGGTTTAATTCGATGCAACGCGAAGAACCTTACCTGGTCTTGACATCCACGGAAGTTTTCAGAGATGAGAATGTGCCTTC GGGAACCGTGAGACAGGTGCTGCATGGCTGTCGTCAGCTCGTGTTGTGAAATGTTGGGTTAAGTCCCGCAACGAGCGCAACCCTTATCCT TTGTTGCCAGCGGTCCGGCCGGGAACTCAAAGGAGACTGCCAGTGATAAACTGGAGGAAGGTGGGGATGACGTCAAGTCATCATGGCCCT TACGACCAGGGCTACACACGTGCTACAATGGCGCATACAAAGAGAAGCGACCTCGCGAGAGCAAGCGGACCTCATAAAGTGCGTCGTAGT CCGGATTGGAGTCTGCAACTCGACTCCATGAAGTCGGAATCGCTAGTAATCGTGGATCAGAATGCCACGGTGAATACGTTCCCGGGCCTT GTACACACCGCCCGTCACACCATGGGAGTGGGTTGCAAAAGAAGTAGGTAGCTGTCTACCGCCCCAGGGAGATATCCCCCCACAGGCCAT ATAAGACAGCGTATACCCGCCGTTGAGCTAACCGGTACTAATGAACCGTGAGGCTTAACCGAGAGGTTAAGCGACTAAGCGTACACGGTG GATGCCCTGGCAGTCAGAGGCGATGAAGGACGTGCTAATCTGCGATAAGCGTCGGTAAGGTGATATGAACCGTTATAACCGGCGATTTCC GAATGGGGAAACCCAGTGTGTTTCGACACACTATCATTAACTGAATCCATAGGTTAATGAGGCGAACCGGGGGAACTGAAACATCTAAGT ACCCCGAGGAAAAGAAATCAACCGAGATTCCCCCAGTAGCGGCGAGCGAACGGGGAGCAGCCCAGAGCCTGAATCAGTGTGTGTGTTAGT GGAAGCGTCTGGAAAGGCGCGCGATACAGGGTGACAGCCCCGTACACAAAAATGCACATGCTGTGAGCTCGATGAGTAGGGCGGGACACG TGGTATCCTGTCTGAATATGGGGGGACCATCCTCCAAGGCTAAATACTCCTGACTGACCGATAGTGAACCAGTACCGTGAGGGAAAGGCG AAAAGAACCCCGGCGAGGGGAGTGAAAAAGAACCTGAAACCGTGTACGTACAAGCAGTGGGAGCACGCTTAGGCGTGTGACTGCGTACCT TTTGTATAATGGGTCAGCGACTTATATTCTGTAGCAAGGTTAACCGAATAGGGGAGCCGAAGGGAAACCGAGTCTTAACTGGGCGTTAAG TTGCAGGGTATAGACCCGAAACCCGGTGATCTAGCCATGGGCAGGTTGAAGGTTGGGTAACACTAACTGGAGGACCGAACCGACTAATGT TGAAAAATTAGCGGATGACTTGTGGCTGGGGGTGAAAGGCCAATCAAACCGGGAGATAGCTGGTTCTCCCCGAAAGCTATTTAGGTAGCG CCTCGTGAATTCATCTCCGGGGGTAGAGCACTGTTTCGGCAAGGGGGTCATCCCGACTTACCAACCCGATGCAAACTGCGAATACCGGAG AATGTTATCACGGGAGACACACGGCGGGTGCTAACGTCCGTCGTGAAGAGGGAAACAACCCAGACCGCCAGCTAAGGTCCCAAAGTCATG GTTAAGTGGGAAACGATGTGGGAAGGCCCAGACAGCCAGGATGTTGGCTTAGAAGCAGCCATCATTTAAAGAAAGCGTAATAGCTCACTG GTCGAGTCGGCCTGCGCGGAAGATGTAACGGGGCTAAACCATGCACCGAAGCTGCGGCAGCGACGCTTATGCGTTGTTGGGTAGGGGAGC GTTCTGTAAGCCTGCGAAGGTGTGCTGTGAGGCATGCTGGAGGTATCAGAAGTGCGAATGCTGACATAAGTAACGATAAAGCGGGTGAAA AGCCCGCTCGCCGGAAGACCAAGGGTTCCTGTCCAACGTTAATCGGGGCAGGGTGAGTCGACCCCTAAGGCGAGGCCGAAAGGCGTAGTC GATGGGAAACAGGTTAATATTCCTGTACTTGGTGTTACTGCGAAGGGGGGACGGAGAAGGCTATGTTGGCCGGGCGACGGTTGTCCCGGT TTAAGCGTGTAGGCTGGTTTTCCAGGCAAATCCGGAAAATCAAGGCTGAGGCGTGATGACGAGGCACTACGGTGCTGAAGCAACAAATGC CCTGCTTCCAGGAAAAGCCTCTAAGCATCAGGTAACATCAAATCGTACCCCAAACCGACACAGGTGGTCAGGTAGAGAATACCAAGGCGC TTGAGAGAACTCGGGTGAAGGAACTAGGCAAAATGGTGCCGTAACTTCGGGAGAAGGCACGCTGATATGTAGGTGAGGTCCCTCGCGGAT GGAGCTGAAATCAGTCGAAGATACCAGCTGGCTGCAACTGTTTATTAAAAACACAGCACTGTGCAAACACGAAAGTGGACGTATACGGTG TGACGCCTGCCCGGTGCCGGAAGGTTAATTGATGGGGTTAGCGCAAGCGAAGCTCTTGATCGAAGCCCCGGTAAACGGCGGCCGTAACTA TAACGGTCCTAAGGTAGCGAAATTCCTTGTCGGGTAAGTTCCGACCTGCACGAATGGCGTAATGATGGCCAGGCTGTCTCCACCCGAGAC TCAGTGAAATTGAACTCGCTGTGAAGATGCAGTGTACCCGCGGCAAGACGGAAAGACCCCGTGAACCTTTACTATAGCTTGACACTGAAC ATTGAGCCTTGATGTGTAGGATAGGTGGGAGGCTTTGAAGTGTGGACGCCAGTCTGCATGGAGCCGACCTTGAAATACCACCCTTTAATG TTTGATGTTCTAACGTTGACCCGTAATCCGGGTTGCGGACAGTGTCTGGTGGGTAGTTTGACTGGGGCGGTCTCCTCCTAAAGAGTAACG GAGGAGCACGAAGGTTGGCTAATCCTGGTCGGACATCAGGAGGTTAGTGCAATGGCATAAGCCAGCTTGACTGCGAGCGTGACGGCGCGA GCAGGTGCGAAAGCAGGTCATAGTGATCCGGTGGTTCTGAATGGAAGGGCCATCGCTCAACGGATAAAAGGTACTCCGGGGATAACAGGC TGATACCGCCCAAGAGTTCATATCGACGGCGGTGTTTGGCACCTCGATGTCGGCTCATCACATCCTGGGGCTGAAGTAGGTCCCAAGGGT ATGGCTGTTCGCCATTTAAAGTGGTACGCGAGCTGGGTTTAGAACGTCGTGAGACAGTTCGGTCCCTATCTGCCGTGGGCGCTGGAGAAC TGAGGGGGGCTGCTCCTAGTACGAGAGGACCGGAGTGGACGCATCACTGGTGTTCGGGTTGTCATGCCAATGGCACTGCCCGGTAGCTAA ATGCGGAAGAGATAAGTGCTGAAAGCATCTAAGCACGAAACTTGCCCCGAGATGAGTTCTCCCTGACCCTTTAAGGGTCCTGAAGGAACG TTGAAGACGACGACGTTGATAGGCCGGGTGTGTAAGCGGCGGGTATACGCAATGACGTATGGTGGCCTGTGGGGGGATATCTGTGAACTG GGGCGAAGTAGCCGGCGCTTACCACTTTGTGATTCATGACTGGGGTGAAGTCGTAACAAGGTAACCGTAGGGGAACCTGCGGTTGGATCA CCTCCTTACCTTAAAGAAGCGTACTTTGTAGTGCTCACACAGATTGTCTGATAGAAAGTGAAAAGCAAGGCGTTTACGCGTTGGGAGTGA GGCTGAAGAGAATAAGGCCGTTCGCTTTCTATTAATGAAAGCTCACCCTACACGAAAATATCACGCAACGCGTGATAAGCAATTTTCGTG TCCCCTTCGTCTAGAGGCCCAGGACACCGCCCTTTCACGGCGGTAACAGGGGTTCGAATCCCCTAGGGGACGCCACTTGCTGGTTTGTGA GTGAAAGTCGCCGACCTTAATATCTCAAAACTCATCTTCGGGTGATGTTTGAGATATTTGCTCTTTAAAAATCTGGATCAAGCTGAAAAT TGAAACACTGAACAACGAGAGTTGTTCGTGAGTCTCTCAAATTTTCGCAACACGATGATGAATCGAAAGAAACATCTTCGGGTTGTGAGC TTAAGCTTACAACGCCGAAGCTGTTTTGGCGGATGAGAGAAGATTTTCAGCCTGATACAGATTAAATCAGAACGCAGAAGCGGTCTGATA AAACAGAATTTGCCTGGCGGCAGTAGCGCGGTGGTCCCACCTGACCCCATGCCGAACTCAGAAGTGAAACGCCGTAGCGCCGATGGTAGT GTGGGGTCTCCCCATGCGAGAGTAGGGAACTGCCAGGCATCAAATAAAACGAAAGGCTCAGTCGAAAGACTGGGCCTTTCGTTTTATCTG TTGTTTGTCGGTGAACGCTCTCCTGAGTAGGACAAATCCGCCGGGAGCGGATTTGAACGTTGCGAAGCAACGGCCCGGAGGGTGGCGGGC AGGACGCCCGCCATAAACTGCCAGGCATCAAATTAAGCAGAAGGCCATCCTGACGGATGGCCTTTTTGCGTTTCTACAAACTCTTCCTGT CGTCATATCTACAAGCCGGCGCGCCGGGAAATGTGCGCGGAACCCCTATTTGTTTATTTTTCTAAATACATTCAAATATGTATCCGCTCA TGAGACAATAACCCTGATAAATGCTTCAATAATATTGAAAAAGGAAGAGTATGAGTATTCAACATTTCCGTGTCGCCCTTATTCCCTTTT TTGCGGCATTTTGCCTTCCTGTTTTTGCTCACCCAGAAACGCTGGTGAAAGTAAAAGATGCTGAAGATCAGTTGGGTGCACGAGTGGGTT ACATCGAACTGGATCTCAACAGCGGTAAGATCCTTGAGAGTTTTCGCCCCGAAGAACGTTTTCCAATGATGAGCACTTTTAAAGTTCTGC

TATGTGGCGCGGTATTATCCCGTGTTGACGCCGGGCAAGAGCAACTCGGTCGCCGCATACACTATTCTCAGAATGACTTGGTTGAGTACT
CACCAGTCACAGAAAAGCATCTTACGGATGGCATGACAGTAAGAGAATTATGCAGTGCTGCAATAACCATGAGTGATAACACTGCGGCCA
ACTTACTTCTGACAACGATCGGAGGACCGAAGGAGCTAACCGCTTTTTTGCACAACATGGGGGATCATGTAACTCGCCTTGATCGTTGGG
AACCGGAGCTGAATGAAGCCATACCAAACGACGAGCGTGACACCACGATGCCTGCAGCAATGGCAACAACGTTGCGCAAACTATTAACTG
GCGAACTACTTACTCTAGCTTCCCGGCAACAATTAATAGACTGGATGGAGGCGGATAAAGTTGCAGGACCACTTCTGCGCTCGGCCCTTC
CGGCTAGCTGGTTTATTGCTGATAAATCTGGAGCCGGTGAGCGTGGGTCTCGCGGTATCATTGCAGCACTGGGGCCAGATGGTAAGCCCT
CCCGTATCGTAGTTATCTACACGACGGGGAGTCAGGCAACTATGGATGAACGAAATAGACAGATCGCTGAGATAGGTGCCTCACTGATTA
AGCATTGGTAACTGCAGACCAAGTTTACTCATATATACTTTAGATTGATTTAAAACTTCATTTTTAATTTAAAAGGATCTAGGTGAAGAT
CCTTTTTGATAATCTCATGACCAAAATCCCTTAACGTGAGTTTTCGTTCCACTGAGCGTCAGACCCCGTAGAAAAGATCAAAGGATCTTC
TTGAGATCCTTTTTTTTCTGCGCGTAATCTGCTGCTTGCAAACAAAAAAACCACCGCTACCAGCGGTGGTTTGTTTGCCGGATCAAGAGCT
ACCAACTCTTTTTCCGAAGGTAACTGGCTTCAGCAGAGCGCAGATACCAAATACTGTCCTTCTAGTGTAGCCGTAGTTAGGCCACCACTT
CAAGAACTCTGTAGCACCGCCTACATACCTCGCTCTGCTAATCCTGTTACCAGTGGCTGCTGCCAGTGGCGATAAGTCGTGTCTTACCGG
GTTGGACTCAAGACGATAGTTACCGGATAAGGCGCAGCGGTCGGGCTGAACGGGGGGTTCGTGCACACAGCCCAGCTTGGAGCGAACGAC
CTACACCGAACTGAGATACCTACAGCGTGAGCTATGAGAAAGCGCCACGCTTCCCGAAGGGAGAAAGGCGGACAGGTATCCGGTAAGCGG
CAGGGTCGGAACAGGAGAGCGCACGAGGGAGCTTCCAGGGGGAAACGCCTGGTATCTTTATAGTCCTGTCGGGTTTCGCCACCTCTGACT
TGAGCGTCGATTTTTGTGATGCTCGTCAGGGGGGCGGAGCCTATGGAAAAACGCCAGCAACGCGGCCTTTTTACGGTTCCTGGCCTTTTG
CTGG

RM_Tether8	GCGGCCGCGATCTCTCACCTACCAAACAATGCCCCCCTGCAAAAAATAAATTCATATAAAAAACATACAGATAACCATCTGCGGTGATAA ATTATCTCTGGCGGTGTTGACATAAATACCACTGGCGGTGATACTGAGCACGGGTACCGGCCGCTGAGAAAAAGCGAAGCGGCACTGCTC TTTAACAATTTATCAGACAATCTGTGTGGGCACTCGAAGATACGGATTCTTAACGTCGCAAGACGAAAAATGAATACCAAGTCTCAAGAG TGAACACGTAATTCATTACGAAGTTTAATTCTTTGAGCGTCAAACTTTTAAATTGAAGAGTTTGATCATGGCTCAGATTGAACGCTGGCG GCAGGCCTAACACATGCAAGTCGAACGGTAACAGGAAGAAGCTTGCTTCTTTGCTGACGAGTGGCGGACGGGTGAGTAATGTCTGGGAAA CTGCCTGATGGAGGGGGATAACTACTGGAAACGGTAGCTAATACCGCATAACGTCGCAAGACCAAAGAGGGGGACCTTCGGGCCTCTTGC CATCGGATGTGCCCAGATGGGATTAGCTAGTAGGTGGGGTAACGGCTCACCTAGGCGACGATCCCTAGCTGGTCTGAGAGGATGACCAGC CACACTGGAACTGAGACACGGTCCAGACTCCTACGGGAGGCAGCAGTGGGGAATATTGCACAATGGGCGCAAGCCTGATGCAGCCATGCC GCGTGTATGAAGAAGGCCTTCGGGTTGTAAAGTACTTTCAGCGGGGAGGAAGGGAGTAAAGTTAATACCTTTGCTCATTGACGTTACCCG CAGAAGAAGCACCGGCTAACTCCGTGCCAGCAGCCGCGGTAATACGGAGGGTGCAAGCGTTAATCGGAATTACTGGGCGTAAAGCGCACG CAGGCGGTTTGTTAAGTCAGATGTGAAATCCCCGGGCTCAACCTGGGAACTGCATCTGATACTGGCAAGCTTGAGTCTCGTAGAGGGGGG TAGAATTCCAGGTGTAGCGGTGAAATGCGTAGAGATCTGGAGGAATACCGGTGGCGAAGGCGGCCCCCTGGACGAAGACTGACGCTCAGG TGCGAAAGCGTGGGGAGCAAACAGGATTAGATACCCTGGTAGTCCACGCCGTAAACGATGTCGACTTGGAGGTTGTGCCCTTGAGGCGTG GCTTCCGGAGCTAACGCGTTAAGTCGACCGCCTGGGGAGTACGGCCGCAAGGTTAAAACTCAAATGAATTGACGGGGGCCCGCACAAGCG GTGGAGCATGTGGTTTAATTCGATGCAACGCGAAGAACCTTACCTGGTCTTGACATCCACGGAAGTTTTCAGAGATGAGAATGTGCCTTC GGGAACCGTGAGACAGGTGCTGCATGGCTGTCGTCAGCTCGTGTTGTGAAATGTTGGGTTAAGTCCCGCAACGAGCGCAACCCTTATCCT TTGTTGCCAGCGGTCCGGCCGGGAACTCAAAGGAGACTGCCAGTGATAAACTGGAGGAAGGTGGGGATGACGTCAAGTCATCATGGCCCT TACGACCAGGGCTACACACGTGCTACAATGGCGCATACAAAGAGAAGCGACCTCGCGAGAGCAAGCGGACCTCATAAAGTGCGTCGTAGT CCGGATTGGAGTCTGCAACTCGACTCCATGAAGTCGGAATCGCTAGTAATCGTGGATCAGAATGCCACGGTGAATACGTTCCCGGGCCTT GTACACACCGCCCGTCACACCATGGGAGTGGGTTGCAAAAGAAGTAGGTAGCTGUCUGACUCGUACGUAGGGCGUCACAGGAGAUACUAA GACAGAAUAUACCCCCCGTTGAGCTAACCGGTACTAATGAACCGTGAGGCTTAACCGAGAGGTTAAGCGACTAAGCGTACACGGTGGATG CCCTGGCAGTCAGAGGCGATGAAGGACGTGCTAATCTGCGATAAGCGTCGGTAAGGTGATATGAACCGTTATAACCGGCGATTTCCGAAT GGGGAAACCCAGTGTGTTTCGACACACTATCATTAACTGAATCCATAGGTTAATGAGGCGAACCGGGGGAACTGAAACATCTAAGTACCC CGAGGAAAAGAAATCAACCGAGATTCCCCCAGTAGCGGCGAGCGAACGGGGAGCAGCCCAGAGCCTGAATCAGTGTGTGTGTTAGTGGAA GCGTCTGGAAAGGCGCGCGATACAGGGTGACAGCCCCGTACACAAAAATGCACATGCTGTGAGCTCGATGAGTAGGGCGGGACACGTGGT ATCCTGTCTGAATATGGGGGGACCATCCTCCAAGGCTAAATACTCCTGACTGACCGATAGTGAACCAGTACCGTGAGGGAAAGGCGAAAA GAACCCCGGCGAGGGGAGTGAAAAAGAACCTGAAACCGTGTACGTACAAGCAGTGGGAGCACGCTTAGGCGTGTGACTGCGTACCTTTTG TATAATGGGTCAGCGACTTATATTCTGTAGCAAGGTTAACCGAATAGGGGAGCCGAAGGGAAACCGAGTCTTAACTGGGCGTTAAGTTGC AGGGTATAGACCCGAAACCCGGTGATCTAGCCATGGGCAGGTTGAAGGTTGGGTAACACTAACTGGAGGACCGAACCGACTAATGTTGAA AAATTAGCGGATGACTTGTGGCTGGGGGTGAAAGGCCAATCAAACCGGGAGATAGCTGGTTCTCCCCGAAAGCTATTTAGGTAGCGCCTC GTGAATTCATCTCCGGGGGTAGAGCACTGTTTCGGCAAGGGGGTCATCCCGACTTACCAACCCGATGCAAACTGCGAATACCGGAGAATG TTATCACGGGAGACACACGGCGGGTGCTAACGTCCGTCGTGAAGAGGGAAACAACCCAGACCGCCAGCTAAGGTCCCAAAGTCATGGTTA AGTGGGAAACGATGTGGGAAGGCCCAGACAGCCAGGATGTTGGCTTAGAAGCAGCCATCATTTAAAGAAAGCGTAATAGCTCACTGGTCG AGTCGGCCTGCGCGGAAGATGTAACGGGGCTAAACCATGCACCGAAGCTGCGGCAGCGACGCTTATGCGTTGTTGGGTAGGGGAGCGTTC TGTAAGCCTGCGAAGGTGTGCTGTGAGGCATGCTGGAGGTATCAGAAGTGCGAATGCTGACATAAGTAACGATAAAGCGGGTGAAAAGCC CGCTCGCCGGAAGACCAAGGGTTCCTGTCCAACGTTAATCGGGGCAGGGTGAGTCGACCCCTAAGGCGAGGCCGAAAGGCGTAGTCGATG GGAAACAGGTTAATATTCCTGTACTTGGTGTTACTGCGAAGGGGGGACGGAGAAGGCTATGTTGGCCGGGCGACGGTTGTCCCGGTTTAA GCGTGTAGGCTGGTTTTCCAGGCAAATCCGGAAAATCAAGGCTGAGGCGTGATGACGAGGCACTACGGTGCTGAAGCAACAAATGCCCTG CTTCCAGGAAAAGCCTCTAAGCATCAGGTAACATCAAATCGTACCCCAAACCGACACAGGTGGTCAGGTAGAGAATACCAAGGCGCTTGA GAGAACTCGGGTGAAGGAACTAGGCAAAATGGTGCCGTAACTTCGGGAGAAGGCACGCTGATATGTAGGTGAGGTCCCTCGCGGATGGAG CTGAAATCAGTCGAAGATACCAGCTGGCTGCAACTGTTTATTAAAAACACAGCACTGTGCAAACACGAAAGTGGACGTATACGGTGTGAC GCCTGCCCGGTGCCGGAAGGTTAATTGATGGGGTTAGCGCAAGCGAAGCTCTTGATCGAAGCCCCGGTAAACGGCGGCCGTAACTATAAC GGTCCTAAGGTAGCGAAATTCCTTGTCGGGTAAGTTCCGACCTGCACGAATGGCGTAATGATGGCCAGGCTGTCTCCACCCGAGACTCAG TGAAATTGAACTCGCTGTGAAGATGCAGTGTACCCGCGGCAAGACGGAAAGACCCCGTGAACCTTTACTATAGCTTGACACTGAACATTG AGCCTTGATGTGTAGGATAGGTGGGAGGCTTTGAAGTGTGGACGCCAGTCTGCATGGAGCCGACCTTGAAATACCACCCTTTAATGTTTG ATGTTCTAACGTTGACCCGTAATCCGGGTTGCGGACAGTGTCTGGTGGGTAGTTTGACTGGGGCGGTCTCCTCCTAAAGAGTAACGGAGG AGCACGAAGGTTGGCTAATCCTGGTCGGACATCAGGAGGTTAGTGCAATGGCATAAGCCAGCTTGACTGCGAGCGTGACGGCGCGAGCAG GTGCGAAAGCAGGTCATAGTGATCCGGTGGTTCTGAATGGAAGGGCCATCGCTCAACGGATAAAAGGTACTCCGGGGATAACAGGCTGAT ACCGCCCAAGAGTTCATATCGACGGCGGTGTTTGGCACCTCGATGTCGGCTCATCACATCCTGGGGCTGAAGTAGGTCCCAAGGGTATGG CTGTTCGCCATTTAAAGTGGTACGCGAGCTGGGTTTAGAACGTCGTGAGACAGTTCGGTCCCTATCTGCCGTGGGCGCTGGAGAACTGAG GGGGGCTGCTCCTAGTACGAGAGGACCGGAGTGGACGCATCACTGGTGTTCGGGTTGTCATGCCAATGGCACTGCCCGGTAGCTAAATGC GGAAGAGATAAGTGCTGAAAGCATCTAAGCACGAAACTTGCCCCGAGATGAGTTCTCCCTGACCCTTTAAGGGTCCTGAAGGAACGTTGA AGACGACGACGTTGATAGGCCGGGTGTGTAAGCGGGGGGUAUAUUCAAUGACGGUAUCCGAGCUGUGACGCUGGCCUACGCAAAUCAGCC GGCGCTTACCACTTTGTGATTCATGACTGGGGTGAAGTCGTAACAAGGTAACCGTAGGGGAACCTGCGGTTGGATCACCTCCTTACCTTA AAGAAGCGTACTTTGTAGTGCTCACACAGATTGTCTGATAGAAAGTGAAAAGCAAGGCGTTTACGCGTTGGGAGTGAGGCTGAAGAGAAT AAGGCCGTTCGCTTTCTATTAATGAAAGCTCACCCTACACGAAAATATCACGCAACGCGTGATAAGCAATTTTCGTGTCCCCTTCGTCTA GAGGCCCAGGACACCGCCCTTTCACGGCGGTAACAGGGGTTCGAATCCCCTAGGGGACGCCACTTGCTGGTTTGTGAGTGAAAGTCGCCG ACCTTAATATCTCAAAACTCATCTTCGGGTGATGTTTGAGATATTTGCTCTTTAAAAATCTGGATCAAGCTGAAAATTGAAACACTGAAC AACGAGAGTTGTTCGTGAGTCTCTCAAATTTTCGCAACACGATGATGAATCGAAAGAAACATCTTCGGGTTGTGAGCTTAAGCTTACAAC GCCGAAGCTGTTTTGGCGGATGAGAGAAGATTTTCAGCCTGATACAGATTAAATCAGAACGCAGAAGCGGTCTGATAAAACAGAATTTGC CTGGCGGCAGTAGCGCGGTGGTCCCACCTGACCCCATGCCGAACTCAGAAGTGAAACGCCGTAGCGCCGATGGTAGTGTGGGGTCTCCCC ATGCGAGAGTAGGGAACTGCCAGGCATCAAATAAAACGAAAGGCTCAGTCGAAAGACTGGGCCTTTCGTTTTATCTGTTGTTTGTCGGTG AACGCTCTCCTGAGTAGGACAAATCCGCCGGGAGCGGATTTGAACGTTGCGAAGCAACGGCCCGGAGGGTGGCGGGCAGGACGCCCGCCA TAAACTGCCAGGCATCAAATTAAGCAGAAGGCCATCCTGACGGATGGCCTTTTTGCGTTTCTACAAACTCTTCCTGTCGTCATATCTACA AGCCGGCGCGCCGGGAAATGTGCGCGGAACCCCTATTTGTTTATTTTTCTAAATACATTCAAATATGTATCCGCTCATGAGACAATAACC CTGATAAATGCTTCAATAATATTGAAAAAGGAAGAGTATGAGTATTCAACATTTCCGTGTCGCCCTTATTCCCTTTTTTGCGGCATTTTG CCTTCCTGTTTTTGCTCACCCAGAAACGCTGGTGAAAGTAAAAGATGCTGAAGATCAGTTGGGTGCACGAGTGGGTTACATCGAACTGGA TCTCAACAGCGGTAAGATCCTTGAGAGTTTTCGCCCCGAAGAACGTTTTCCAATGATGAGCACTTTTAAAGTTCTGCTATGTGGCGCGGT

ATTATCCCGTGTTGACGCCGGGCAAGAGCAACTCGGTCGCCGCATACACTATTCTCAGAATGACTTGGTTGAGTACTCACCAGTCACAGA
AAAGCATCTTACGGATGGCATGACAGTAAGAGAATTATGCAGTGCTGCAATAACCATGAGTGATAACACTGCGGCCAACTTACTTCTGAC
AACGATCGGAGGACCGAAGGAGCTAACCGCTTTTTTGCACAACATGGGGGATCATGTAACTCGCCTTGATCGTTGGGAACCGGAGCTGAA
TGAAGCCATACCAAACGACGAGCGTGACACCACGATGCCTGCAGCAATGGCAACAACGTTGCGCAAACTATTAACTGGCGAACTACTTAC
TCTAGCTTCCCGGCAACAATTAATAGACTGGATGGAGGCGGATAAAGTTGCAGGACCACTTCTGCGCTCGGCCCTTCCGGCTAGCTGGTT
TATTGCTGATAAATCTGGAGCCGGTGAGCGTGGGTCTCGCGGTATCATTGCAGCACTGGGGCCAGATGGTAAGCCCTCCCGTATCGTAGT
TATCTACACGACGGGGAGTCAGGCAACTATGGATGAACGAAATAGACAGATCGCTGAGATAGGTGCCTCACTGATTAAGCATTGGTAACT
GCAGACCAAGTTTACTCATATATACTTTAGATTGATTTAAAACTTCATTTTTAATTTAAAAGGATCTAGGTGAAGATCCTTTTTGATAAT
CTCATGACCAAAATCCCTTAACGTGAGTTTTCGTTCCACTGAGCGTCAGACCCCGTAGAAAAGATCAAAGGATCTTCTTGAGATCCTTTT
TTTCTGCGCGTAATCTGCTGCTTGCAAACAAAAAAACCACCGCTACCAGCGGTGGTTTGTTTGCCGGATCAAGAGCTACCAACTCTTTTT
CCGAAGGTAACTGGCTTCAGCAGAGCGCAGATACCAAATACTGTCCTTCTAGTGTAGCCGTAGTTAGGCCACCACTTCAAGAACTCTGTA
GCACCGCCTACATACCTCGCTCTGCTAATCCTGTTACCAGTGGCTGCTGCCAGTGGCGATAAGTCGTGTCTTACCGGGTTGGACTCAAGA
CGATAGTTACCGGATAAGGCGCAGCGGTCGGGCTGAACGGGGGGTTCGTGCACACAGCCCAGCTTGGAGCGAACGACCTACACCGAACTG
AGATACCTACAGCGTGAGCTATGAGAAAGCGCCACGCTTCCCGAAGGGAGAAAGGCGGACAGGTATCCGGTAAGCGGCAGGGTCGGAACA
GGAGAGCGCACGAGGGAGCTTCCAGGGGGAAACGCCTGGTATCTTTATAGTCCTGTCGGGTTTCGCCACCTCTGACTTGAGCGTCGATTT
TTGTGATGCTCGTCAGGGGGGCGGAGCCTATGGAAAAACGCCAGCAACGCGGCCTTTTTACGGTTCCTGGCCTTTTGCTGG

	GCGGCCGCGATCTCTCACCTACCAAACAATGCCCCCCTGCAAAAAATAAATTCATATAAAAAACATACAGATAACCATCTGCGGTGATAA
	ATTATCTCTGGCGGTGTTGACATAAATACCACTGGCGGTGATACTGAGCACGGGTACCGGCCGCTGAGAAAAAGCGAAGCGGCACTGCTC
	TTTAACAATTTATCAGACAATCTGTGTGGGCACTCGAAGATACGGATTCTTAACGTCGCAAGACGAAAAATGAATACCAAGTCTCAAGAG
	TGAACACGTAATTCATTACGAAGTTTAATTCTTTGAGCGTCAAACTTTTAAATTGAAGAGTTTGATCATGGCTCAGATTGAACGCTGGCG
	GCAGGCCTAACACATGCAAGTCGAACGGTAACAGGAAGAAGCTTGCTTCTTTGCTGACGAGTGGCGGACGGGTGAGTAATGTCTGGGAAA
	CTGCCTGATGGAGGGGGATAACTACTGGAAACGGTAGCTAATACCGCATAACGTCGCAAGACCAAAGAGGGGGACCTTCGGGCCTCTTGC
	CATCGGATGTGCCCAGATGGGATTAGCTAGTAGGTGGGGTAACGGCTCACCTAGGCGACGATCCCTAGCTGGTCTGAGAGGATGACCAGC
	CACACTGGAACTGAGACACGGTCCAGACTCCTACGGGAGGCAGCAGTGGGGAATATTGCACAATGGGCGCAAGCCTGATGCAGCCATGCC
	GCGTGTATGAAGAAGGCCTTCGGGTTGTAAAGTACTTTCAGCGGGGAGGAAGGGAGTAAAGTTAATACCTTTGCTCATTGACGTTACCCG
	CAGAAGAAGCACCGGCTAACTCCGTGCCAGCAGCCGCGGTAATACGGAGGGTGCAAGCGTTAATCGGAATTACTGGGCGTAAAGCGCACG
	CAGGCGGTTTGTTAAGTCAGATGTGAAATCCCCGGGCTCAACCTGGGAACTGCATCTGATACTGGCAAGCTTGAGTCTCGTAGAGGGGGG
	TAGAATTCCAGGTGTAGCGGTGAAATGCGTAGAGATCTGGAGGAATACCGGTGGCGAAGGCGGCCCCCTGGACGAAGACTGACGCTCAGG
	TGCGAAAGCGTGGGGAGCAAACAGGATTAGATACCCTGGTAGTCCACGCCGTAAACGATGTCGACTTGGAGGTTGTGCCCTTGAGGCGTG
	GCTTCCGGAGCTAACGCGTTAAGTCGACCGCCTGGGGAGTACGGCCGCAAGGTTAAAACTCAAATGAATTGACGGGGGCCCGCACAAGCG
	GTGGAGCATGTGGTTTAATTCGATGCAACGCGAAGAACCTTACCTGGTCTTGACATCCACGGAAGTTTTCAGAGATGAGAATGTGCCTTC
	GGGAACCGTGAGACAGGTGCTGCATGGCTGTCGTCAGCTCGTGTTGTGAAATGTTGGGTTAAGTCCCGCAACGAGCGCAACCCTTATCCT
	TTGTTGCCAGCGGTCCGGCCGGGAACTCAAAGGAGACTGCCAGTGATAAACTGGAGGAAGGTGGGGATGACGTCAAGTCATCATGGCCCT
	TACGACCAGGGCTACACACGTGCTACAATGGCGCATACAAAGAGAAGCGACCTCGCGAGAGCAAGCGGACCTCATAAAGTGCGTCGTAGT
	CCGGATTGGAGTCTGCAACTCGACTCCATGAAGTCGGAATCGCTAGTAATCGTGGATCAGAATGCCACGGTGAATACGTTCCCGGGCCTT
	GTACACACCGCCCGTCACACCATGGGAGTGGGTTGCAAAAGAAGTAGGTAGCTGGGTAACTGTCGTATAGATGGAAGTGGATTCACACCC
	GATATAAGACAGAATATGGACCCCGTTGAGCTAACCGGTACTAATGAACCGTGAGGCTTAACCGAGAGGTTAAGCGACTAAGCGTACACG
	GTGGATGCCCTGGCAGTCAGAGGCGATGAAGGACGTGCTAATCTGCGATAAGCGTCGGTAAGGTGATATGAACCGTTATAACCGGCGATT
	TCCGAATGGGGAAACCCAGTGTGTTTCGACACACTATCATTAACTGAATCCATAGGTTAATGAGGCGAACCGGGGGAACTGAAACATCTA
	AGTACCCCGAGGAAAAGAAATCAACCGAGATTCCCCCAGTAGCGGCGAGCGAACGGGGAGCAGCCCAGAGCCTGAATCAGTGTGTGTGTT
	AGTGGAAGCGTCTGGAAAGGCGCGCGATACAGGGTGACAGCCCCGTACACAAAAATGCACATGCTGTGAGCTCGATGAGTAGGGCGGGAC
	ACGTGGTATCCTGTCTGAATATGGGGGGACCATCCTCCAAGGCTAAATACTCCTGACTGACCGATAGTGAACCAGTACCGTGAGGGAAAG
	GCGAAAAGAACCCCGGCGAGGGGAGTGAAAAAGAACCTGAAACCGTGTACGTACAAGCAGTGGGAGCACGCTTAGGCGTGTGACTGCGTA
	CCTTTTGTATAATGGGTCAGCGACTTATATTCTGTAGCAAGGTTAACCGAATAGGGGAGCCGAAGGGAAACCGAGTCTTAACTGGGCGTT
	AAGTTGCAGGGTATAGACCCGAAACCCGGTGATCTAGCCATGGGCAGGTTGAAGGTTGGGTAACACTAACTGGAGGACCGAACCGACTAA
	TGTTGAAAAATTAGCGGATGACTTGTGGCTGGGGGTGAAAGGCCAATCAAACCGGGAGATAGCTGGTTCTCCCCGAAAGCTATTTAGGTA
	GCGCCTCGTGAATTCATCTCCGGGGGTAGAGCACTGTTTCGGCAAGGGGGTCATCCCGACTTACCAACCCGATGCAAACTGCGAATACCG
	GAGAATGTTATCACGGGAGACACACGGCGGGTGCTAACGTCCGTCGTGAAGAGGGAAACAACCCAGACCGCCAGCTAAGGTCCCAAAGTC
	ATGGTTAAGTGGGAAACGATGTGGGAAGGCCCAGACAGCCAGGATGTTGGCTTAGAAGCAGCCATCATTTAAAGAAAGCGTAATAGCTCA
	CTGGTCGAGTCGGCCTGCGCGGAAGATGTAACGGGGCTAAACCATGCACCGAAGCTGCGGCAGCGACGCTTATGCGTTGTTGGGTAGGGG
	AGCGTTCTGTAAGCCTGCGAAGGTGTGCTGTGAGGCATGCTGGAGGTATCAGAAGTGCGAATGCTGACATAAGTAACGATAAAGCGGGTG
	AAAAGCCCGCTCGCCGGAAGACCAAGGGTTCCTGTCCAACGTTAATCGGGGCAGGGTGAGTCGACCCCTAAGGCGAGGCCGAAAGGCGTA
	GTCGATGGGAAACAGGTTAATATTCCTGTACTTGGTGTTACTGCGAAGGGGGGACGGAGAAGGCTATGTTGGCCGGGCGACGGTTGTCCC
	GGTTTAAGCGTGTAGGCTGGTTTTCCAGGCAAATCCGGAAAATCAAGGCTGAGGCGTGATGACGAGGCACTACGGTGCTGAAGCAACAAA
	TGCCCTGCTTCCAGGAAAAGCCTCTAAGCATCAGGTAACATCAAATCGTACCCCAAACCGACACAGGTGGTCAGGTAGAGAATACCAAGG
	CGCTTGAGAGAACTCGGGTGAAGGAACTAGGCAAAATGGTGCCGTAACTTCGGGAGAAGGCACGCTGATATGTAGGTGAGGTCCCTCGCG
	GATGGAGCTGAAATCAGTCGAAGATACCAGCTGGCTGCAACTGTTTATTAAAAACACAGCACTGTGCAAACACGAAAGTGGACGTATACG
	GTGTGACGCCTGCCCGGTGCCGGAAGGTTAATTGATGGGGTTAGCGCAAGCGAAGCTCTTGATCGAAGCCCCGGTAAACGGCGGCCGTAA
	CTATAACGGTCCTAAGGTAGCGAAATTCCTTGTCGGGTAAGTTCCGACCTGCACGAATGGCGTAATGATGGCCAGGCTGTCTCCACCCGA
	GACTCAGTGAAATTGAACTCGCTGTGAAGATGCAGTGTACCCGCGGCAAGACGGAAAGACCCCGTGAACCTTTACTATAGCTTGACACTG
	AACATTGAGCCTTGATGTGTAGGATAGGTGGGAGGCTTTGAAGTGTGGACGCCAGTCTGCATGGAGCCGACCTTGAAATACCACCCTTTA
	ATGTTTGATGTTCTAACGTTGACCCGTAATCCGGGTTGCGGACAGTGTCTGGTGGGTAGTTTGACTGGGGCGGTCTCCTCCTAAAGAGTA
	ACGGAGGAGCACGAAGGTTGGCTAATCCTGGTCGGACATCAGGAGGTTAGTGCAATGGCATAAGCCAGCTTGACTGCGAGCGTGACGGCG
	CGAGCAGGTGCGAAAGCAGGTCATAGTGATCCGGTGGTTCTGAATGGAAGGGCCATCGCTCAACGGATAAAAGGTACTCCGGGGATAACA
	GGCTGATACCGCCCAAGAGTTCATATCGACGGCGGTGTTTGGCACCTCGATGTCGGCTCATCACATCCTGGGGCTGAAGTAGGTCCCAAG
	GGTATGGCTGTTCGCCATTTAAAGTGGTACGCGAGCTGGGTTTAGAACGTCGTGAGACAGTTCGGTCCCTATCTGCCGTGGGCGCTGGAG
	AACTGAGGGGGGCTGCTCCTAGTACGAGAGGACCGGAGTGGACGCATCACTGGTGTTCGGGTTGTCATGCCAATGGCACTGCCCGGTAGC
	TAAATGCGGAAGAGATAAGTGCTGAAAGCATCTAAGCACGAAACTTGCCCCGAGATGAGTTCTCCCTGACCCTTTAAGGGTCCTGAAGGA
	ACGTTGAAGACGACGACGTTGATAGGCCGGGTGTGTAAGGGGGTCCATATTCAATGACGTATCGAAGGTGTGAATCCATGGACTATACGA
	TTGTTACCCCGGCGCTTACCACTTTGTGATTCATGACTGGGGTGAAGTCGTAACAAGGTAACCGTAGGGGAACCTGCGGTTGGATCACCT
	CCTTACCTTAAAGAAGCGTACTTTGTAGTGCTCACACAGATTGTCTGATAGAAAGTGAAAAGCAAGGCGTTTACGCGTTGGGAGTGAGGC
	TGAAGAGAATAAGGCCGTTCGCTTTCTATTAATGAAAGCTCACCCTACACGAAAATATCACGCAACGCGTGATAAGCAATTTTCGTGTCC
	CCTTCGTCTAGAGGCCCAGGACACCGCCCTTTCACGGCGGTAACAGGGGTTCGAATCCCCTAGGGGACGCCACTTGCTGGTTTGTGAGTG
	AAAGTCGCCGACCTTAATATCTCAAAACTCATCTTCGGGTGATGTTTGAGATATTTGCTCTTTAAAAATCTGGATCAAGCTGAAAATTGA
	AACACTGAACAACGAGAGTTGTTCGTGAGTCTCTCAAATTTTCGCAACACGATGATGAATCGAAAGAAACATCTTCGGGTTGTGAGCTTA
	AGCTTACAACGCCGAAGCTGTTTTGGCGGATGAGAGAAGATTTTCAGCCTGATACAGATTAAATCAGAACGCAGAAGCGGTCTGATAAAA
	CAGAATTTGCCTGGCGGCAGTAGCGCGGTGGTCCCACCTGACCCCATGCCGAACTCAGAAGTGAAACGCCGTAGCGCCGATGGTAGTGTG
	GGGTCTCCCCATGCGAGAGTAGGGAACTGCCAGGCATCAAATAAAACGAAAGGCTCAGTCGAAAGACTGGGCCTTTCGTTTTATCTGTTG
	TTTGTCGGTGAACGCTCTCCTGAGTAGGACAAATCCGCCGGGAGCGGATTTGAACGTTGCGAAGCAACGGCCCGGAGGGTGGCGGGCAGG
RM	ACGCCCGCCATAAACTGCCAGGCATCAAATTAAGCAGAAGGCCATCCTGACGGATGGCCTTTTTGCGTTTCTACAAACTCTTCCTGTCGT
_T	CATATCTACAAGCCGGCGCGCCGGGAAATGTGCGCGGAACCCCTATTTGTTTATTTTTCTAAATACATTCAAATATGTATCCGCTCATGA
eth	GACAATAACCCTGATAAATGCTTCAATAATATTGAAAAAGGAAGAGTATGAGTATTCAACATTTCCGTGTCGCCCTTATTCCCTTTTTTG
er	CGGCATTTTGCCTTCCTGTTTTTGCTCACCCAGAAACGCTGGTGAAAGTAAAAGATGCTGAAGATCAGTTGGGTGCACGAGTGGGTTACA
9	TCGAACTGGATCTCAACAGCGGTAAGATCCTTGAGAGTTTTCGCCCCGAAGAACGTTTTCCAATGATGAGCACTTTTAAAGTTCTGCTAT

GTGGCGCGGTATTATCCCGTGTTGACGCCGGGCAAGAGCAACTCGGTCGCCGCATACACTATTCTCAGAATGACTTGGTTGAGTACTCAC
CAGTCACAGAAAAGCATCTTACGGATGGCATGACAGTAAGAGAATTATGCAGTGCTGCAATAACCATGAGTGATAACACTGCGGCCAACT
TACTTCTGACAACGATCGGAGGACCGAAGGAGCTAACCGCTTTTTTGCACAACATGGGGGATCATGTAACTCGCCTTGATCGTTGGGAAC
CGGAGCTGAATGAAGCCATACCAAACGACGAGCGTGACACCACGATGCCTGCAGCAATGGCAACAACGTTGCGCAAACTATTAACTGGCG
AACTACTTACTCTAGCTTCCCGGCAACAATTAATAGACTGGATGGAGGCGGATAAAGTTGCAGGACCACTTCTGCGCTCGGCCCTTCCGG
CTAGCTGGTTTATTGCTGATAAATCTGGAGCCGGTGAGCGTGGGTCTCGCGGTATCATTGCAGCACTGGGGCCAGATGGTAAGCCCTCCC
GTATCGTAGTTATCTACACGACGGGGAGTCAGGCAACTATGGATGAACGAAATAGACAGATCGCTGAGATAGGTGCCTCACTGATTAAGC
ATTGGTAACTGCAGACCAAGTTTACTCATATATACTTTAGATTGATTTAAAACTTCATTTTTAATTTAAAAGGATCTAGGTGAAGATCCT
TTTTGATAATCTCATGACCAAAATCCCTTAACGTGAGTTTTCGTTCCACTGAGCGTCAGACCCCGTAGAAAAGATCAAAGGATCTTCTTG
AGATCCTTTTTTTCTGCGCGTAATCTGCTGCTTGCAAACAAAAAAACCACCGCTACCAGCGGTGGTTTGTTTGCCGGATCAAGAGCTACC
AACTCTTTTTCCGAAGGTAACTGGCTTCAGCAGAGCGCAGATACCAAATACTGTCCTTCTAGTGTAGCCGTAGTTAGGCCACCACTTCAA
GAACTCTGTAGCACCGCCTACATACCTCGCTCTGCTAATCCTGTTACCAGTGGCTGCTGCCAGTGGCGATAAGTCGTGTCTTACCGGGTT
GGACTCAAGACGATAGTTACCGGATAAGGCGCAGCGGTCGGGCTGAACGGGGGGTTCGTGCACACAGCCCAGCTTGGAGCGAACGACCTA
CACCGAACTGAGATACCTACAGCGTGAGCTATGAGAAAGCGCCACGCTTCCCGAAGGGAGAAAGGCGGACAGGTATCCGGTAAGCGGCAG
GGTCGGAACAGGAGAGCGCACGAGGGAGCTTCCAGGGGGAAACGCCTGGTATCTTTATAGTCCTGTCGGGTTTCGCCACCTCTGACTTGA
GCGTCGATTTTTGTGATGCTCGTCAGGGGGGCGGAGCCTATGGAAAAACGCCAGCAACGCGGCCTTTTTACGGTTCCTGGCCTTTTGCTG
G

Supplementary Table 5.3 Tether designs that were designed, built, and characterized in the Squires strain.

Sample	Avg doubling time (min)	Tether 1 (5' - 3')	Tether 2 (5' - 3')
WT	67.43	None	None
Ribo-T v1	163.45	AAAAAAAA	AAAAAAAAA
Ribo-T v2	129.62	CAAUGAACAAUUGGA	GAUAACUAGU
Ribo-switch 3	232.92	TTTTTTGATGAGGATTACCCATCTTTAAAAA	TTTTTTGATGAGGAATTACCCATCTTTTTT
Ribo-switch 6	269.44	TTTTTTGATGAGGATTACCCATCTTTAAAAA	TTTTTTGATGAGGAATTACCCATCTTTTTT
Ribo-switch 7	281.93	TTTTTTGATGAGGATTACCCATCTTTAAAAA	TTTTTTGATGAGGAATTACCCATCTTTTTT
Ribo-switch 10	293.55	TTTCGTACACCATTAGGGTACGTTTTTCGTACACCATTAGGGTACGTTTAA	TTTCGTACACCATTAGGGTACGTTT
v1.0 UUU-MS2-Ribo-T	278.07	TTTGATGAGGAATTACCCATCTTT	TTTAAAGATGGGTAATCCTCATCAAA
v3.0UUU-MS2-Ribo-T	247.4	TTTGATGAGGATTACCCATCTTT	TTTAAAGATGGGTAATCCTCATCAAA

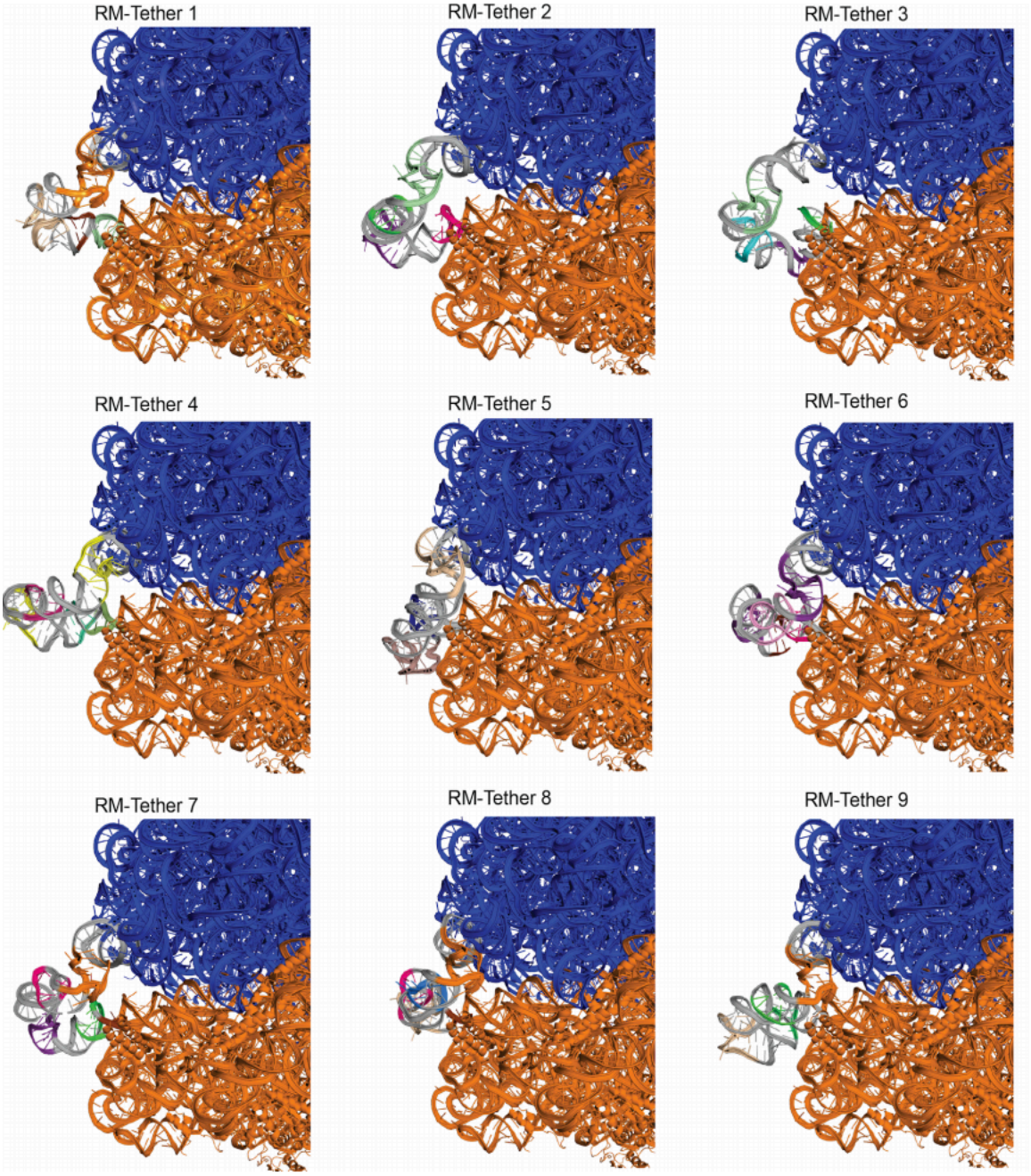

Supplementary Figure 5.1 All 9 RNAMake RM-Tether designs, colored according to the motifs that were used to generate it, helices (gray), small subunit (orange), and large subunit (blue).

CHAPTER 6

Dissertation Overview and Future Outlook

6.1 Dissertation Overview

In this dissertation, we have used both *in vitro* and *in vivo* methods to both understand and engineer the cell's protein synthesis machine: the ribosome. Specifically, in chapter 1, we presented an overview of the ribosome and the current literature on studying and engineering the ribosome. In chapter 2, we investigated the mutationally flexibility of the ribosome in an in vitro ribosome synthesis, assembly, and translation (iSAT) platform. Importantly, an important finding was that despite the highly conserved nature of the ribosome's active site, almost every location is still amenable to some mutation. In chapter 3, we extended the use of our iSAT platform to design, build, and characterize ribosomes capable of incorporating β-amino acids. This chapter represents an important steppingstone for future ribosome engineers, as it sets the stage for an efficient workflow for design, building, and testing mutant ribosome isolated from cells, or built *in vitro*. In chapter 4, we shifted to *in vivo* ribosome biochemistry and engineering work, with the goal of optimizing a system for ribosome engineering in the cell. Importantly, this work resulted in the new state-of-the-art *in vivo* orthogonal tethered ribosome platform, Ribo-T v2. This new platform permitted the incorporation of up to 5 ncAAs. In chapter 5, we extended our *in vivo* tethered ribosome platform to design, build, and study novel tether sequences. Towards the goal of computationally designing RNA nanomachines, we demonstrated for the first time, the ability to de novo design ribosomal tethers that maintain translation functionality without getting cleaved. Finally, in chapters 6 and 7, we summarize our work, gather our conclusions, and give an outlook on future work. In the appendix, we present work that is ongoing.

"You can't use up creativity. The more you use, the more you have." – Maya Angelou

6.2 Future work

The following sections outline what I believe is the most relevant future work that has either been spearheaded and requires continued efforts, or represents proposed work directly related to one or more of the chapters described above.

6.2.1 Probing single and multi-mutations in other key regions of the ribosome

The iSAT system is uniquely poised to permit the study of other important mutations within key regions of the ribosome. One future project idea is to study the evolution of the ribosome's anatomy through mutational studies. We can imagine sequencing aligning 3 other key locations within the ribosome: (1) the nucleotides surrounding the L1 stalk, (2) the Sarcin-ricin loop (SRL) nucleotides, (3) Nucleotides surrounding other important stalks such as the L7/L12 stalk, and (4) nucleotides surrounding L27, which has been implicated in the peptidyl transferase reaction. These are important parts of the ribosome that still need further studies. Specifically, the L1 stalk is a mobile structure implicated in directing tRNA movement during translocation through the ribosome [289]. This stalk interacts with the E-site tRNA. The SRL is an interesting structure on the ribosome, the precise role is still not fully understood. Recent biochemical and structural studies indicate that the SRL is critical for triggering GTP hydrolysis on elongation factor Tu (EF-Tu) and elongation factor G (EF-G) [290,291]. The L7/L12 stalk is highly mobile. It makes key interactions with the 50S subunit and interacts with bound elongation factors and is involved in ribosomal proteins eliciting their GTPas activity [292]. And finally, L27 has been highly debated in its function within PTC activity [155,156]. Better understanding the nucleotides around this ribosomal protein will be important for future basic biology and engineering efforts.

6.2.2 Leveraging SHAPE-Seq for characterizing mutant rRNA interactions

I believe that an important direction for the lab is to deepen our collaboration with the Lucks lab and move forward with structurally analyzing our in vitro and in vivo ribosome variants using SHAPE-Seq [293]. Specifically, using SHAPE-Seq will enhance our understanding of the structure-function impacts of mutational changes to the ribosome's active site (or other locations within the ribosome), as well as changes to different tethered constructs (Figure 6.1).

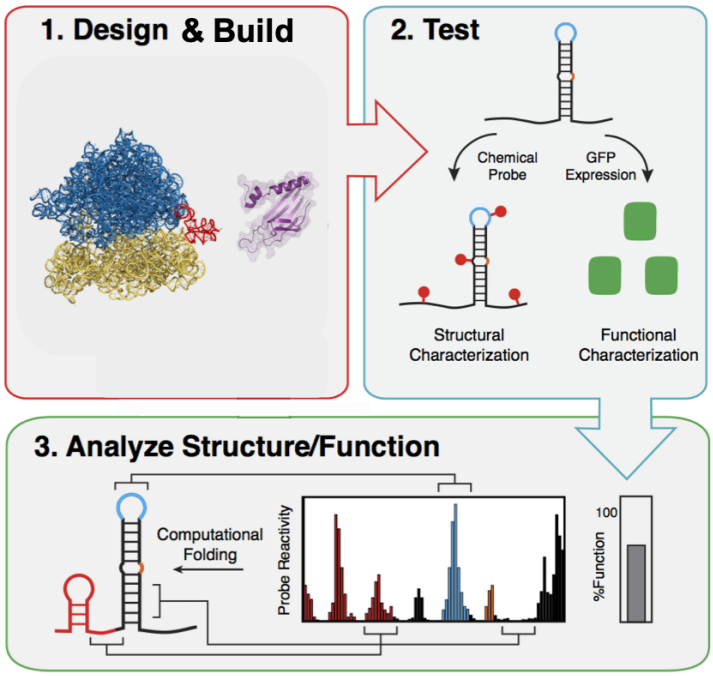

Figure 6.1 Using SHAPE-Seq in combination with iSAT ribosome synthesis or orthogonal tethered ribosomes (Ribo-T) will enhance our understanding of structure and function relationships within RNA designs and the ribosome.

6.2.3 Rescuing translation and improving ncAA incorporation with translation factors

Another important direction in the lab is to begin merging our ribosome engineering efforts with that of engineered translation factors in a novel way. Specifically, previous work has demonstrated that the addition of purified elongation factor P (EF-P) improves the incorporation of ncAAs [137]. I imagine future work investigating the impact of titrating other translation factors with different mutant ribosomes (Figure 6.2).

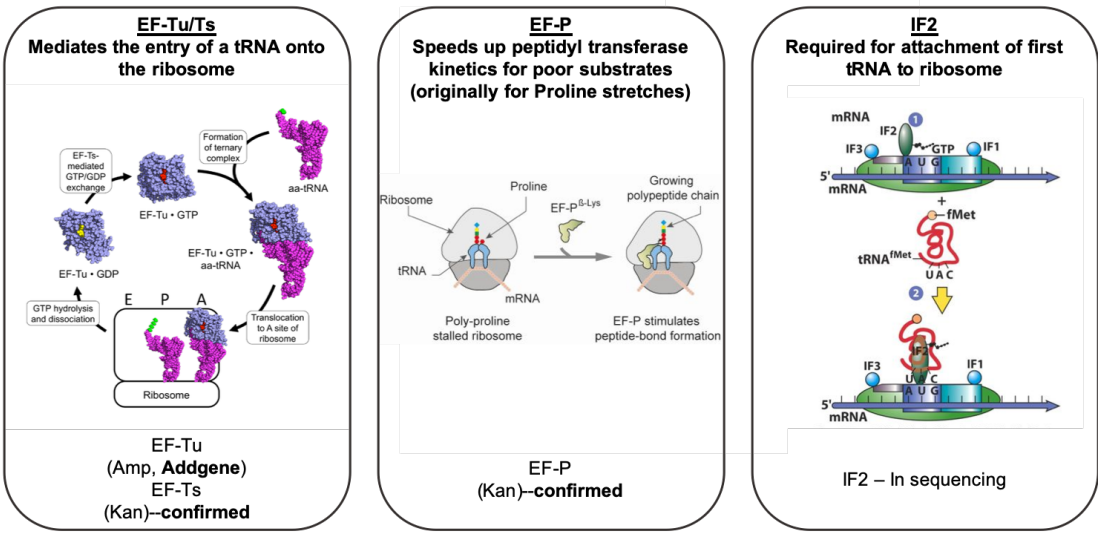

Figure 6.2 Schematics of the various translation factors that could be used in ribosome and translation engineering. Titrating in these factors may help elucidate basic biology of their structural and functional impacts in translation, while also aiding the improved incorporation of ncAAs.

6.2.4 Novel circular permutations with computationally designed tethers

Finally, I see our lab further collaborating with the lab of Dr. Rhiju Das at Stanford to further probe novel circular permutations on our Ribo-T construct. Importantly, by investigating new circular permutations and designing computationally designed tethers between these new locations, we will learn basic design rules around how and where we can tether the ribosome, and what loops and helices are permissible to drastic engineering. Furthermore, this represents an important opportunity for computational biologists to improve their design and modeling algorithms, bringing us closer to a gold standard for de novo designing RNA nanomachines, and more broadly, RNA.

CHAPTER 7

Conclusion

Inspired by the ribosome's incredible catalytic capacity, researchers have sought to study and engineer this nanomachine for the synthesis of sequence defined polymers (SDPs). However, because the ribosome is such a crucial component for cell-life, cell viability constraints have stymied these efforts. *In vitro* and *in vivo* ribosome engineering platforms have lead to a better understanding of structure, function relationships and has better informed complex RNA and ribosome design rules. With these tools in hand, we can now imagine understanding key components of the ribosome that were previously inaccessible for study. We can also imagine preparing specialized ribosomes, which possess the capacity to incorporate different novel monomers. We can even imagine evolving ribosomes back into more ancient forms, or forward into future forms; to better understand how the ribosome came to be.

This dissertation focused on our recent advances in the construction engineered ribosomes for the advancement of basic and synthetic biology. Libraries of ribosome active site mutants were designed, constructed, and characterized. This work resulted in the first and only comprehensive mutational map of the ribosome's PTC. Then, further work investigated multi-mutations for the incorporation of expanded backbone monomers; resulting in a standardized workflow for studying and engineering ribosomes for ncAA incorporation. Finally, using an in vivo ribosome engineering platform, we developed a state-of-the-art orthogonal ribosome system, which was used for the incorporation of ncAA in a cell. This work was further expanded for the study of computationally designed ribosome variants *in vivo*. The principles developed in this work, gave rise to design rules and basic biology insight that will help shape the future of ribosome engineering both *in vivo* and *in vitro*. Our studies suggest that the ribosome, despite being an ancient and highly conserved macromolecular structure, can indeed be engineered and mutated for novel purposes.

CHAPTER 8

Appendix

The work described in this chapter is unpublished and ongoing.

8.1 Improving ribosome orthogonality with translational riboregulators

8.1.1 Background

Orthogonal 16S/SD pairs and translational riboregulators (like toehold switches) regulate translation by functionally distinct mechanisms: orthogonal ribosomes act by base-pairing, whereas toehold switches function by structural inhibition. Strong secondary structure around the ribosome binding site (RBS) cannot be unwound by the ribosome, preventing translation initiation; translation can only be initiated when this structure is unwound by an invading trigger RNA. Given that toehold switches and ribosomes regulate translation differently, it should be possible to combine them to add their effects (Figure 8.1).

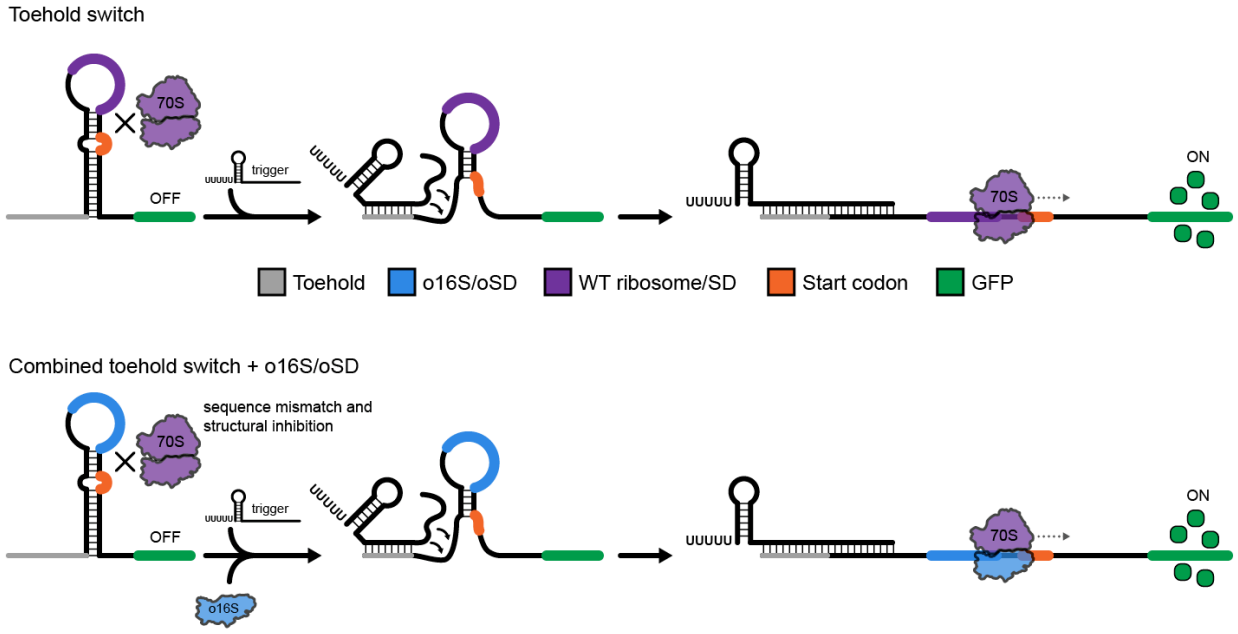

Figure 8.1 Cartoon depiction of the process of combining toehold switches and orthogonal ribosomes to selectively regulate translation.

In collaborative work that was initiated between Dr. Paul D. Carlson from the Lucks lab, and Dr. Erik D. Carlson, we aimed to combine toehold (TH) switches with orthogonal ribosomes to demonstrate the following:

1) Combined regulation enhances ON/OFF expression: Some leak (translation by WT ribosomes in the OFF state) is observed for both orthogonal ribosomes and toehold switches. The combined system should have a lower OFF state, giving a much larger ON/OFF ratio. There's some precedent for this basic idea – the Lucks Lab has shown that coupling transcription and translational control accomplishes a similar effect [294].
2) Orthogonal TH switches can minimize crosstalk between o-ribosomes: The ability to multiplex orthogonal ribosomes would be an advantage; for example, expressing multiple proteins in the same cell using different o-ribosomes that can be turned ON and OFF independently. It is easy to generate libraries of orthogonal toehold switches, although it is unclear whether the oSD/o16S pairs evolved in the RiboT v2 paper are mutually orthogonal (does one o16S significantly translate from a non-cognate oSD?). We should be able to leverage orthogonal toehold switches to minimize crosstalk between o-ribosome variants. For example, if you have 4 variably orthogonal o16S/oSD pairs, you could couple each of them to an orthogonal toehold switch-trigger pair, which will give a set of 4 *very* orthogonal regulators (Figure 8.2).

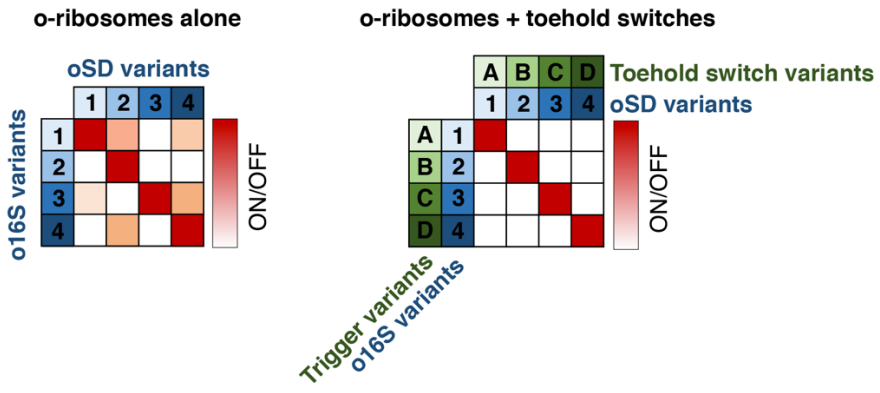

Figure 8.2 Hypothetical combinations of orthogonal ribosomes and toehold switches to generate translation regulators.

3) Orthogonal TH switches + orthogonal ribosomes can be combined to create a large set of mutually orthogonal regulators: A set of 4 toehold switches and 4 o-ribosomes could be mixed-and-matched to create a 16x16 orthogonality matrix (Figure 8.3).

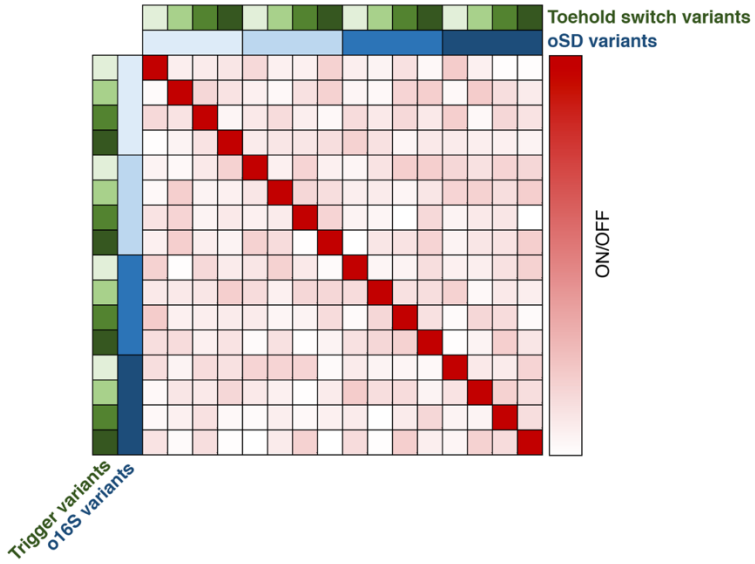

Figure 8.3 An example set of 4 toehold switches and 4 o-ribosomes combined to produce an orthogonality matrix.

8.1.2 Experimental setup and future work

Design and construction of the key parts and elements for this project have thus far been completed by Dr. Erik Carlson, Anne d'Aquino, and Dr. Paul Carlson. Future work would involve carrying out the following set of basic experiments:

First, future work would involve testing a single oSD/o16S pair with a toehold switch, resulting in a simple 3-plasmid setup:

- Target (reporter) (p15A / chloramphenicol, sfGFP reporter)
    i. Toehold switch (WT SD)
    ii. oSD (no TH switch)
    iii. Toehold switch w/ oSD
- Toehold switch trigger (pCDF / spectinomycin): we typically use ColE1 to express triggers, but pCDF should work fine (lower copy number but still in excess compared to p15A)
- o-ribosome (ColE1 / Carbenicillin)
    i. WT (pAM552)
    ii. o16S

The second step would involve testing every combination of oSD/o16S pairs from the original Ribo-T paper [175] and Ribo-T v2 [287] (6 mRNAs and 10 aSD total). Not all of these will be orthogonal, but testing every combination will let us pull out the largest set. Next, we would test o-ribosomes identified in the previous step, each expressed with a different orthogonal toehold switch – trigger pair, which have been extensively characterized previously. Finally, if some o-ribosomes show good orthogonality in the second step, mix-and-match with several toehold switch-trigger pairs to give a larger set of orthogonal regulators. This would demonstrate a more

general concept: if you have two independent methods of orthogonal gene regulation, they can be "multiplied" to give a much larger set. To our knowledge, nobody has demonstrated this before; however, it could be useful in cases where identifying new orthogonal pairs is challenging.

8.2 Expressing ribosomal proteins *in vitro*

8.2.1 Background

Crystal structures have elucidated an RNA-catalyzed peptidyl transferase mechanism in the large subunit of the ribosome, wherein residues from domain V of 23S rRNA contact and position substrates in catalysis[11]. However, it has been demonstrated that this catalytic activity still requires r-proteins[23].

The 54 r-protein coding genes are highly organized and regulated temporally and spatially in their synthesis in order to guarantee stoichiometric expression during assembly[19,295]. The genes of functionally or structurally related proteins are arranged into 19 operons respectively[1]. The most established mechanism of r-protein regulation is autogenous feedback regulation, wherein r-proteins, when in excess, can negatively regulate the translation by binding to the mRNA of their own or related operons [296,297]. Evidence exists for additional mechanisms of regulation, including non-autogenous regulation, transcriptional regulation, and protein degradation[1,298,299].

The expression of all the 54 r-proteins and their feedback regulation has been elucidated *in vivo* and *in vitro*[42,297,300-304]. A few studies have used individual recombinant r-proteins for *in vitro* 30S assembly studies. Culver and Noller demonstrated that 30S r-proteins could be recombinantly over-expressed, purified and assembled into clusters onto rRNA to form functional 30S particles[42,305]. However, no such achievements have been reported for 50S assembly. A small

number of studies have been reported for 50S assembly from extracted total proteins of the 50S (TP50) (in contrast to recombinant 50S proteins); however such 50S particles possess extremely poor functionality mainly due to disordered stoichiometry, rRNA misfolding and poor post-transcriptional modifications[50]. Green and Noller have illustrated inefficiencies in ribosome assembly without 23S rRNA post-transcriptional modifications[46]. Even *in vivo*, 50S assembly can be disrupted by a lack of post-transcriptional 23S methylation[306].

The functions of r-proteins range from structural, to mRNA interactions and chaperone and factor binding activity near the PTC[20]. Mutations in r-proteins have been shown to convey resistance to antibiotics such as streptomycin and erythromycin through direct and indirect disruption of antibiotic binding sites[21,22], but their precise roles in translation have yet to be elucidated.

While the *E. coli* ribosome is said to require 54 r-proteins, ribosomal mutants have been found that lack certain r-proteins[24], and gene knockout studies have shown that 22 r-proteins can be individually deleted from the *E. coli* genome without lethality[25]. Work from Noller and colleagues has suggested a minimum number of macromolecules required for peptidyl transferase, specifically the 23S rRNA and r-proteins L2 and L3[26]. L2 and L3 reside in close proximity to the PTC[27-29] (Figure 8.4). Additionally, Schulze, Nierhaus and Mankin demonstrated, *via* single-omission tests, that L2 and L3 (as well as L4) are essential for peptidyl transferase activity[30,31].

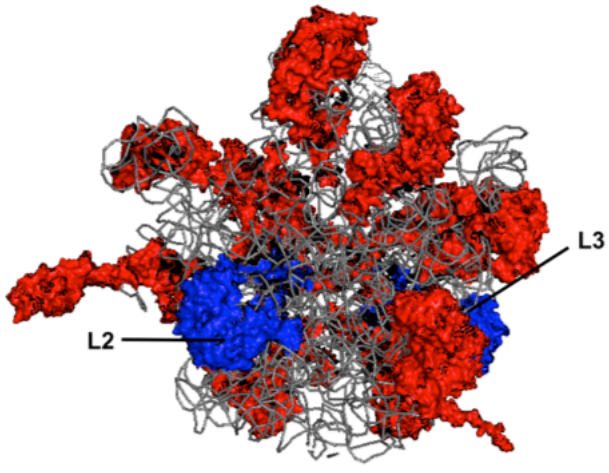

Figure 8.4 The front view, or the interface between the subunits of the 50S ribosomal subunit, with r-proteins L2 and L3 highlighted in blue. Additional interface r-proteins are in red.

Studies in which all 54 r-proteins are synthesized *in vitro* will provide a platform for r-protein mutagenesis and study. Specifically, work in this area will improve studies on ribosome biogenesis and elucidate individual r-protein functions and the impact of mutations on ribosome activity and promiscuity.

8.2.2 Experimental setup and future work

As a first step in approaching this problem, Dr. Brian Fritz and I both worked on synthesizing all of the ribosomal proteins in a cell-free system (See Dr. Brian Fritz's dissertation). Specifically, cell-free reactions were performed similarly to iSAT reactions; however, reactions took place in an S30 extract with plasmids encoding for each r-protein (instead of an sfGFP reporter). S30 extracts possessed the cell's native ribosomes, permitting the synthesis of r-proteins. S30 reactions were prepared as previously described[193,307] from MRE600 cell strain. R-protein synthesis was analyzed by radioactive amino acid incorporation as described previously[51] (Figure 8.5). In future work, a number of ribosomal proteins' expression needs to be optimized in the pJL1 vector in an S30 extract. Once the expression of all proteins is optimized, this system can be

engineered and optimized for the synthesis and study of individual ribosomal proteins, as well as the construction of completely synthetic ribosomes (synthetic rRNA and rProteins).

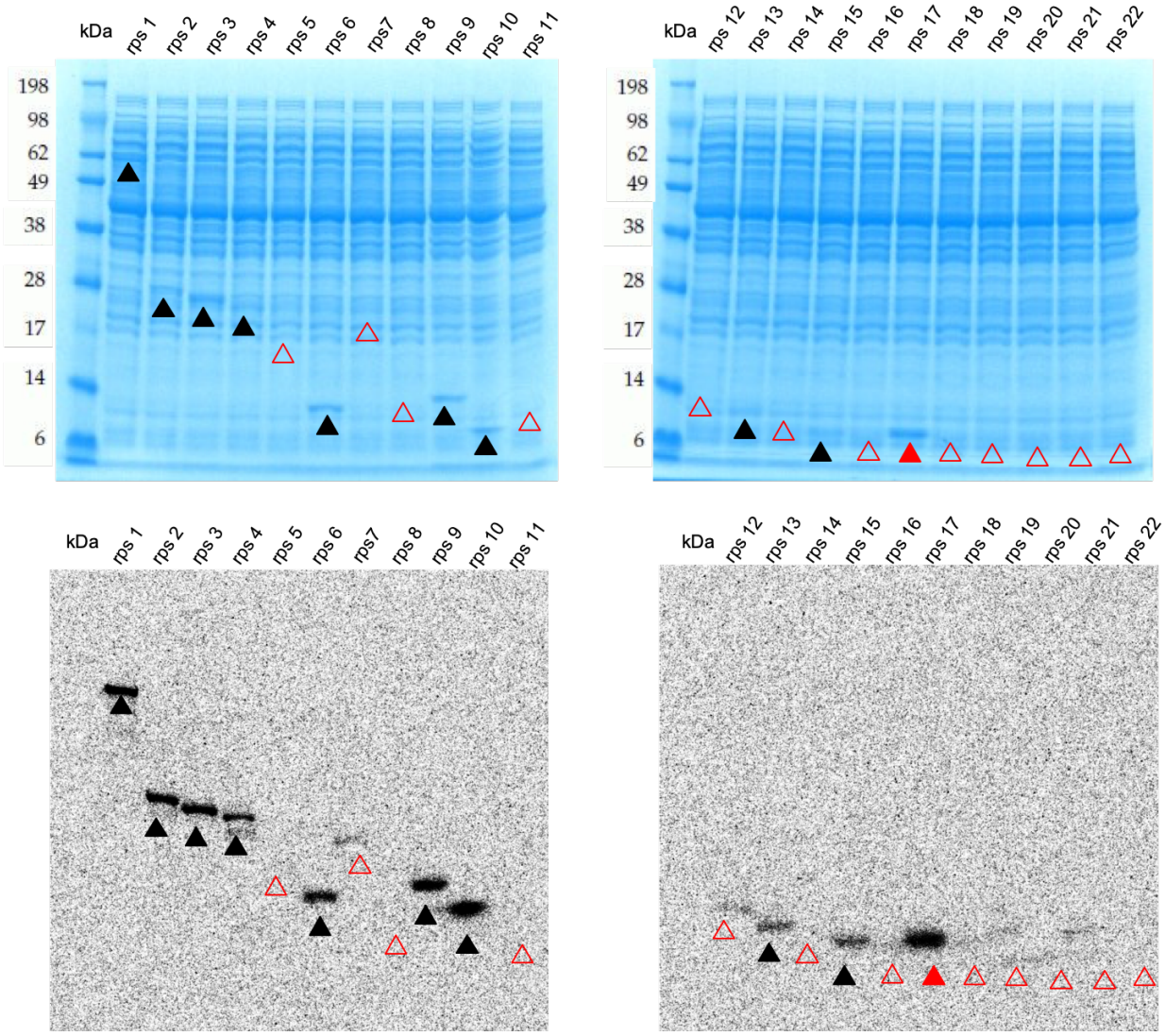

Figure 8.5 R-protein synthesis was analyzed by radioactive amino acid incorporation. S5, S8, S11, S12, S14, S7, S13, and S16 need expression optimization in the future.

8.3 Educational tools: studying mutations in protein structure and function

8.3.1 Background

Structure function relationships in biology can be effectively taught using cell-free biology techniques. Using kits such as BioBits [179,180], we can imagine studying the impact of mutations on protein structure and function using fluorescent reporters such as sfGFP. One such direction could involve using CRISPR Cas9 in an educational tools kit to introduce two mutations (Y66H / Y145F) to change the green fluorescence to blue fluorescence in a reporter protein. This has been done previously for Cell Biology labs, but is not necessarily easily portable or accessible [308]. I imagine future work involving constructs used in the Jewett lab (pJL1-sfGFP) being repurposed to generate a BioBits kit that reflects what was done in previous work surrounding this project [308].

8.3.2 Experimental setup and future work

There are a number of potential mutations in the sfGFP construct that could highlight important and interesting structural and functional change to young scientists. Importantly, teaching students about severe impacts of mutations (destroying fluorescence) or changing functionality (green to blue fluorescence) marks to key learning objectives. An analysis of these two potential changes in sfGFP are listed below:

T64 is coded by ACC (ACC) codon

- Place a missense mutation at this position to kill fluorescence
- Make a missense mutation corresponding to an alanine mutation (polar uncharged side chain to small hydrophobic side chain)
- T64A → ACC to GCC

Y66 is encoded by TAT (UAU) codon

- Place mutation Y66H mutation here to make fluorescence in sfGFP Blue
- To make Y66H missense mutation, clone point mutation UAU to CAU

8.4 Nature Protocols: A ribosome tethering strategy for an orthogonal ribosome-messenger RNA system

8.4.1 Abstract

Escherichia coli's ribosomes possess an incredible catalytic capability that has long motivated efforts to understand and harness artificial versions for biotechnology. However, repurposing ribosomes for synthetic biology requires new engineering approaches, decoupled from growth. Recently, the development of an orthogonal ribosome-mRNA system in cells, where a sub-population of ribosomes are available for engineering and are independent from wild-type ribosomes supporting cell life. This was achieved by constructing a ribosome with covalently tethered subunits called Ribo-T (the core 16S and 23S ribosomal RNAs form a single chimeric molecule). Surprisingly, Ribo-T can support life in the absence of wild-type ribosomes, and can be evolved to select otherwise dominantly lethal mutations when used in an orthogonal Ribo-T–mRNA system. Here, we describe protocols necessary to use and apply tethred ribosome systems, which includes common fitness and functional assays both *in vivo* and in *in vitro* systems. Importantly, engineering and mutating Ribo-T can be achieved by simple cloning techniques, as the system is controlled entirely by plasmids. These attributes render our protocol both functional and easily transferrable and sets the stage to explore poorly understood functions of the ribosome, enabling orthogonal genetic systems, and engineering ribosomes with altered chemical properties (Figure 8.6).

8.4.2 Overview of the technique

Ribo-T variant construction: All Ribo-T variants can be constructed using simple and efficient cloning techniques. For instance, whether introducing point mutations (such as A2058G

for conferring antibiotic resistance), various circular permutations, or novel tethers in various locations with unique sequences, inverse PCR with custom DNA oligos can be used to introduce these variations into the Ribo-T template. Subsequently, PCR is followed by recircularization by Gibson assembly reactions. The Ribo-T template is available in the non-profit plasmid repository, Addgene (Addgene catalog numbers -- 69344: SQ171fg/pCSacB; 69343: SQ171fg/pRibo-T; 69342: SQ171/pRibo-T).

Key feature unique to our technique: Our Ribo-T construct is the first ever full-orthogonal tethered ribosome. Through engineering efforts, we meticulously identified viable linkers as well as circular permutation locations. Additionally, we have further optimized and improved our tethers for greater usability. Our tether locations between the loop of helix 101 (H101) on the 23S rRNA and the apex loop of helix 44 (h44) on the 16S rRNA were key milestones in generating a hybrid 16S-23S rRNA molecule for a tethered ribosome, and can now be leveraged for specific tether engineering.

Using POP cells / plasmid shuttling: Importantly, cloning of the variant Ribo-T constructs are carried out in a construct whose parent is the pAM552 plasmid. The pAM552 plasmid is a derivative of pLK35 from which the unessential segments of the pBR322 cloning vector have been removed. pAM552 contains the entire *rrnB* operon of *E. coli* under the control of the phage lambda P_L promoter which is constitutively active in the conventional *E. coli* strains but is silent at 30ºC in the strain POP2136 (30ºC) carrying the cI857 gene of the temperature-sensitive lambda repressor. When screening single or libraries of constructs, plasmids are shuttled through POP2136 cells at 30ºC to suppress the expression of lethal variants. Shuttling in the POP2136 strain permits a simple and efficient way of confirming desired sequences, and assessing

library diversity. After an overnight culture at 30ºC, the Ribo-T plasmid(s) can be extracted and the resulting clones can be analyzed and verified by plasmid sequencing.

Key feature unique to our technique: One major challenge for cloning Ribo-T is the expression of lethal or toxic ribosome designs, leading to unintended mutations by the host cell to turn off expression. In order to overcome this, a system for turning expression off or on is required for reliable cloning. Our plasmid shuttling system in POP cells provides an effective platform for analyzing tethered ribosome sequences without impacting cell health or plasmid stability.

Ribo-T in the Squires strain / working with the Squires strain: Beyond the orthogonal system, Ribo-T with a wild-type Shine-Dalgarno initiation sequence is able to fully support cell growth in the absence of wild-type ribosomal RNA. The experimental preparation and testing of Ribo-T variants requires a strain lacking all seven ribosomal operons (Δ7 *rrn*): the Squires (SQ171) strain. The pRibo-T plasmids are transformed into Δ7 *rrn* SQ171 strain carrying pCSacB plasmid, (which carries a wt rRNA operon) and transformants resistant to ampicillin (plasmid antibiotic resistance), erythromycin (antibiotic resistance mutation, A2058G, introduced directly into the 23S rRNA) and sucrose (for functional replacement of the pCSacB plasmid) are selected. Due to the poor health of these cells, introducing Ribo-T into the SQ171fg strain requires careful attention to detail. When shuttling the Ribo-T variants from POP2136 to SQ171fg, a number of recovery steps must be taken upon transformation to ensure proper transfer. After transforming variants into SQ171fg cells, transformations are rapidly recovered in 800 µL of SOC media. This recovery should be undertaken at 37ºC for one to two hours with shaking (250 rpm). After incubating, overnight recovery cultures are prepared. A 750 µL aliquot of the 1-2 hour recovery is introduced into 1.25 mL of SOC supplemented with 50 µg/mL of ampicillin and 0.25% sucrose. This

overnight recovery allows cells to slowly acclimate to running completely off Ribo-T ribosomes without wild-type untethered ribosomes. After a 10-14 hour overnight recovery, these cells can be plated on full selection LB-agar plates possessing ampicillin (select for Ribo-T plasmid), erythromycin (A2058G resistance mutation on Ribo-T), and 5% sucrose (counter-select pCSacB plasmid).

Key feature unique to our technique: In our work, we evolved a version of the Squires strain that possesses a fast growing phenotype when using Ribo-T in the absence of wild-type ribosomes. Despite having been the principle ribosome-deletion strain for the past 20 years, the Squires strain is still difficult to work with due to its slow growth rate. Our evolved strain, termed SQ171fg exhibits better growth characteristics and shorter doubling time (70+/- 2 min). The strain still lacks wild type rDNA and rRNA, confirming that every ribosome in this strain was assembled with the tethered rRNA. Upon deeper characterization, the following two mutations were discovered in our strain: a nonsense mutation in the ybeX gene encoding a putative Mg2+/Co2+ transporter, and a missense mutation in the rpsA gene encoding ribosomal protein S1. Either rpsA alone or their combined effect account for the faster growth of SQ171fg. Importantly, this faster growing phenotype is extremely useful, as it permits faster design-build-test cycles, and gives a healthier, and thus more facile strain to work with.

Characterizing Ribo-T (confirming tethering and viability): Characterizing activity, tethering, and viability of Ribo-T is carried out through several assays. A key first step is to confirm viability and tethering of Ribo-T. First, viability is screened in clones grown from transformation into SQ171 or SQ171fg strains. Upon plating SQ171fg cells possessing Ribo-T variants on LB-agar plates containing sucrose (and appropriate antibiotics), the sucrose efficiently kicks out the

pCSacB plasmid (which carries a wt rRNA operon), leaving the Ribo-T variant as the sole rRNA source. If clones grow on the LB-Agar plates supplemented with sucrose and ampicillin, then Ribo-T successfully replaced pCSacB and now sustains the life of the cell. Second, complete replacement of pCSacB with pRibo-T is further verified by a three-primer diagnostic PCR. A primer can be extended across the T1 linker in the presence of ddCTP terminator and a primer can be extended across the T2 linker in the presence of ddGTP terminator. DNA-agarose gels can be used to analyze the extent of primer extension and amplification. Third, agarose gel electrophoresis of total RNA prepared from SQ171fg cells expressing WT ribosomes and Ribo-T are carried out an analyzed. rRNA extracted from isolated WT ribosomes or Ribo-T can be assessed in a denaturing (4% - 8%) polyacrylamide gel. Model gels representing untethered and tethered controls can be found in the original manuscript, “Protein synthesis with tethered ribosomes”. Total RNA gels represent the key determinate of successful subunit tethering. Lastly, to confirm tethering structurally, sucrose gradient fractionations of polysomes prepared from cells expressing WT ribosomes and Ribo-T are carried out. Sucrose gradient analysis is carried out under 15 mM MgCl2 or 1.5 mM MgCl2 (dissociating) conditions. The position of the peaks corresponding to separate (50S and 30S) and tethered (70S and Ribo-T) ribosomes are analyzed under both conditions. In low magnesium conditions (1.5 mM MgCl2), untethered ribosomes dissociate, forming separate 50S and 30S subunits. If Ribo-T variants are indeed tethered, a single major shifted peak at 65S will remain under 1.5 mM MgCl2 conditions.

When characterizing activity of the tethered ribosomes, protein synthesis and translation rates can be assessed. *In vivo* protein synthesis rates can be probed in SQ171fg cells expressing wild-type ribosomes or Ribo-T. Protein synthesis is measured by quantifying the incorporation of

[^{35}S] L-methionine into TCA-insoluble protein fractions during incubation at 37C in minimal medium. Subsequently, 2D gel electrophoresis analysis of the proteins expressed in exponentially growing SQ171fg cells with WT or Ribo-T constructs can be carried out. *In vitro* translation rates can be measured using the PURExpress system supplemented with purified WT or Ribo-T ribosomes and [^{35}S] L-methionine. The respective ribosomes are introduced into *in vitro* transcription-translation reactions, and probed for dihydrofolate reductase (DHFR) protein synthesis. SDS-PAGE analysis can be used to assess the quantity and quality of protein synthesized. Rates of translation can be determined from the initial slopes. Finally, a deep biochemical probing of Ribo-T translation can be probed using toe-printing assays. Toeprinting analysis of translation of a 20-codon synthetic gene, RST1, can be carried out to assess ribosome initiation arrests. The position of toeprint bands represent where ribosome variants initiate and stop translation.

Key feature unique to our technique: One essential requirement in the tethered ribosome system is the need to validate the preservation of an intact tether. An RNA extraction from the Squires strain possessing Ribo-T permits the visualization of the tether's status. This step is unique to Ribo-T, as it confirms that the tether is not cleaved, and Ribo-T indeed remains tethered.

Using o-RiboT: A core application of this protocol is the effective translation of orthogonal genes by orthogonal Ribo-T (oRibo-T) *in vivo* and *in vitro*. To accomplish this, we express an orthogonal *sf-GFP* reporter in *E. coli* cells transformed with pAM552 plasmid encoding WT rRNA, and pAM552 with an orthogonal SD sequence in 16S rRNA of a non-tethered ribosome (oRbs) or poRibo-T1 expressing an orthogonal Ribo-T. Cells lacking a GFP reporter should be used as a background fluorescence control.

Key feature unique to our technique: With our fully-orthogonal tethered ribosome, one can, for the first time evolve the ribosomal active site in the context both subunits. Exploring the role of ribosomal active site mutations has thus far been difficult because of the lethal nature of peptidyl transferase center (PTC) mutations. We demonstrated active site evolution with our system by evolving key PTC nucleotides to bypass peptide stalling and arrest. A similar strategy can be carried out for other active site evolution goals, including: antibiotic resistance, unique monomer incorporation, abiological polymer synthesis, and more.

Applications and target audience: Tethered ribosomes, such as Ribo-T, currently represent the only method for synthesizing, engineering, and studying fully orthogonal ribosomes both *in vitro* and *in vivo*. This innovative and accessible protocol permits applications in basic biology as well as synthetic biology and engineering. Importantly, our approach allows, for the first time, an *in vivo* method for probing and evolving dominant lethal nucleotide mutations in the ribosome's active site (the peptidyl transferase center), as well as the only fully orthogonal *in vivo* system that can be evolved and leveraged for novel functions without interfering with native translation.

For example, one main use may be to probe the ribosome's active site for novel antibiotic resistance mutations. Furthermore, other basic biological discoveries can be made with this platform. These include, but are not limited to, characterizing nucleotides involved in peptide stalling, probing necessity and sufficiency of helices, and deeper characterization of ribosome initiation and decoding. Engineers will find our platform especially appealing, as it represents the only resource for evolving a ribosome for new functions in the context of both the large and small subunits. Importantly, scaling up the synthesis of novel tethered ribosomes and/or the products

they synthesize can easily be achieved with this *in vivo* platform. Researchers who will find our method of interest include synthetic biologists, ribosome biochemists, and molecular biologists.

Advantages, limitations and adaptations: The random exchange of ribosomal subunits between recurrent acts of protein biosynthesis presents an obstacle for making fully orthogonal ribosomes, a task with important implications for fundamental science, bioengineering, and synthetic biology. Previously, it was possible to redirect a subpopulation of the small ribosomal subunits from translating indigenous mRNAs to instead translating a specific mRNA by placing an alternative Shine–Dalgarno sequence in a reporter mRNA and introducing the complementary changes in the anti-Shine–Dalgarno region in 16S rRNA, which enabled selection of mutant 30S subunits with new decoding properties. However, because large subunits freely exchange between native and orthogonal small subunits, creating a fully orthogonal ribosome has been impossible, thereby limiting the engineering of the 50S subunit, including the peptidyl transferase center (PTC) and the nascent peptide exit tunnel, for specialized new properties.

By linking the small and large subunit rRNA into a continuous molecule, our tethered ribosome technique achieves full orthogonality of the entire ribosomal core rRNA (both small and large subunits) for *in vivo* ribosome engineering.

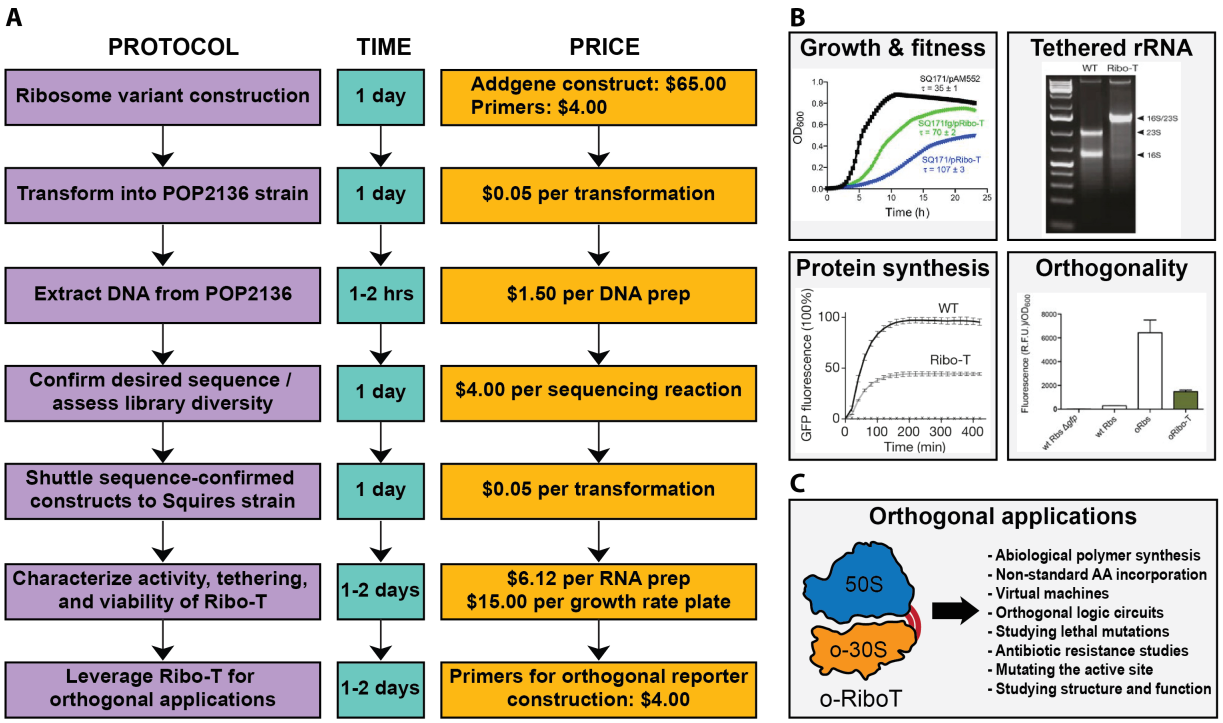

Figure 8.6 An efficient and low cost workflow permits Ribo-T designs to be readily built, tested, characterized, and leveraged for orthogonal applications. **(**a) The workflow time and cost of designing, building, and characterizing Ribo-T variants. (b) Standard characterization assays for Ribo-T *in vitro* and *in vivo*. (c) Orthogonal applications of Ribo-T.

8.5 Giving back to the scientific and broader community

Giving back to the scientific and broader community through scientific communication, outreach, education, and mentorship is a key aspect of any dissertation work. The dissertation marks the transition from a student to a scholar; and as part of a scholar's responsibility, one must train, teach, mentor and give back to the community that supported their own education and scholarly growth.

During a PhD, you are asked to focus in on an extremely narrow subject. You are asked to immerse yourself in this narrow subject, study everything about this narrow subject, and become

an expert on this narrow subject. This is very important; however, it is equally important to not lose sight of the larger community and world around you.

With these two items in mind, I have compiled a brief non-comprehensive list of some of the ways that I have found greater meaning in my work by sharing my knowledge and mentorship with the greater Chicago community. I hope that future graduate students might find inspiration in these opportunities and either contribute to one of these programs, or begin their own unique outreach and mentoring efforts.

- Jugando Con La Ciencia
- Northwestern HerStory
- Mentorship Opportunities for Research Engagement (MORE)
- Northwestern's Prison Education Program (NPEP)
- BioBuilder
- Research Experience for Teachers (RET)
- The TRiO Program
- Mentoring and undergraduate student or high school student
- MSI Jr. Science Cafes
- MSI Science Works

"When you learn, teach. When you get, give." – Maya Angelou

REFERENCES

1 Kaczanowska, M. & Rydén-Aulin, M. Ribosome biogenesis and the translation process in Escherichia coli. *Microbiology and Molecular Biology Reviews* **71**, 477-494 (2007).

2 Shajani, Z., Sykes, M. T. & Williamson, J. R. Assembly of bacterial ribosomes. *Annu Rev Biochem* **80**, 501-526, doi:10.1146/annurev-biochem-062608-160432 (2011).

3 Bremer, H. & Dennis, P. Modulation of Chemical Composition and Other Parameters of the Cell at Different Exponential Growth Rates. *EcoSal Plus*, doi:doi:10.1128/ecosal.5.2.3 (2008).

4 Parker, J. Errors and alternatives in reading the universal genetic code. *Microbiological Reviews* **53**, 273-298 (1989).

5 Brosius, J., Palmer, M. L., Kennedy, P. J. & Noller, H. F. Complete nucleotide sequence of a 16S ribosomal RNA gene from Escherichia coli. *Proceedings of the National Academy of Sciences of the United States of America* **75**, 4801-4805 (1978).

6 Brosius, J., Dull, T. J. & Noller, H. F. Complete nucleotide sequence of a 23S ribosomal RNA gene from Escherichia coli. *Proceedings of the National Academy of Sciences of the United States of America* **77**, 201-204 (1980).

7 Brownlee, G. G., Sanger, F. & Barrell, B. G. Nucleotide sequence of 5S-ribosomal RNA from Escherichia coli. *Nature* **215**, 735-736 (1967).

8 Kruger, K. *et al.* Self-splicing RNA: autoexcision and autocyclization of the ribosomal RNA intervening sequence of Tetrahymena. *Cell* **31**, 147-157 (1982).

9 Zaug, A. J., Grabowski, P. J. & Cech, T. R. Autocatalytic cyclization of an excised intervening sequence RNA is a cleavage-ligation reaction. *Nature* **301**, 578-583 (1983).

10 Green, R. & Noller, H. F. Ribosomes and translation. *Annu Rev Biochem* **66**, 679-716, doi:10.1146/annurev.biochem.66.1.679 (1997).

11 Nissen, P., Hansen, J., Ban, N., Moore, P. B. & Steitz, T. A. The Structural Basis of Ribosome Activity in Peptide Bond Synthesis. *Science* **289**, 920-930 (2000).

12 Gray, M. W., Burger, G. & Lang, B. F. Mitochondrial evolution. *Science* **283**, 1476-1481 (1999).

13 Gongadze, G. M. 5S rRNA and ribosome. *Biochemistry (Moscow)* **76**, 1450-1464, doi:10.1134/s0006297911130062 (2011).

14 Shine, J. & Dalgarno, L. The 3'-Terminal Sequence of Escherichia coli 16S Ribosomal RNA: Complementarity to Nonsense Triplets and Ribosome Binding Sites. *Proceedings of the National Academy of Sciences* **71**, 1342-1346 (1974).

15 Qin, D., Abdi, N. M. & Fredrick, K. Characterization of 16S rRNA mutations that decrease the fidelity of translation initiation. *Rna* **13**, 2348-2355, doi:10.1261/rna.715307 (2007).

16 Carter, A. P. *et al.* Functional insights from the structure of the 30S ribosomal subunit and its interactions with antibiotics. *Nature* **407**, 340-348, doi:10.1038/35030019 (2000).

17 Kimura, S. & Suzuki, T. Fine-tuning of the ribosomal decoding center by conserved methyl-modifications in the Escherichia coli 16S rRNA. *Nucleic Acids Res* **38**, 1341-1352, doi:10.1093/nar/gkp1073 (2010).

18 Welch, M., Chastang, J. & Yarus, M. An Inhibitor of Ribosomal Peptidyl Transferase Using the Transition-State Analogy. *Biochemistry* **34**, 385-390, doi:10.1021/bi00002a001 (1995).

19 Hardy, S. J. The stoichiometry of the ribosomal proteins of Escherichia coli. *Mol Gen Genet* **140**, 253-274 (1975).

20 Wilson, D. N. & Nierhaus, K. H. Ribosomal proteins in the spotlight. *Crit Rev Biochem Mol Biol* **40**, 243-267, doi:10.1080/10409230500256523 (2005).

21 Gregory, S. T. & Dahlberg, A. E. Erythromycin resistance mutations in ribosomal proteins L22 and L4 perturb the higher order structure of 23 S ribosomal RNA. *J Mol Biol* **289**, 827-834, doi:10.1006/jmbi.1999.2839 (1999).

22 Ozaki, M., Mizushima, S. & Nomura, M. Identification and Functional Characterization of the Protein controlled by the Streptomycin-resistant Locus in E. coli. *Nature* **222**, 333-339 (1969).

23 Hampl, H., Schulze, H. & Nierhaus, K. H. Ribosomal components from Escherichia coli 50 S subunits involved in the reconstitution of peptidyltransferase activity. *Journal of Biological Chemistry* **256**, 2284-2288 (1981).

24 Dabbs, E. R. Selection for Escherichia coli mutants with proteins missing from the ribosome. *J Bacteriol* **140**, 734-737 (1979).

25 Shoji, S., Dambacher, C. M., Shajani, Z., Williamson, J. R. & Schultz, P. G. Systematic chromosomal deletion of bacterial ribosomal protein genes. *J Mol Biol* **413**, 751-761, doi:10.1016/j.jmb.2011.09.004 (2011).

26 Khaitovich, P., Mankin, A. S., Green, R., Lancaster, L. & Noller, H. F. Characterization of functionally active subribosomal particles from Thermus aquaticus. *Proceedings of the National Academy of Sciences* **96**, 85-90, doi:10.1073/pnas.96.1.85 (1999).

27 Wower, J., Hixson, S. S. & Zimmermann, R. A. Photochemical cross-linking of yeast tRNAPhe containing 8-azidoadenosine at positions 73 and 76 to the Escherichia coli ribosome. *Biochemistry* **27**, 8114-8121, doi:10.1021/bi00421a021 (1988).

28 Eilat, D. A. N. *et al.* Affinity labelling the acceptor site of the peptidyl transferase centre of the Escherichia coli ribosome. *Nature* **250**, 514-516 (1974).

29 Abdurashidova, G. G., Tsvetkova, E. A. & Budowsky, E. I. Direct tRNA-protein interactions in ribosomal complexes. *Nucleic Acids Research* **19**, 1909-1915, doi:10.1093/nar/19.8.1909 (1991).

30 Schulze, H. & Nierhaus, K. H. Minimal set of ribosomal components for reconstitution of the peptidyltransferase activity. *The EMBO journal* **1**, 609-613 (1982).

31 Khaitovich, P. & Mankin, A. S. in *The Ribosome* (American Society of Microbiology, 2000).

32 Hockenberry, A. J., Pah, A. R., Jewett, M. C. & Amaral, L. A. N. Leveraging genome-wide datasets to quantify the functional role of the anti-Shine–Dalgarno sequence in regulating translation efficiency. *Open Biology* **7**, 160239, doi:10.1098/rsob.160239 (2017).

33 Hockenberry, A. J., Pah, A. R., Jewett, M. C. & Amaral, L. A. N. Defining the anti-Shine-Dalgarno sequence interaction and quantifying its functional role in regulating translation efficiency. *bioRxiv* (2016).

34 Steitz, J. A. & Jakes, K. How ribosomes select initiator regions in mRNA: base pair formation between the 3' terminus of 16S rRNA and the mRNA during initiation of protein synthesis in Escherichia coli. *Proceedings of the National Academy of Sciences* **72**, 4734-4738 (1975).

35 Kenner, R. A. A protein-nucleic acid crosslink in 30S ribosomes. *Biochemical and biophysical research communications* **51**, 932-938 (1973).

36 Held, W. A., Gette, W. R. & Nomura, M. Structure and function of bacterial ribosomes. 24. Role of 16S ribosomal ribonucleic acid and the 30S ribosomal protein S12 in the initiation of natural messenger ribonucleic acid translation. *Biochemistry* **13**, 2115-2122, doi:10.1021/bi00707a019 (1974).

37 de Boer, H. A., Hui, A., Comstock, L. J., Wong, E. & Vasser, M. Portable Shine-Dalgarno regions: a system for a systematic study of defined alterations of nucleotide sequences within E. coli ribosome binding sites. *DNA (Mary Ann Liebert, Inc.)* **2**, 231-235, doi:10.1089/dna.1983.2.231 (1983).

38 Rodnina, M. V., Daviter, T., Gromadski, K. & Wintermeyer, W. Structural dynamics of ribosomal RNA during decoding on the ribosome. *Biochimie* **84**, 745-754, doi:http://dx.doi.org/10.1016/S0300-9084(02)01409-8 (2002).

39 Yusupov, M. M. *et al.* Crystal Structure of the Ribosome at 5.5 Å Resolution. *Science* **292**, 883-896, doi:10.1126/science.1060089 (2001).

40 Marquez, V., Wilson, D. N., Tate, W. P., Triana-Alonso, F. & Nierhaus, K. H. Maintaining the ribosomal reading frame: the influence of the E site during translational regulation of release factor 2. *Cell* **118**, 45-55, doi:10.1016/j.cell.2004.06.012 (2004).

41 Traub, P. & Nomura, M. Structure and function of E. coli ribosomes. V. Reconstitution of functionally active 30S ribosomal particles from RNA and proteins. *Proceedings of the National Academy of Sciences of the United States of America* **59**, 777-784 (1968).

42 Culver, G. M. & Noller, H. F. Efficient reconstitution of functional Escherichia coli 30S ribosomal subunits from a complete set of recombinant small subunit ribosomal proteins. *Rna* **5**, 832-843 (1999).

43 Maki, J. A. & Culver, G. M. Recent developments in factor-facilitated ribosome assembly. *Methods* **36**, 313-320, doi:10.1016/j.ymeth.2005.04.008 (2005).

44 Nierhaus, K. H. & Dohme, F. Total Reconstitution of Functionally Active 50S Ribosomal Subunits from Escherichia coli. *Proceedings of the National Academy of Sciences of the United States of America* **71**, 4713-4717 (1974).

45 Herold, M. & Nierhaus, K. H. Incorporation of six additional proteins to complete the assembly map of the 50 S subunit from Escherichia coli ribosomes. *The Journal of biological chemistry* **262**, 8826-8833 (1987).

46 Green, R. & Noller, H. F. In vitro complementation analysis localizes 23S rRNA posttranscriptional modifications that are required for Escherichia coli 50S ribosomal subunit assembly and function. *Rna* **2**, 1011-1021 (1996).

47 Erlacher, M. D., Chirkova, A., Voegele, P. & Polacek, N. Generation of chemically engineered ribosomes for atomic mutagenesis studies on protein biosynthesis. *Nature protocols* **6**, 580-592, doi:10.1038/nprot.2011.306 (2011).

48 Nierhaus, K. H. *Reconstitution of ribosomes, in Ribosomes and Protein Synthesis, A Practical Approach*. (Oxford University Press, 1990).

49 Polacek, N. The ribosome meets synthetic biology. *Chembiochem* **12**, 2122-2124, doi:10.1002/cbic.201100259 (2011).

50 Semrad, K. & Green, R. Osmolytes stimulate the reconstitution of functional 50S ribosomes from in vitro transcripts of Escherichia coli 23S rRNA. *Rna* **8**, 401-411 (2002).

51 Jewett, M. C., Fritz, B. R., Timmerman, L. E. & Church, G. M. In vitro integration of ribosomal RNA synthesis, ribosome assembly, and translation. *Mol Syst Biol* **9**, 678, doi:10.1038/msb.2013.31 (2013).

52 Fritz, B. R. & Jewett, M. C. The impact of transcriptional tuning on in vitro integrated rRNA transcription and ribosome construction. *Nucleic Acids Res* **42**, 6774-6785, doi:10.1093/nar/gku307 (2014).

53 Fritz, B. R., Jamil, O. K. & Jewett, M. C. Implications of macromolecular crowding and reducing conditions for in vitro ribosome construction. *Nucleic Acids Res* (2015).

54 Forster, A. C. & Church, G. M. Towards synthesis of a minimal cell. *Mol Syst Biol* **2**, 45, doi:10.1038/msb4100090 (2006).

55 Jewett, M. C. & Forster, A. C. Update on designing and building minimal cells. *Current opinion in biotechnology* **21**, 697-703, doi:10.1016/j.copbio.2010.06.008 (2010).

56 Shimizu, Y. *et al.* Cell-free translation reconstituted with purified components. *Nat Biotechnol* **19**, 751-755, doi:10.1038/90802
90802 [pii] (2001).
57 Li, J., Wassie, B. & Church, G. M. Physiological Assembly Of Functionally Active 30S Ribosomal Subunits From In Vitro Synthesized Parts. *bioRxiv*, doi:10.1101/137745 (2017).
58 Prince, J. B., Taylor, B. H., Thurlow, D. L., Ofengand, J. & Zimmermann, R. A. Covalent crosslinking of tRNA1Val to 16S RNA at the ribosomal P site: identification of crosslinked residues. *Proceedings of the National Academy of Sciences* **79**, 5450-5454 (1982).
59 Wower, J., Hixson, S. S. & Zimmermann, R. A. Labeling the peptidyltransferase center of the Escherichia coli ribosome with photoreactive tRNA(Phe) derivatives containing azidoadenosine at the 3' end of the acceptor arm: a model of the tRNA-ribosome complex. *Proceedings of the National Academy of Sciences of the United States of America* **86**, 5232-5236 (1989).
60 Sato, N. S., Hirabayashi, N., Agmon, I., Yonath, A. & Suzuki, T. Comprehensive genetic selection revealed essential bases in the peptidyl-transferase center. *Proceedings of the National Academy of Sciences* **103**, 15386-15391, doi:10.1073/pnas.0605970103 (2006).
61 Yassin, A. & Mankin, A. S. Potential new antibiotic sites in the ribosome revealed by deleterious mutations in RNA of the large ribosomal subunit. *The Journal of biological chemistry* **282**, 24329-24342, doi:10.1074/jbc.M703106200 (2007).
62 Hui, A. & de Boer, H. A. Specialized ribosome system: preferential translation of a single mRNA species by a subpopulation of mutated ribosomes in Escherichia coli. *Proceedings of the National Academy of Sciences of the United States of America* **84**, 4762-4766 (1987).
63 Leonov, A. A., Sergiev, P. V., Bogdanov, A. A., Brimacombe, R. & Dontsova, O. A. Affinity purification of ribosomes with a lethal G2655C mutation in 23 S rRNA that affects the translocation. *The Journal of biological chemistry* **278**, 25664-25670, doi:10.1074/jbc.M302873200 (2003).
64 Youngman, E. M., Brunelle, J. L., Kochaniak, A. B. & Green, R. The Active Site of the Ribosome Is Composed of Two Layers of Conserved Nucleotides with Distinct Roles in Peptide Bond Formation and Peptide Release. *Cell* **117**, 589-599, doi:10.1016/S0092-8674(04)00411-8.
65 Ederth, J., Mandava, C. S., Dasgupta, S. & Sanyal, S. A single-step method for purification of active His-tagged ribosomes from a genetically engineered Escherichia coli. *Nucleic Acids Research* **37**, e15-e15, doi:10.1093/nar/gkn992 (2009).
66 Asai, T., Zaporojets, D., Squires, C. & Squires, C. L. An Escherichia coli strain with all chromosomal rRNA operons inactivated: complete exchange of rRNA genes between bacteria. *Proc Natl Acad Sci U S A* **96**, 1971-1976 (1999).
67 Vázquez-Laslop, N., Ramu, H., Klepacki, D., Kannan, K. & Mankin, A. S. The key function of a conserved and modified rRNA residue in the ribosomal response to the nascent peptide. *The EMBO journal* **29**, 3108-3117, doi:10.1038/emboj.2010.180 (2010).
68 Sahu, B., Khade, P. K. & Joseph, S. Functional Replacement of Two Highly Conserved Tetraloops in the Bacterial Ribosome(). *Biochemistry* **51**, 7618-7626, doi:10.1021/bi300930r (2012).
69 Burakovsky, D. E. *et al.* Mutations at the accommodation gate of the ribosome impair RF2-dependent translation termination. *Rna* **16**, 1848-1853, doi:10.1261/rna.2185710 (2010).
70 Davis, L. & Chin, J. W. Designer proteins: applications of genetic code expansion in cell biology. *Nature reviews Molecular cell biology* **13**, 168-182 (2012).
71 Dumas, A., Lercher, L., Spicer, C. D. & Davis, B. G. Designing logical codon reassignment–expanding the chemistry in biology. *Chemical Science* **6**, 50-69 (2015).

72 Forster, A. C. *et al.* Programming peptidomimetic syntheses by translating genetic codes designed de novo. *Proceedings of the National Academy of Sciences* **100**, 6353-6357 (2003).
73 O'donoghue, P., Ling, J., Wang, Y.-S. & Söll, D. Upgrading protein synthesis for synthetic biology. *Nature chemical biology* **9**, 594-598 (2013).
74 Wang, L., Brock, A., Herberich, B. & Schultz, P. G. Expanding the Genetic Code of Escherichia coli. *Science* **292**, 498 (2001).
75 Wang, L., Xie, J. & Schultz, P. G. Expanding the genetic code. *Annu. Rev. Biophys. Biomol. Struct.* **35**, 225-249 (2006).
76 Rackham, O. & Chin, J. W. Cellular Logic with Orthogonal Ribosomes. *Journal of the American Chemical Society* **127**, 17584-17585, doi:10.1021/ja055338d (2005).
77 Rackham, O. & Chin, J. W. A network of orthogonal ribosome· mRNA pairs. *Nature chemical biology* **1**, 159-166 (2005).
78 Neumann, H., Wang, K., Davis, L., Garcia-Alai, M. & Chin, J. W. Encoding multiple unnatural amino acids via evolution of a quadruplet-decoding ribosome. *Nature* **464**, 441-444, doi:http://www.nature.com/nature/journal/v464/n7287/suppinfo/nature08817_S1.html (2010).
79 Zhang, Y. *et al.* A semi-synthetic organism that stores and retrieves increased genetic information. *Nature* **551**, 644, doi:10.1038/nature24659 https://www.nature.com/articles/nature24659#supplementary-information (2017).
80 Davis, L. & Chin, J. W. Designer proteins: applications of genetic code expansion in cell biology. *Nature reviews. Molecular cell biology* **13**, 168-182, doi:10.1038/nrm3286 (2012).
81 Forster, A. C. *et al.* Programming peptidomimetic syntheses by translating genetic codes designed de novo. *Proc Natl Acad Sci U S A* **100**, 6353-6357, doi:10.1073/pnas.1132122100 (2003).
82 O'Donoghue, P., Ling, J., Wang, Y. S. & Soll, D. Upgrading protein synthesis for synthetic biology. *Nat Chem Biol* **9**, 594-598, doi:10.1038/nchembio.1339 (2013).
83 Fahnestock, S. & Rich, A. Ribosome-catalyzed polyester formation. *Science* **173**, 340-343 (1971).
84 Ohta, A., Murakami, H., Higashimura, E. & Suga, H. Synthesis of polyester by means of genetic code reprogramming. *Chem Biol* **14**, 1315-1322, doi:S1074-5521(07)00370-5 [pii] 10.1016/j.chembiol.2007.10.015 (2007).
85 Ohta, A., Murakami, H. & Suga, H. Polymerization of alpha-hydroxy acids by ribosomes. *Chembiochem* **9**, 2773-2778, doi:10.1002/cbic.200800439 (2008).
86 Ellman, J. A., Mendel, D. & Schultz, P. G. Site-specific incorporation of novel backbone structures into proteins. *Science* **255**, 197-200 (1992).
87 Kawakami, T., Murakami, H. & Suga, H. Ribosomal synthesis of polypeptoids and peptoid-peptide hybrids. *J Am Chem Soc* **130**, 16861-16863, doi:10.1021/ja806998v (2008).
88 Guo, J., Wang, J., Anderson, J. C. & Schultz, P. G. Addition of an alpha-hydroxy acid to the genetic code of bacteria. *Angew Chem Int Ed* **47**, 722-725 (2008).
89 Subtelny, A. O., Hartman, M. C. T. & Szostak, J. W. Ribosomal synthesis of n-methyl peptides. *Journal of the American Chemical Society* **130**, 6131-6136, doi:10.1021/ja710016v (2008).
90 Englander, M. T. *et al.* The ribosome can discriminate the chirality of amino acids within its peptidyl-transferase center. *Proc Natl Acad Sci USA* **112**, 6038-6043, doi:10.1073/pnas.1424712112 (2015).
91 Dedkova, L. M. *et al.* beta-Puromycin selection of modified ribosomes for in vitro incorporation of beta-amino acids. *Biochemistry* **51**, 401-415, doi:10.1021/bi2016124 (2012).

92 Maini, R. *et al.* Incorporation of beta-amino acids into dihydrofolate reductase by ribosomes having modifications in the peptidyltransferase center. *Bioorg Med Chem* **21**, 1088-1096, doi:10.1016/j.bmc.2013.01.002 (2013).

93 Maini, R. *et al.* Protein Synthesis with Ribosomes Selected for the Incorporation of β-Amino Acids. *Biochemistry*, doi:10.1021/acs.biochem.5b00389 (2015).

94 Ohta, A., Yamagishi, Y. & Suga, H. Synthesis of biopolymers using genetic code reprogramming. *Current Opinion in Chemical Biology* **12**, 159-167, doi:10.1016/j.cbpa.2007.12.009 (2008).

95 Wu, N., Deiters, A., Cropp, T. A., King, D. & Schultz, P. G. A genetically encoded photocaged amino acid. *Journal of the American Chemical Society* **126**, 14306-14307, doi:10.1021/ja040175z (2004).

96 Summerer, D. *et al.* A genetically encoded fluorescent amino acid. *Proceedings of the National Academy of Sciences of the United States of America* **103**, 9785-9789, doi:10.1073/pnas.0603965103 (2006).

97 Chin, J. W., Martin, A. B., King, D. S., Wang, L. & Schultz, P. G. Addition of a photocrosslinking amino acid to the genetic code of Escherichiacoli. *Proceedings of the National Academy of Sciences of the United States of America* **99**, 11020-11024, doi:10.1073/pnas.172226299 (2002).

98 Chin, J. W. *et al.* Addition of p-azido-L-phenylalanine to the genetic code of Escherichia coli. *Journal of the American Chemical Society* **124**, 9026-9027, doi:10.1021/ja027007w (2002).

99 Liu, C. C. & Schultz, P. G. Adding new chemistries to the genetic code. *Annu. Rev. Biochem.* **79**, 413-444, doi:doi:10.1146/annurev.biochem.052308.105824 (2010).

100 Neumann, H. *et al.* A method for genetically installing site-specific acetylation in recombinant histones defines the effects of H3 K56 acetylation. *Mol Cell* **36**, 153-163, doi:10.1016/j.molcel.2009.07.027 (2009).

101 Lee, S. *et al.* A facile strategy for selective incorporation of phosphoserine into histones. *Angewandte Chemie* **52**, 5771-5775, doi:10.1002/anie.201300531 (2013).

102 Hubbell, J. A. Drug development: Longer-lived proteins. *Nature* **467**, 1051-1052, doi:10.1038/4671051a (2010).

103 Wals, K. & Ovaa, H. Unnatural amino acid incorporation in E. coli: current and future applications in the design of therapeutic proteins. *Frontiers in chemistry* **2**, 15, doi:10.3389/fchem.2014.00015 (2014).

104 Zimmerman, E. S. *et al.* Production of site-specific antibody–drug conjugates using optimized non-natural amino acids in a cell-free expression system. *Bioconjug. Chem.* **25**, 351-361, doi:10.1021/bc400490z (2014).

105 Cohen, P. Protein kinases--the major drug targets of the twenty-first century? *Nature reviews. Drug discovery* **1**, 309-315, doi:10.1038/nrd773 (2002).

106 Pray, L. A. Gleevec: the breakthrough in cancer treatment. *Nature Education* **1**, 37 (2008).

107 Ramos, J. W. Cancer research center hotline: PEA-15 phosphoprotein: a potential cancer drug target. *Hawaii medical journal* **64**, 77-80 (2005).

108 Voronkov, M., Braithwaite, S. P. & Stock, J. B. Phosphoprotein phosphatase 2A: a novel druggable target for Alzheimer's disease. *Future medicinal chemistry* **3**, 821-833, doi:10.4155/fmc.11.47 (2011).

109 Krishnamoorthy, S. *et al.* A Novel Phosphopeptide Microarray Based Interactome Map in Breast Cancer Cells Reveals Phosphoprotein-GRB2 Cell Signaling Networks. *PLoS One* **8**, e67634, doi:10.1371/journal.pone.0067634 (2013).

110 Axup, J. Y. *et al.* Synthesis of site-specific antibody-drug conjugates using unnatural amino acids. *Proceedings of the National Academy of Sciences of the United States of America* **109**, 16101-16106, doi:10.1073/pnas.1211023109 (2012).

111 Cho, H. *et al.* Optimized clinical performance of growth hormone with an expanded genetic code. *Proc. Natl. Acad. Sci. U. S. A.* **108**, 9060-9065, doi:10.1073/pnas.1100387108 (2011).

112 Romano, N. H., Sengupta, D., Chung, C. & Heilshorn, S. C. Protein-engineered biomaterials: nanoscale mimics of the extracellular matrix. *Biochimica et biophysica acta* **1810**, 339-349, doi:10.1016/j.bbagen.2010.07.005 (2011).

113 Zhong, Z., Yang, H., Zhang, C. & Lewis, J. C. Synthesis and Catalytic Activity of Amino Acids and Metallopeptides with Catalytically Active Metallocyclic Side Chains. *Organometallics* **31**, 7328-7331, doi:10.1021/om300848p (2012).

114 Albayrak, C. & Swartz, J. R. Direct polymerization of proteins. *ACS Synth Biol* **3**, 353-362, doi:10.1021/sb400116x (2014).

115 Hoesl, M. G. & Budisa, N. Recent advances in genetic code engineering in *Escherichia coli*. *Curr. Opin. Biotechnol.* **23**, 751-757, doi:10.1016/j.copbio.2011.12.027 (2012).

116 Des Soye, B. J., Patel, J. R., Isaacs, F. J. & Jewett, M. C. Repurposing the translation apparatus for synthetic biology. *Curr Opin Chem Biol* **28**, 83-90, doi:10.1016/j.cbpa.2015.06.008 (2015).

117 Quast, R. B., Mrusek, D., Hoffmeister, C., Sonnabend, A. & Kubick, S. Cotranslational incorporation of non-standard amino acids using cell-free protein synthesis. *FEBS letters* **589**, 1703-1712, doi:10.1016/j.febslet.2015.04.041 (2015).

118 Czekster, C. M., Robertson, W. E., Walker, A. S., Söll, D. & Schepartz, A. In vivo biosynthesis of a β-amino acid-containing protein. *J. Am. Chem. Soc* **138**, 5194-5197 (2016).

119 Rogerson, D. T. *et al.* Efficient genetic encoding of phosphoserine and its nonhydrolyzable analog. *Nature chemical biology* **11**, 496-503 (2015).

120 Gallagher, R. R., Li, Z., Lewis, A. O. & Isaacs, F. J. Rapid editing and evolution of bacterial genomes using libraries of synthetic DNA. *Nature protocols* **9**, 2301-2316, doi:10.1038/nprot.2014.082 (2014).

121 Wang, H. H. *et al.* Programming cells by multiplex genome engineering and accelerated evolution. *Nature* **460**, 894-898, doi:10.1038/nature08187 (2009).

122 Amiram, M. *et al.* Evolution of translation machinery in recoded bacteria enables multi-site incorporation of nonstandard amino acids. *Nature biotechnology* **33**, 1272-1279 (2015).

123 Murakami, H., Ohta, A., Goto, Y., Sako, Y. & Suga, H. in *Nucleic Acids Symposium Series.* 35-36 (Oxford University Press).

124 Goto, Y., Katoh, T. & Suga, H. Flexizymes for genetic code reprogramming. *Nature protocols* **6**, 779-790 (2011).

125 Niwa, N., Yamagishi, Y., Murakami, H. & Suga, H. A flexizyme that selectively charges amino acids activated by a water-friendly leaving group. *Bioorganic & medicinal chemistry letters* **19**, 3892-3894 (2009).

126 Ohuchi, M., Murakami, H. & Suga, H. The flexizyme system: a highly flexible tRNA aminoacylation tool for the translation apparatus. *Current opinion in chemical biology* **11**, 537-542 (2007).

127 Hipolito, C. J. & Suga, H. Ribosomal production and in vitro selection of natural product-like peptidomimetics: the FIT and RaPID systems. *Current opinion in chemical biology* **16**, 196-203 (2012).

128 Ohshiro, Y. *et al.* Ribosomal Synthesis of Backbone-Macrocyclic Peptides Containing γ-Amino Acids. *ChemBioChem* **12**, 1183-1187 (2011).

129 Ohta, A., Murakami, H., Higashimura, E. & Suga, H. Synthesis of polyester by means of genetic code reprogramming. *Chemistry & biology* **14**, 1315-1322 (2007).

130 Ohta, A., Murakami, H. & Suga, H. Polymerization of α-Hydroxy Acids by Ribosomes. *ChemBioChem* **9**, 2773-2778 (2008).

131 Sako, Y., Goto, Y., Murakami, H. & Suga, H. Ribosomal synthesis of peptidase-resistant peptides closed by a nonreducible inter-side-chain bond. *ACS chemical biology* **3**, 241-249 (2008).
132 Sako, Y., Morimoto, J., Murakami, H. & Suga, H. Ribosomal synthesis of bicyclic peptides via two orthogonal inter-side-chain reactions. *Journal of the American Chemical Society* **130**, 7232-7234 (2008).
133 Fujino, T., Goto, Y., Suga, H. & Murakami, H. Ribosomal Synthesis of Peptides with Multiple β-Amino Acids. *Journal of the American Chemical Society* **138**, 1962-1969, doi:10.1021/jacs.5b12482 (2016).
134 Katoh, T., Tajima, K. & Suga, H. Consecutive Elongation of D-Amino Acids in Translation. *Cell chemical biology* **24**, 46-54 (2017).
135 Kawakami, T., Murakami, H. & Suga, H. Messenger RNA-programmed incorporation of multiple N-methyl-amino acids into linear and cyclic peptides. *Chemistry & biology* **15**, 32-42 (2008).
136 Katoh, T., Iwane, Y. & Suga, H. Logical engineering of D-arm and T-stem of tRNA that enhances d-amino acid incorporation. *Nucleic Acids Res*, doi:10.1093/nar/gkx1129 (2017).
137 Katoh, T., Wohlgemuth, I., Nagano, M., Rodnina, M. V. & Suga, H. Essential structural elements in tRNA(Pro) for EF-P-mediated alleviation of translation stalling. *Nat Commun* **7**, 11657, doi:10.1038/ncomms11657 (2016).
138 Englander, M. T. *et al.* The ribosome can discriminate the chirality of amino acids within its peptidyl-transferase center. *Proceedings of the National Academy of Sciences* **112**, 6038-6043, doi:10.1073/pnas.1424712112 (2015).
139 Park, H.-S. *et al.* Expanding the genetic code of Escherichia coli with phosphoserine. *Science* **333**, 1151-1154 (2011).
140 Melnikov, S. *et al.* Molecular insights into protein synthesis with proline residues. *EMBO reports*, e201642943 (2016).
141 Katoh, T., Wohlgemuth, I., Nagano, M., Rodnina, M. V. & Suga, H. Essential structural elements in tRNAPro for EF-P-mediated alleviation of translation stalling. *Nat Commun* **7**, 11657, doi:10.1038/ncomms11657
https://www.nature.com/articles/ncomms11657#supplementary-information (2016).
142 Doerfel, L. K. *et al.* Entropic Contribution of Elongation Factor P to Proline Positioning at the Catalytic Center of the Ribosome. *Journal of the American Chemical Society* **137**, 12997-13006, doi:10.1021/jacs.5b07427 (2015).
143 Polikanov, Y. S., Steitz, T. A. & Innis, C. A. A proton wire to couple aminoacyl-tRNA accommodation and peptide-bond formation on the ribosome. *Nature structural & molecular biology* **21**, 787-793 (2014).
144 Sievers, A., Beringer, M., Rodnina, M. V. & Wolfenden, R. The ribosome as an entropy trap. *Proceedings of the National Academy of Sciences of the United States of America* **101**, 7897-7901 (2004).
145 Maini, R. *et al.* Protein synthesis with ribosomes selected for the incorporation of β-amino acids. *Biochemistry* **54**, 3694 (2015).
146 Maini, R. *et al.* Ribosome-mediated incorporation of dipeptides and dipeptide analogues into proteins in vitro. *Journal of the American Chemical Society* **137**, 11206-11209 (2015).
147 Maini, R. *et al.* Incorporation of β-amino acids into dihydrofolate reductase by ribosomes having modifications in the peptidyltransferase center. *Bioorganic & medicinal chemistry* **21**, 1088-1096 (2013).

148 Wang, K., Neumann, H., Peak-Chew, S. Y. & Chin, J. W. Evolved orthogonal ribosomes enhance the efficiency of synthetic genetic code expansion. *Nat Biotechnol* **25**, 770-777, doi:10.1038/nbt1314 (2007).

149 Chubiz, L. M. & Rao, C. V. Computational design of orthogonal ribosomes. *Nucleic acids research* **36**, 4038-4046 (2008).

150 Orelle, C. *et al.* Protein synthesis by ribosomes with tethered subunits. *Nature* **524**, 119-124 (2015).

151 Fried, S. D., Schmied, W. H., Uttamapinant, C. & Chin, J. W. Ribosome subunit stapling for orthogonal translation in E. coli. *Angewandte Chemie International Edition* **54**, 12791-12794 (2015).

152 Terasaka, N., Hayashi, G., Katoh, T. & Suga, H. An orthogonal ribosome-tRNA pair via engineering of the peptidyl transferase center. *Nature chemical biology* **10**, 555-557 (2014).

153 Voorhees, R. M., Weixlbaumer, A., Loakes, D., Kelley, A. C. & Ramakrishnan, V. Insights into substrate stabilization from snapshots of the peptidyl transferase center of the intact 70S ribosome. *Nature Structural & Molecular Biology* **16**, 528-533, doi:10.1038/nsmb.1577 (2009).

154 Jenner, L., Demeshkina, N., Yusupova, G. & Yusupov, M. Structural rearrangements of the ribosome at the tRNA proofreading step. *Nature Structural & Molecular Biology* **17**, 1072-1078, doi:10.1038/nsmb.1880 (2010).

155 Maguire, B. A., Beniaminov, A. D., Ramu, H., Mankin, A. S. & Zimmermann, R. A. A protein component at the heart of an RNA machine: the importance of protein l27 for the function of the bacterial ribosome. *Mol Cell* **20**, 427-435, doi:10.1016/j.molcel.2005.09.009 (2005).

156 Wower, I. K., Wower, J. & Zimmermann, R. A. Ribosomal protein L27 participates in both 50 S subunit assembly and the peptidyl transferase reaction. *J Biol Chem* **273**, 19847-19852, doi:10.1074/jbc.273.31.19847 (1998).

157 Polacek, N. & Mankin, A. S. The ribosomal peptidyl transferase center: structure, function, evolution, inhibition. *Crit Rev Biochem Mol Biol* **40**, 285-311, doi:10.1080/10409230500326334 (2005).

158 Kim, D. F. & Green, R. Base-pairing between 23S rRNA and tRNA in the ribosomal A site. *Mol Cell* **4**, 859-864 (1999).

159 Samaha, R. R., Green, R. & Noller, H. F. A base pair between tRNA and 23S rRNA in the peptidyl transferase centre of the ribosome. *Nature* **377**, 309-314, doi:10.1038/377309a0 (1995).

160 Marks, J. *et al.* Context-specific inhibition of translation by ribosomal antibiotics targeting the peptidyl transferase center. *Proceedings of the National Academy of Sciences* **113**, 12150-12155, doi:10.1073/pnas.1613055113 (2016).

161 Beringer, M. & Rodnina, M. V. The Ribosomal Peptidyl Transferase. *Molecular Cell* **26**, 311-321, doi:https://doi.org/10.1016/j.molcel.2007.03.015 (2007).

162 Arenz, S. *et al.* Molecular basis for erythromycin-dependent ribosome stalling during translation of the ErmBL leader peptide. *Nat Commun* **5**, 3501, doi:10.1038/ncomms4501 (2014).

163 Gumbart, J., Schreiner, E., Wilson, Daniel N., Beckmann, R. & Schulten, K. Mechanisms of SecM-Mediated Stalling in the Ribosome. *Biophysical Journal* **103**, 331-341, doi:10.1016/j.bpj.2012.06.005 (2012).

164 Brunelle, J. L., Youngman, E. M., Sharma, D. & Green, R. The interaction between C75 of tRNA and the A loop of the ribosome stimulates peptidyl transferase activity. *RNA* **12**, 33-39, doi:10.1261/rna.2256706 (2006).

165 Green, R., Switzer, C. & Noller, H. F. Ribosome-catalyzed peptide-bond formation with an A-site substrate covalently linked to 23S ribosomal RNA. *Science* **280**, 286-289 (1998).

166 Beringer, M. & Rodnina, M. V. Importance of tRNA interactions with 23S rRNA for peptide bond formation on the ribosome: studies with substrate analogs. *Biol Chem* **388**, 687-691, doi:10.1515/bc.2007.077 (2007).

167 Ogle, J. M., Carter, A. P. & Ramakrishnan, V. Insights into the decoding mechanism from recent ribosome structures. *Trends Biochem Sci* **28**, 259-266, doi:10.1016/s0968-0004(03)00066-5 (2003).

168 Culver, G. M. & Noller, H. F. In vitro reconstitution of 30S ribosomal subunits using complete set of recombinant proteins. *Methods Enzymol* **318**, 446-460, doi:10.1016/s0076-6879(00)18069-3 (2000).

169 Tamaru, D., Amikura, K., Shimizu, Y., Nierhaus, K. H. & Ueda, T. Reconstitution of 30S ribosomal subunits in vitro using ribosome biogenesis factors. *RNA (New York, N.Y.)* **24**, 1512-1519, doi:10.1261/rna.065615.118 (2018).

170 Bubunenko, M. *et al.* 30S ribosomal subunits can be assembled in vivo without primary binding ribosomal protein S15. *Rna* **12**, 1229-1239, doi:10.1261/rna.2262106 (2006).

171 Thompson, J. *et al.* Analysis of mutations at residues A2451 and G2447 of 23S rRNA in the peptidyltransferase active site of the 50S ribosomal subunit. *Proceedings of the National Academy of Sciences of the United States of America* **98**, 9002-9007, doi:Doi 10.1073/Pnas.151257098 (2001).

172 Lieberman, K. R. & Dahlberg, A. E. The importance of conserved nucleotides of 23 S ribosomal RNA and transfer RNA in ribosome catalyzed peptide bond formation. *J Biol Chem* **269**, 16163-16169 (1994).

173 Green, R., Samaha, R. R. & Noller, H. F. Mutations at nucleotides G2251 and U2585 of 23 S rRNA perturb the peptidyl transferase center of the ribosome 1 1 Edited by P. E. Wright. *Journal of Molecular Biology* **266**, 40-50, doi:https://doi.org/10.1006/jmbi.1996.0780 (1997).

174 d'Aquino, A. E., Kim, D. S. & Jewett, M. C. Engineered Ribosomes for Basic Science and Synthetic Biology. *Annual Review of Chemical and Biomolecular Engineering* **9**, 311-340, doi:10.1146/annurev-chembioeng-060817-084129 (2018).

175 Orelle, C. *et al.* Protein synthesis by ribosomes with tethered subunits. *Nature* **524**, 119-124, doi:10.1038/nature14862 (2015).

176 Liu, Y., Kim, D. S. & Jewett, M. C. Repurposing ribosomes for synthetic biology. *Current Opinion in Chemical Biology* **40**, 87-94, doi:https://doi.org/10.1016/j.cbpa.2017.07.012 (2017).

177 Carlson, E. D., Gan, R., Hodgman, C. E. & Jewett, M. C. Cell-free protein synthesis: Applications come of age. *Biotechnology Advances* **30**, 1185-1194, doi:10.1016/j.biotechadv.2011.09.016 (2012).

178 Martin, R. W. *et al.* Cell-free protein synthesis from genomically recoded bacteria enables multisite incorporation of noncanonical amino acids. *Nature communications* **9**, 1203, doi:10.1038/s41467-018-03469-5 (2018).

179 Huang, A. *et al.* BioBits™ Explorer: A modular synthetic biology education kit. *Science Advances* **4**, eaat5105, doi:10.1126/sciadv.aat5105 (2018).

180 Stark, J. C. *et al.* BioBits™ Bright: A fluorescent synthetic biology education kit. *Science Advances* **4**, eaat5107, doi:10.1126/sciadv.aat5107 (2018).

181 Kightlinger, W. *et al.* Design of glycosylation sites by rapid synthesis and analysis of glycosyltransferases. *Nat Chem Biol* **14**, 627-635, doi:10.1038/s41589-018-0051-2 (2018).

182 Jaroentomeechai, T. *et al.* Single-pot glycoprotein biosynthesis using a cell-free transcription-translation system enriched with glycosylation machinery. *Nat Commun* **9**, 2686, doi:10.1038/s41467-018-05110-x (2018).

183 Clementi, N., Chirkova, A., Puffer, B., Micura, R. & Polacek, N. Atomic mutagenesis reveals A2660 of 23S ribosomal RNA as key to EF-G GTPase activation. *Nat Chem Biol* **6**, 344-351, doi:10.1038/nchembio.341 (2010).

184 Erlacher, M. D., Chirkova, A., Voegele, P. & Polacek, N. Generation of chemically engineered ribosomes for atomic mutagenesis studies on protein biosynthesis. *Nat. Protocols* **6**, 580-592, doi:http://www.nature.com/nprot/journal/v6/n5/abs/nprot.2011.306.html#supplementary-information (2011).

185 Willi, J. *et al.* Oxidative stress damages rRNA inside the ribosome and differentially affects the catalytic center. *Nucleic Acids Res* **46**, 1945-1957, doi:10.1093/nar/gkx1308 (2018).

186 Liu, Y., Fritz, B. R., Anderson, M. J., Schoborg, J. A. & Jewett, M. C. Characterizing and Alleviating Substrate Limitations for Improved in vitro Ribosome Construction. *ACS Synth Biol*, doi:10.1021/sb5002467 (2014).

187 Green, R. & Noller, H. F. Reconstitution of Functional 50S Ribosomes from in Vitro Transcripts of Bacillus stearothermophilus 23S rRNA. *Biochemistry* **38**, 1772-1779, doi:10.1021/bi982246a (1999).

188 O'Connor, M., Thomas, C. L., Zimmermann, R. A. & Dahlberg, A. E. Decoding fidelity at the ribosomal A and P sites: influence of mutations in three different regions of the decoding domain in 16S rRNA. *Nucleic Acids Research* **25**, 1185-1193 (1997).

189 Moine, H. & Dahlberg, A. E. Mutations in helix 34 of Escherichia coli 16 S ribosomal RNA have multiple effects on ribosome function and synthesis. *J Mol Biol* **243**, 402-412, doi:10.1006/jmbi.1994.1668 (1994).

190 O'Connor, M. & Dahlberg, A. E. Mutations at U2555, a tRNA-protected base in 23S rRNA, affect translational fidelity. *Proceedings of the National Academy of Sciences* **90**, 9214-9218 (1993).

191 Yarza, P. *et al.* Update of the All-Species Living Tree Project based on 16S and 23S rRNA sequence analyses. *Systematic and Applied Microbiology* **33**, 291-299, doi:https://doi.org/10.1016/j.syapm.2010.08.001 (2010).

192 Nierhaus, K. H. in *Ribosomes and Protein Synthesis: A Practical Approach* (ed G. Spedding) 161-189 (IRL Press, 1990).

193 Swartz, J. R., Jewett, M. C. & Woodrow, K. A. Cell-free protein synthesis with prokaryotic combined transcription-translation. *Methods Mol Biol* **267**, 169-182, doi:10.1385/1-59259-774-2:169 (2004).

194 Polacek, N., Gaynor, M., Yassin, A. & Mankin, A. S. Ribosomal peptidyl transferase can withstand mutations at the putative catalytic nucleotide. *Nature* **411**, 498-501 (2001).

195 Laurberg, M. *et al.* Structural basis for translation termination on the 70S ribosome. *Nature* **454**, 852-857, doi:10.1038/nature07115 (2008).

196 Simonovic, M. & Steitz, T. A. A structural view on the mechanism of the ribosome-catalyzed peptide bond formation. *Biochim Biophys Acta* **1789**, 612-623, doi:10.1016/j.bbagrm.2009.06.006 (2009).

197 Schmeing, T. M., Huang, K. S., Strobel, S. A. & Steitz, T. A. An induced-fit mechanism to promote peptide bond formation and exclude hydrolysis of peptidyl-tRNA. *Nature* **438**, 520-524, doi:10.1038/nature04152 (2005).

198 Gregory, S. T., Lieberman, K. R. & Dahlberg, A. E. Mutations in the peptidyl transferase region of E.coli 23S rRNA affecting translational accuracy. *Nucleic Acids Research* **22**, 279-284, doi:10.1093/nar/22.3.279 (1994).

199 Scolnick, E., Tompkins, R., Caskey, T. & Nirenberg, M. Release factors differing in specificity for terminator codons. *Proceedings of the National Academy of Sciences of the United States of America* **61**, 768-774, doi:10.1073/pnas.61.2.768 (1968).

200 Scolnick, E. M. & Caskey, C. T. Peptide chain termination. V. The role of release factors in mRNA terminator codon recognition. *Proceedings of the National Academy of Sciences of the United States of America* **64**, 1235-1241, doi:10.1073/pnas.64.4.1235 (1969).

201 Hesslein, A. E. *et al.* Exploration of the conserved A+C wobble pair within the ribosomal peptidyl transferase center using affinity purified mutant ribosomes. *Nucleic Acids Research* **32**, 3760-3770, doi:10.1093/nar/gkh672 (2004).

202 Porse, B. T., Thi-Ngoc, H. P. & Garrett, R. A. The Donor Substrate Site within the Peptidyl Transferase Loop of 23 S rRNA and its Putative Interactions with the CCA-end of N-blocked Aminoacyl-tRNAPhe. *Journal of Molecular Biology* **264**, 472-483, doi:https://doi.org/10.1006/jmbi.1996.0655 (1996).

203 Sigmund, C. D. & Morgan, E. A. Erythromycin resistance due to a mutation in a ribosomal RNA operon of Escherichia coli. *Proc Natl Acad Sci U S A* **79**, 5602-5606 (1982).

204 Weisblum, B. Erythromycin resistance by ribosome modification. *Antimicrob Agents Chemother* **39**, 577-585, doi:10.1128/aac.39.3.577 (1995).

205 Vester, B. & Douthwaite, S. Macrolide resistance conferred by base substitutions in 23S rRNA. *Antimicrobial agents and chemotherapy* **45**, 1-12, doi:10.1128/aac.45.1.1-12.2001 (2001).

206 Bocchetta, M., Xiong, L. & Mankin, A. S. 23S rRNA positions essential for tRNA binding in ribosomal functional sites. *Proceedings of the National Academy of Sciences* **95**, 3525 (1998).

207 Chirkova, A. *et al.* The role of the universally conserved A2450–C2063 base pair in the ribosomal peptidyl transferase center. *Nucleic Acids Research* **38**, 4844-4855, doi:10.1093/nar/gkq213 (2010).

208 Bayfield, M. A., Thompson, J. & Dahlberg, A. E. The A2453-C2499 wobble base pair in Escherichia coli 23S ribosomal RNA is responsible for pH sensitivity of the peptidyltransferase active site conformation. *Nucleic Acids Research* **32**, 5512-5518, doi:10.1093/nar/gkh888 (2004).

209 Korostelev, A. A. Structural aspects of translation termination on the ribosome. *RNA (New York, N.Y.)* **17**, 1409-1421, doi:10.1261/rna.2733411 (2011).

210 Pape, T., Wintermeyer, W. & Rodnina, M. V. Complete kinetic mechanism of elongation factor Tu-dependent binding of aminoacyl-tRNA to the A site of the E.coli ribosome. *The EMBO Journal* **17**, 7490-7497, doi:10.1093/emboj/17.24.7490 (1998).

211 O'Connor, M., Lee, W.-C. M., Mankad, A., Squires, C. L. & Dahlberg, A. E. Mutagenesis of the peptidyltransferase center of 23S rRNA: the invariant U2449 is dispensable. *Nucleic Acids Research* **29**, 710-715, doi:10.1093/nar/29.3.710 (2001).

212 O'Connor, M., Willis, N. M., Bossi, L., Gesteland, R. F. & Atkins, J. F. Functional tRNAs with altered 3' ends. *Embo j* **12**, 2559-2566 (1993).

213 Melo Czekster, C., Robertson, W. E., Walker, A. S., Söll, D. & Schepartz, A. In Vivo Biosynthesis of a β-Amino Acid-Containing Protein. *Journal of the American Chemical Society* **138**, 5194-5197, doi:10.1021/jacs.6b01023 (2016).

214 Aleksashin, N. A. *et al.* Assembly and functionality of the ribosome with tethered subunits. *Nat Commun* **10**, 930, doi:10.1038/s41467-019-08892-w (2019).

215 Fried, S. D., Schmied, W. H., Uttamapinant, C. & Chin, J. W. Ribosome Subunit Stapling for Orthogonal Translation in E. coli. *Angewandte Chemie (International Ed. in English)* **54**, 12791-12794, doi:10.1002/anie.201506311 (2015).

216 Schmied, W. H. *et al.* Controlling orthogonal ribosome subunit interactions enables evolution of new function. *Nature* **564**, 444-448, doi:10.1038/s41586-018-0773-z (2018).

217 Dedkova, L. M. & Hecht, S. M. Expanding the Scope of Protein Synthesis Using Modified Ribosomes. *Journal of the American Chemical Society* **141**, 6430-6447, doi:10.1021/jacs.9b02109 (2019).

218 Liu, C. C., Jewett, M. C., Chin, J. W. & Voigt, C. A. Toward an orthogonal central dogma. *Nature Chemical Biology* **14**, 103, doi:10.1038/nchembio.2554 (2018).

219 Noeske, J. *et al.* High-resolution structure of the Escherichia coli ribosome. *Nat Struct Mol Biol* **22**, 336-341, doi:10.1038/nsmb.2994 (2015).

220 Cheloha, R. W. *et al.* Consequences of Periodic α-to-β3 Residue Replacement for Immunological Recognition of Peptide Epitopes. *ACS Chemical Biology* **10**, 844-854, doi:10.1021/cb500888q (2015).

221 Webb, A. I. *et al.* T Cell Determinants Incorporating β-Amino Acid Residues Are Protease Resistant and Remain Immunogenic In Vivo. *The Journal of Immunology* **175**, 3810-3818, doi:10.4049/jimmunol.175.6.3810 (2005).

222 Liu, C. C. & Schultz, P. G. Adding new chemistries to the genetic code. *Annu Rev Biochem* **79**, 413-444, doi:10.1146/annurev.biochem.052308.105824 (2010).

223 Hoesl, M. G. & Budisa, N. Recent advances in genetic code engineering in Escherichia coli. *Curr Opin Biotechnol* **23**, 751-757, doi:10.1016/j.copbio.2011.12.027 (2012).

224 Davis, L. & Chin, J. W. Designer proteins: applications of genetic code expansion in cell biology. *Nature Reviews in Molecular Cell Biology* **13**, 168-182, doi:10.1038/nrm3286 (2012).

225 Englander, M. T. *et al.* The ribosome can discriminate the chirality of amino acids within its peptidyl-transferase center. *Proc Natl Acad Sci U S A* **112**, 6038-6043, doi:10.1073/pnas.1424712112 (2015).

226 Guichard, G. *et al.* Melanoma Peptide MART-1(27−35) Analogues with Enhanced Binding Capacity to the Human Class I Histocompatibility Molecule HLA-A2 by Introduction of a β-Amino Acid Residue: Implications for Recognition by Tumor-Infiltrating Lymphocytes. *Journal of Medicinal Chemistry* **43**, 3803-3808, doi:10.1021/jm000909s (2000).

227 Reinelt, S. *et al.* β-Amino Acid Scan of a Class I Major Histocompatibility Complex-restricted Alloreactive T-cell Epitope. *Journal of Biological Chemistry* **276**, 24525-24530, doi:10.1074/jbc.M102772200 (2001).

228 Raguse, T. L., Porter, E. A., Weisblum, B. & Gellman, S. H. Structure-activity studies of 14-helical antimicrobial beta-peptides: probing the relationship between conformational stability and antimicrobial potency. *J Am Chem Soc* **124**, 12774-12785 (2002).

229 Albericio, F. Developments in peptide and amide synthesis. *Curr Opin Chem Biol* **8**, 211-221, doi:10.1016/j.cbpa.2004.03.002 (2004).

230 Guichard, G. & Seebach, D. Solid-phase synthesis of beta-oligopeptides. *Chimia* **51**, 315-318 (1997).

231 Arvidsson, P. I. *et al.* Antibiotic and hemolytic activity of a beta2/beta3 peptide capable of folding into a 12/10-helical secondary structure. *Chembiochem* **4**, 1345-1347, doi:10.1002/cbic.200300698 (2003).

232 Murray, J. K. *et al.* Efficient synthesis of a beta-peptide combinatorial library with microwave irradiation. *J Am Chem Soc* **127**, 13271-13280, doi:10.1021/ja052733v (2005).

233 Heckler, T. G., Zama, Y., Naka, T. & Hecht, S. M. Dipeptide formation with misacylated tRNAPhes. *J Biol Chem* **258**, 4492-4495 (1983).

234 Noren, C. J., Anthony-Cahill, S. J., Griffith, M. C. & Schultz, P. G. A general method for site-specific incorporation of unnatural amino acids into proteins. *Science* **244**, 182-188 (1989).
235 Goto, Y., Katoh, T. & Suga, H. Flexizymes for genetic code reprogramming. *Nat Protoc* **6**, 779-790, doi:10.1038/nprot.2011.331 (2011).
236 Youngman, E. M. & Green, R. Affinity purification of in vivo-assembled ribosomes for in vitro biochemical analysis. *Methods* **36**, 305-312, doi:https://doi.org/10.1016/j.ymeth.2005.04.007 (2005).
237 Keryer-Bibens, C., Barreau, C. & Osborne, H. B. Tethering of proteins to RNAs by bacteriophage proteins. *Biol Cell* **100**, 125-138, doi:10.1042/bc20070067 (2008).
238 Beckert, B. *et al.* Structure of a hibernating 100S ribosome reveals an inactive conformation of the ribosomal protein S1. *Nature Microbiology* **3**, 1115-1121, doi:10.1038/s41564-018-0237-0 (2018).
239 Ramakrishnan, V. Ribosome Structure and the Mechanism of Translation. *Cell* **108**, 557-572, doi:https://doi.org/10.1016/S0092-8674(02)00619-0 (2002).
240 Ban, N., Nissen, P., Hansen, J., Moore, P. B. & Steitz, T. A. The Complete Atomic Structure of the Large Ribosomal Subunit at 2.4 Å Resolution. *Science* **289**, 905 (2000).
241 Schluenzen, F. *et al.* Structure of Functionally Activated Small Ribosomal Subunit at 3.3 Å Resolution. *Cell* **102**, 615-623, doi:https://doi.org/10.1016/S0092-8674(00)00084-2 (2000).
242 Wimberly, B. T. *et al.* Structure of the 30S ribosomal subunit. *Nature* **407**, 327-339, doi:10.1038/35030006 (2000).
243 Stern, S., Powers, T., Changchien, L. M. & Noller, H. F. RNA-protein interactions in 30S ribosomal subunits: folding and function of 16S rRNA. *Science* **244**, 783-790 (1989).
244 Viani Puglisi, E., Green, R., Noller, H. F. & Puglisi, J. D. Structure of a conserved RNA component of the peptidyl transferase centre. *Nature Structural Biology* **4**, 775, doi:10.1038/nsb1097-775 (1997).
245 Des Soye, B. J., Patel, J. R., Isaacs, F. J. & Jewett, M. C. Repurposing the translation apparatus for synthetic biology. *Current Opinion in Chemical Biology* **28**, 83-90, doi:https://doi.org/10.1016/j.cbpa.2015.06.008 (2015).
246 Davis, L. & Chin, J. W. Designer proteins: applications of genetic code expansion in cell biology. *Nature Reviews Molecular Cell Biology* **13**, 168, doi:10.1038/nrm3286 https://www.nature.com/articles/nrm3286#supplementary-information (2012).
247 Roesser, J. R., Xu, C., Payne, R. C., Surratt, C. K. & Hecht, S. M. Preparation of misacylated aminoacyl-tRNAPhe's useful as probes of the ribosomal acceptor site. *Biochemistry* **28**, 5185-5195 (1989).
248 Hui, A. & de Boer, H. A. Specialized ribosome system: preferential translation of a single mRNA species by a subpopulation of mutated ribosomes in Escherichia coli. *Proceedings of the National Academy of Sciences* **84**, 4762-4766, doi:10.1073/pnas.84.14.4762 (1987).
249 Rackham, O. & Chin, J. W. A network of orthogonal ribosome x mRNA pairs. *Nat Chem Biol* **1**, 159-166, doi:10.1038/nchembio719 (2005).
250 Neumann, H., Wang, K., Davis, L., Garcia-Alai, M. & Chin, J. W. Encoding multiple unnatural amino acids via evolution of a quadruplet-decoding ribosome. *Nature* **464**, 441, doi:10.1038/nature08817 https://www.nature.com/articles/nature08817#supplementary-information (2010).
251 Wang, K., Neumann, H., Peak-Chew, S. Y. & Chin, J. W. Evolved orthogonal ribosomes enhance the efficiency of synthetic genetic code expansion. *Nature Biotechnology* **25**, 770, doi:10.1038/nbt1314 https://www.nature.com/articles/nbt1314#supplementary-information (2007).

252 Kitahara, K. & Suzuki, T. The ordered transcription of RNA domains is not essential for ribosome biogenesis in Escherichia coli. *Mol Cell* **34**, 760-766, doi:10.1016/j.molcel.2009.05.014 (2009).
253 An, W. & Chin, J. W. Synthesis of orthogonal transcription-translation networks. *Proceedings of the National Academy of Sciences* **106**, 8477-8482, doi:10.1073/pnas.0900267106 (2009).
254 Datsenko, K. A. & Wanner, B. L. One-step inactivation of chromosomal genes in Escherichia coli K-12 using PCR products. *Proceedings of the National Academy of Sciences* **97**, 6640-6645, doi:10.1073/pnas.120163297 (2000).
255 Gibson, D. G. *et al.* Enzymatic assembly of DNA molecules up to several hundred kilobases. *Nat Meth* **6**, 343-345, doi:http://www.nature.com/nmeth/journal/v6/n5/suppinfo/nmeth.1318_S1.html (2009).
256 Melançon, C. E. & Schultz, P. G. One Plasmid Selection System for the Rapid Evolution of Aminoacyl-tRNA Synthetases. *Bioorganic & medicinal chemistry letters* **19**, 3845-3847, doi:10.1016/j.bmcl.2009.04.007 (2009).
257 Inouye, S. & Inouye, M. Up-promoter mutations in the lpp gene of Escherichia coli. *Nucleic Acids Research* **13**, 3101-3110, doi:10.1093/nar/13.9.3101 (1985).
258 Lajoie, M. J. *et al.* Genomically Recoded Organisms Expand Biological Functions. *Science* **342**, 357-360, doi:10.1126/science.1241459 (2013).
259 Wang, H. H. *et al.* Programming cells by multiplex genome engineering and accelerated evolution. *Nature* **460**, 894-898, doi:http://www.nature.com/nature/journal/v460/n7257/suppinfo/nature08187_S1.html (2009).
260 Gan, R. *et al.* Translation system engineering in Escherichia coli enhances non-canonical amino acid incorporation into proteins. *Biotechnology and bioengineering* **114**, 1074-1086, doi:10.1002/bit.26239 (2017).
261 Chin, J. W. *et al.* Addition of p-Azido-l-phenylalanine to the Genetic Code of Escherichia coli. *Journal of the American Chemical Society* **124**, 9026-9027, doi:10.1021/ja027007w (2002).
262 Reuter, J. S. & Mathews, D. H. RNAstructure: software for RNA secondary structure prediction and analysis. *BMC Bioinformatics* **11**, 129, doi:10.1186/1471-2105-11-129 (2010).
263 Heinig, M. & Frishman, D. STRIDE: a web server for secondary structure assignment from known atomic coordinates of proteins. *Nucleic Acids Res* **32**, W500-502, doi:10.1093/nar/gkh429 (2004).
264 Salis, H. M., Mirsky, E. A. & Voigt, C. A. Automated design of synthetic ribosome binding sites to control protein expression. *Nat Biotech* **27**, 946-950, doi:http://www.nature.com/nbt/journal/v27/n10/suppinfo/nbt.1568_S1.html (2009).
265 Espah Borujeni, A., Channarasappa, A. S. & Salis, H. M. Translation rate is controlled by coupled trade-offs between site accessibility, selective RNA unfolding and sliding at upstream standby sites. *Nucleic Acids Research* **42**, 2646-2659, doi:10.1093/nar/gkt1139 (2014).
266 Amiram, M. *et al.* Evolution of translation machinery in recoded bacteria enables multi-site incorporation of nonstandard amino acids. *Nat Biotech* **33**, 1272-1279 (2015).
267 Jaroentomeechai, T. *et al.* Author Correction: Single-pot glycoprotein biosynthesis using a cell-free transcription-translation system enriched with glycosylation machinery. *Nature Communications* **9**, 3396, doi:10.1038/s41467-018-05620-8 (2018).
268 Mukai, T., Lajoie, M. J., Englert, M. & Söll, D. Rewriting the Genetic Code. *Annual Review of Microbiology* **71**, 557-577, doi:10.1146/annurev-micro-090816-093247 (2017).
269 Arranz-Gibert, P., Vanderschuren, K. & Isaacs, F. J. Next-generation genetic code expansion. *Current Opinion in Chemical Biology* **46**, 203-211, doi:https://doi.org/10.1016/j.cbpa.2018.07.020 (2018).

270 Chin, J. W. Expanding and reprogramming the genetic code. *Nature* **550**, 53, doi:10.1038/nature24031 (2017).

271 Arranz-Gibert, P., Vanderschuren, K. & Isaacs, F. J. Next-generation genetic code expansion. *Curr Opin Chem Biol* **46**, 203-211, doi:10.1016/j.cbpa.2018.07.020 (2018).

272 Chong, S., Chen, C., Ge, H. & Xie, X. S. Mechanism of Transcriptional Bursting in Bacteria. *Cell* **158**, 314-326, doi:10.1016/j.cell.2014.05.038.

273 Shearwin, K. E., Callen, B. P. & Egan, J. B. Transcriptional interference-a crash course. *Trends in Genetics* **21**, 339-345, doi:10.1016/j.tig.2005.04.009.

274 Yeung, E. *et al.* The Effect of Compositional Context on Synthetic Gene Networks. *bioRxiv*, 083329 (2016).

275 Gan, R. *et al.* Translation system engineering in Escherichia coli enhances non-canonical amino acid incorporation into proteins. *Biotechnol Bioeng* **114**, 1074-1086, doi:10.1002/bit.26239 (2017).

276 Chatterjee, A., Xiao, H. & Schultz, P. G. Evolution of multiple, mutually orthogonal prolyl-tRNA synthetase/tRNA pairs for unnatural amino acid mutagenesis in *Escherichia coli*. *Proc. Natl. Acad. Sci. U. S. A.* **109**, 14841-14846, doi:10.1073/pnas.1212454109 (2012).

277 Carlson, E. D. Creating Ribo-T: (Design, Build, Test)n. *ACS Synth Biol* **4**, 1173-1175, doi:10.1021/acssynbio.5b00218 (2015).

278 Guo, P. The emerging field of RNA nanotechnology. *Nature nanotechnology* **5**, 833-842, doi:10.1038/nnano.2010.231 (2010).

279 Leontis, N. B., Lescoute, A. & Westhof, E. The building blocks and motifs of RNA architecture. *Curr Opin Struct Biol* **16**, 279-287, doi:10.1016/j.sbi.2006.05.009 (2006).

280 Jaeger, L. & Chworos, A. The architectonics of programmable RNA and DNA nanostructures. *Curr Opin Struct Biol* **16**, 531-543, doi:10.1016/j.sbi.2006.07.001 (2006).

281 Jasinski, D., Haque, F., Binzel, D. W. & Guo, P. Advancement of the Emerging Field of RNA Nanotechnology. *ACS Nano* **11**, 1142-1164, doi:10.1021/acsnano.6b05737 (2017).

282 Afonin, K. A. *et al.* Computational and experimental characterization of RNA cubic nanoscaffolds. *Methods (San Diego, Calif.)* **67**, 256-265, doi:10.1016/j.ymeth.2013.10.013 (2014).

283 Jossinet, F., Ludwig, T. E. & Westhof, E. Assemble: an interactive graphical tool to analyze and build RNA architectures at the 2D and 3D levels. *Bioinformatics* **26**, 2057-2059, doi:10.1093/bioinformatics/btq321 (2010).

284 Yesselman, J. D. *et al.* Computational design of three-dimensional RNA structure and function. *Nat Nanotechnol* **14**, 866-873, doi:10.1038/s41565-019-0517-8 (2019).

285 Cheatham, T. E., 3rd, Brooks, B. R. & Kollman, P. A. Molecular modeling of nucleic acid structure. *Curr Protoc Nucleic Acid Chem* **Chapter 7**, Unit-7.5, doi:10.1002/0471142700.nc0705s06 (2001).

286 Lee, J. *et al.* RNA design rules from a massive open laboratory. *Proc Natl Acad Sci U S A* **111**, 2122-2127, doi:10.1073/pnas.1313039111 (2014).

287 Carlson, E. D. *et al.* Engineered ribosomes with tethered subunits for expanding biological function. *Nat Commun* **10**, 3920, doi:10.1038/s41467-019-11427-y (2019).

288 LeCuyer, K. A., Behlen, L. S. & Uhlenbeck, O. C. Mutants of the Bacteriophage MS2 Coat Protein That Alter Its Cooperative Binding to RNA. *Biochemistry* **34**, 10600-10606, doi:10.1021/bi00033a035 (1995).

289 Trabuco, L. G. *et al.* The role of L1 stalk-tRNA interaction in the ribosome elongation cycle. *J Mol Biol* **402**, 741-760, doi:10.1016/j.jmb.2010.07.056 (2010).

290 Voorhees, R. M., Schmeing, T. M., Kelley, A. C. & Ramakrishnan, V. The mechanism for activation of GTP hydrolysis on the ribosome. *Science* **330**, 835-838, doi:10.1126/science.1194460 (2010).

291 Shi, X., Khade, P. K., Sanbonmatsu, K. Y. & Joseph, S. Functional role of the sarcin-ricin loop of the 23S rRNA in the elongation cycle of protein synthesis. *J Mol Biol* **419**, 125-138, doi:10.1016/j.jmb.2012.03.016 (2012).

292 Carlson, M. A. *et al.* Ribosomal protein L7/L12 is required for GTPase translation factors EF-G, RF3, and IF2 to bind in their GTP state to 70S ribosomes. *FEBS J* **284**, 1631-1643, doi:10.1111/febs.14067 (2017).

293 Lucks, J. B. *et al.* Multiplexed RNA structure characterization with selective 2'-hydroxyl acylation analyzed by primer extension sequencing (SHAPE-Seq). *Proceedings of the National Academy of Sciences* **108**, 11063, doi:10.1073/pnas.1106501108 (2011).

294 Westbrook, A. M. & Lucks, J. B. Achieving large dynamic range control of gene expression with a compact RNA transcription–translation regulator. *Nucleic Acids Research* **45**, 5614-5624, doi:10.1093/nar/gkx215 (2017).

295 Weber, H. J. Stoichiometric measurements of 30S and 50S ribosomal proteins from Escherichia coli. *Mol Gen Genet* **119**, 233-248 (1972).

296 Yates, J. L. & Nomura, M. Feedback regulation of ribosomal protein synthesis in E. coli: localization of the mRNA target sites for repressor action of ribosomal protein L1. *Cell* **24**, 243-249 (1981).

297 Yates, J. L., Arfsten, A. E. & Nomura, M. In vitro expression of Escherichia coli ribosomal protein genes: autogenous inhibition of translation. *Proc Natl Acad Sci U S A* **77**, 1837-1841 (1980).

298 Sykes, M. T., Sperling, E., Chen, S. S. & Williamson, J. R. Quantitation of the ribosomal protein autoregulatory network using mass spectrometry. *Anal Chem* **82**, 5038-5045, doi:10.1021/ac9028664 (2010).

299 Wikstrom, P. M., Bystrom, A. S. & Bjork, G. R. Non-autogenous control of ribosomal protein synthesis from the trmD operon in Escherichia coli. *J Mol Biol* **203**, 141-152 (1988).

300 Semrad, K., Green, R. & Schroeder, R. RNA chaperone activity of large ribosomal subunit proteins from Escherichia coli. *Rna* **10**, 1855-1860, doi:10.1261/rna.7121704 (2004).

301 Brot, N., Caldwell, P. & Weissbach, H. Autogenous control of Escherichia coli ribosomal protein L10 synthesis in vitro. *Proc Natl Acad Sci U S A* **77**, 2592-2595 (1980).

302 Yates, J. L. & Nomura, M. E. coli ribosomal protein L4 is a feedback regulatory protein. *Cell* **21**, 517-522 (1980).

303 Dean, D., Yates, J. L. & Nomura, M. Identification of ribosomal protein S7 as a repressor of translation within the str operon of E. coli. *Cell* **24**, 413-419 (1981).

304 Dean, D., Yates, J. L. & Nomura, M. Escherichia coli ribosomal protein S8 feedback regulates part of spc operon. *Nature* **289**, 89-91 (1981).

305 Grondek, J. F. & Culver, G. M. Assembly of the 30S ribosomal subunit: positioning ribosomal protein S13 in the S7 assembly branch. *Rna* **10**, 1861-1866, doi:10.1261/rna.7130504 (2004).

306 Alix, J. H., Hayes, D. & Nierhaus, K. H. Properties of ribosomes and RNA synthesized by Escherichia coli grown in the presence of ethionine. V. Methylation dependence on the assembly of E. coli 50 S ribosomal subunits. *J Mol Biol* **127**, 375-395 (1979).

307 Jewett, M. C., Calhoun, K. A., Voloshin, A., Wuu, J. J. & Swartz, J. R. An integrated cell-free metabolic platform for protein production and synthetic biology. *Mol Syst Biol* **4**, 220, doi:msb200857 [pii]
10.1038/msb.2008.57 (2008).

308 Giron, M. D. & Salto, R. From green to blue: site-directed mutagenesis of the green fluorescent protein to teach protein structure-function relationships. *Biochem Mol Biol Educ* **39**, 309-315, doi:10.1002/bmb.20467 (2011).

Anne d'Aquino

545 Hinman Ave. Apt L2. Evanston, IL 60202 | 224-420-7096 |
annedaquino2019@u.northwestern.edu

EDUCATION

B.S.: Western Washington University, June 2014, Biochemistry, Mathematics Minor
Ph.D.: Northwestern University, Expected: Winter 2020, Biological Sciences

RESEARCH AND PROFESSIONAL EXPERIENCE

2014 – Present | Northwestern University Interdisciplinary Biological Sciences Program
Advisor: Dr. Michael Jewett
Studying and engineering the ribosome active site for extended backbone monomer incorporation.

Winter 2012 – July 2014 | Western Washington University Department of Chemistry
Advisor: Dr. Paul Spiegel
Studied the structure and function of an engineered human-porcine blood coagulation factor VIII protein.

Summer 2013 | Northwestern University Summer Research Opportunity Program
Advisor: Dr. Heather Pinkett, Chosen keynote speaker for SROP research symposium
Studied the structure and function of transcription factors involved in pleiotropic drug resistance.

Summer 2012 | University of California Irvine; National Science Foundation REU
Advisor: Dr. Douglas Tobias
Conducted research on the molecular dynamics of wild-type and mutant γ crystallin protein molecules in water.

2011 – 2012 | Western Washington University, Vietnam and America Study Abroad
Advisor: Dr. Mart Stewart
Studied the impacts of dioxin within fatty tissues and the environment; investigated the epidemiology associated with Agent Orange sprayed over 40 years ago during the war.

AWARDS, FELLOWSHIPS & GRANTS

January 2019 – 2019 Ribosome conference travel award recipient (Merida Mexico) ($500)

January 2019 – 2019 ASBMB Travel award for the 2019 ASBMB annual meeting in Orlando ($1000)

February 2019 – 2019 Stanford University Postdoctoral Recruitment Initiative in Sciences and Medicine Program (PRISM)
Selected for an early postdoc interview opportunity with the PRISM program at Stanford.

March 2018 – Present, Northwestern University Presidential Fellowship
The Presidential Fellowship is the most prestigious award presented annually to graduate students who are nominated by their academic programs and represent a combination of intellectual and creative ability. As Presidential Fellows, recipients take on a leadership role in the Society of Fellows--faculty members and past Presidential Fellows.

June 2017 – Present, Northwestern University Ryan Fellowship
The Ryan Fellowship supports graduate students dedicated to the exploration of fundamental nanoscale science and to advancing this knowledge into practical applications of benefit to society.

April 2014 – Present, National Science Foundation Graduate Research Fellowship
The NSF GRFP recognizes and supports outstanding graduate students in NSF-supported science, technology, engineering, and mathematics disciplines. Fellows are anticipated to become knowledge experts who can contribute significantly to research, teaching, and innovations in science and engineering.

June 2015 – 2017, NIH Molecular Biophysics Training Grant Fellow and Trainee (Funded by the National Institute of Health)
The Molecular Biophysics Training Program is funded by the National Institute of General Medical Sciences of the National Institutes of Health (5T32 GM008382). The program serves as a hub for all research and training activities in biophysics at Northwestern. Fellows receive in depth training in biophysical techniques, attend core biophysical courses, and organize and present in seminars.

January 2018 – Northwestern University Building on Diversity (NU BonD) Travel Grant
The NUBonD travel grant enabled me to present my research in the form of an oral presentation at the 2018 International Conference on Biomolecular Engineering Asia conference (ICBE Asia).

April 2017 – National Science Foundation Graduate Research in Data Program (GRID)
This program exposed me to data science training and applications. I was selected to attend workshops in data science, career panels with professionals in various fields, and was selected as one of 8 students to travel to Washington D.C. to meet with the NSF, NIH, Blue Labs, The Advisory Board Company and the Institute for Defense Analyses.

April 2017-January 2018 – Northwestern IBiS Travel Award
The IBiS Travel Award is enabled me to present my research at the Synthetic Biology: Engineering, Evolution, and Design (SEED) conference in Vancouver BC in June 2017, as well as the International Conference on Biomolecular Engineering in Singapore in January 2018.

April 2017 – Northwestern Graduate School (TGS) Travel Grant
The TGS Travel Grant is enabling me to present my research at the Synthetic Biology: Engineering, Evolution, and Design (SEED) conference in Vancouver BC in June 2017.

November 2016 – Engineering Biology Research Consortium (EBRC) Conference 1st place poster

June 2015 – Chicago Communication in Science Conference Fellow (ComSciCon)
The Chicago ComSciCon workshop series is designed to empower graduate students to communicate the complex concepts in science, engineering and other technical fields to diverse audiences. Attendees interact with fellow graduate student leaders in science communication, learn from expert writers and communicators including journalists, communication researchers, and scientists, and produce original writing for publication.

April 2016 – Evanston Engagement Grant
A service and community engagement grant, which aims to encourage positive student interaction with the Evanston community. Awarded for my proposed work with the HerStory event at the Museum of Science and Industry. This event aims to inspire young women around Chicago to pursue higher education and careers in science ($500). https://nuherstory.weebly.com/

January 2016- 2018 – GLAC Co-Sponsorship Funds Recipient
Funding to co-sponsor events that develop graduate student leadership and advocacy efforts. I was awarded funding for my work with Jugando Con La Ciencia on developing an arts and science fair at the Evanston

Public Library ($200), as well as two years of funding for my work in organizing HerStory ($200 each year).

June 2016 – American Society for Cell Biology (ASCB) COMPASS Outreach Grant
Funding to organize and carry out an event that brought Biology experiments and knowledge to underrepresented minorities. I was awarded funding for my work with Jugando Con La Ciencia on developing "*Un dia con la biologia*" wherein we brought 7 different biology demos to an Oakton Elementary School. Oakton has a high population of Spanish-speaking students ($700).

June 2014 – Western Washington University Spring Commencement Speaker
The commencement speaker of WWU is granted to a student from WWU's entire graduating class. The award honors a graduating senior for their exceptional scholarship and service to the university and community.

May 2014 – Outstanding Undergraduate Poster -WWU Scholar's Week Symposium
1st Place Poster Prize in the Division of Biochemistry

June 2012 – National Science Foundation Research Experience for Undergraduates
Received the NSF REU to conduct summer research at The University of California, Irvine under the supervision of Dr. Douglas Tobias.

June 2013 – National Science Foundation Summer Research Opportunity Program
Received the SROP to conduct summer research at Northwestern University under the supervision of Dr. Heather Pinkett. I was subsequently chosen as the STEM speaker in the final research symposium and offered early admission to the IBiS PhD program.

September 2012 - 2014 – Marion Van Nostrand STEM Scholarship Recipient
The Marion Van Nostrand Scholarship is awarded to women who are majors in physics, biology, chemistry, computer science, engineering or mathematics.

June 2013 – Julia Ann Rutherford Memorial Scholarship (Puget Sound section of ACS)
This scholarship is awarded to outstanding undergraduate students studying chemistry or biochemistry and plan on pursuing careers in these fields.

September 2013 – All Nations Louis Stokes Alliance for Minority Participation Scholarship
The ANLSAMP program is funded by the National Science Foundation, with the goal of increasing the number of minority and Native American students successfully completing degrees in STEM.

September 2012 – 2014 – Barbara French Duzan Scholarship (WWU Chemistry Dept)
This scholarship is intended for a B.S.-Biochemistry or B.S.-Chemistry major who demonstrates both academic achievement and financial need.

September 2012 – Washington State Opportunity Scholarship

September 2011 – 2013, Dr. Ralph and Ms. Eleanor Rinne Scholarship (WWU)

COMMUNITY/VOLUNTEER SERVICE

December 2018 – Present, Northwestern Prison Education Program (NPEP), Co-director of media and campus relations, Co-director of Cook County Jail Partnership, Northwestern University, CCDOC & IDOC, Stateville Correctional Center Education

June 2019, TRiO College & Career Summer Academy, Workshop leader, College of Lake County, Grayslake IL

October 2018 – Present – Annual Museum of Science and Industry (MSI) Science Works
Volunteer, Northwestern University, Museum of Science and Industry, Chicago

June 2018 – Present, BioBuilder workshop leader
Lead & organize workshops to train teachers in engineering biology skills and curriculum

September 2015 – Present, HerStory Outreach Program Director
Director and Lead organizer, volunteer, Northwestern University

September 2015 – 2018, Mentorship Opportunities for Research Engagement (MORE)
Director, Operations manager, Volunteer and mentor, Northwestern University

March 2014 – Present, International Science Engineering Fair (ISEF) judge /volunteer
Volunteer judge for the annual Chicago Public Schools ISEF finalists'
Northwestern University and the Chicago Museum of Science and Industry

Fall 2017 – Summer 2018 – The Museum of Science and Industry Jr. Science Café
Volunteer STEM professional presenter, Museum of Science & Industry

December 2014 – Summer 2019, Jugando con la Ciencia (JCLC – "Playing with Science")
Volunteer and activities coordinator, Northwestern University

September 2014 – 2015, Science in Society HELIX Magazine
Scientific writer/blogger, Northwestern University

September 2014 – 2016, IBiS Student Organization (ISO)
Outreach coordinator and director, Northwestern University

September 2011 – 2018, National Society for the Advancement of Hispanics/Chicanos and Native Americans in Science (SACNAS)
President and volunteer, Western Washington University (2011–2014) and volunteer and member for Northwestern University SACNAS (2014–Present)

January 2014 – 2018, Mentor Matching Engine
Volunteer mentor, Northwestern University

September 2012 – June 2014, ACS Student Chapter Chemistry Club
Volunteer, Western Washington University

May 2011 – September 2013, Food Sense Nutrition Education Program
Volunteer, Western Washington University

LEADERSHIP POSITIONS

April 2017–2018, Outreach/education liaison-Engineering Biology Research Consortium
As the outreach and education liaison for the EBRC, I worked with other team members to organize education outreach demos at the spring EBRC workshop at the University of Washington. We also compiled outreach opportunities for the synthetic biology community to access, share, and utilize in their volunteer efforts.

September 2015–2018, Mentorship Opportunities for Research Engagement (MORE)
As the Director and operations manager, I planned, organized and facilitated outreach and mentorship events for graduate students across Northwestern. I have directed 3 branches of the program: MORE@NW, MORE@ETHS, and MORE REACH.

September 2015 – Present, Founder and Director of HerStory
As the founder and director of HerStory, I establish and implement HerStory which is an outreach event aimed to inspire middle and high school females to pursue higher education and careers in science.

September 2015–Present, Jugando Con La Ciencia volunteer / lead coordinator
As a lead coordinator with Jugando Con La Ciencia, I have helped organize and execute outreach events spanning weekly activity sessions with children and their families, to one day biology fairs, to weekend events at the public library.

September 2016–Present, Graduate Research Mentor
As a graduate research mentor, I have spent over 3 years mentoring and training 3 undergraduate students on their own research projects. My mentorship has resulted in my first mentee, Tasfia, receiving the Alumnae of Northwestern University Scholarship award for women in STEM, her first co-authored paper, an invitation to give an oral presentation at the 2017 American Institute of Chemical Engineers (AIChE) annual meeting (where she won a 2nd place poster award in the Biotechnology, Food, and Pharma III Division), and travel grants from Northwestern's office of Undergraduate Research and the NU BonD (Building on Diversity) organization. Additionally, Tasfia presented her work as a poster at the Northwestern Undergraduate Research & Arts Exposition, as an oral presentation at the American Institute of Chemical Engineers (AIChE) Midwest Regional Conference, and was invited to present at the 2018 Stanford Undergraduate Research Conference. Finally, Tasfia was selected as a top-3 finalist for the Northwestern Gotaas Award recognizing one graduating senior in engineering who has demonstrated excellence in research as an undergraduate. My work with her will also culminate in her honors thesis and resulted in her enrollment in a graduate PhD program in Chemical Engineering at Rice University. My second mentee was Alysse, who was awarded a Northwestern Summer Research Grant through NU's office of undergraduate research and was hired to perform research in the lab of Dr. Kate Adamala at the University of Minnesota. My third undergraduate, Kim, was awarded a paid internship experience through her University (Johnson and Wales University), and presented posters at The Central US Synthetic Biology Workshop, and the Midwest Enzyme Chemistry Conference. Her work in the lab has culminated in her acceptance and enrollment in a graduate PhD program in Biology.

September 2016 – Present, Research Experience for Teachers (RET)
In July of each year, I help organize and run a two-week research experience for 5 teachers from Chicago Public middle and high schools. Teachers conduct hands-on research activities and develop lesson plans designed to expose students to engineering research and careers.

September 2015–2018, Distinguished Researcher in the Life Sciences (DRiLS) committee
As an organizer of the DRiLS lecture series, I have helped invite, host and organize distinguished researchers to speak at Northwestern and meet with graduate students. Speakers include Eva Nogales (attended), Maryanne Bonner (attended), Elizabeth Blackburn (invited), and Ben Barres (invited).

September 2016-2017, Biophysics Symposium Organizing committee and speaker host
As a part of the organizing committee, I took part in assisting with A/V and tech support on the day of the symposium. Furthermore, I worked with the committee to organize details of the event such as food, gifts for speakers, prizes, etc. I also helped host speakers before and during the symposium.

May 2015, IBiS Student Organization's Career Day organizer
I invited 8 academic and non-academic professionals to visit Northwestern and discuss their careers with IBiS students. The professionals spanned industry, medical writing, publishing, undergraduate teaching, directors of core facilities, academic administration, consulting, and academic professorships. I also organized a cocktail hour and round robin following the discussion.

September 2014 – 2016, IBiS Student Organization (ISO)
As the outreach coordinator of ISO, I take on the responsibility of planning; organizing and facilitating outreach and volunteer activities for graduate students in IBiS.

Fall 2012 – August 2014, Bellingham Police Explorer
The Bellingham Police Explorer post is part of the volunteer services program within the police department. The post allows young men and women the opportunity to explore and learn about a career in the criminal justice field while serving as a volunteer within the department. The program is service oriented with explorers helping people, assisting at community events, and aiding police officers with their work. Explorers also attend police academies every six months.

Fall 2012 – June 2014, President of SACNAS, WWU Chapter
As the president of WWU's SACNAS Chapter, I helped organize and implement outreach events geared toward underrepresented minorities in science.

January 2012 – June 2014, Lead Chemistry Tutor
I was the lead subject tutor for undergraduate General Chemistry.

September 2019 – June 2014, Tennis coach
I volunteered as a lead tennis coach for a local high school (Squalicum High School in Bellingham). In my work, I coached students from 3rd grade to seniors in high school.

June – September 2010, Math and Science Teacher at Mount Baker High School
I was a summer school math and science teacher to underrepresented students. This NOYCE summer internship was funded by the National Science Foundation.

HONORS, DISTINCTIONS

April 2018; Northwestern University Presidential Fellowship, Northwestern University
June 2017; Northwestern Ryan Fellow, Northwestern University
June 2015; NIH Molecular Biophysics Trainee, Northwestern University
April 2014; NSF Graduate Fellow; Western Washington University – Northwestern University
April 2014; WWU commencement Speaker; Western Washington University
June 2014; Graduated Cum Laude; Western Washington University

PROFESSIONAL SOCIETY MEMBERSHIPS

September 2018 – Present; ASCB
October 2018 – Present; ASBMB
January 2017 – Present; AAAS
March 2016 – 2018; Society for Biological Engineering (SBE)
September 2012 – Present; Society for the Advancement of Hispanics/Chicanos and Native Americans in Science (SACNAS)
September 2012 – 2014; American Chemical Society

TEACHING

January 2017 – March 2017, Advanced Cellular Biology (Biol_Sci 315), TA
Northwestern University, 12 hours/week for 1 quarter
Fall 2016 – New TA Conference (NTAC), Workshop Leader
Northwestern University, 2 days
January 2016 – March 2016, Cellular Processes Lab (Biol_Sci 221), Teaching Assistant,
Northwestern University, 20 hours/week for 1 quarter
September 2012 – June 2014, Organic Chemistry, Teaching Assistant
Western Washington University, 15 hours/week
June 2010 – NSF NOYCE Summer School Teacher, Primary Instructor,
Western Washington University, 40 hours/week

PUBLICATIONS

1. d'Aquino, A.E.; Kim, D.S.; and Jewett, M.C., Engineered Ribosomes for Basic and Synthetic Biology. **2018**. Annual Reviews of Chemical and Biomolecular Engineering. 9: 311-340.

2. *Caschera, F.; *Karim, A.; Gazzola, G.; d'Aquino, A. E.; Packard, N.H.; Jewett, M.C., High-throughput optimization cycle of a cell-free ribosome assembly and protein synthesis system. **2018**. ACS Synthetic Biology. Doi: 10.1021/acssynbio.8b00276. 7 (12): 22841-2853.

3. Yesselman, J.D.; Eiler, D.; Carlson, E.D.; Gotrik, M.R.; d'Aquino, A.E.; Ooms, A.N.; Kladwang, W.; Carlson, P.; Shi, X.; Costantino, D.A.; Herschlag, D.; Lucks, J.; Jewett, M.C.; Kieft, J.S.; and Das, R., Computational Design of Three-dimensional RNA Structure and Function. **2019**. Nature Nanotechnology. DOI: 10.1038/s41565-019-0517-8. [Epub ahead of print].

4. *Carlson, E. D.; *d'Aquino, A. E.; Kim, D.; Fulk, E. M.; Szal, T.; Mankin, A.; Jewett, M. C., Engineered ribosomes with tethered subunits for expanding biological function. **2019.** Nature Communications. DOI: 10.1038/s41467-019-11427-y.
*These authors contributed equally to this work.

5. d'Aquino, A. E.; Azim, T.; Aleksashin, N.; Hockenberry, A.J.; Mankin, A.; Jewett, M. C., Mutating the ribosomal peptidyl transferase center *in vitro*. **2019.** *Manuscript in revision (NAR).*

6. Aleksashin, A.A.; Szal, T.; d'Aquino, A.E.; Jewett, M.C.; and Mankin, A.S., Orthogonal protein translation systems based on dissociable ribosomes. 2019. *Manuscript submitted (Nature).*

7. Ian W. Smith, Anne E. d'Aquino, Ernest T. Parker, Christopher B. Doering, P. Clint Spiegel, Jr., The 3.2 A Crystal structure of a bioengineered variant of blood coagulation factor VIII indicates two distinct conformations of the C2 domain. **2019**. Journal of Thrombosis and Haemostasis. DOI: 10.1111/jth.14621.

8. d'Aquino, A. E.*; Carlson, E. D.*; Jewett, M. C., A ribosome tethering strategy for a fully orthogonal ribosome-messenger RNA system. **2019.** *Manuscript in preparation (Invited article; Nature Protocols).*

9. Anne E. d'Aquino, Andrea I. d'Aquino, Lauren Sutton, Mart Stewart, "Agent Orange and Narratives of Suffering," *Occam's Razor* 2 (**2012**): 36-64.

10. Jewett, M.C.; Carlson, E.D.; d'Aquino, A.E.; Kim, D.S., Ribosomes with Tethered Subunits. **2016**. *US Patent Application Serial No. 15/363,828*.

11. Jewett, M.C.; d'Aquino, A.E.; Ribosome Variants for Sequence Defined Polymer Synthesis. **2018**. *US Patent Application Serial No. 62/694,553*.

CONFERENCE PRESENTATIONS

1. "Mutating the ribosome peptidyl transferase center in vitro." ASBMB Meeting/ Experimental Biology 2019, Orlando FL, Poster Presentation, April 8, 2019. (Flash talk competition finalist)
2. "Engineered ribosomes with tethered subunits for expanding biological function." The RNA Club, Oral Presentation, University of Chicago GCIS, Chicago, March 18, 2019.
3. "Mutating the ribosomal peptidyl transferase center in vitro." Ribosome Structure and Function 2019, Poster Presentation, Merida MX, January 8, 2019.
4. "Mutational characterization and mapping of the 70S ribosomal active site." ASCB Meeting 2019, Poster Presentation, San Diego CA, December 11, 2018.
5. "Mutating the ribosomal peptidyl transferase center *in vitro*." Northwestern University Interdisciplinary Program in Biological Sciences Annual Retreat, Oral presentation, September 2018.
6. "Lost in translation: Mapping Ribosomal Mutations *in vitro*." The RNA Club, Oral Presentation, Northwestern Stanley Manne Children's Research Institute, June 11, 2018.
7. "Lost in translation: Mutating the ribosome active site *in vitro*." Northwestern University Computational Research Day, Poster Presentation, April 22, 2018.
8. "Lost in translation: Mapping Ribosomal Active Site Mutations *in vitro*." Engineering Biology Research Consortium (EBRC) Conference, University of Washington Seattle, Poster Presentation, March 2018.
9. "Lost in translation: Mapping Ribosomal Active Site Mutations *in vitro*." The International Conference for Biomolecular Engineering, Singapore, Oral Presentation, January 2018. (Awarded NUBonD travel grant)
10. "Lost in translation: Mapping the active site of the *E. coli* 70S Ribosome." Northwestern's 8th Annual Molecular Biophysics Symposium, Oral Presentation, June 2017.
11. "Mapping the PTC of the 70S ribosomal 23S rRNA." Northwestern University Interdisciplinary Program in Biological Sciences Annual Retreat, Poster presentation, September 2016.
12. "Characterizing the *E. coli* 70S Ribosome 23S rRNA peptidyl transferase center." Engineering Biology Research Consortium (EBRC) Conference, Poster Presentation, March 2017.
13. "Characterizing the *E. coli* 70S Ribosome 23S rRNA peptidyl transferase center." The Inaugural Engineering Biology Research Consortium (EBRC) Conference, Poster Presentation, November 2016, (1st place best poster award winner).
14. "Mutating and characterizing the *E. coli* Ribosomal 23S rRNA." Synthetic Biology: Engineering, Evolution & Design Conference (SEED), Poster Presentation, July 2016.
15. "Probing the role of 23S rRNA PTC interactions in translation fidelity." Northwestern's 7th Annual Molecular Biophysics Symposium, Poster Presentation, June 2016.

16. “Investigating the impact of 70S ribosomal 23S rRNA PTC mutations.” Northwestern University Interdisciplinary Program in Biological Sciences Annual Retreat, Poster presentation, September 2016.
17. “The Regulation of Drug Resistance by Transcription Factors Pdr1p and Pdr3p.” Summer Research Opportunity Program Research Symposium (Selected as best STEM oral presenter, and offered early admission to IBiS PhD program), Oral Presentation, May 2013.
18. “Structural Studies of Hybrid Human-Porcine Blood Coagulation Factor VIII.” Western Washington University Scholar’s Week Symposium (1st place Best Poster Award Winner), Poster Presentation, 2014.
19. “Analysis of Molecular Dynamics Simulations of Wild-type and Mutant γ Crystallin Molecules in Water.” University of California, Irvine Research Symposium, Oral Presentation, August 2012.
20. “Structural Studies of Homing Endonuclease I-SscI.” Western Washington University Scholar’s Week Symposium, Poster Presentation, May 2013.